DESIGN OF DETAILED MODELS FOR USE IN FAST AEROELASTIC SIMULATIONS OF PERMANENT-MAGNET DIRECT-DRIVE WIND TURBINES

by

DAVID S. OCHS

B.S, Kansas State University, 2010

A THESIS

submitted in partial fulfillment of the requirements for the degree

MASTER OF SCIENCE

Department of Electrical and Computer Engineering
College of Engineering

KANSAS STATE UNIVERSITY
Manhattan, Kansas

2012

Approved by:

Major Professor
Ruth Douglas Miller

Copyright

Abstract

This thesis presents the design of two models for permanent-magnet direct-drive wind turbines. The models are of a 10 kW and a 5 MW wind turbine, which are representative of residential scale and commercial scale turbines respectively. The models include aerodynamic and mechanical simulations through the FAST software, as well as concurrent electrical simulations through the SimPowerSystems toolbox for MATLAB/Simulink. The aim is to provide wind turbine designers and researchers with a comprehensive simulation tool that they can use to design and test many different aspects of a wind turbine. The particular novelty of these models is their high level of detail in electromechanical simulations. For each model, a generator speed controller was designed in a reference frame attached to the generator's rotor, and was executed with a 3-phase active rectifier using space-vector pulse-width modulation. Also for each model, active and reactive power controllers were designed in a reference frame synchronous with the grid, and were executed with a 3-phase inverter using space-vector pulse-width modulation. Additionally, a blade pitch controller was designed for the 5 MW model. Validation of the models was carried out in the MATLAB/Simulink environment with satisfactory results.

Table of Contents

List of Figures

List of Tables

Acknowledgements

I would like to acknowledge the efforts of Dr. Miller and Dr. White on this project. I spent lots of time in my office with my head spinning, and you were always ready and willing to straighten it out. I would also like to thank Dr. Mirafzal for serving on my committee. Many thanks also to Tod Hanley of Bergey Windpower for providing data on the 10 kW system and patiently answering my many questions. Finally, thank you to my family and friends for supporting me throughout graduate school.

Dedication

I dedicate this work to my wife, Marinda. You have been unbelievably patient with me through the ups and downs of my graduate school experience. I put a lot of effort into this project, and you put just as much or more into our marriage over the last two years.

Chapter 1 - Introduction

1.1 The Electric Power Grid

The electric power grid was essentially born in 1891 when the first large-scale demonstration of AC power transmission was performed in Germany [1, p. 17]. Since then it has been powered in large part by power plants that burn fossil fuels. Each part of the power system can be classified into one of four major categories: generation, transmission, distribution, or load. Energy is converted to electrical form by generators, moved across town or across the country by transmission and/or distribution systems, and finally powers everything from televisions to large industrial plants (loads). Following is a very brief description of each part of the power system.

Any description of the power system must start with generation. All types of power generation, with the exception of photovoltaics and fuel cells, work on basically the same principle: capture mechanical energy with a turbine, and then convert it to electrical energy with a generator. In coal, nuclear, geothermal, solar thermal, oil, and diesel power plants, water is boiled to make steam, which is then forced through a turbine, making it spin. The shaft of the turbine is connected to the shaft of the generator, so the generator spins as well. Natural gas plants use either a combustion turbine, which is basically a jet engine on a stand, or both a combustion turbine and a steam turbine. Wind power plants also use a turbine/generator combination, but instead of steam forcing the turbine to spin, the wind does it. A certain type of generator used in some wind turbines (permanent-magnet synchronous) will be discussed in detail in Chapter 3. All generators work on the basic same principles. According to Faraday's law, a conductor that is moving in the presence of a magnetic field will have an induced voltage. In mathematical form, this is [2, p. 177]

$$e_{ind} = (\boldsymbol{v} \times \boldsymbol{B}) \cdot \boldsymbol{L} \tag{1.1}$$

Where $\boldsymbol{v}$ is the velocity of the conductor, $\boldsymbol{B}$ is the flux density of the magnetic field, and $\boldsymbol{L}$ is the length of the conductor. Then according to Ohm's law,

$$V = IR, \tag{1.2}$$

if a load is attached to the conductor, current will flow. Electric power can then be defined as:

$$P = I^2R = \frac{V^2}{R}. \tag{1.3}$$

Equations (1.2) and (1.3) only consider resistive loads, but they can be generalized for non-resistive loads easily. The distinction is not important for this discussion.

Once energy is converted from mechanical to electrical form, it must be moved from the generating station to the loads, which may be very far away. This is the job of the transmission and distribution systems. Transmission and distribution systems have basically the same purpose: moving power. This is done with the use of long wires made out of a conducting material, copper or aluminum. Transmission systems move much larger amounts of power than distribution systems. They use large, long, wires that are energized to high voltages in order to minimize the energy lost as heat. Distribution systems use shorter wires that are energized to lower voltages for moving power smaller distances, usually within a city or a town.

Finally, after the energy has been converted to electricity and moved from power plants to loads, it can be converted into work by customers' devices. Those devices may be anything from very large motors at industrial facilities to toasters and lights in homes. Figure 1.1 shows a good visualization of the entire electric power grid.

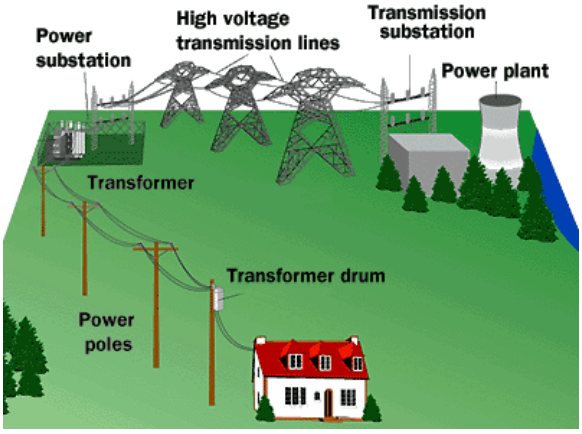

Figure 1.1 The Electric Power Grid [3]

1.2 Wind Energy

Throughout the history of the power grid in the United States, the generation sector has been dominated by fossil fuel power plants. Among the different types of fossil fuel plants, coal plants are the most prevalent, making up 54% of power generation in the United States [4]. When fossil fuels such as coal are burned, they release toxic gases such as CO_2, NO_x, SO_x, and others into the atmosphere. Due in large part to a desire to decrease those emissions, wind energy has experienced very high growth in the last 10 years. Between 2001 and 2011, over 41,000 MW of wind power was installed in the United States, bringing the total installed capacity to 46,919 MW [5]. The recent enthusiasm for wind power is evidenced by the various goals set for it in the coming years. The U.S Department of Energy has a goal of 20% of our power coming from wind by 2030 [6]. President Obama stated in his 2011 State of the Union Address that his goal is for 80% of our energy to come from renewable sources, not just wind, by 2035 [7]. Even though a large amount of wind energy capacity has been installed recently, there are still some major barriers to achieving a high penetration of wind in our county's energy portfolio.

One major drawback of wind energy is that it is inherently variable. Using historical data, the average wind speed in a particular area can be determined, but it is impossible to predict exactly how fast the wind will blow in a given location on a given day. Wind forecasts help, but as anyone who has left their umbrella at home at the local meteorologist's advice, and then gotten soaked by rain can attest, weather forecasts are not always accurate. Wind turbines are reduced to mere decorations on the horizon if the wind is not blowing. Meanwhile a "conventional" generation asset such as a coal or nuclear plant can produce power independently from Mother Nature. A fossil fuel plant can be dispatched, or scheduled, to produce a certain amount of power at a certain time to match the expected load at that time, but a wind turbine cannot. A robust and wide-area transmission system can help with this issue, and multi-MW energy storage could probably solve it, but neither of those is the subject of this thesis. The models and ideas presented here will help engineers design wind turbines better, making them more reliable and cost effective over their lifespans.

1.3 Modern Wind Turbine Operation

There are many different types of wind turbines. The precursors to today's multi-megawatt behemoths were simple drag machines. They were incapable of spinning faster than the wind was blowing and they were mainly used to pump water. The windmills that dot the Kansas plains are predominately drag machines. Modern wind turbines, on the other hand, are lift machines. The blades are aerodynamically designed to achieve lift when the wind hits them. Modern wind turbine blades are essentially highly engineered wings attached to a hub. The lift they achieve allows them to spin faster than the wind is blowing, greatly increasing the amount of power they can capture from the wind. From the 1970's, when utility scale wind turbines started to gain popularity, through the 1990's, the generators used in wind turbines were almost exclusively induction machines. Induction machines were attractive for wind turbines due to their relatively low cost and rugged construction. However, the speed at which an induction machine must rotate in order to be most efficient is significantly higher than that at which utility scale wind turbines spin. That fact necessitated a gearbox in those machines. Gearboxes are still used today in turbines that use doubly fed induction generators (DFIGs). Gearboxes have proven to be a prime source of failures in modern wind turbines [8]. A different type of generator, a synchronous machine excited by permanent magnets instead of a field winding, can eliminate the need for a gearbox. Permanent-magnet synchronous generators (PMSGs) can be designed to operate at low speeds with high torque, thereby achieving efficient operation at lower speeds than induction machines [9]. Lower speed operation eliminates the need for the gearbox. Wind turbines without a gearbox are called "direct-drive."

The focus of this thesis is exclusively on permanent-magnet direct-drive (PMDD) wind turbines, but the basic physics behind how all variable speed wind turbines extract power from the wind is the same. The equation for the power captured by a horizontal axis wind turbine is:

$$P = \frac{1}{2}\rho C_p A_s U^3, \tag{1.4}$$

where ρ is the air density, A_s is the swept area of the blades, U is the wind speed, and C_p is the coefficient of performance. The theoretical limit, called the Betz limit, of C_p is 16/27 (approximately 0.59) [10, p. 61]. From (1.4) it is clear that the higher the C_p, the more power a

turbine will produce for a given wind speed. This project began as a collaboration with some colleagues in the Department of Mechanical and Nuclear Engineering at Kansas State University, whose work entails maximizing C_p - a highly nonlinear control problem. C_p is a function of both tip speed ratio (λ) and blade pitch (β). Figure 1.2 shows a graphical representation of an example C_p function.

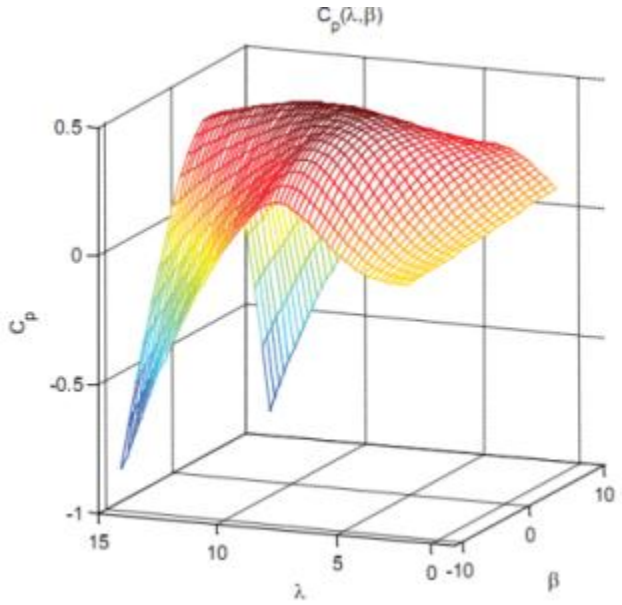

Figure 1.2 C_p plot [11]

Tip speed ratio (TSR) is defined as the ratio of the speed of a turbine's blade tip to the wind speed [10, p. 60]. In equation form:

$$\lambda \triangleq \frac{\omega R}{U}, \tag{1.5}$$

where ω is the angular velocity of the rotor, R is the radius of the rotor, and U is the wind speed. In a direct drive wind turbine, ω is the same as the angular velocity of the generator shaft. Because a control system cannot affect the blade length or the wind speed, ω is what must be controlled in order to change TSR, which must be controlled to maximize C_p. Controlling the speed of a PMSG will allow our collaborators' controller to adjust TSR in order to maximize C_p.

For a direct drive wind turbine, the angular velocity of the rotor and the frequency of the generated power are related by:

$$f = \frac{\omega p}{2\pi}. \tag{1.6}$$

In (1.6), p is the number of generator pole pairs, and ω is still the angular velocity of the rotor. In order to be connected to the grid, a generator must have a frequency of almost exactly 60 Hz at all times. Because ω will vary, sometimes wildly, with the wind in order to maximize C_p, some sort of interface must be used to ensure the frequency of the power injected to the grid is always 60 Hz. That interface is called a "full converter" or a "back-to-back converter". It is generally made up of two or three pieces of power electronic equipment: a rectifier (AC/DC converter), sometimes a chopper (DC/DC converter), and an inverter (DC/AC converter). A schematic for a direct-drive wind turbine with a full converter is shown in Figure 1.3.

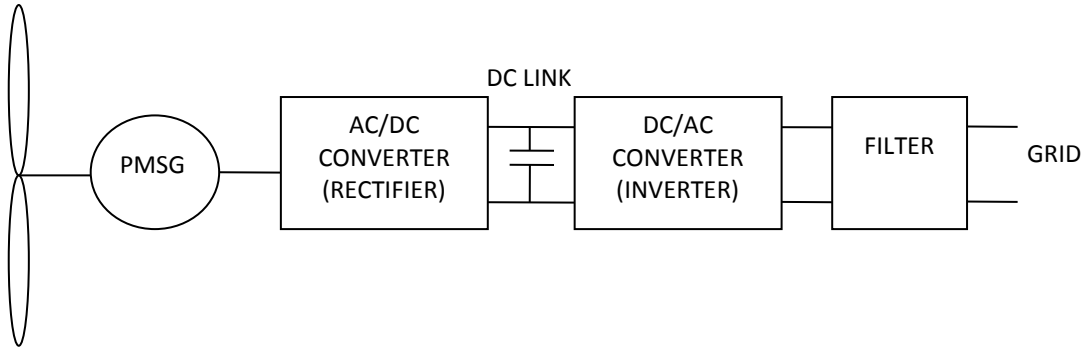

Figure 1.3 Full Converter

Much research continues to be done on the design of the various parts of full converters [12] [13] [14]. A major focus of this thesis is the control system design for both an active rectifier and a grid-tied inverter that together make up a full converter. That converter model can then be used in conjunction with a model for a permanent-magnet synchronous generator and the FAST aeroelastic wind turbine simulator developed by the National Renewable Energy Laboratory (NREL) to perform detailed simulations of direct-drive wind turbines. Those simulations can have many different uses, including studying the interaction of the electrical and mechanical parts of the turbine and designing control systems to maximize the power extracted from it.

Chapter 2 - FAST Aeroelastic Simulations and Literature Review of Electromechanical FAST Simulations

The motivation behind computer simulations of wind turbines is obvious: wind turbines are large, expensive machines. It would be prohibitively costly and dangerous to test new ideas on real wind turbines. However, even a modest PC can simulate various parts of them. Simulations aid in design and testing of many aspects of wind turbines, including the control systems and power electronics that are the subject of this thesis. Of course, there is no way to make a perfect simulator, and there is no substitute for field testing before a product is deployed, but modern wind turbine simulators are powerful and can accurately simulate many different variables. This chapter provides background on the wind turbine simulator used in this thesis: FAST. It also provides a review of the published literature on FAST simulations involving both mechanical and electrical components, henceforth called electromechanical simulations.

2.1. NREL CAE Tools

FAST is an aeroelastic simulator, developed by Jonkman, Buhl, and others at the NREL in Boulder, Colorado, designed to predict loads on horizontal-axis wind turbines (HAWT's) [15]. It is part of a set of modular, open-source, computer-aided engineering (CAE) tools distributed by NREL. Four such tools are used in this thesis: Modes, TurbSim, AeroDyn, and FAST. Modes is used to find the mode shapes of towers and blades, which are then used by AeroDyn and FAST. TurbSim is used to generate turbulent wind data sets, AeroDyn does aerodynamic calculations, and FAST uses those calculations to calculate many different loads on a HAWT. A brief summary of each tool is presented in the next four subsections.

2.1.1 Modes

FAST considers the blade and tower to be flexible elements modeled by a linear modal representation, so mode shapes must be included in the input file. For the benefit of us non-mechanical engineers, a mode shape is basically the direction a body takes as it vibrates. An example of tower mode shapes is shown in Figure 2.1.

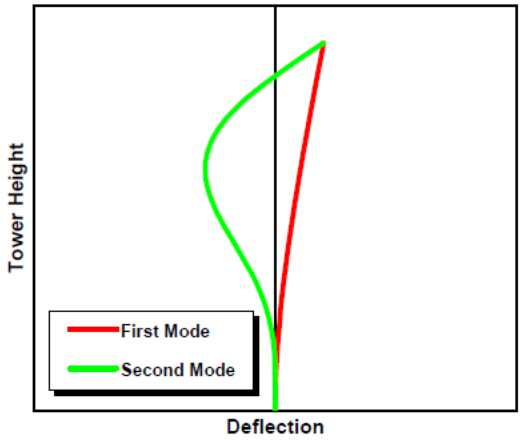

Figure 2.1 Exemplar Tower Mode Shapes [15]

Both the tower and the blades must also have mode shapes defined in the input file. The Modes code is based on Hassan's GH Bladed code; it was modernized by Buhl in 2000 [16]. Modes takes information about the tower and the mass of the nacelle and rotor and finds the mode shapes and natural frequencies of the system. For this thesis, Modes was used to find the mode shapes of the tower used for the 10 kW system, which is described in Section 2.2.1.

2.1.2 TurbSim

TurbSim uses stochastic models to simulate turbulent wind [17]. It simulates "time series of three-component wind-speed vectors at points in a two-dimensional vertical rectangular grid that is fixed in space [17]." This is more clearly understood with the help of Figure 2.2, which shows how this idea works with a wind turbine.

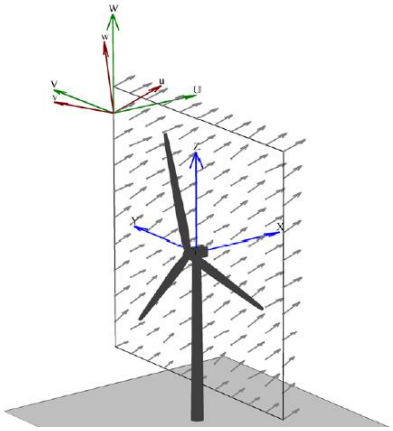

Figure 2.2 TurbSim Wind Field Visualization [17]

TurbSim output files can be used as AeroDyn input files. AeroDyn, discussed below, is a code that is used in conjunction with an aeroelastic simulator, such as FAST, to "predict the aerodynamics of HAWT's [18]." When used with AeroDyn, a TurbSim-generated wind file consists of many fields of wind, such as the one in Figure 2.2, that are "marched through" the wind turbine in time. This process is visualized in Figure 2.3.

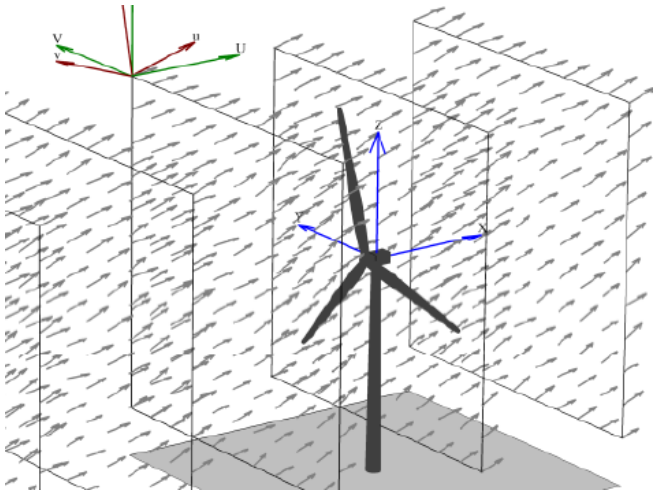

Figure 2.3 TurbSim Wind Data Used with AeroDyn [17]

This means that very complicated sets of turbulent, high-resolution wind data can be generated by TurbSim and used in FAST simulations. Such data sets would be very difficult to obtain from conventional wind monitoring systems.

2.1.3 AeroDyn

As previously mentioned, AeroDyn does HAWT aerodynamics. It is meant to be used with an aeroelastic simulator such as FAST or ADAMS® (henceforth written as ADAMS). When prompted by such a simulator, "AeroDyn calculates the aerodynamic lift, drag, and pitching moment of airfoil sections along the wind turbine blades [18]." An AeroDyn input file specifies discrete segments of the blade along the span [18]. AeroDyn uses information from input files on turbine geometry, as well as data from the aeroelastic simulator such as operating condition, blade-element velocity and location, and wind inflow, to calculate forces for each blade segment [18]. It uses both blade element momentum (BEM) theory and generalized dynamic wake theory for calculating the effects of turbine wake [18]. AeroDyn also includes the capability to consider

dynamic stall and tower shadow. Much more on the theory behind AeroDyn can be found in the AeroDyn Theory Guide by Moriarty and Hansen [18].

Wind input files for AeroDyn can be generated using TurbSim, but they do not have to be. A hub height wind input file consists of time series of wind speed, direction, vertical speed, horizontal speed, horizontal shear, vertical shear, linear vertical shear, and gust speed [19]. This allows for quite a bit of flexibility in wind input. One can collect real wind data, correct for hub height using the power law, or something similar, and use it in AeroDyn. Many simulations were run using constant wind velocities in the design process for the controllers in this thesis. Figure 2.4 shows an example of the total wind speed used by AeroDyn using a wind file from TurbSim, and Figure 2.5 shows the same for a hub height wind file with some arbitrary gusts.

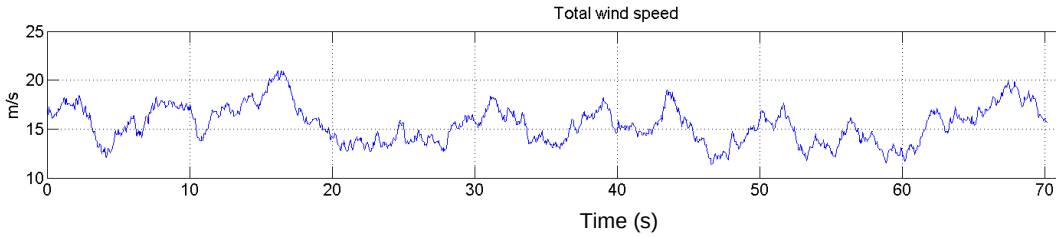

Figure 2.4 Total Wind Speed Used by AeroDyn from a TurbSim Wind File

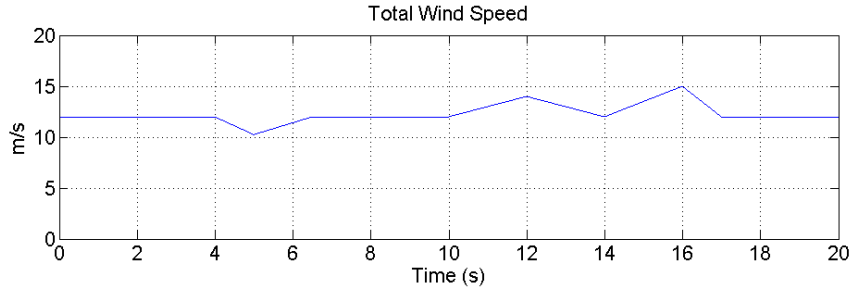

Figure 2.5 Total Wind Speed Used by AeroDyn for an Arbitrary Hub Height Wind File

2.1.4 FAST

At one time, FAST was an acronym for Fatigue, Aerodynamics, Structures, and Turbulence, but it is known simply as FAST today. FAST is a publicly available aeroelastic simulator for two or three-bladed HAWTs. Aeroelastic basically means it simulates the interactions of aerodynamic forces (wind) with mechanical bodies (tower, nacelle, rotor, etc). FAST, in its present form, had

its genesis in 2002 from the combination of two different codes for modeling two and three-bladed wind turbines [15]. FAST is often compared to, and verified against, a commercial program called ADAMS that can be used to simulate wind turbines. In fact, FAST can be used to generate data for use in ADAMS simulations. FAST and ADAMS, along with AeroDyn, were determined suitable for "the calculation of onshore wind turbine loads for design and certification [20]". There are over 1,000 possible output variables from a FAST simulation, including wind motions, motions of each blade, teeter motions, shaft motions, nacelle motions, yaw motions, local tower motions, and others [15]. FAST is written in FORTRAN 90, but a dynamic linked library (DLL) is available so that FAST may be used in MATLAB® Simulink® (henceforth written as MATLAB and Simulink) simulations as an S-function block. Without this functionality, this thesis would not be possible, as all of the electrical components and control systems used are part of a Simulink toolbox. FAST is complicated software and it is outside the scope of this thesis to completely explain how it works. Instead, a brief overview of the theory behind the software and how to use it as part of Simulink simulations will be provided.

FAST has twenty four degrees of freedom (DOF) for a three-bladed wind turbine (only three-bladed turbines are used in this thesis) [15]. Twenty two of the twenty four DOF are illustrated nicely in Figure 2.6. The two not shown are rotor-furl hinge and tail-furl hinge. The six DOF for the platform are used for offshore turbine simulations.

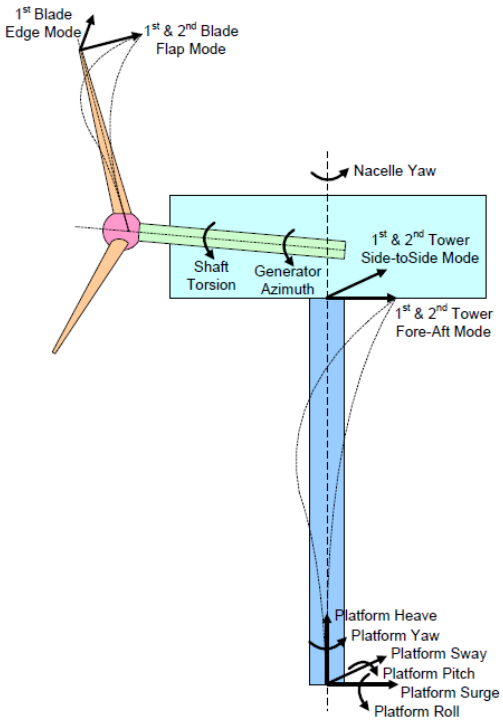

Figure 2.6 FAST Degrees of Freedom [21]

FAST uses both multi-body and modal dynamics in its formulation [15]. The resulting nonlinear equations of motion are ordinary differential equations (ODE's) and they are solved using the 4th order Adams-Bashforth-Adams-Moulton (ABAM) predictor-corrector fixed-step-size explicit integration scheme [21]. The platform motions assume small angles but all other DOF motions may be large and accuracy is retained [21]. FAST uses several different coordinate systems for different DOF, all of which may be found in the FAST User's Guide [15].

The drivetrain model is an equivalent shaft between the generator and the hub with an optional linear torsion spring and damper [15].

There are several options in FAST for generators, ranging from simple induction generator to user-defined models. The generator model in this thesis is a user-defined model from Simulink. The Simulink generator model calculates the generator torque and passes it to FAST for use in calculations at every time step.

The nacelle yaw DOF can be used to specify whether or not the turbine is allowed to yaw. If it is allowed to passively yaw, constants can be set to govern the dynamics of yawing. Active yaw, which is used in utility-scale turbines, can be simulated as well using a yaw control scheme defined in a separate input file or in Simulink [15]. FAST also includes both rotor furling and tail furling (for turbines with a tail) effects.

FAST has the option of simulating active pitch control, which is used on large turbines to regulate the power captured by the wind. A pitch control system can be implemented in Simulink much in the same way that a yaw controller can. FAST does not include the dynamics of blade pitch actuators.

2.2 FAST Wind Turbine Models

Two different wind turbines were considered for this thesis. Both are permanent-magnet direct-drive (PMDD) systems. The first is a 10 kW system based heavily on the Bergey Excel 10 machine. The second is a 5 MW system based on the fictional NREL 5 MW turbine. Systems of such different sizes were chosen intentionally so that the final products would be one testbed representative of small wind turbines and one representative of large turbines. Following is a short summary of the FAST models for each machine. The electrical models are presented in later chapters.

2.2.1 10 kW Wind Turbine

The FAST model used for the 10 kW system is based on the Small Wind Research Turbine (SWRT) provided by NREL. The SWRT is a real turbine tested at the National Wind Test Center (NWTC) in Boulder, Colorado in 2005. It was still installed at the NWTC as of this author's visit in March 2012. The SWRT is a modified Bergey Excel 10 kW turbine [22]. It is an upwind, 3-bladed turbine that furls horizontally out of the wind. It has a tail boom that is designed to furl the turbine when the rotor moment becomes greater than the gravity restoring moment of the tail [22]. The rotor diameter is 5.6 m so the swept area is 26.4 m^2. It has a cut-in wind speed of 3.1 m/s and no cut-out wind speed. The rotor is designed to spin between 0 – 400 rpm. Figure 2.7 shows the SWRT installed at the NWTC. Some of the extra instrumentation installed by NWTC personnel for research purposes is clearly seen in Figure 2.7. The Bergy Excel 10kW has

received several upgrades since it was used as the basis for the SWRT. The most notable upgrades are the increased rotor diameter from 5.8 m to 7 m and a new generator with ferrous magnets rather than neodymium ones. Both of these changes have been incorporated into the models used in this thesis.

Figure 2.7 Small Wind Research Turbine at the National Wind Technology Center [22]

The SWRT was mounted on a 34.5 m tower at the NWTC, but the FAST model distributed by NREL does not have real mode shapes for the tower. However, Jonkman and others published a detailed characterization of an 11.5 m tower used in their research on the UAE wind turbine [23]. Data from their report was used with the Modes code described in Section 2.1.1 to find mode shapes for the tower with the SWRT mounted on top of it. Those mode shapes come in the form of 6^{th}-order polynomials. The first two coefficients of the polynomials are always zero because the tower is considered cantilevered at its base so the mode shapes' deflection and slope must be zero [15]. The mode shapes found are given in Table 1. A plot of the normalized mode shapes is shown in Figure 2.8.

Table 1 UAE Tower Mode Shapes

	Mode 1	Mode 2

Frequency (Hz)	3.1267	17.0941
x^2	1.2789	-9.4878
x^3	-2.5586	-4.2045
x^4	6.8578	43.4360
x^5	-6.8267	-38.1498
x^6	2.2486	9.4062

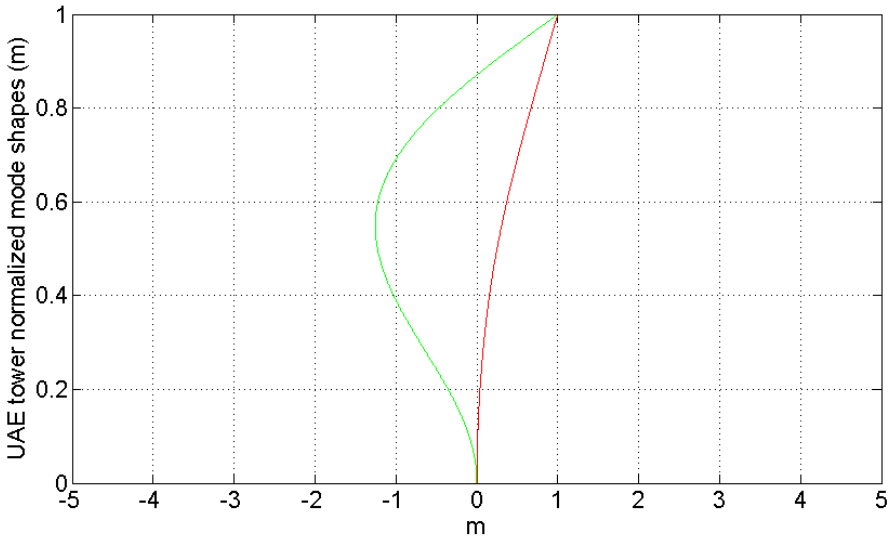

Figure 2.8 Normalized UAE Tower Mode Shapes

Sixteen of the possible 24 DOF in FAST are used when simulating the 10 kW system. They are: two longitudinal modes and two lateral modes of the tower displacement, nacelle yawing angle, and generator azimuth angle; flapwise tip motions of the first and second modes of each blade; edgewise tip displacement of each blade; and tail furl. The platform DOF are used for simulations of offshore wind turbines, so they were excluded from the simulations in this thesis. The torsion stiffness and damping DOF are not used in the simulation of the 10 kW system because its blades are bolted directly to the generator [24]. Rotor furl was neglected because tail furl dominates for this turbine.

2.2.2 5 MW Wind Turbine

The 5 MW system in this thesis is based almost exclusively on the NREL 5 MW model. The NREL 5 MW turbine is fictional, but is based heavily on the Repower 5M turbine. Though intended for use in simulations of offshore simulations, it is perfectly valid to use the model for onshore simulations, as was done for this thesis. The turbine model has an 87.6 m tower, 63 m blades, and a rated speed of 12.1 RPM at 11.4 m/s wind. Details on the model can be found in [25].

The only change made to the model was the insertion of the electrical system models described below. The model's creators intended for the turbine to use a DFIG. The insertion of a PMSG into the turbine would most likely change some mechanical and aerodynamic properties of the system, including mass and inertia values. Those changes were neglected in this thesis; the system is assumed to have exactly the same mechanical properties as if it had a DFIG. This means that mechanical outputs of the simulation are most likely wrong. Someone wishing to use the model in this thesis for a true electromechanical simulation would need to correct the necessary values to reflect the inclusion of the PMSG. However, because the blades need not change when a PMSG is used, the aerodynamic results are still valid. As shown in Chapter 11, the model produces a realistic power curve, as well as realistic results for the effects of blade pitching. Therefore, the model presented in this thesis could still be used to design blade pitch and maximum power capture controllers.

2.3 Review of Literature on Electromechanical FAST Simulations

One of the main goals of this thesis is to document the creation of the most comprehensive electromechanical FAST models to date. Therefore it is appropriate to review the current state of electromechanical FAST simulations.

Fadaeinedjad et. al used FAST to simulate a wind turbine with a fixed-speed induction generator in studying power quality in a wind-diesel system [26]. They also used FAST to study the power quality of an entire wind farm composed of fixed-speed induction generators [27]. They continued to model a fixed-speed induction generator in their FAST simulations examining how mechanical dynamics of wind turbines affect flicker [28].

Fadaeinedjad et. al successfully completed electromechanical simulations in FAST using a DFIG, which uses a gearbox [29] [30]. Their DFIG model was implemented in Simulink and it did not include power converter switching dynamics. They designed their grid-side controller to output a certain amount of power depending on the rotor speed according to a pre-defined curve. They used both generator torque control and blade pitch control in their power tracking scheme. Their model was then used to explore the mechanical problems caused by electrical disturbances such as voltage sag caused by faults. Boukhezzar and Siguerdidjane also used a DFIG in FAST simulations to design a maximum power capture control scheme [31] [32]. They assumed that all electrical systems in the turbine are "well controlled" so they did not consider generator or converter control in their work. Beltran et. al simulated a DFIG as part of FAST simulations as part of the design of sliding-mode controllers for maximum power capture [33] [34] [35]. They also used their models to test the grid fault tolerance of their system [35]. Their published work states that they implemented electrical systems in Simulink but no converter design, dynamics, or control were presented so it is impossible to say how detailed their models were. Xing-Jia et. al used a very basic DFIG model to design a maximum power capture scheme for a 650 kW two-bladed turbine and they conducted their simulations in FAST [36]. Frost et. al used FAST simulations of the same 650 kW turbine with a simple induction generator model in their work developing an adaptive control scheme for speed control [37].

Corbus and Meadors performed detailed modeling of the SWRT in FAST as part of their efforts to validate FAST to experimental results [22]. Their generator model was simply a torque-speed curve and they did not model the power electronic converters. Gong and Qiao modeled a 10 kW PMDD turbine in FAST as part of their effort to detect faults from observing generator currents [38]. They did not model any of the power electronics, however, as it was not necessary for their investigations. Bywater, et. al used FAST to calculate aerodynamic and mechanical loads as part of the WindPACT drive train study conducted at NREL [39]. Though they did not model electrical components as part of FAST simulations, they used FAST results as a consideration in evaluating different drive train options. Zhang et. al modeled a 1.5 MW PMDD machine in FAST for testing a control design [40]. The basis for their model came from Bywater et. al's

work at NREL. They modeled only the PMSG torque equation and did not present models or controllers for the converters.

Deliverables of this thesis project are models of two direct-drive permanent-magnet wind turbines: a 10 kW machine and a 5 MW machine. The models will use FAST and AeroDyn for aerodynamic and mechanical simulations, with detailed models for the active rectifier, DC link capacitor, 3-phase inverter, filter, and transformer integrated directly into the simulations. Complete feedback control systems for the rectifier and inverter will be included in the simulations as well. Simulations completed with the models take an unprecedented amount of dynamics into account. For instance, previous work on torque control in the research listed above assumed that the dynamics of the converters were fast compared to all other dynamics, so they were not modeled. Many assumed current setpoints were realized instantly. In this thesis, the dynamics of the converters and their control systems are taken into account. Instead of desired currents appearing instantaneously, a control system is tasked with realizing them by actual switching of the power electronic converter model. Simulations of this magnitude are very computationally expensive, but they provide a more realistic picture of what goes on in a real wind turbine than previous simulations have. They also offer opportunities for experiments that were not possible before.

Chapter 3 - Generators

A large amount of literature exists that details the design and operation of permanent-magnet synchronous machines (PMSMs), mostly focusing on their use as motors. But the equations are the same for motor and generator operation. Some of the best PMSM theory can be found in [41] and [42]. This chapter begins with fundamentals that apply to all electric motors/generators, and then narrows to explore only permanent-magnet synchronous machines.

3.1 Fundamental Energy Conversion Theory

3.1.1 Faraday's Law and Lenz's Law

Arguably the most basic equation of energy conversion, Faraday's law, was presented in Chapter 1 as the basis for how a generator works. It is repeated, in a slightly different form, as [41],

$$e_{ind}(t) = -\frac{d\lambda}{dt} = -N\frac{d\varphi}{dt}. \tag{3.1}$$

Equation (3.1) tells us that a coiled conductor in the presence of a changing magnetic field will have an induced voltage. λ is the flux linkage of the coil, and it is defined as the flux linkage of a single turn (φ), multiplied by the number of turns in the coil, or:

$$\lambda = N \cdot \varphi. \tag{3.2}$$

Understanding flux linkage is essential to understanding how electric machines work, but it is often assumed in the literature that the reader already knows what flux linkage is. This can lead to considerable confusion depending on how well the reader remembers his or her undergraduate Physics II class. Therefore, some discussion of flux linkage is in order.

Starting with a magnetic field of intensity H, magnetic flux density is defined as B=μH, where μ is magnetic permeability. Then, the total flux crossing some cross sectional area, A, is defined as flux linkage:

$$\lambda = \int_A B dA. \tag{3.3}$$

The cross sectional area may be that of a single wire or of a coil of wire, for example. If the subject is a coil of wire (a winding), and if the winding encloses (links) the total flux, then the total flux links each turn of the winding. Flux linkage has units of webers (Wb) or volt.seconds (V.s). From the units alone, one could deduce that the time derivative of flux linkage is voltage. Another somewhat intuitive way to think of flux linkage is in terms of inductance. Inductance and flux linkage are related by [43, p. 51]

$$\lambda = L \cdot i. \tag{3.4}$$

Although there is a negative sign in (3.1), it is somewhat arbitrary. The polarity of the induced voltage is really determined by Lenz's law. Lenz's law says that when a voltage is induced according to Faraday's law, its polarity will be such that if a resistance were connected to the voltage, a current would flow in such a direction as to produce a flux to oppose the change in flux linkage that induced the voltage. A fair question to ask would then be how does one know what flux is produced by a given current? The answer is given by Lenz's law and one of the venerable "right hand rules" of electromagnetism. This particular right hand rule says that if a person coils his fingers (on their right hand of course) in the direction of current flow, his thumb will point in the direction of the flux produced by that current [41].

The classic demonstration of Faraday's law and Lenz's law using a rod, a magnetic field, and a conductor is repeated here, as it illustrates the simplest possible generator. This thought experiment is described very well in [41], and the discussion here borrows heavily from it.

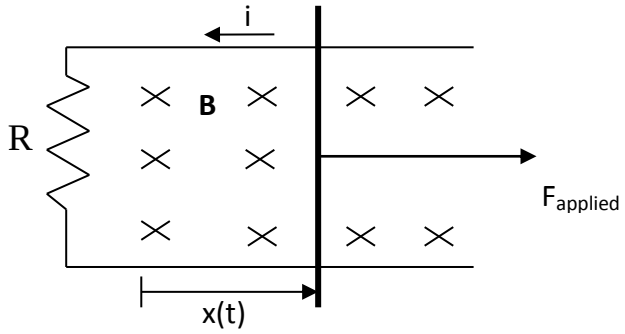

Figure 3.1 Linear Generator

The dark vertical line in Figure 3.1 represents a conductor that is free to move. It is in contact with the two lighter horizontal lines, which are fixed conductors. R is the lumped equivalent resistance of all of the conductors, and it must be present in order for current to flow. The magnetic flux density, **B**, has some arbitrary magnitude, and is directed into the page as denoted by "x" in Figure 3.1. **B** is static (unchanging). When a force is applied to the conductor, it moves, and the amount of flux "contained" within the conductive loop changes. A voltage is induced according to Faraday's law, whose magnitude is proportional to the time rate of change in flux within the loop. Because **B** is static, the magnitude of the voltage is related to the speed at which the conductor moves. The current that flows must produce **B'** to oppose the increase in total flux. Because **B** is directed into the page, and the conductor is moving to the right to increase the enclosed surface area, **B'** must be out of the page and by the right hand rule, current flows counterclockwise around the loop. Using conventional current flow rules, the positive "side" of the induced voltage is that which current flows into. Figure 3.2 shows this in a circuit.

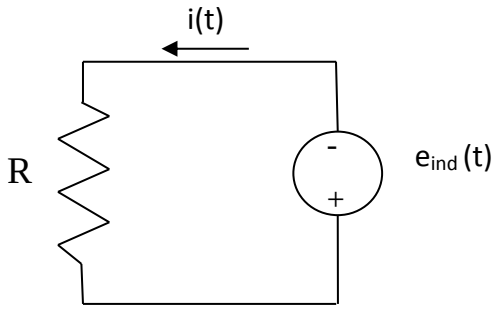

Figure 3.2 Linear Generator Equivalent Circuit

Alternately, one could switch the polarity of the voltage as well as the direction of the current flow and get the same result. Doing that is using the "motor" or "load" sign convention (as opposed to the generator sign convention), and it is used in most of the literature, so it will be used throughout this thesis. When the motor sign convention is used, the negative sign is dropped from (3.1).

Returning to the definition of Faraday's law, if B is constant, (3.3) becomes:

$$\Phi = \lambda = N \cdot \varphi = B \cdot A = B \cdot Y \cdot x(t), \tag{3.5}$$

where Y is the length of the conductor in Figure 3.1. Obviously, the area of the loop formed by the conductors changes as the conductor moves, as reflected in (3.5). Substituting (3.5) into (3.1) and dropping the negative sign gives [41]:

$$e_{ind}(t) = \frac{d\lambda}{dt} = \frac{d\big(BYx(t)\big)}{dt} = BY\frac{dx(t)}{dt}. \tag{3.6}$$

$\frac{dx(t)}{dt}$ is the definition of velocity so (3.6) can be written as [41]:

$$e_{ind}(t) = B \cdot Y \cdot v. \tag{3.7}$$

Equation (3.7) is known as the "BLv law".

Not much has been said yet about R from Figure 3.1 and Figure 3.2. It does not appear in Faraday's law, so it does not play any role in inducing voltage. However, it is an important part of Figure 3.1, as the next section explains.

3.1.2 Lorentz's Force Law

Lorentz's force law is defined as [43, p. 25]

$$\boldsymbol{F} = q \cdot \boldsymbol{v} \times \boldsymbol{B}, \tag{3.8}$$

where q is the charge of a particle and $\boldsymbol{v}$ is its velocity vector. $\boldsymbol{B}$ is the flux density vector of the magnetic field in which the charged particle is moving. Engineers usually prefer to work in terms of current (i=dq/dt) as opposed to charge. If the charged particle is swapped for a current-carrying conductor of length Y, and it is assumed that the magnetic field is uniform, (3.8) can be rewritten as [44, p. 226]

$$\boldsymbol{F} = i(\boldsymbol{Y} \text{ x } \boldsymbol{B}). \tag{3.9}$$

Equation (3.9) is usually used to help explain how motors work, as it is the simplest equation that shows a force as a result of a current. However, it is important for generators as well, as it is the basis for the generator torque.

The cross product of the length of the conductor and the flux density brings us to another right hand rule, this one attributed to Flemming [44, p. 226]. It says that, using the right hand, point the index finger in the direction of current flow along the conductor (direction of $\boldsymbol{Y}$) and the middle finger in the direction of $\boldsymbol{B}$. Then, the thumb points in the direction of $\boldsymbol{F}$. Note that if $\boldsymbol{Y}$ is perpendicular to $\boldsymbol{B}$ the cross product becomes simple multiplication. In that case, (3.9) becomes simply:

$$F = B \cdot Y \cdot i. \tag{3.10}$$

Equation (3.10) is known as the "BLi law" [41].

Consider Figure 3.1 again. Using Flemming's right hand rule, it can be deduced that there will be another force present, called $F_{counter}$, that will be applied to the conductor as a result of the current and the magnetic field it induces (**B'**). Since the flux density and the conductor are perpendicular, the magnitude of $F_{counter}$ can be found with (3.10). Figure 3.3 shows the linear generator from Figure 3.1 with $F_{counter}$ included.

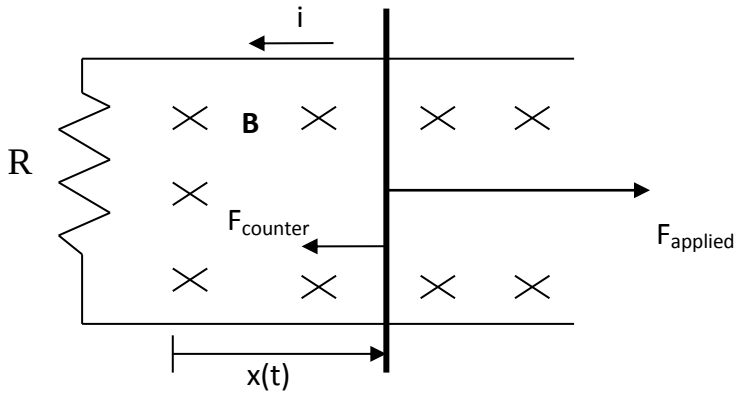

Figure 3.3 Linear Generator With Counter Force

Ohm's law then reveals the role R plays in Figure 3.1 and Figure 3.3. The value of R will influence the magnitude of i according to Ohm's law. The magnitude of i influences the magnitude of $F_{counter}$, which then determines the magnitude of $F_{applied}$ that is needed to keep the rod moving at a constant velocity in order to keep the induced voltage constant.

3.1.3 The Biot-Savart Law

For the final bit of electromagnetic theory, we'll step away from the linear generator and consider only a current-carrying conductor. Biot-Savart's law is given as [2, p. 228]:

$$\boldsymbol{B}_{induced} = \mu_0 \boldsymbol{H} = \frac{\mu_o I}{4\pi} \int_l \frac{d\boldsymbol{l} \times \hat{\boldsymbol{R}}}{R^2}. \tag{3.11}$$

Equation (3.11) gives the magnetic flux density produced by a current flowing through a conductor. $\boldsymbol{R}$ is the vector from a current element to the observer, $\boldsymbol{l}$ is the path along which the current flows, and μ_o is the permeability of free space. For the purposes of this thesis, the Biot-Savart law says that a current flowing in a conductor produces a magnetic field. The orientation of the magnetic field is found by, big surprise, a right hand rule! This one says to point the right thumb along the direction of current flow and the fingers will coil in the direction of the magnetic field. This is the basis of making a magnet with electricity: an electromagnet.

3.2 Synchronous Machine Theory of Operation

The energy conversion physics presented in the previous section is the basis of all electric machines (motors and generators). This thesis is only concerned with the control of a specific type of machine: the permanent-magnet synchronous variety. Therefore, discussion will be limited to synchronous machines. This section begins with the theory of all synchronous machines, then focuses only on PMSMs for more detailed analysis.

The key characteristic of synchronous machines is given away in their name: synchronous. Synchronous machines operating stably always spin at a constant speed. That speed, called synchronous speed, is given by:

$$n = \frac{60f}{p}, \tag{3.12}$$

where n is the rotational speed in revolutions per minute (rpm), f is the electrical frequency in Hz, and p is the number of pole pairs of the machine.

To begin the theory on how synchronous machines work, consider a conductor. Equation (3.11) shows that a current-carrying conductor produces a magnetic field. It can be shown that if the conductor is coiled, the magnetic field produced is larger for a given current [1, p. 5]. It can also be shown that if three currents of equal magnitude and 120^o phase shifts flow through a balanced (120^o physical degrees apart and equal inductance) 3-phase winding, a magnetic field with flux of constant magnitude is developed in the machine [1, p. 24]. This magnetic field rotates around the machine at the same frequency as the currents that produced it [1, p. 24]. Let the 3-phase winding be called the "stator winding," as it remains stationary during the operation of the machine.

Next, consider another winding that is attached to the shaft of the machine. Let that winding be called the "rotor winding," as it rotates when the machine operates. If that winding were to have a DC current passed through it, a stationary or "DC" magnetic field would be induced by (3.11). If this magnetic field and the one from the stator winding were formed at the same time, they would interact. Anyone who has played with bar magnets as a child knows that the type of interaction depends on the orientation of the magnets. Consider the bar magnets in Figure 3.4.

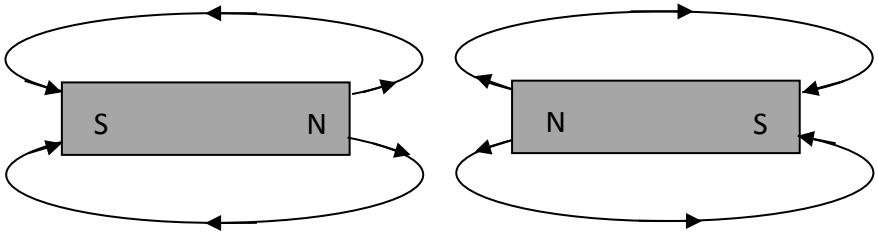

Figure 3.4 Bar Magnets Repelling

The thin lines going from the magnets' north poles to their south poles are lines of flux. Because the directions of the fluxes in Figure 3.4 are opposite, those magnets will repel. Because the lines of flux are in the same direction in Figure 3.5, those magnets will attract. Another way to put it is that opposite magnetic poles attract, or magnetic fluxes tend to align.

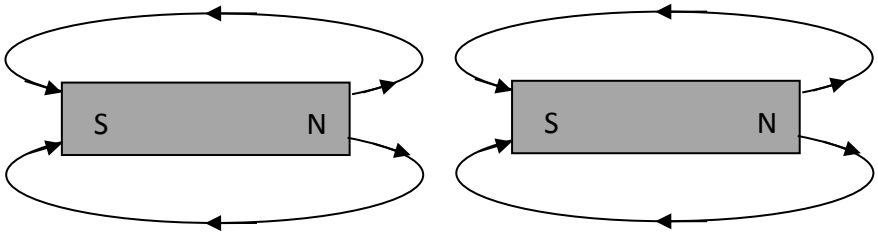

Figure 3.5 Bar Magnets Attracting

The same principle of flux alignment holds for the magnetic fields inside of a synchronous machine. Figure 3.6 shows a simple 2-pole synchronous machine. The stator, or armature, winding is not shown.

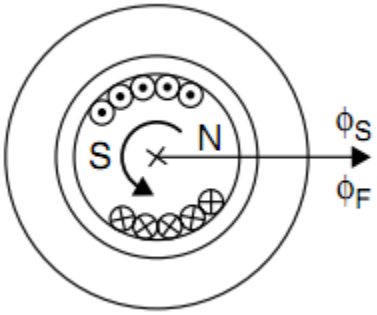

Figure 3.6 2-Pole Synchronous Machine [1, p. 26]

The "dots" and "x's" represent the rotor winding, also called the field winding. The "dots" represent current flowing out of the page and the "x's" represent current flowing into the page. By the right hand rule, if one curls his fingers in that direction, his thumb points towards the "N." The "N" and "S" represent the electromagnet formed by the field winding. From Figure 3.4, we know that flux arrows "leave" the north poles of magnets, hence the arrow pointing to the right in Figure 3.6. The current in the field winding makes ϕ_F, the flux from the field, point to the right. The ϕ_S arrow, which happens to be aligned with the ϕ_F arrow in Figure 3.6, corresponds to the flux from the stator. The simple bar magnet thought experiment shows that magnetic fields tend to align, as shown in Figure 3.6. What would happen, though, if the two fluxes were forced to be slightly misaligned? Consider the bar magnets again: if a north pole is stuck to a south pole and you pull them apart, you can feel them try and pull themselves back together. That "pulling" is the force that tries to realign the magnetic fields. When a synchronous machine acts as a

motor, ϕ_S rotates as discussed above. ϕ_F tries to stay aligned with ϕ_S, and the shaft moves in order to do so. Though the magnetic fields will not align exactly, they will rotate at exactly the same speed. One way to think of it is that ϕ_F "chases" ϕ_S around the machine, and in steady state operation, it stays exactly the same distance behind. Alternately, when a synchronous machine acts as a generator, the field electromagnet is formed as before (the field is excited) and the shaft is made to rotate by a prime mover. The prime mover may be a steam turbine, a wind turbine, or a hamster wheel; the generator does not care what makes it spin! ϕ_F then induces a voltage in each of the field windings as Faraday's law predicts. Then, if a load is connected, a current will flow. When current flows in the armature windings, ϕ_S is formed. For generator operation, ϕ_S "chases" ϕ_F around the machine. Figure 3.7 shows the single phase equivalent circuit of a synchronous machine. If the machine is balanced, the single phase equivalent is sufficient to predict the performance of the machine.

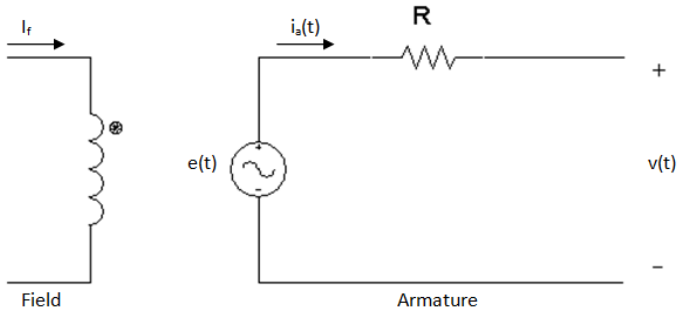

Figure 3.7 Synchronous Machine Single Phase Equivalent Circuit

R in Figure 3.7 represents the lumped resistance of the stator winding (1 phase). As previously stated, when acting as a generator, the armature develops an induced voltage according to Faraday's law. This is shown as $e(t)$ in Figure 3.7. Writing a KVL equation for Figure 3.7 gives:

$$v(t) = e(t) - i_a(t)R = \frac{d\lambda}{dt} - i_a(t)R. \tag{3.13}$$

Notice that flux linkage (λ) has turned up again in (3.13). Figure 3.7 is not the equivalent circuit normally shown for a synchronous machine. The more commonly used equivalent circuit is shown in Figure 3.8.

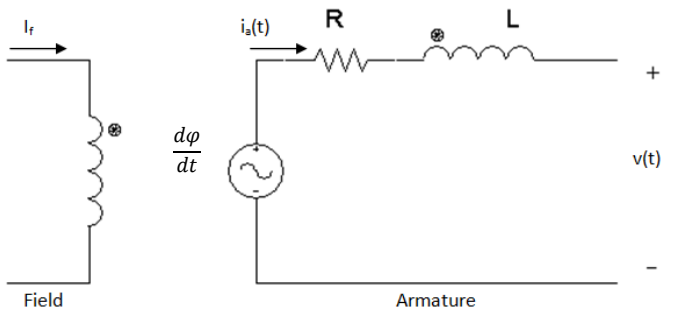

Figure 3.8 Synchronous Machine Single Phase Equivalent Circuit with Inductor

Figure 3.8 breaks the induced voltage into two different terms: one for the stator's flux linkage from the rotor (mutual flux linkage), and one for the flux linkage of the stator winding's own current (self flux linkage) [41]. Recalling (3.4) and assuming L is constant, the resulting voltage equation is:

$$v(t) = -i(t)R - L\frac{di(t)}{dt} + \frac{d\varphi}{dt}, \tag{3.14}$$

where φ is the mutual flux linkage and Li(t) is the self flux linkage. The $\frac{d\varphi}{dt}$ term in (3.14) represents the terminal voltage if there is no load attached, called the "back-emf (electromotive force)".

A designer could easily replace the "DC electromagnet" of the field winding with a permanent magnet. From a magnetic point of view, a coil excited by DC current and a permanent magnet are basically the same. The only difference is that the flux of a "DC electromagnet" can be changed by changing the field current, while that of a permanent magnet is fixed. That is, for a permanent-magnet machine, $|\varphi| = |\varphi_{PM}|$, which is constant. Though the magnitude of φ stays constant, $\frac{d\varphi}{dt}$ is non-negative because the permanent magnets rotate through space as the shaft spins.

3.3 Permanent-Magnet Synchronous Machines

3.3.1 Required characteristics

As stated in the previous section, it does not matter if ϕ_F comes from an exciter and a field winding or from a permanent magnet; it will still act like a "DC magnet." It is outside the scope of this thesis to completely classify all types of permanent-magnet machines. Rather, the goal of this section is to make clear which types of machines the controllers presented later would theoretically work for.

The first level of categorization used for this thesis is by magnetic saliency. Magnetic saliency refers to the physical path that flux must travel through a machine. A convenient way to characterize flux paths is with a parameter called "reluctance." Reluctance in a magnetic system or a magnetic circuit is akin to resistance in an electrical circuit. Reluctance is defined as [44, p. 61]:

$$Re = \frac{l}{\mu A} \ , \tag{3.15}$$

where l is the mean length of a physical flux path, A is the area of the material, and μ is the material's magnetic permeability. As stated succinctly by Mevey, "when stator and rotor slotting is ignored, a machine is non-salient if all flux paths through the center of the rotor have the same reluctance; any machine that is not non-salient is salient [41]." Another way of classifying machines according to saliency is by their method of torque production. Machines that produce torque only by the interaction of two magnetic fields (mutual torque) are non-salient machines [41]. Machines that produce torque by the interaction of a magnetic field and an element with variable reluctance (reluctance torque) and by mutual torque are salient machines [41]. The first criterion a machine must meet in order to work with the controllers presented in this thesis is it must be non-salient.

The second criterion a machine must meet is that it must have a sinusoidal back-emf. The shape of a machine's back-emf refers to its time domain expression, or the shape it would appear as on an oscilloscope. The shape of the back-emf is determined by shape of the permanent magnets

with respect to the stator coils. Consider Figure 3.9 and Figure 3.10 that show simple models of PMSMs with the two most common back-emf shapes: trapezoidal and sinusoidal.

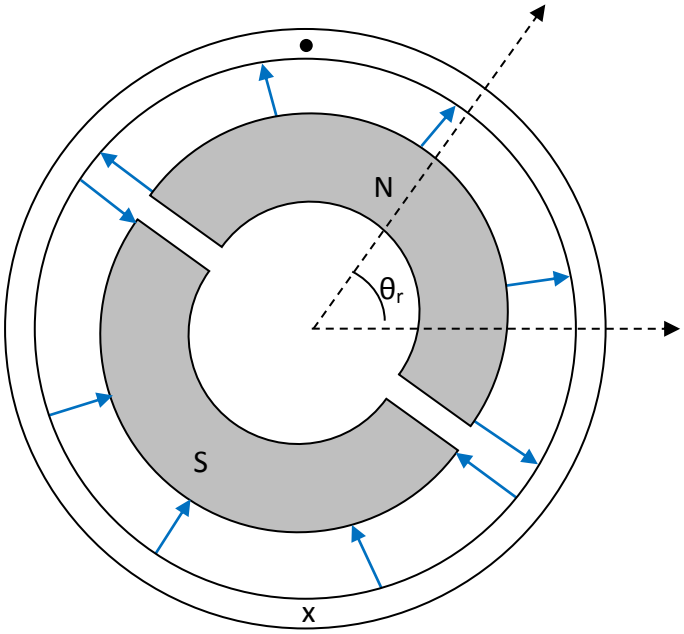

Figure 3.9 Trapezoidal PMSM

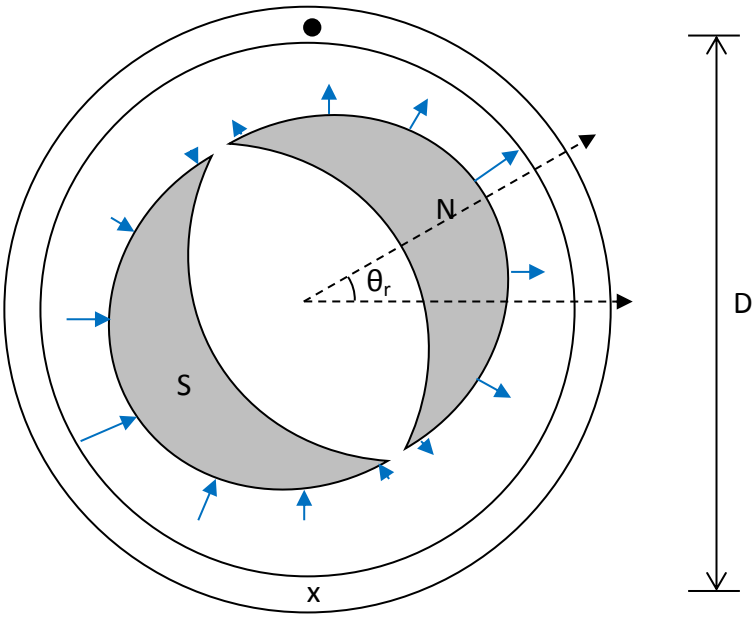

Figure 3.10 Sinusoidal PMSM

The solid arrows in the two preceding figures represent the magnetic flux density produced by the magnets. The “dot” and “x” in each figure represents a single stator winding. These figures are gross simplifications of real machines, but they serve to illustrate a couple of key points about real machines. As the magnets, which are attached to the rotor of each machine spin, the flux density seen by the stator winding changes, tracing out a pattern. Consider the flux density with respect to the “x” side of the stator coil. If arrows pointing away from the magnets represent positive flux density and arrows pointing into them represent negative flux density, the normalized flux density, B, as a function of rotor angle, θ_r, is shown in Figure 3.11 for each motor.

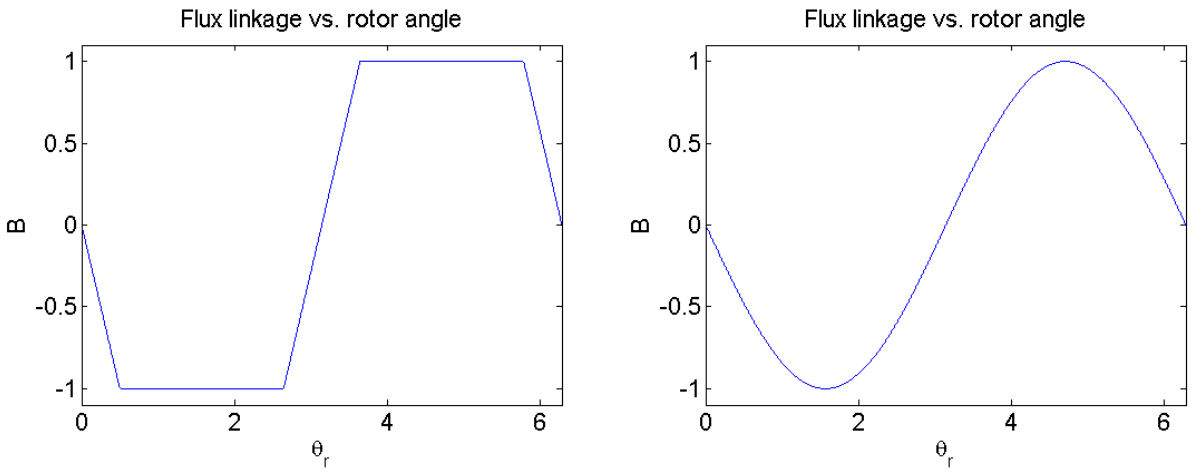

Figure 3.11 Flux Densities as Functions of Rotor Angle

The left-hand plot in Figure 3.11 is difficult to describe with a mathematical function, but the right-hand plot is clearly given by (3.16),

$$B = -B_p \sin(\theta_r). \tag{3.16}$$

Because the flux links both sides of the coil in the same direction in Figure 3.10, the induced voltage (back-emf) can be written from the BLv law as [41]:

$$e(t) = 2N \cdot B \cdot Y \cdot v. \tag{3.17}$$

Substituting (3.16) into (3.17) and changing from linear velocity to rotational velocity gives:

$$\begin{aligned} e(\theta_r) = 2N\left[-B_p \sin(\theta_r)\right] Y \left[\frac{D}{2}\omega(t)\right] &= -N \cdot D \cdot Y \cdot B_p \sin(\theta_r)\,\omega(t) \\ &= -K_e \sin(\theta_r)\,\omega(t), \end{aligned} \tag{3.18}$$

where D is the diameter of the coil as seen in Figure 3.10 and N is the number of turns it has. K_e is called the "voltage constant." The voltage constant is related to the flux established by the permanent magnets by:

$$\psi = \frac{K_e\sqrt{3}}{100\pi p}, \tag{3.19}$$

where K_e has units of $V_{peak,LL}$ / krpm. From (3.18) it is clear that if the sinusoidal PMSM operates at a constant speed, it will have a sinusoidal back-emf. It can be shown that a trapezoidal PMSM will have a trapezoidal back-emf if it spins at a constant speed. Because the

trapezoidal shape may be approximated as a square wave, a trapezoidal PMSM can use a simple square wave inverter with a DC voltage input to run as a motor. Such motors are often called "brushless DC machines," as the input signal to the motor/inverter combination is DC and the inverter eliminates the need for a mechanical commutator.

There are many different ways that a PMSM may be constructed: with magnets on the surface of the rotor or embedded in the rotor, with the rotor outside of stator or inside of it, axial flux, radial flux, etc. No matter how it is constructed, in order to work with the controller types presented in this thesis, a PMSM must be non-salient and have a sinusoidal back-emf. The reasoning behind those specifications will be made clear in later chapters. The machine model used in this thesis assumes that every machine that has a sinusoidal back-emf (also called "round rotor" machines) is non-salient.

3.3.2 Torque

To investigate torque in PMSMs, consider (3.20) and (3.21), which give the mechanical/electrical energy balance of a theoretical 3-phase, sinusoidal machine,

$$P_m = \tau\omega = e_a(t)i_a(t) + e_b(t)i_b(t) + e_c(t)i_c(t) = P_e, \tag{3.20}$$

then

$$\tau = \frac{e_a(t)}{\omega(t)}i_a(t) + \frac{e_b(t)}{\omega(t)}i_b(t) + \frac{e_c(t)}{\omega(t)}i_c(t). \tag{3.21}$$

Equation (3.18) may be rearranged as:

$$\frac{e(t)}{\omega(t)} = -K_e \sin(\theta_r). \tag{3.22}$$

If each phase winding is 120^o apart physically, then the torque functions of each phase will be displaced by 120^o as well [41]. With that in mind, substituting (3.22) into (3.21) gives:

$$\tau = -K_e \sin(\theta_r)\, i_a(t) - K_e \sin(\theta_r - 120°) i_b(t) - K_e \sin(\theta_r + 120°)\, i_c(t). \tag{3.23}$$

Using the same K_e for each term in (3.23) implies the machine is balanced. Next, consider what happens if the phase currents are sinusoidal and some arbitrary angle, γ, out of phase with the back-emf,

$$\begin{aligned}\tau = [-K_e \sin(\theta_r)] \cdot \left[-I_p \sin(\theta_r + \gamma)\right] + [-K_e \sin(\theta_r - 120°)] \\ \cdot \left[-I_p \sin(\theta_r - 120° + \gamma)\right] + [-K_e \sin(\theta_r + 120°)] \\ \cdot \left[-I_p \sin(\theta_r + 120° + \gamma)\right].\end{aligned} \tag{3.24}$$

Using the fact that:

$$\sin(x + y) = \sin(x) \cdot \cos(y) + \cos(x) \cdot \sin(y), \tag{3.25}$$

(3.24) may be simplified as:

$$\begin{aligned}\tau = K_e I_p \{&\sin(\theta_r)\,[\sin(\theta_r)\cos(\gamma) + \cos(\theta_r)\sin(\gamma)] \\ &+ \sin(\theta_r - 120°)\,[\sin(\theta_r - 120°)\ \cos(\gamma) \\ &+ \cos(\theta_r - 120°)\sin(\gamma)] \\ &+ \sin(\theta_r + 120°)\,[\sin(\theta_r + 120°)\cos(\gamma) \\ &+ \cos(\theta_r + 120°)\sin(\gamma)]\},\end{aligned} \tag{3.26}$$

and then further simplified to:

$$\begin{aligned}\tau = K_e I_p \{&\cos(\gamma)\,[\sin^2(\theta_r) + \sin^2(\theta_r - 120°) + \sin^2(\theta_r + 120°)] \\ &+ \sin(\gamma)[\sin(\theta_r)\cos(\theta_r) + \sin(\theta_r - 120°)\cos(\theta_r - 120°) \\ &+ \sin(\theta_r + 120°)\cos(\theta_r + 120°)]\}.\end{aligned} \tag{3.27}$$

Another identity is useful here:

$$\sin(x + y)\cos(x + y) = \frac{1}{2}\sin(2x + 2y). \tag{3.28}$$

Equation (3.28) can be applied to (3.27) with the result:

$$\begin{aligned}\tau = K_e I_p \Big\{&\cos(\gamma)\,[\sin^2(\theta_r) + \sin^2(\theta_r - 120°) + \sin^2(\theta_r + 120°)] \\ &+ \sin(\gamma)\left[\frac{1}{2}\sin(2\theta_r) + \frac{1}{2}\sin(2\theta_r - 240°)\right. \\ &\left.+ \frac{1}{2}\sin(2\theta_r + 240°)\ \right]\Big\}.\end{aligned} \tag{3.29}$$

A third identity,

$$\sin^2(x) = \frac{1}{2} - \frac{1}{2}\cos(2x), \tag{3.30}$$

can be used in (3.29) to obtain

$$\begin{aligned} \tau = K_e I_p \Big\{ & \cos(\gamma) \left[\frac{1}{2} - \frac{1}{2}\cos(2\theta_r) + \frac{1}{2} - \frac{1}{2}\cos(2\theta_r - 240°) + \frac{1}{2} - \frac{1}{2}\cos(2\theta_r \right. \\ & \left. + 240°) \right] \\ & + \sin(\gamma) \left[\frac{1}{2}\sin(2\theta_r) + \frac{1}{2}\sin(2\theta_r - 240°) \right. \\ & \left. + \frac{1}{2}\sin(2\theta_r + 240°) \right] \Big\}. \end{aligned} \tag{3.31}$$

It can be shown that the terms multiplying $\cos(\gamma)$ sum to 3/2 and the terms multiplying $\sin(\gamma)$ sum to 0, so (3.31) can be simplified to:

$$\tau = \frac{3}{2} K_e I_p \cos(\gamma). \tag{3.32}$$

The key takeaway from (3.32) is that if the phase currents are balanced and sinusoidal in a 3-phase machine, torque will be constant.

Chapter 4 - Reference Frame Theory

There are many different ways to control electric machines. The one used in this thesis is called "field-oriented control" (FOC) or "vector control." The vectors being controlled are called "space-vectors" (SV's), but what is a space-vector? In order to answer that question, two changes of variables are in needed, which is where reference frame theory comes in. Reference frame theory provides the means by which 3-phase quantities such as voltage and current may be expressed as a single complex number. Furthermore, that complex number can undergo another change of reference frame and become a constant value. The first change of variables is performed with the Clarke Transform, which the subject of Section 4.1.

4.1 The Clarke Transform

The Clarke Transform, named for Edith Clarke, will allow us to express 3-phase quantities as a single complex number [45]. The most straightforward way to develop the Clarke Transform is to start with a figure. Figure 4.1 shows three vectors (x_i) which represent any instantaneous quantity. It should be emphasized that these *are not phasors*. The x_i vectors are basis vectors that 3-phase quantities may be thought of as lying along. They are shown as unit vectors in Figure 4.1, but they may have any length.

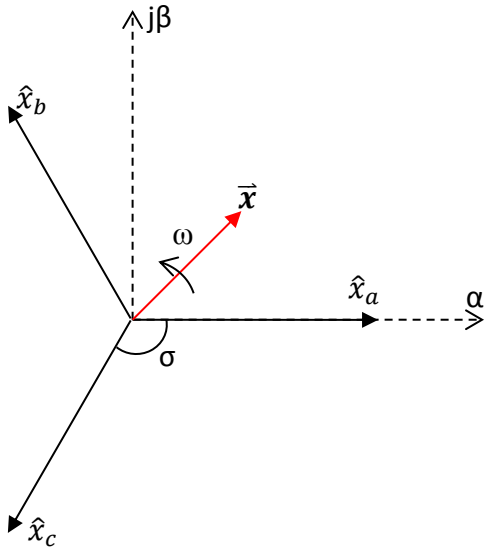

Figure 4.1 Axis system for the Clarke Transform

Figure 4.1 also shows a set of complex, orthogonal axes (αβ). The angle between each successive basis vector is the same, σ. $\vec{\boldsymbol{x}}$ may be written as:

$$\vec{\boldsymbol{x}} = x_a + x_b e^{j\sigma} + x_c e^{-j\sigma}. \tag{4.1}$$

When (4.1) is multiplied by a simple scaling factor, the definition of the complex space-vector is obtained as [46]:

$$\vec{\boldsymbol{x}} = k\left[x_a + x_b e^{j\sigma} + x_c e^{-j\sigma}\right]. \tag{4.2}$$

The need for the scaling factor will become apparent soon. From Figure 4.1, it seems reasonable that $\vec{\boldsymbol{x}}$ could also be written in terms of the orthogonal complex basis vectors (axes), α and β, which is the point of the Clarke Transform.

Let the x_{abc} vectors now be 3-phase variables in a positive sequence. They could be voltages, currents, flux densities, etc.

$$\begin{aligned} x_A &= X_m \cos(\omega t) \\ x_B &= X_m \cos(\omega t - \sigma) \\ x_C &= X_m \cos(\omega t + \sigma) \end{aligned} \tag{4.3}$$

Each term in (4.3) may be written as a sum of complex exponentials using Euler's formula [47, p. 19]:

$$\begin{aligned} x_A &= \frac{X_p}{2}\left[e^{j\omega t} + e^{-j\omega t}\right] \\ x_B &= \frac{X_p}{2}\left[e^{j(\omega t-\sigma)} + e^{-j(\omega t-\sigma)}\right] \\ x_C &= \frac{X_p}{2}\left[e^{j(\omega t+\sigma)} + e^{-j(\omega t+\sigma)}\right], \end{aligned} \tag{4.4}$$

Substituting (4.4) into (4.2) gives

$$\vec{\boldsymbol{x}} = \frac{kX_p}{2}\left[e^{j\omega t} + e^{-j\omega t} + \left(e^{j(\omega t-\sigma)} + e^{-j(\omega t-\sigma)}\right)e^{j\sigma} + \left(e^{j(\omega t+\sigma)} + e^{-j(\omega t+\sigma)}\right)e^{-j\sigma}\right]. \tag{4.5}$$

Note that $e^{j(\omega t-\sigma)} \cdot e^{j\sigma} = e^{j\omega t} \cdot e^{-j\sigma} \cdot e^{j\sigma} = e^{j\omega t}$ and $e^{j(\omega t+\sigma)} \cdot e^{-j\sigma} = e^{j\omega t}$. Therefore, (4.5) can be simplified to:

$$\begin{aligned}\vec{\boldsymbol{x}} &= \frac{kX_p}{2}\left[e^{j\omega t} + e^{-j\omega t} + e^{j\omega t} + e^{-j(\omega t-\sigma)} \cdot e^{j\sigma} + e^{j\omega t} + e^{-j(\omega t+\sigma)} \cdot e^{-j\sigma}\right] \\ &= \frac{kX_p}{2}\left[3e^{j\omega t} + e^{-j\omega t} + e^{-j(\omega t-2\sigma)} + e^{-j(\omega t+2\sigma)}\right].\end{aligned} \tag{4.6}$$

If $\sigma = \frac{2\pi}{3}$, as it would be in a balanced 3-phase power system or electric machine, (4.6) becomes:

$$\vec{\boldsymbol{x}} = \frac{3kX_p}{2}e^{j\omega t}. \tag{4.7}$$

Equation (4.7) shows that a 3-phase quantity such as voltage or current can be represented as a single complex vector (SV). In order to find the α and β components of that vector, one only needs to use $\sigma = \frac{2\pi}{3}$ in the definition of the space-vector, (4.2):

$$\begin{aligned}\vec{\boldsymbol{x}} &= k\left[x_a + x_b\left(-\frac{1}{2} + \frac{j\sqrt{3}}{2}\right) + x_c\left(-\frac{1}{2} - \frac{j\sqrt{3}}{2}\right)\right] \\ &= k\left[x_a - \frac{1}{2}x_b - \frac{1}{2}x_c + \frac{j\sqrt{3}}{2}(x_b - x_c)\right].\end{aligned} \tag{4.8}$$

When (4.8) is put into matrix form with the real and complex parts separated, the result is:

$$\begin{bmatrix} x_\alpha \\ jx_\beta \end{bmatrix} = k\begin{bmatrix} 1 & -\frac{1}{2} & -\frac{1}{2} \\ 0 & j\frac{\sqrt{3}}{2} & -j\frac{\sqrt{3}}{2} \end{bmatrix}\begin{bmatrix} x_a \\ x_b \\ x_c \end{bmatrix}. \tag{4.9}$$

For most practical applications the imaginary operator is not important, so it is left off of the transform and assumed to be implicit. From (4.7) it is clear that if $k = \frac{2}{3}$ the magnitude of the SV

will be the same as the peak value of the phase variables. When $k = \frac{2}{3}$, the Clarke Transform is said to be "magnitude invariant." The magnitude-invariant Clarke Transform is given by:

$$\begin{bmatrix} x_\alpha \\ x_\beta \end{bmatrix} = \frac{2}{3}\begin{bmatrix} 1 & -\frac{1}{2} & -\frac{1}{2} \\ 0 & \frac{\sqrt{3}}{2} & -\frac{\sqrt{3}}{2} \end{bmatrix}\begin{bmatrix} x_a \\ x_b \\ x_c \end{bmatrix} = \frac{2}{3} C \boldsymbol{x_{abc}}. \tag{4.10}$$

Equation (4.10) is the form of the Clarke Transform that is most commonly found in the literature. It is meant to be used with instantaneous values of 3-phase variables. If the variables used are positive sequence, such as (4.3), the SV will trace a counterclockwise circle around the αβ plane in time. Since the $\hat{x}_{abc}$ basis vectors correspond to the magnetic axes of a 3-phase ac machine, such as a PMSG, it is often said that performing a Clarke Transform on machine variables references those voltages to the machine's stator. That is, one can observe the variables from a stationary reference frame "attached to the stator."

Of course, the Clarke Transform would not be very useful if it was not possible to transform back into the phase variables. There are a number of ways to find the inverse Clark Transform, but using Figure 4.1 and trigonometric relationships is probably the most straightforward. Trigonometry is used to derive both the forward and inverse Clarke Transforms in Appendix A. The inverse Clark Transform is given by:

$$\begin{bmatrix} x_a \\ x_b \\ x_c \end{bmatrix} = \frac{2}{3}\begin{bmatrix} 1 & 0 \\ -\frac{1}{2} & \frac{\sqrt{3}}{2} \\ -\frac{1}{2} & -\frac{\sqrt{3}}{2} \end{bmatrix}\begin{bmatrix} x_\alpha \\ x_\beta \end{bmatrix} = \frac{2}{3} C^{-1} \boldsymbol{x_{\alpha\beta}}. \tag{4.11}$$

Conveniently, the αβ components of line-to-neutral voltage may be found using only two line-to-line voltage measurements. This is convenient for two reasons: it eliminates one voltage measurement, which decreases costs and increases reliability for the whole system, and there is usually no neutral brought outside the case of a PMSM. This particular version of the Clarke Transform is derived in Appendix A with the result:

$$\begin{bmatrix} v_\alpha \\ v_\beta \end{bmatrix} = \frac{1}{3}\begin{bmatrix} 2 & 1 \\ 0 & \sqrt{3} \end{bmatrix}\begin{bmatrix} v_{ab} \\ v_{bc} \end{bmatrix}. \tag{4.12}$$

4.2 The Park Transform

The previous section showed how a 3-phase quantity such as voltage or current may be expressed as a single complex number. Performing a Clarke Transform on machine variables is said to reference them to the stator. As made clear from (4.7), the complex space-vector rotates around the complex αβ plane at the same angular frequency (ω) as the original variable. The Park Transform places another set of basis vectors onto the αβ plane. This third set of basis vectors, after abc and αβ, are called the direct axis and quadrature axis (dq axes). The dq axes rotate around the complex plane at some frequency. If that frequency is made to be the same as the original variable, the d- and q-axis components of the variable will be constant. Performing a Park Transform allows us to find those d- and q-axis values. Since the dq axes rotate at the same frequency as the rotor for a synchronous machine, performing a Park Transform is known as changing to a reference frame attached to the rotor. To visualize how this works, consider Figure 4.2, which shows an arbitrary, positive sequence, sinusoidal, 3-phase variable.

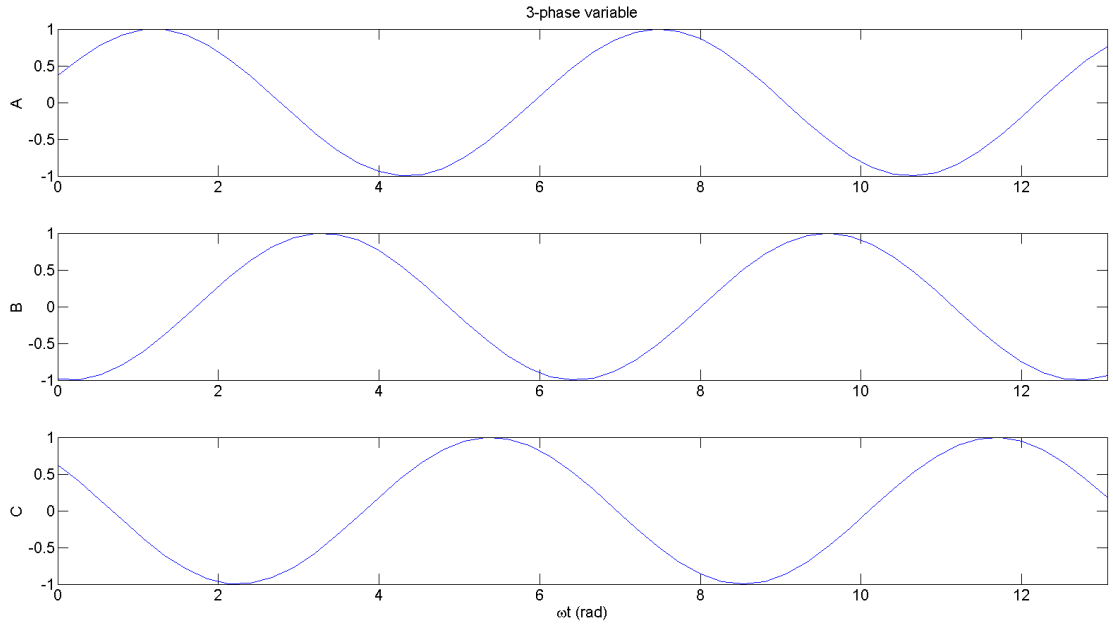

Figure 4.2 Arbitrary, Positive Sequence, 3-phase Signal

Figure 4.3 shows the Park Transform “in action.” In the top left section, the dashed vector is a space-vector that rotates counter clockwise with time. The d and q axes do the same, so that when the space-vector is decomposed into its d-axis and q-axis components, those components are constant. This is seen in a couple of different ways in the other three parts of Figure 4.3.

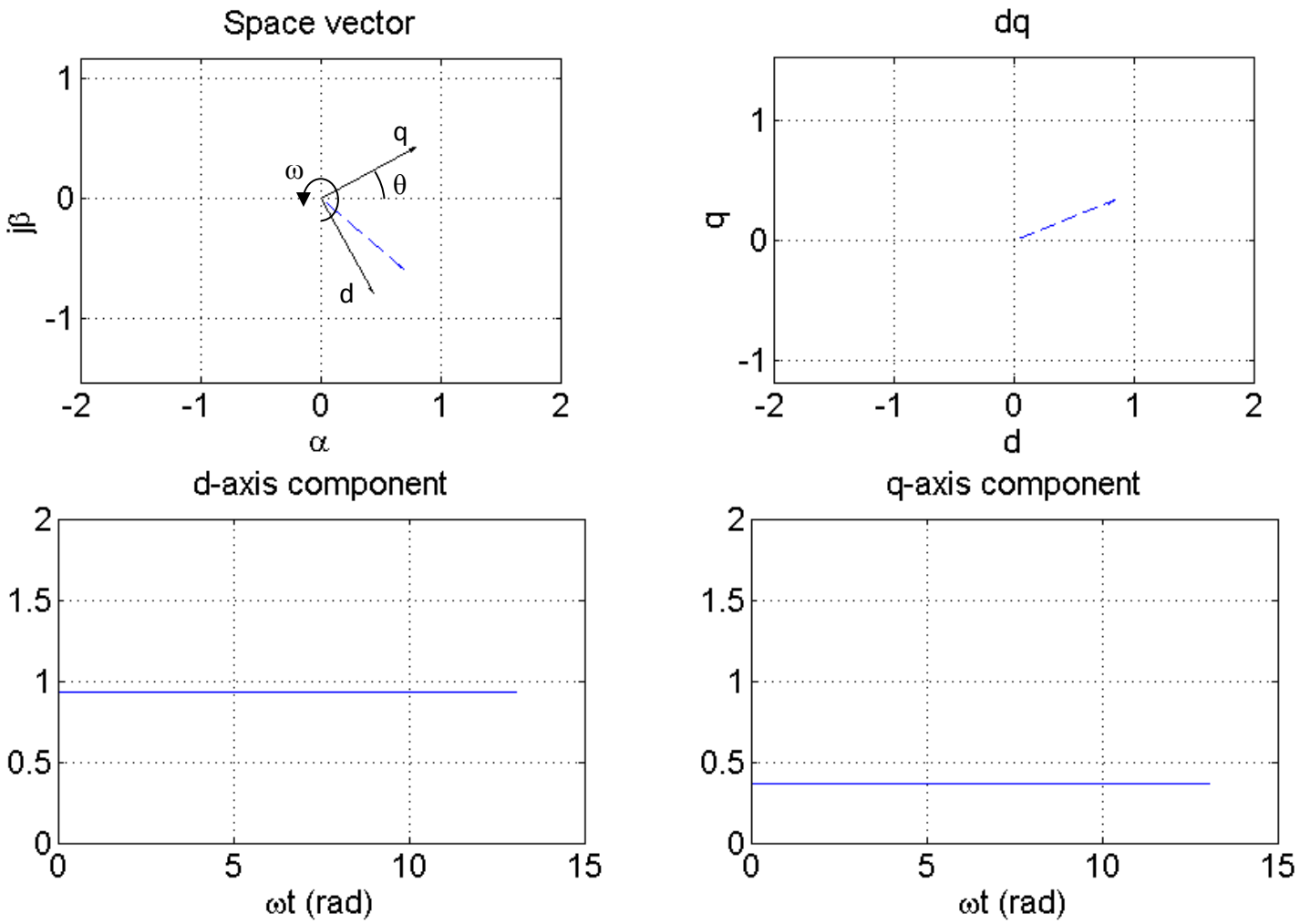

Figure 4.3 3-Phase Signal with Clarke and Park Transforms

The Park Transform is named after R.H. Park, who was the first to refer variables to the rotor reference frame in his landmark paper [48]. There are several ways to derive the transformation, one of which is to use trigonometry after referring the original variables to the stator reference frame with the Clarke Transform. Figure 4.4 shows an arbitrary space-vector decomposed into four different d-axis and q-axis components. The total q-axis component of $\vec{x}$ has a contribution from both the α and β components of $\vec{x}$; likewise for the d-axis component. Figure 4.4 shows how those components can be represented on a vector diagram.

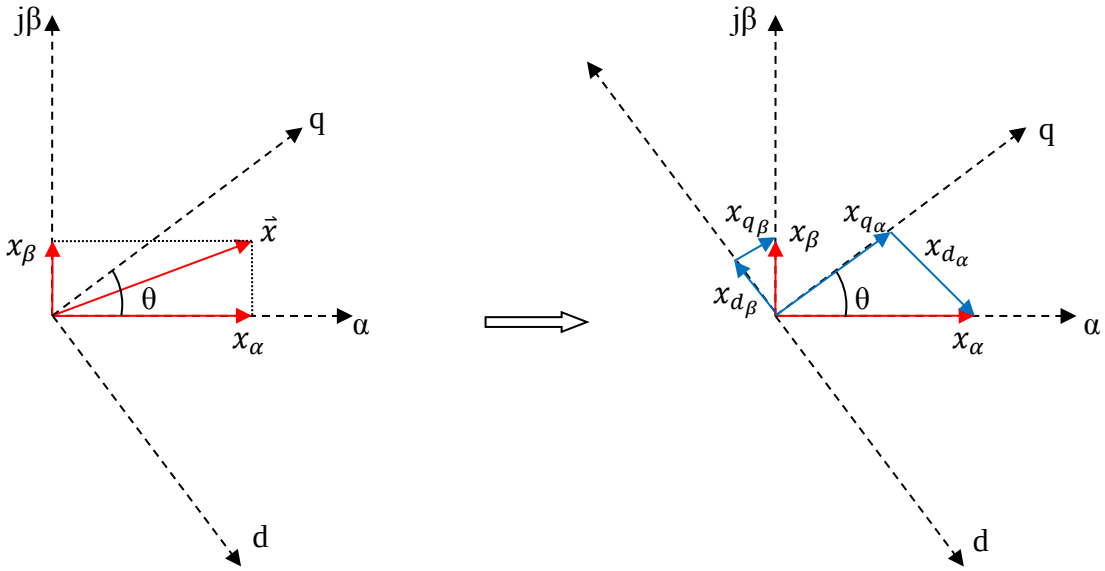

Figure 4.4 Space-vector Decomposed into d-axis and q-axis Components

The trigonometric relationships that yield the Park Transform can be easily found from Figure 4.4,

$$\begin{aligned} x_d &= x_{d_\alpha} + x_{d_\beta} = x_\alpha \sin(\theta) - x_\beta \cos(\theta) \\ x_q &= x_{q_\alpha} + x_{q_\beta} = x_\alpha \cos(\theta) + x_\beta \sin(\theta), \end{aligned} \tag{4.13}$$

$$\begin{bmatrix} x_d \\ x_q \end{bmatrix} = \begin{bmatrix} \sin(\theta) & -\cos(\theta) \\ \cos(\theta) & \sin(\theta) \end{bmatrix} \begin{bmatrix} x_\alpha \\ x_\beta \end{bmatrix} = P \begin{bmatrix} x_\alpha \\ x_\beta \end{bmatrix}. \tag{4.14}$$

Equation (4.14) is the Park Transform. Figure 4.5 shows the results of the Park Transform from Figure 4.4.

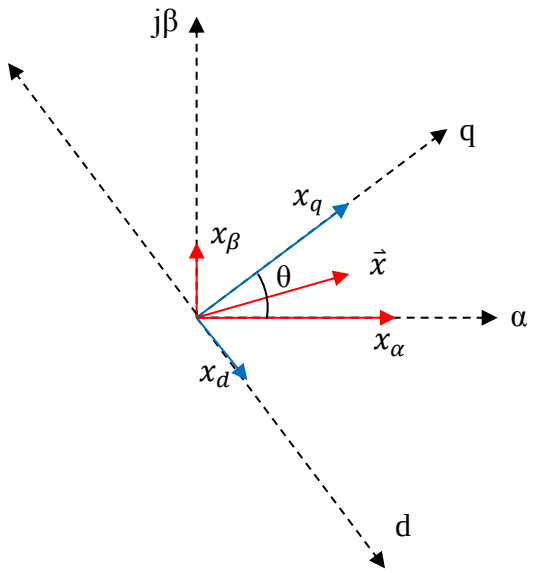

Figure 4.5 Graphical Park Transform

An important note: this Park Transform is slightly different from others presented in some of the literature [41]. The reason is the definition of θ. The software used to develop the controllers defined θ as shown in Figure 4.4, as does some of the literature [42, p. 113] [49]. Many other authors define θ as the angle between the d-axis and the α-axis. As this author learned after many frustrating hours, the distinction is important. θ will be defined as shown in Figure 4.4 for the duration of this thesis.

Like the Clarke Transform, the Park Transform has an inverse that can be used to transform the variables back into the αβ reference frame. There are several ways of finding the inverse Park Transform, including trigonometrically. The most straightforward way, though, is to simply find the inverse of P from (4.14). Doing so yields the inverse Park Transform,

$$\begin{bmatrix} x_\alpha \\ x_\beta \end{bmatrix} = \begin{bmatrix} \sin(\theta) & \cos(\theta) \\ -\cos(\theta) & \sin(\theta) \end{bmatrix} \begin{bmatrix} x_d \\ x_q \end{bmatrix} = P^{-1} \begin{bmatrix} x_d \\ x_q \end{bmatrix}. \tag{4.15}$$

4.3 The Combined Clarke and Park Transform

Because the Park Transform is performed on data that has already been referred to the stator reference frame, it is a natural extension to perform both transforms at once. Combining the transforms makes referring machine variables to the synchronous reference frame possible with only one step. The combination is straightforward and is presented here.

$$\begin{bmatrix} x_d \\ x_q \end{bmatrix} = P \cdot C \cdot \begin{bmatrix} x_a \\ x_b \\ x_c \end{bmatrix}$$

$$= \begin{bmatrix} \sin(\theta) & -\cos(\theta) \\ \cos(\theta) & \sin(\theta) \end{bmatrix} \cdot \frac{2}{3} \begin{bmatrix} 1 & -\frac{1}{2} & -\frac{1}{2} \\ 0 & \frac{\sqrt{3}}{2} & -\frac{\sqrt{3}}{2} \end{bmatrix} \begin{bmatrix} x_a \\ x_b \\ x_c \end{bmatrix}$$

$$= \frac{2}{3} \cdot \begin{bmatrix} \sin(\theta) & -\frac{1}{2}\sin(\theta) - \frac{\sqrt{3}}{2}\cos(\theta) & -\frac{1}{2}\sin(\theta) + \frac{\sqrt{3}}{2}\cos(\theta) \\ \cos(\theta) & -\frac{1}{2}\cos(\theta) + \frac{\sqrt{3}}{2}\sin(\theta) & -\frac{1}{2}\cos(\theta) - \frac{\sqrt{3}}{2}\sin(\theta) \end{bmatrix} \begin{bmatrix} x_a \\ x_b \\ x_c \end{bmatrix} \quad (4.16)$$

$$= \frac{2}{3} \cdot \begin{bmatrix} \sin(\theta) & \cos\left(\theta + \frac{5\pi}{6}\right) & \cos\left(\theta + \frac{\pi}{6}\right) \\ \cos(\theta) & \cos\left(\theta - \frac{2\pi}{3}\right) & \cos\left(\theta + \frac{2\pi}{3}\right) \end{bmatrix} \begin{bmatrix} x_a \\ x_b \\ x_c \end{bmatrix}$$

$$= \frac{2}{3} \cdot \begin{bmatrix} \sin(\theta) & \sin\left(\theta - \frac{2\pi}{3}\right) & \sin\left(\theta + \frac{2\pi}{3}\right) \\ \cos(\theta) & \cos\left(\theta - \frac{2\pi}{3}\right) & \cos\left(\theta + \frac{2\pi}{3}\right) \end{bmatrix} \begin{bmatrix} x_a \\ x_b \\ x_c \end{bmatrix} = K\boldsymbol{x}_{abc}.$$

The final result of (4.16) is the expression that Krause and Thomas used to describe the transformation to an arbitrary reference frame [50]. It is also the method that the SimPowerSystems toolbox for Simulink uses to perform reference frame conversions.

A similar method can be used to find the transform from the dq reference frame to 3-phase variables. That transform is [42, p. 111]:

$$\begin{bmatrix} x_a \\ x_b \\ x_c \end{bmatrix} = \begin{bmatrix} \sin(\theta) & \cos(\theta) \\ \sin\left(\theta - \frac{2\pi}{3}\right) & \cos\left(\theta - \frac{2\pi}{3}\right) \\ \sin\left(\theta + \frac{2\pi}{3}\right) & \cos\left(\theta + \frac{2\pi}{3}\right) \end{bmatrix} \begin{bmatrix} x_d \\ x_q \end{bmatrix} = K^{-1}\boldsymbol{x}_{dq}. \quad (4.17)$$

Chapter 5 - PMSM Model

From a review of the literature associated with PMSG wind turbines, it seems that a fairly standard machine model has emerged, with some minor variations (sign conventions, simplifying assumptions). The most commonly used electrical model for a PMSM is given by some form of [13] [41] [51] [52] [53] [54]:

$$v_d = Ri_d - p\omega_r L_q i_q + L_d \frac{di_d}{dt} \tag{5.1}$$

$$v_q = Ri_q + p\omega_r (L_d i_d + \psi) + L_q \frac{di_q}{dt} \tag{5.2}$$

$$\tau_e = \frac{3}{2} p\left(i_d i_q \left(L_d - L_q\right) + \psi i_q\right). \tag{5.3}$$

In addition to the preceding three equations, two others that describe the mechanical dynamics of the turbine/generator are commonly used. The first mechanical equation is found in the literature as well, also with some slight variations due to sign conventions and simplifying assumptions, [11] [42, p. 266] [55]:

$$\dot{\omega_r} = \frac{1}{J}(\tau_e - C_D \omega_r - \tau_{aero}). \tag{5.4}$$

The other mechanical equation is simple physics,

$$\dot{\theta_r} = \omega_r. \tag{5.5}$$

Table 2 gives descriptions of each parameter in (5.1) - (5.5).

Table 2 PMSM Model Parameters

Symbol	Parameter	Units
v_d	d-axis voltage	V
v_q	q-axis voltage	V
i_d	d-axis current	A
i_q	q-axis current	A
ψ	flux established by PM's	Wb
R	per-phase stator resistance	Ω
L_d	d-axis inductance	H
L_q	q-axis inductance	H
ω_r	PMSG rotor angular velocity	rad/s
θ_r	rotor angle	rad
τ_e	PMSG torque	N.m
τ_{aero}	torque on the PMSG rotor from wind	N.m
J	Combined turbine rotor and generator inertia	$kg.m^2$
C_D	lumped damping term	N.m.s
p	pole pairs	unit-less

The rest of this chapter is devoted to deriving (5.1) - (5.3) in detail.

5.1 Voltage Equations

From the preceding chapter it is clear the some angle, θ, must be known in order to refer machine variables to the rotor reference frame. It turns out that that angle must be θ_e, the electrical angle of the back-emf.

Figure 5.1 shows a 2-pole, 3-phase PMSM with the d and q-axes superimposed on the machine. The as, bs, and cs axes are the magnetic axes of the machine. In a PMSM, θ_r could be measured by an encoder. θ_r is related to θ_e by:

$$\theta_e = p\theta_r. \tag{5.6}$$

For the remainder of this chapter, θ in the Park Transform will be the PMSG back-emf angle, θ_e.

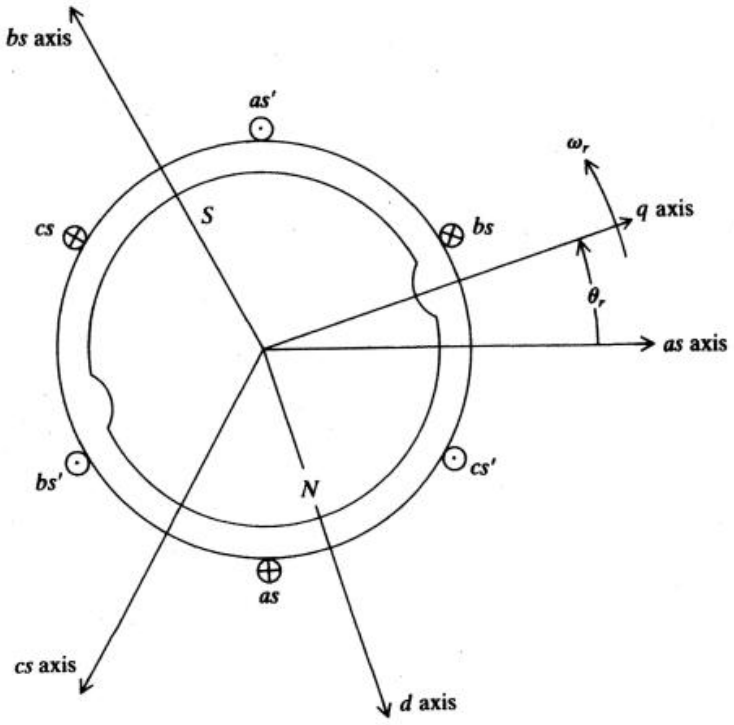

Figure 5.1 PMSM with dq coordinate system [42, p. 262]

Consider (3.13) with the opposite current sign convention as Figure 3.7 (motor sign convention). The PMSM block in the SimPowerSystems toolbox for Simulink, which was used for all of the simulations in this thesis, uses the motor sign convention, so it will be used from this point on. The following derivation is very similar to that in Krause, et. al [42, pp. 261-267]. It is reproduced and expanded upon here as it is vital to understanding how the controllers presented in later chapters work. Equation (3.13) with the motor sign convention is:

$$v(t) = i(t) \cdot R + \frac{d\lambda}{dt}. \tag{5.7}$$

Equation (5.7) is only for a single phase. If the machine for which (5.7) is written is a 3-phase, wye-connected machine, it may be extended to:

$$\begin{bmatrix} v_a(t) \\ v_b(t) \\ v_c(t) \end{bmatrix} = \begin{bmatrix} R & 0 & 0 \\ 0 & R & 0 \\ 0 & 0 & R \end{bmatrix} \begin{bmatrix} i_a(t) \\ i_b(t) \\ i_c(t) \end{bmatrix} + \frac{d}{dt} \begin{bmatrix} \lambda_a(t) \\ \lambda_b(t) \\ \lambda_c(t) \end{bmatrix} \tag{5.8}$$

$$\boldsymbol{v}_{abc} = \boldsymbol{r}_s \cdot \boldsymbol{i}_{abc} + \frac{d}{dt}\boldsymbol{\lambda}_{abc}.$$

Equation (5.8) assumes that the stator resistance, R, of all three phases is the same, which is most often the case. Because $\boldsymbol{x}_{abc} = K^{-1}\boldsymbol{x}_{dq}$ and $KK^{-1} = I$, (5.8) may be written as:

$$K \cdot \left(\boldsymbol{v}_{abc} = \boldsymbol{r}_s \boldsymbol{i}_{abc} + \frac{d}{dt}\boldsymbol{\lambda}_{abc}\right) = \boldsymbol{v}_{dq} = K\boldsymbol{r}_s K^{-1}\boldsymbol{i}_{dq} + K\frac{d}{dt}\left(K^{-1}\boldsymbol{\lambda}_{dq}\right). \tag{5.9}$$

Because the resistance is assumed to be the same for all phases,

$$K\boldsymbol{r}_s K^{-1} = \begin{bmatrix} R & 0 \\ 0 & R \end{bmatrix} = \boldsymbol{r}. \tag{5.10}$$

Using (5.10) and expanding the last term of (5.9) with the chain rule, (5.9) may be rewritten as:

$$\boldsymbol{v}_{dq} = \boldsymbol{r}\boldsymbol{i}_{dq} + K\frac{dK^{-1}}{dt}\boldsymbol{\lambda}_{dq} + KK^{-1}\frac{d\boldsymbol{\lambda}_{dq}}{dt}. \tag{5.11}$$

The second term of (5.11) may be simplified using the fact that:

$$\begin{aligned} \frac{dK^{-1}}{dt} &= \frac{d}{dt}\begin{bmatrix} \sin(\theta_e(t)) & \cos(\theta_e(t)) \\ \sin\left(\theta_e(t) - \frac{2\pi}{3}\right) & \cos\left(\theta_e(t) - \frac{2\pi}{3}\right) \\ \sin\left(\theta_e(t) + \frac{2\pi}{3}\right) & \cos\left(\theta_e(t) + \frac{2\pi}{3}\right) \end{bmatrix} \\ &= \begin{bmatrix} \frac{\mathrm{d}\theta_e}{dt}\cos(\theta_e) & -\frac{\mathrm{d}\theta_e}{dt}\sin(\theta_e) \\ \frac{\mathrm{d}\theta_e}{dt}\cos\left(\theta_e - \frac{2\pi}{3}\right) & -\frac{\mathrm{d}\theta_e}{dt}\sin\left(\theta_e - \frac{2\pi}{3}\right) \\ \frac{\mathrm{d}\theta_e}{dt}\cos\left(\theta_e + \frac{2\pi}{3}\right) & -\frac{\mathrm{d}\theta_e}{dt}\sin\left(\theta_e - \frac{2\pi}{3}\right) \end{bmatrix}. \end{aligned} \tag{5.12}$$

Because $\frac{\mathrm{d}\theta_e}{dt}$ is the angular frequency of the back-emf, ω_e, (5.12) may be further simplified,

$$\frac{dK^{-1}}{dt} = \omega_e \begin{bmatrix} \cos(\theta_e) & -\sin(\theta_e) \\ \cos\left(\theta_e - \frac{2\pi}{3}\right) & -\sin\left(\theta_e - \frac{2\pi}{3}\right) \\ \cos\left(\theta_e + \frac{2\pi}{3}\right) & -\sin\left(\theta_e - \frac{2\pi}{3}\right) \end{bmatrix}. \tag{5.13}$$

It can then be shown that:

$$K\frac{dK^{-1}}{dt} = \begin{bmatrix} 0 & -\omega_e \\ \omega_e & 0 \end{bmatrix}. \tag{5.14}$$

Using (5.14), (5.11) can be simplified to:

$$\boldsymbol{v}_{dq} = \boldsymbol{r}\boldsymbol{i}_{dq} + \omega_e \begin{bmatrix} -\lambda_q \\ \lambda_d \end{bmatrix} + \frac{d\boldsymbol{\lambda}_{dq}}{dt} = \boldsymbol{r}\boldsymbol{i}_{dq} + \omega_e \boldsymbol{\lambda}_{-qd} + \frac{d\boldsymbol{\lambda}_{dq}}{dt}. \tag{5.15}$$

The next step is to further simplify the flux linkages. After reading Chapter 3, it should be no surprise to learn that the flux linkages of the stator coils in a PMSM have both self flux linkage and mutual flux linkage. Furthermore, the stator coils will each link some flux from the permanent magnets. The total flux linked by a coil is partly due to the current flowing through that coil, partly due to the currents in other windings, and partly due to the permanent magnets on the rotor. Recall from (3.4) that inductance is a measure of the flux linked by a wire as a function of the current through that wire. Krause, et al, define self-inductance and mutual inductance by stating that,

> *"In a magnetically linear system the self-inductance of a winding is the ratio of the flux linked by a winding to the current flowing in the winding with all other winding currents zero. Mutual inductance is the ratio of flux linked by one winding due to current flowing in a second winding with all other winding currents zero including the winding for which the flux linkages are being determined [42, p. 48]."*

Using detailed information about the machine's construction, a precise expression can be found for the total inductance of each stator coil. Such an expression is given by [42, p. 195],

$$\boldsymbol{L}_s = \begin{bmatrix} L_{ls} + L_A - L_B\cos(2\theta_e) & -\frac{1}{2}L_A - L_B\cos\left(2\left(\theta_e - \frac{\pi}{3}\right)\right) & -\frac{1}{2}L_A - L_B\cos\left(2\left(\theta_e + \frac{\pi}{3}\right)\right) \\ -\frac{1}{2}L_A - L_B\cos\left(2\left(\theta_e - \frac{\pi}{3}\right)\right) & L_{ls} + L_A - L_B\cos\left(2\left(\theta_e - \frac{2\pi}{3}\right)\right) & -\frac{1}{2}L_A - L_B\cos(2(\theta_e + \pi)) \\ -\frac{1}{2}L_A - L_B\cos\left(2\left(\theta_e + \frac{\pi}{3}\right)\right) & -\frac{1}{2}L_A - L_B\cos(2(\theta_e + \pi)) & L_{ls} + L_A - L_B\cos\left(2\left(\theta_e + \frac{2\pi}{3}\right)\right) \end{bmatrix}. \quad (5.16)$$

As stated above, the total flux linkage of each stator winding in a PMSM has contributions from self-inductance, mutual inductance, and the permanent magnets. This is captured in (5.17) [42, p. 263],

$$\boldsymbol{\lambda}_{abc} = \boldsymbol{L}_s \boldsymbol{i}_{abc} + \boldsymbol{\lambda}_m. \quad (5.17)$$

$\boldsymbol{\lambda}_m$ in (5.17) is the flux linkage contribution from the permanent magnets. If the stator coils are placed in a sinusoidal manner around the machine, $\boldsymbol{\lambda}_m$ given by,

$$\boldsymbol{\lambda}_m = \psi \begin{bmatrix} \sin(\theta_e) \\ \sin\left(\theta_e - \frac{2\pi}{3}\right) \\ \sin\left(\theta_e + \frac{2\pi}{3}\right) \end{bmatrix}, \quad (5.18)$$

where ψ is the magnitude of the flux established by the permanent magnets. In order to find $\boldsymbol{\lambda}_{dq}$, (5.17) is pre-multiplied by K,

$$\begin{aligned} \boldsymbol{\lambda}_{dq} &= K(\boldsymbol{L}_s \boldsymbol{i}_{abc} + \boldsymbol{\lambda}_m) = K\left(\boldsymbol{L}_s K^{-1} \boldsymbol{i}_{dq} + \boldsymbol{\lambda}_m\right) \\ &= K\boldsymbol{L}_s K^{-1} \boldsymbol{i}_{dq} + K\boldsymbol{\lambda}_m. \end{aligned} \quad (5.19)$$

It can be shown, most conveniently with a symbolic math processor, that:

$$K\boldsymbol{L}_s K^{-1} = \begin{bmatrix} \frac{3}{2}(L_A + L_B) + L_{ls} & 0 \\ 0 & \frac{3}{2}(L_A + L_B) - L_{ls} \end{bmatrix}. \quad (5.20)$$

Then, considering the following definitions:

$$
\begin{aligned}
L_{mq} &\triangleq \frac{3}{2}(L_A - L_B) \\
L_{md} &\triangleq \frac{3}{2}(L_A - L_B) \\
L_{md} + L_{ls} &\triangleq L_d \\
L_{mq} + L_{ls} &\triangleq L_q,
\end{aligned}
\tag{5.21}
$$

(5.20) may be rewritten as [42, p. 264]:

$$
K\boldsymbol{L}_s K^{-1} = \begin{bmatrix} L_{md} + L_{ls} & 0 \\ 0 & L_{mq} + L_{ls} \end{bmatrix} = \begin{bmatrix} L_d & 0 \\ 0 & L_q \end{bmatrix}. \tag{5.22}
$$

In order to further simplify (5.19), it can be shown that:

$$
K\boldsymbol{\lambda}_m = \begin{bmatrix} \psi \\ 0 \end{bmatrix}. \tag{5.23}
$$

Taking both (5.22) and (5.23) into account, (5.19) can be simplified to:

$$
\boldsymbol{\lambda}_{dq} = \begin{bmatrix} \lambda_d \\ \lambda_q \end{bmatrix} = \begin{bmatrix} L_d & 0 \\ 0 & L_q \end{bmatrix} \begin{bmatrix} i_d \\ i_q \end{bmatrix} + \begin{bmatrix} \psi \\ 0 \end{bmatrix}. \tag{5.24}
$$

Using (5.24), (5.15) becomes:

$$
\begin{aligned}
\boldsymbol{v}_{dq} = \begin{bmatrix} v_d \\ v_q \end{bmatrix} = \begin{bmatrix} R & 0 \\ 0 & R \end{bmatrix} \begin{bmatrix} i_d \\ i_q \end{bmatrix} + \omega_e \left(\begin{bmatrix} 0 & -L_q \\ L_d & 0 \end{bmatrix} \begin{bmatrix} i_d \\ i_q \end{bmatrix} + \begin{bmatrix} 0 \\ \psi \end{bmatrix} \right) \\
+ \frac{d}{dt} \left(\begin{bmatrix} L_d & 0 \\ 0 & L_q \end{bmatrix} \begin{bmatrix} i_d \\ i_q \end{bmatrix} + \begin{bmatrix} \psi \\ 0 \end{bmatrix} \right).
\end{aligned}
\tag{5.25}
$$

Equation (5.25) may then be simplified to

$$
v_d = Ri_d - \omega_e L_q i_q + L_d \frac{di_d}{dt} \tag{5.26}
$$

$$
v_q = Ri_q + \omega_e (L_d i_d + \psi) + L_q \frac{di_q}{dt}. \tag{5.27}
$$

Then (5.26) and (5.27) can be extended to machines with more than two poles with the simple relationships [43, p. 89]:

$$\begin{aligned} \omega_e &= p\omega_r \\ \theta_e &= p\theta_r, \end{aligned} \tag{5.28}$$

where ω_e the frequency of the generator's back-emf and p is the number of generator pole pairs . Considering (5.28), (5.26) and (5.27) become the final equations for line-to-neutral voltage in the synchronous reference frame:

$$v_d = Ri_d - p\omega_r L_q i_q + L_d \frac{di_d}{dt} \tag{5.29}$$

$$v_q = Ri_q + p\omega_r(L_d i_d + \psi) + L_q \frac{di_q}{dt}. \tag{5.30}$$

5.2 Torque Equation

As will be shown in Chapter 7, torque control is an important part of a PMSG FOC speed controller. An equation relating torque to variables in the synchronous reference frame is useful to that end. There are at least two ways other than the one shown here to derive such an equation [41] [42, pp. 206-207,265]. The derivation shown below is the simplest of the three known to the author.

Let the line-to-neutral terminal voltages of a 3-phase PMSM be:

$$\begin{aligned} v_a &= V_m \cos(\theta_e + \delta) \\ v_b &= V_m \cos\left(\theta_e - \frac{2\pi}{3} + \delta\right) \\ v_b &= V_m \cos\left(\theta_e + \frac{2\pi}{3} + \delta\right), \end{aligned} \tag{5.31}$$

and let the phase machine's phase currents be:

$$
\begin{aligned}
i_a &= I_m \cos(\theta_e + \gamma) \\
i_b &= I_m \cos\left(\theta_e - \frac{2\pi}{3} + \gamma\right) \\
i_c &= I_m \cos\left(\theta_e + \frac{2\pi}{3} + \gamma\right).
\end{aligned}
\tag{5.32}
$$

Let positive currents flow into the machine. It can be shown that the *instantaneous* 3-phase power generated by the machine is [56, p. 67]:

$$
P_{3\phi} = \frac{3}{2} V_m I_m \cos(\delta - \gamma).
\tag{5.33}
$$

Next, let the voltages and currents be referred to the rotor reference frame as:

$$
\begin{bmatrix} v_d \\ v_q \end{bmatrix} = \frac{2}{3} \cdot \begin{bmatrix} \sin(\theta_e) & \sin\left(\theta_e - \frac{2\pi}{3}\right) & \sin\left(\theta_e + \frac{2\pi}{3}\right) \\ \cos(\theta_e) & \cos\left(\theta_e - \frac{2\pi}{3}\right) & \cos\left(\theta_e + \frac{2\pi}{3}\right) \end{bmatrix} \begin{bmatrix} v_a \\ v_b \\ v_c \end{bmatrix} = V_m \begin{bmatrix} -\sin(\delta) \\ \cos(\delta) \end{bmatrix}
\tag{5.34}
$$

and

$$
\begin{bmatrix} i_d \\ i_q \end{bmatrix} = \frac{2}{3} \cdot \begin{bmatrix} \sin(\theta_e) & \sin\left(\theta_e - \frac{2\pi}{3}\right) & \sin\left(\theta_e + \frac{2\pi}{3}\right) \\ \cos(\theta_e) & \cos\left(\theta_e - \frac{2\pi}{3}\right) & \cos\left(\theta_e + \frac{2\pi}{3}\right) \end{bmatrix} \begin{bmatrix} i_a \\ i_b \\ i_c \end{bmatrix} = I_m \begin{bmatrix} -\sin(\gamma) \\ \cos(\gamma) \end{bmatrix}.
\tag{5.35}
$$

Then:

$$
\begin{bmatrix} v_d & v_q \end{bmatrix} \begin{bmatrix} i_d \\ i_q \end{bmatrix} = V_m I_m \cos(\delta - \gamma).
\tag{5.36}
$$

By inspection it is clear that (5.36) only differs from (5.33) by a factor of 3/2. Compensating for that, the instantaneous power can be written as:

$$
P_{3\phi} = \frac{3}{2} \left(v_d i_d + v_q i_q \right).
\tag{5.37}
$$

Then (5.29) and (5.30) can be substituted into (5.37), which becomes:

$$
\begin{aligned}
P_{3\phi} = \frac{3}{2} &\left(R i_d - p \omega_r L_q i_q + L_d \frac{d i_d}{dt} \right) i_d \\
&+ \frac{3}{2} \left(R i_q + p \omega_r L_d i_d + p \omega_r \psi + L_q \frac{d i_q}{dt} \right) i_q.
\end{aligned}
\tag{5.38}
$$

Equation (5.38) can then be simplified to:

$$P_{3\phi} = \frac{3}{2}R\left(i_d^2 + i_q^2\right) + \frac{3}{2}\left(L_d i_d \frac{di_d}{dt} + L_q i_q \frac{di_q}{dt}\right) + \frac{3}{2}p\omega_r\left(i_d i_q\left(L_d - L_q\right) + \psi i_q\right). \quad (5.39)$$

The first term in (5.39) describes the machine's conduction losses, the second term describes the power stored in the stator's magnetic field if the currents are changing, and the third term describes the conversion from mechanical power to electrical power [52]. Assuming the first term is negligible and the machine is operating at steady state $\left(\frac{di_d}{dt} = \frac{di_q}{dt} = 0\right)$, the mechanical power can be set equal to the electromechanical conversion term:

$$\tau_e\omega_r = \frac{3}{2}p\omega_r\left(i_d i_q\left(L_d - L_q\right) + \psi i_q\right) \rightarrow \tau_e = \frac{3}{2}p\left(i_d i_q\left(L_d - L_q\right) + \psi i_q\right), \quad (5.40)$$

and (5.3) has been derived.

5.3 Non-Salient, Sinusoidal, PMSM Model

The equations presented in the previous two sections are valid for any PMSM. As stated in Section 3.3.1 though, not all PMSMs will work with the controllers developed in this thesis. In order to work with the type of controller used in this project, the machine must be non-salient. In a non-salient machine, $L_d = L_q = L_s$, where L_s is the synchronous inductance [41]. That simplifying assumption is the reason the controllers presented later will not work with every PMSM. If the d- and q-axis inductances are not approximately equal, the structure of the controller must be different. In the case of non-salient machines, (5.1), (5.2), and (5.3) can be simplified to

$$v_d = Ri_d + L_s\left(\frac{di_d}{dt} - p\omega_r i_q\right) \quad (5.41)$$

$$v_q = Ri_q + L_s\left(\frac{di_q}{dt} + p\omega_r i_d\right) + p\omega_r\psi \quad (5.42)$$

$$\tau_e = \frac{3}{2}p\psi i_q. \quad (5.43)$$

Equations (5.41) - (5.43) along with (5.4) and (5.5) make up the machine model used to design the controllers presented later.

The generator parameters for the 10 kW machine are proprietary to Bergey Windpower, so only their ranges can be reported here. Those ranges and the parameters for the 5 MW model are given in Table 3.

Table 3 PMSM Model Parameters Used in Simulations of 5 MW Machine

Parameter	Value (10 kW)	Value (5 MW)
R_s	0.05-0.2 Ω	$4.76*10^{-4}$ Ω
L_s	1-4 mH	0.177 mH
ψ	0.25 – 0.5 Wb	1.0567 Wb
J	83.34 kg.m^2	$116.469*10^3$ kg.m^2
p	14-18	9

The parameters for the 5 MW machine were chosen based on reasonable ranges provided by engineers at ABB Inc. It is important to note that J is not part of the PMSG model for FAST simulations. J was used in non-FAST simulations that could be completed quickly and were used to design the controllers, which were then tested in FAST. Also, (5.4) is only used in non-FAST simulations, as FAST includes much more complicated dynamics than (5.4) represents.

Chapter 6 - Solid-State Rectifiers and Inverters

6.1 3-Phase Passive Rectifiers

A rectifier is a device that converts AC current into DC current. A solid-state rectifier performs this conversion using semiconductor devices; namely diodes, thyristors, or transistors. Figure 6.1 shows the simplest type of 3-phase rectifier: a diode rectifier. A diode rectifier is sometimes called "passive" as there is no way to control when the diodes conduct.

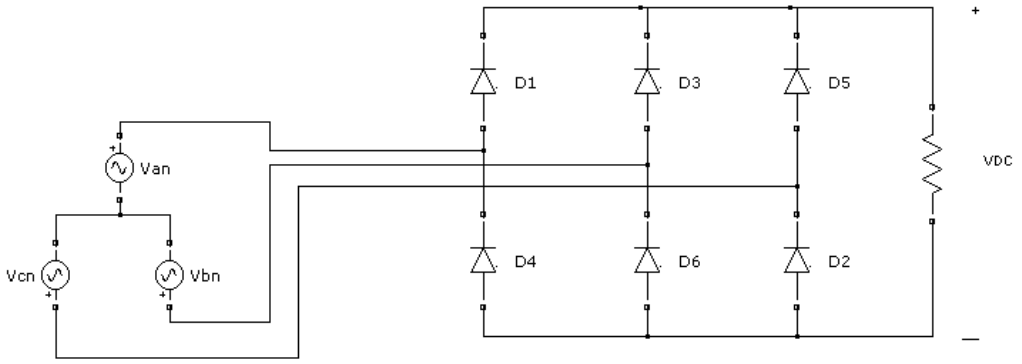

Figure 6.1 3-Phase Passive Rectifier

A diode conducts when the voltage at its anode is some V_D greater than the voltage at its cathode. V_D is traditionally assumed to be 0.7 V, but it varies from device to device. With that knowledge, one can predict when each diode will conduct. In a 3-phase passive rectifier, the two diodes that are connected to the phases with the highest *magnitude* line-to-line voltage at any instant will conduct [57, p. 71]. Figure 6.2 shows the line-to-line input voltages and the output current (with conducting diodes indicated) for a circuit such as Figure 6.1. The magnitudes in Figure 6.2 are arbitrary. Figure 6.2 shows some ripple in the output current; that can be minimized by placing a capacitor across the load. A rectifier with such a capacitor is sometimes called a "peak rectifier," as the output voltage is approximately equal to the peak value of the input voltage.

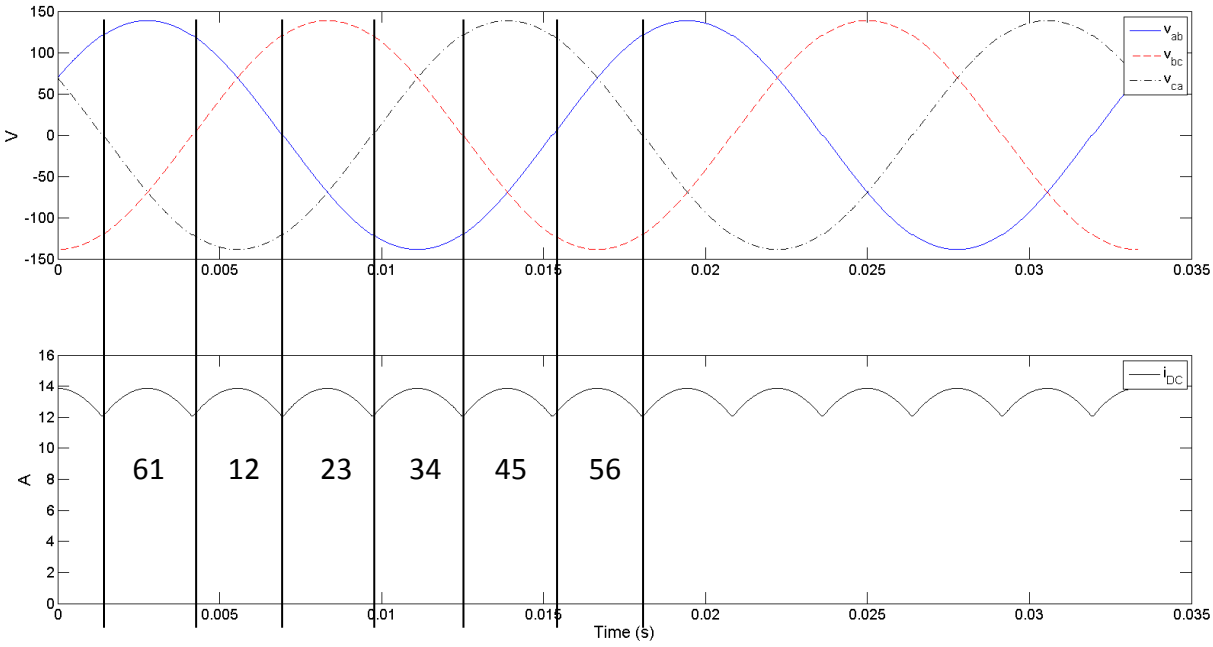

Figure 6.2 Input Voltage and Output Current for a 3-Phase Passive Rectifier

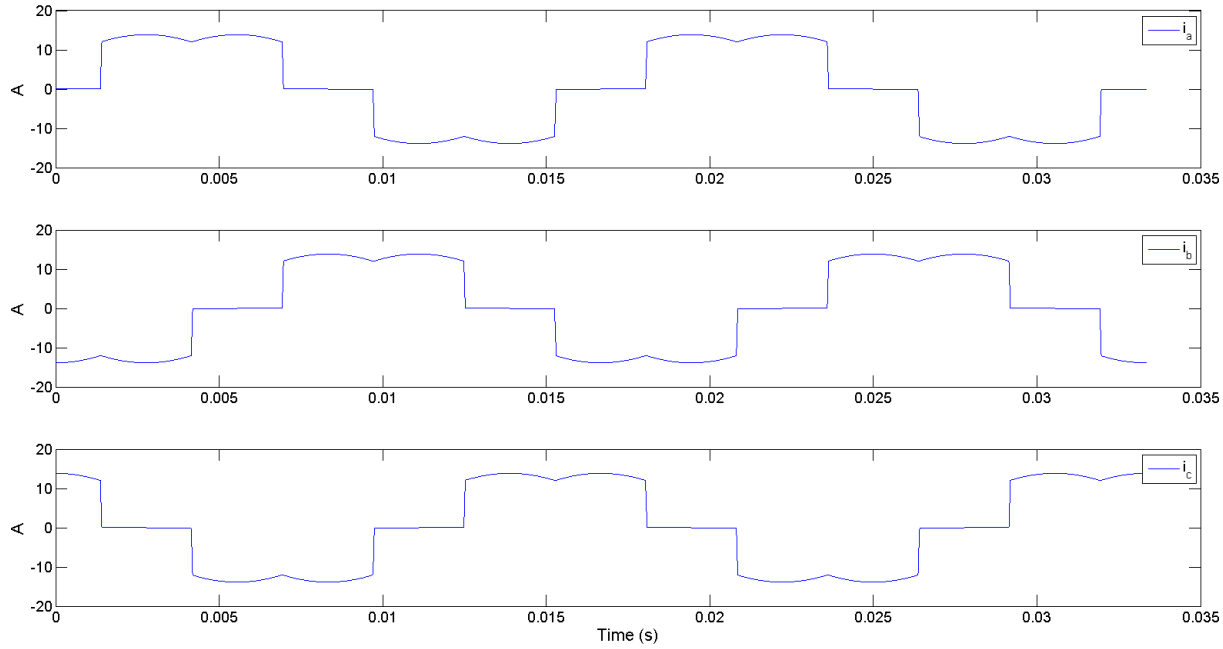

Figure 6.3 3-Phase Passive Rectifier Input Currents

Figure 6.3 shows the input currents for a circuit such as Figure 6.1. By inspection it is clear that the input currents have high levels of harmonics (they are very "un-sinusoidal"). Recall from Section 3.3.2 that sinusoidal currents in a sinusoidal PMSM give the machine constant torque. If the input voltage sources in Figure 6.1 were actually a PMSG, the generator's torque would not be constant. Constant torque in a direct-drive wind turbine generator means the machine will spin smoothly, with reduced mechanical stress.

Because diodes cannot be made to conduct or block at will, the rectifier input currents cannot be controlled and they can only be made sinusoidal by a large filter. However, passive rectifiers are cheaper and easier to use than active ones due to their simplicity. Despite the lack of control, it is still possible to find works published recently that include passive rectifiers for wind turbine applications and they are still in use in wind turbines being manufactured today [54].

6.2 3-Phase Voltage-Source Converters

In contrast to passive rectifiers, active rectifiers perform the same basic function, and they can be controlled. An active rectifier is shown with a PMSG connected to its input in Figure 6.4.

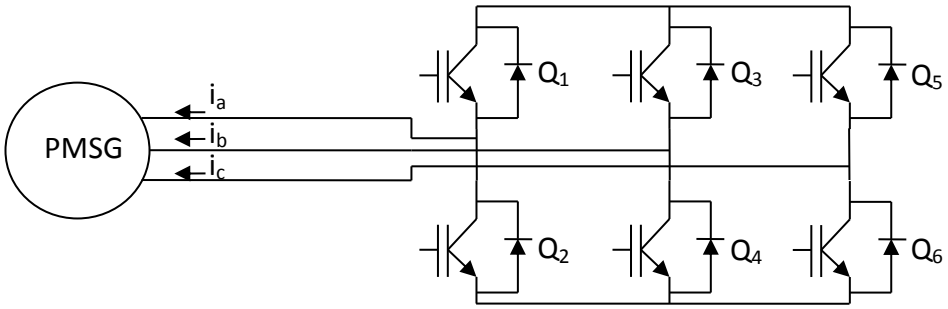

Figure 6.4 3-Phase IGBT Bridge

In Figure 6.4, the diodes from Figure 6.1 have been replaced with insulated-gate bipolar transistors (IGBTs) with anti-parallel diodes. An IGBT is basically a MOSFET/BJT hybrid. Like MOSFETs, IGBTs have high input impedance. Also, IGBTs can handle more current than MOSFETs, and they have lower conduction and switching losses than BJTs [57, p. 289]. IGBTs are controlled by the voltage between their gate and source, and their switching speed is somewhere in between those of a BJT and MOSFET [57, p. 289]. When a sufficient voltage is applied between gate and source, the device conducts current. When that voltage is removed,

conduction ceases. This process is known as gating. A good comparison of different semiconductor switches is given in Mohan [58, pp. 16-30]. For the purposes of designing controllers, it is assumed that IGBTs act as ideal switches. However, some of their non-idealities are accounted for in the simulations.

The current directions shown in Figure 6.4 reflect the motor sign convention. The topology of this active rectifier, called a 3-phase IGBT bridge, can be used for either an active rectifier or a voltage source inverter. The principles of operation are very similar for both applications. The main idea behind both applications is that the IGBTs should be turned on and off in such a way as to ensure a balanced 3-phase sinusoidal voltage on the AC side and nearly constant DC on the DC side. As an example, consider the motor drive circuit in Figure 6.5.

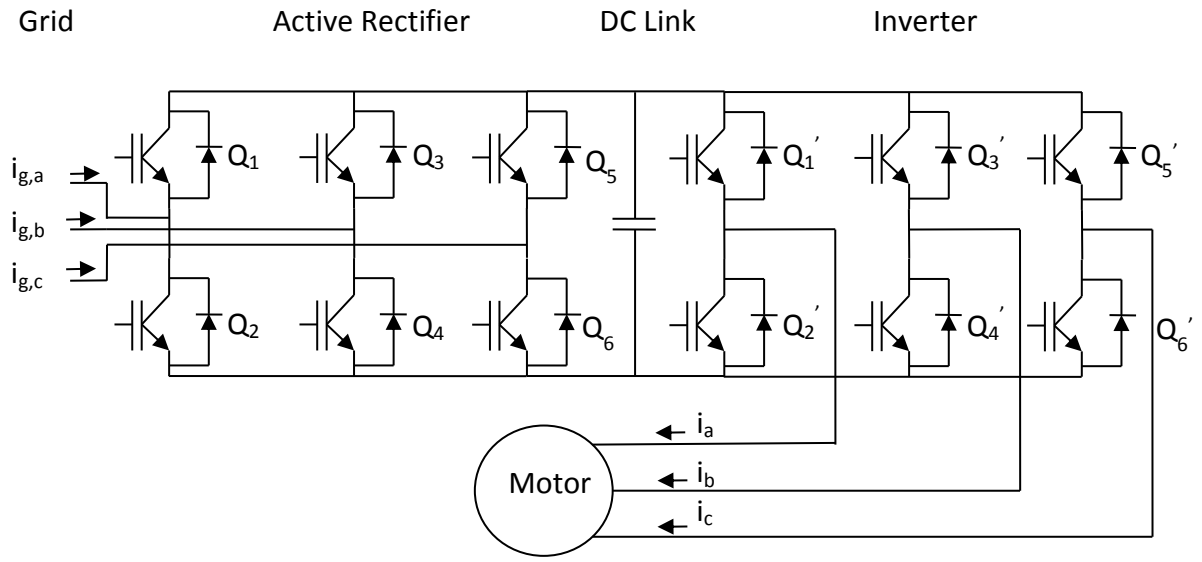

Figure 6.5 Back-to-Back Converter in a Motor Drive

A motor's speed can be controlled by controlling the magnitude and frequency of its input voltage. It is the inverter's job to do just that; it takes the DC voltage at the DC link and converts it to AC at the desired frequency and magnitude. The active rectifier's job is to set the DC link voltage to a desired level by converting the AC grid current to DC. Because an active rectifier is controllable, this can be done in such a way as to not adversely affect the grid (high power factor, low harmonics). The back-to-back converter in a wind turbine works on the same principles as this drive, but in reverse. In a wind turbine, it is the rectifier's job to control the machine and the

inverter's job to make sure that current flows smoothly into the grid. Either converter could theoretically keep the DC link voltage constant, but it is more commonly a task for the inverter's control system [13] [51]. Both of the converters used in this thesis are voltage-source converters, meaning their terminal voltages may be controlled.

Consider Figure 6.6, which shows the 3-phase bridge as envisioned by Malinowski [59].

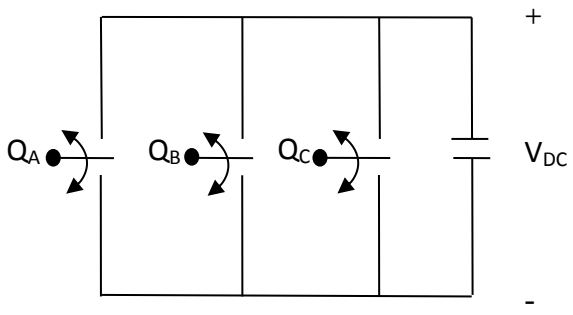

Figure 6.6 3-Switch Bridge

The IGBTs of Figure 6.4 have been replaced by three theoretical two-way ideal switches. Each switch has two possible states: up or down. If a switch is up, let the value of some function, S, be 1. If a switch is down, let the value of that function be 0. There are eight possible switch combinations, or states. The line-to-line voltages of the bridge's terminals can be found in terms of S and V_{DC}. For example, Figure 6.7 shows $(S_a, S_b, S_c) = (1,0,0)$. Clearly:

$$\begin{aligned} v_{ab} &= V_{DC} \\ v_{bc} &= 0 \\ v_{ca} &= -V_{DC} \end{aligned} \tag{6.1}$$

for Figure 6.7.

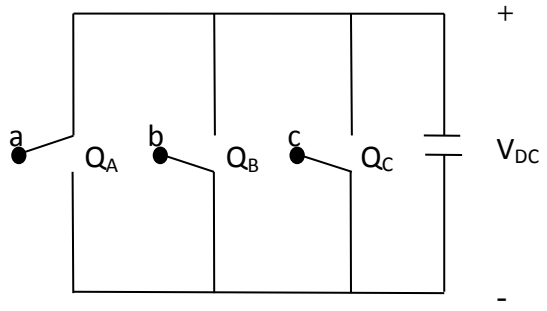

Figure 6.7 3-Switch Bridge, (1,0,0)

If all eight switch states are considered, it can be shown that [59]:

$$v_{ab} = V_{DC}(S_a - S_b) \tag{6.2}$$

$$v_{bc} = V_{DC}(S_b - S_c) \tag{6.3}$$

$$v_{ca} = V_{DC}(S_c - S_a). \tag{6.4}$$

Though not as intuitive as the line-to-line voltage relationships, the line-to-neutral voltages can also be written as functions of S and V_{DC} simply by examining each switch state with a wye-connected load attached to the bridge [59],

$$v_{an} = \frac{V_{DC}(2S_a - S_b - S_c)}{3} \tag{6.5}$$

$$v_{bn} = \frac{V_{DC}(2S_b - S_a - S_c)}{3} \tag{6.6}$$

$$v_{an} = \frac{V_{DC}(2S_c - S_a - S_b)}{3}. \tag{6.7}$$

If the switches are operated in the sequence given in Table 4, the line-to-neutral voltages would be those shown in Figure 6.8. This manner of switching is called "180^o conduction mode," as each switch operates for half of the cycle (180^o), or "six-step operation" because there are six distinct states that the switches may occupy.

Table 4 Positive Sequence Switch States for 180° Conduction Mode

ωt	(S_a,S_b,S_c)
$0 - \pi/3$	(1,0,0)
$\pi/3 - 2\pi/3$	(1,1,0)
$2\pi/3 - \pi$	(0,1,0)
$\pi - 4\pi/3$	(0,1,1)
$4\pi/3 - 5\pi/3$	(0,0,1)
$5\pi/3 - 2\pi$	(1,0,1)

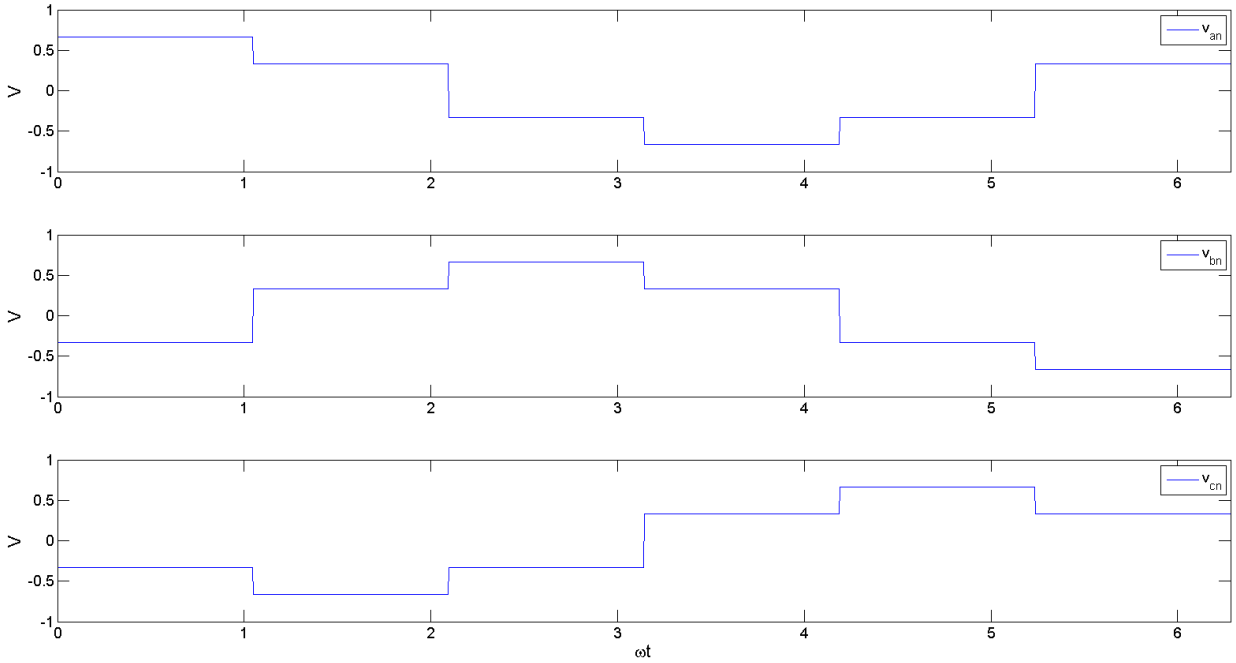

Figure 6.8 3-Phase Bridge L-N Voltages in 180° Conduction Mode

Because the waveforms in Figure 6.8 have instantanous transitions from one voltage to another, the equations describing them are infinite series of sinusoids [47, pp. 202-204]. The components of those voltages, called "harmonics," whose frequencies are greater than the fundamental (60 Hz for a grid-tied application) are undesirable. Such harmonics can cause overheating of transformers and torque ripple in electric machines, and they cannot transfer any active power. Therefore it is common practice to filter harmonics out of the waveform. Though it is outside the scope of this thesis to derive, it can be shown that by proper switching at frequencies many times

greater than the fundamental, harmonics can be shifted up to higher frequencies where they are easier to filter [60, p. 183]. This process is called "pulse-width modulation" (PWM). One popular type of PWM is called "space-vector pulse-width modulation" (SVPWM), or simply "space-vector modulation" (SVM). SVPWM is commonly used in motor drives and back-to-back converters for wind turbines [13] [41] [42, pp. 506-510] [51] [61]. SVPWM was used for both converters in this thesis and it is described in the next section.

6.3 Space-vector Pulse-Width Modulation

Since the voltages in Figure 6.8 are 3-phase, the Clarke Transform can be applied to them. Because the voltages are constant for each switch state, the result is six discrete space-vectors. For example, for $0< \omega t< \pi/3$:

$$\begin{bmatrix} v_\alpha \\ v_\beta \end{bmatrix} = \frac{2}{3}\boldsymbol{C}\begin{bmatrix} \frac{2}{3} \\ -\frac{1}{3} \\ -\frac{1}{3} \end{bmatrix} V_{DC} = \begin{bmatrix} \frac{2}{3} \\ 0 \end{bmatrix} V_{DC}. \tag{6.8}$$

Equation (6.8) can be expanded for the entire cycle as:

$$\begin{aligned} \frac{2}{3}\boldsymbol{C}\begin{bmatrix} 2/3 & 1/3 & -1/3 & -2/3 & -1/3 & 1/3 \\ -1/3 & 1/3 & 2/3 & 1/3 & -1/3 & -2/3 \\ -1/3 & -2/3 & -1/3 & 1/3 & 2/3 & 1/3 \end{bmatrix} V_{DC} \\ = V_{DC}\begin{bmatrix} \frac{2}{3} & \frac{1}{3} & -\frac{1}{3} & -\frac{2}{3} & -\frac{1}{3} & \frac{1}{3} \\ 0 & \frac{\sqrt{3}}{3} & \frac{\sqrt{3}}{3} & 0 & -\frac{\sqrt{3}}{3} & -\frac{\sqrt{3}}{3} \end{bmatrix}. \end{aligned} \tag{6.9}$$

Each column of (6.9) is a space-vector that corresponds to a particular switch state. When those space-vectors are plotted in the αβ plane for V_{DC}=1V, the result is Figure 6.9.

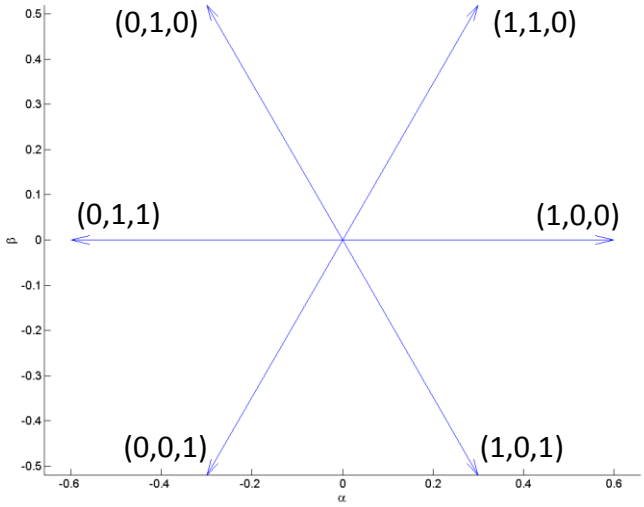

Figure 6.9 Base Space-vectors for a 3-Phase Bridge

The numbers in parentheses in Figure 6.9 are (S_a, S_b, S_c). Figure 6.9 is simply another way of visualizing Figure 6.8; it is Figure 6.8 from a different frame of reference. As ωt increases in Figure 6.8, the voltage changes from one space-vector to the next in a counter-clockwise fashion in Figure 6.9, beginning with the (1,0,0) SV. In addition to the six switch states in Figure 6.9, there are two more possible states: (0,0,0) and (1,1,1). Both of these states make all three line-to-neutral voltages 0. They can be represented in a SV diagram such as Figure 6.9 by two points located at the origin. The eight possible SV's are called the "base space-vectors," as they are the basis for synthesizing other space-vectors. For simplicity's sake, the base SVs will be named as shown in Figure 6.10.

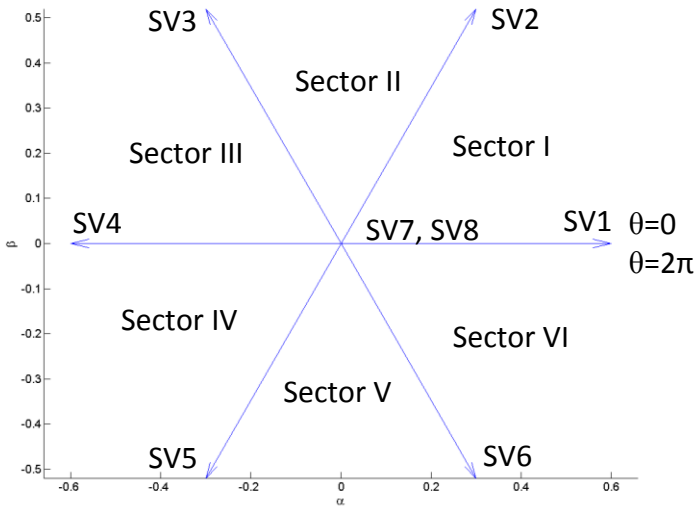

Figure 6.10 Base SVs with Naming Conventions

The sector numbers in Figure 6.10 can be used to keep track of the range of ωt for a given instant. It should be noted that SV7=(1,1,1) and SV8=(0,0,0).

Like a passive rectifier, an active rectifier using 180^{o} modulation does not allow for any control of the voltage or current. However, unlike a passive rectifier, a controller can be designed to turn the switches of an active rectifier on and off at will. That is, a controller can choose which of the base space-vectors in Figure 6.10 is active at any time. If the capacitor in Figure 6.4 is large enough so that V_{DC} varies slowly with respect to the switching of space-vectors, an active rectifier can set the voltage at the terminals of a generator, or an inverter can set the voltage at its terminals. This is the principle behind SVPWM.

SVPWM was first developed by H.W van der Broeck and others in the 1980's [62]. The formulation used in this thesis is very similar to their original one. Consider Figure 6.11.

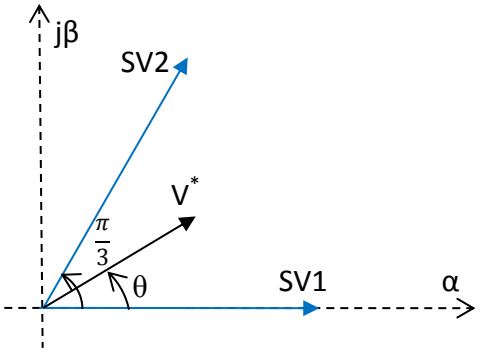

Figure 6.11 SVPWM in Sector I

Suppose it is desired that $\mathbf{V}^*$ be the voltage SV at the terminals of an electric machine. Because the only possible SVs when using a 3-phase bridge are given in Figure 6.10, the controller cannot simply turn a set of switches on and realize $\mathbf{V}^*$. However, SVPWM makes it possible to achieve an *average* SV of $\mathbf{V}^*$. A useful definition for the average SV that results from switching between two adjacent base SVs and the zero SVs is given by [63]:

$$d_x \cdot SV1 + d_y \cdot SV2 = \boldsymbol{V}^* = mVe^{j\theta} \tag{6.10}$$

and

$$d_x + d_y + d_0 = 1. \tag{6.11}$$

d_x, d_y, and d_0 in (6.10) and (6.11) are the duty cycles of the space-vectors being used to realize $\mathbf{V}^*$. Let the period over which the average SV is desired to be $\mathbf{V}^*$ be T_s seconds. Then for Sector I,

$$\begin{aligned} d_1 &\triangleq \frac{Time\ that\ SV1\ is\ active}{T_s} \\ d_2 &\triangleq \frac{Time\ that\ SV2\ is\ active}{T_s} \\ d_0 &\triangleq \frac{Time\ that\ SV7\ and\ SV8\ are\ active}{T_s}. \end{aligned} \tag{6.12}$$

Of course, if $\mathbf{V}^*$ were in a sector other than Sector I, base space-vectors other than SV1 and SV2 would be used. Also, in (6.10), m is called the "modulation index," and it is defined as:

$$m = \frac{V}{V_{DC}}. \tag{6.13}$$

As in most power electronics applications, m must be between 0 and 1. However, using a linear technique, such as that described by (6.10) and (6.11), for SVPWM puts an upper bound on m that is less than 1 [59]. Recall from Chapter 4 that a balanced, 3-phase, sinusoidal signal is the same as a constant-magnitude SV that rotates smoothly in a circular fashion around the αβ plane. If the goal of SVPWM is to approximate a constant-magnitude voltage SV at the terminals of the machine, then the average SV must rotate smoothly and have constant magnitude. Figure 6.12 shows the SV diagram for when $\mathbf{V}^*$ is halfway between SV1 and SV2, and its magnitude is as large as possible. In other words, $d_1 = d_2 = 0.5$ and $d_0 = 0$ in order to satisfy (6.11). Then from (6.10):

$$0.5 \cdot \frac{2V_{DC}}{3} + 0.5 \cdot \frac{2V_{DC}}{3} e^{\frac{j\pi}{3}} = \frac{\sqrt{3}}{3} V_{DC} e^{\frac{j\pi}{3}}. \tag{6.14}$$

Equation (6.11) can be satisfied with $d_0 = 0$ many other ways, but the magnitude of $\mathbf{V}^*$ will be greater than $\frac{\sqrt{3}}{3} V_{DC}$ for every case except that in (6.14). For example, if $d_1 = 0.25,\ d_2 = 0.75$ and $d_0 = 0$,

$$0.25 \cdot \frac{2V_{DC}}{3} + 0.75 \cdot \frac{2V_{DC}}{3} e^{\frac{j\pi}{3}} = \frac{\sqrt{13}}{6} V_{DC} e^{j0.2426}. \tag{6.15}$$

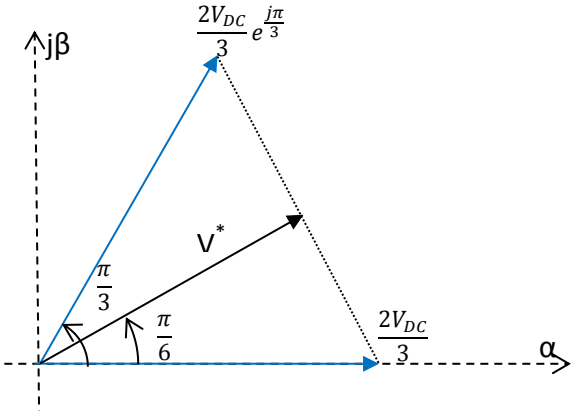

Figure 6.12 SVPWM in Sector I Example

Therefore, in order that the average of $\mathbf{V}^*$ traces out a circle around the αβ plane with constant magnitude,

$$0 \leq m \leq \frac{\sqrt{3}}{3}. \tag{6.16}$$

Equation (6.16) is visualized in Figure 6.13, where the dashed circle represents the path of $\mathbf{V}^*$ with $m = \frac{\sqrt{3}}{3}$ [59]. V_{DC} is normalized in Figure 6.13.

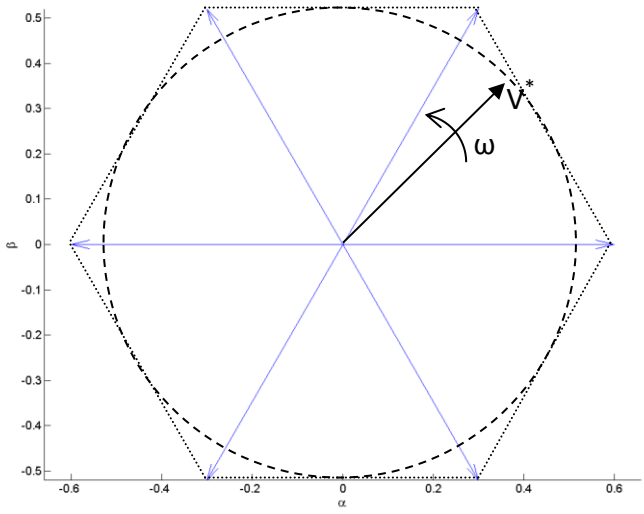

Figure 6.13 SV Diagram Showing the Upper Bound of Linear SVPWM

In order to effectively use SVPWM, the controller must be able to synthesize any $\mathbf{V}^*$ average along the circle in Figure 6.13. This means that d_1 and d_2 must be found for every $\mathbf{V}^*$. In Figure 6.11 the angle of $\mathbf{V}^*$ (θ) was measured with respect to the α axis. Let θ_{rel} be defined as the angle of a desired average SV, $\mathbf{V}^*$, with respect to the nearest base SV in the clockwise direction. This is shown in Figure 6.14 for Sector II.

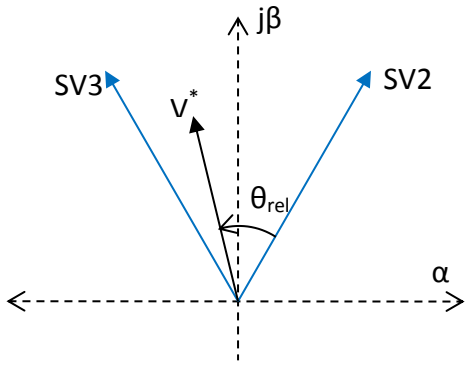

Figure 6.14 Definition of θ_{rel}

A general solution can be found for d_x, d_y, and d_0 in terms of the length of m and θ_{rel}. For operation in a given sector, let d_x be the duty cycle of the more clockwise base SV, and d_y be that for the more counterclockwise one. Let d_0 be the duty cycle for the zero SV, which could be any combination of SV7 and SV8. From (6.10):

$$\boldsymbol{V}^* = mV_{DC}e^{j\theta_{rel}} = mV_{DC}[\cos(\theta_{rel}) + jsin(\theta_{rel})] = d_x\frac{2V_{DC}}{3} + d_y\frac{2V_{DC}}{3}e^{\frac{j\pi}{3}}$$

$$= d_x\frac{2V_{DC}}{3} + d_y\frac{V_{DC}}{3} + j\left(d_yV_{DC}\frac{\sqrt{3}}{3}\right). \tag{6.17}$$

When (6.17) is resolved into its real and imaginary components the result is:

$$m\cdot\cos(\theta_{rel}) = d_x\frac{2}{3} + d_y\frac{1}{3} \tag{6.18}$$

and

$$m\cdot\sin(\theta_{rel}) = d_y\frac{1}{\sqrt{3}} \rightarrow d_y = \sqrt{3}m\cdot\sin(\theta_{rel}). \tag{6.19}$$

Substituting (6.19) into (6.18) and solving for d_x gives:

$$d_x = \sqrt{3}m\cdot\cos\left(\theta_{rel} + \frac{\pi}{6}\right). \tag{6.20}$$

Finally, from (6.11) it follows that:

$$d_0 = 1 - d_x - d_y. \tag{6.21}$$

It is common in the literature to find m defined such that $\boldsymbol{V}^* = mV_{max}e^{j\theta_{rel}}$, where V_{max} is the base space-vector length. If that is the case, d_x and d_y can be found with a slightly simpler computation [64, pp. 254-265] [65]. However, this author feels that defining m as (6.13) is more intuitive and aligns better with other PWM schemes.

One of the reasons that SVPWM is used in this thesis is that it lends itself very well to controlling variables in a rotating reference frame. For instance, there may be a certain dq voltage that is desired in order to control d-axis and q-axis current of a machine. That dq voltage setpoint can be referred to the stator through an inverse Clarke Transform to obtain a $V_{\alpha\beta}$ setpoint ($\mathbf{V}^*$). Then m and θ_{rel} can be determined and the duty cycles calculated with (6.19) - (6.21).

After the duty cycles are found, the appropriate gating signals can be applied to the IGBTs. Because the sector must be found as part of finding θ_{rel}, the two base space-vectors (SV_x and SV_y) for a given averaging period (T_s) are known. The simplest way to synthesize $\mathbf{V}^*$ is to gate the IGBTs associated with SV_x for the first d_x*T_s seconds of the averaging period, and then gate the SV_y IGBTs for the next d_y*T_s seconds. Finally, any combination of SV7 and SV8 is gated for the remaining time in the averaging period (d_0*T_s). This is shown in Figure 6.15 for an arbitrary $\mathbf{V}^*$ in Sector I.

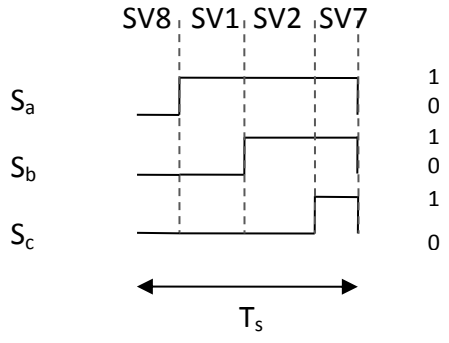

Figure 6.15 Simple SVPWM Switching Pattern

However, there are many other ways to distribute the switching through a switching period, which is the subject of the following section.

6.4 Improved SVPWM Switching Patterns

In any pulse-width-modulated power electronic device, lower switching frequency means lower losses. This is because solid-state switches don't turn on and off instantaneously and they dissipate power during the transitions. Recall, though, that in order for torque to be constant, the phase currents must be sinusoidal and balanced. The less sinusoidal the phase currents, the greater their total harmonic distortion (THD). THD is a measure of how similar a signal is to a pure sinusoid and it is defined as [57, p. 359]

$$THD = \frac{1}{I_1}\left(\sum_{n=2,3,\ldots}^{\infty} I_n^2\right)^{1/2}, \tag{6.22}$$

where n denotes the harmonic number. Low THD is desirable because one of the stated goals of this rectifier is to force the machine to have nearly constant torque. Two different switching patterns are presented here: one that reduces switching frequency and one that reduces THD.

Figure 6.15 shows that only one switch leg (2 IGBTs that are vertically aligned in Figure 6.4) changes state during each transition. However, when a new averaging period begins, all three legs must change states. Therefore there are three turn-on operations and three turn-off operations every cycle. The simple type of SVPWM switching is the benchmark against which the two improved schemes are compared to below.

6.4.1 Switching to minimize losses

As discussed above, lowering the switching frequency reduces the losses in any power electronic circuit. The "low-loss" scheme shown for Sector I in Figure 6.16 cuts the effective switching frequency in half [65].

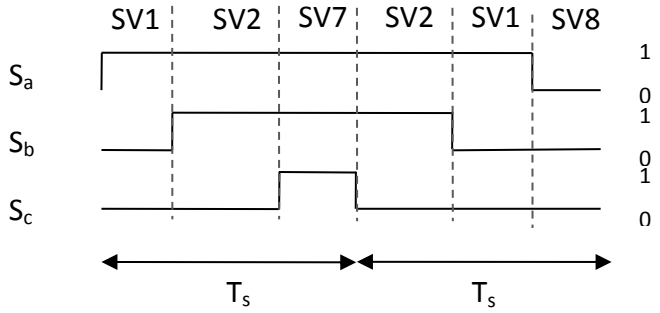

Figure 6.16 Low-Loss SVPWM Switching Pattern in Sector I

From Figure 6.16 it is clear that there are either three turn-on's or three turn-off's every cycle, meaning the effective switching frequency is halved. Because the switching frequency is halved, the losses should be approximately halved as well. One clear downside to this pattern is that it is more complicated to implement due to the necessity to reverse the order of the SVs and change the zero SV every switching cycle. Another consideration is that the order of the zero SVs should be swapped for every other sector. Figure 6.17 uses an example in Sector II to show why this is necessary.

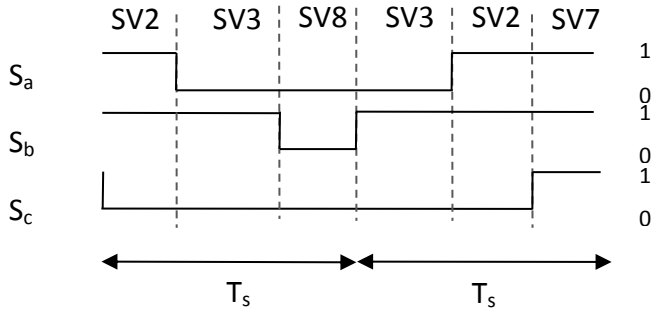

Figure 6.17 Low-Loss SVPWM Switching Pattern in Sector II

Clearly if the zero SVs' order had not been swapped between Figure 6.16 and Figure 6.17 there would have been more than three switching actions every cycle. The other downside to low-loss switching is that there will be harmonics at half of the switching frequency. Those lower-frequency harmonics will not be filtered as well by the machine's inductance, resulting in higher THD and less-constant torque.

6.4.2 Switching to minimize THD

Though it is not immediately obvious, a switching pattern that is more symmetrical than the previous two provides lower THD than they do. Such a symmetrical pattern is shown in Figure 6.18.

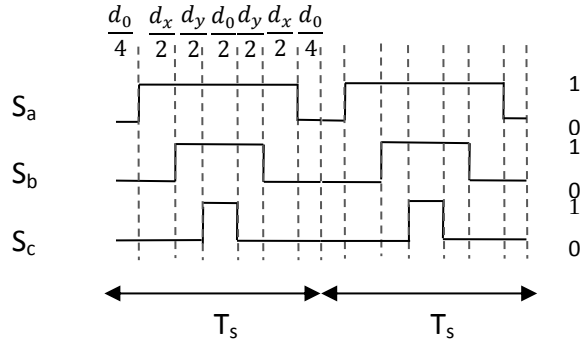

Figure 6.18 Symmetrical SVPWM Switching Pattern in Sector I

Figure 6.18 shows that there are three turn-on's and three turn-off's every cycle, so the losses should be similar to the simple pattern. For the same reasons as the low-loss pattern, either the zero SVs should be swapped or the order of d_x and d_y should be reversed for every other sector in order to avoid extraneous switching. This pattern will produce significant harmonics at integer multiples of the switching frequency, making filtering by the machine's inductance relatively easier than when low-loss switching is used. This is the switching pattern used for all of the converters in this thesis.

Chapter 7 - Torque and Speed Control of Permanent-Magnet Synchronous Generators

The generator-side control scheme's ultimate goal is to control the speed of the generator. Controlling generator speed allows a controller such as the one proposed in [11] to capture as much power as possible from the wind. Recall (5.4), repeated below as (7.1), which describes the rotational dynamics of a wind turbine,

$$\dot{\omega_r} = \frac{1}{J}(\tau_e - C_D\omega_r - \tau_{aero}). \tag{7.1}$$

The inertia and damping coefficients are obviously not controllable. τ_{aero}, the torque on the generator shaft due to the wind, could be controlled by changing the blade pitch, but that is left for a later section. For now, assume that the blade pitch is fixed. Therefore, the term in (7.1) that can be used to control generator speed is τ_e, the generator torque. A high-level representation of the generator-side control scheme is shown in Figure 7.1. All of the variables in Figure 7.1 have been defined in previous chapters except CCT_1 and CCT_2, which are defined below. Variables with "*" superscripts in Figure 7.1 are setpoints.

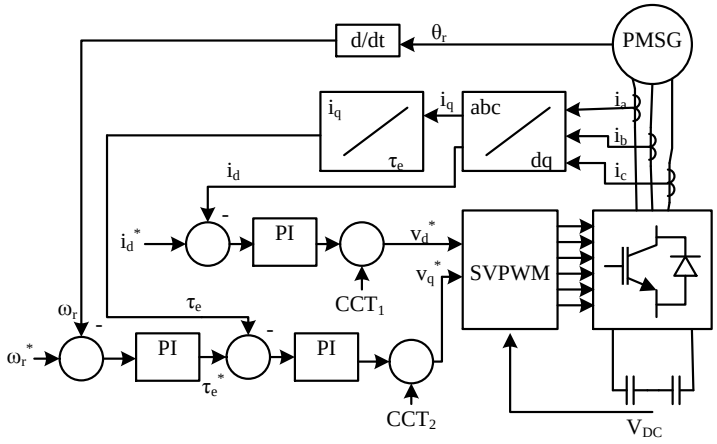

Figure 7.1 Generator-Side Control Scheme

7.1 Torque Control

To understand how torque can be controlled, consider (5.43), which is repeated here,

$$\tau_e = \frac{3}{2}p\psi i_q. \tag{7.2}$$

Recall from Section 5.3 that one of the conditions that a given PMSG must meet in order to work with the controllers presented here is that it must be non-salient. Equation (5.43) can be rearranged to solve for i_q and substituted into (5.42) with the result:

$$v_q = \frac{2R\tau_e}{3p\psi} + L_s\left(\frac{2}{3p\psi}\frac{d\tau_e}{dt} + p\omega_r i_d\right) + p\omega_r\psi. \tag{7.3}$$

Because neither ω_r nor i_d are constant, (7.3) is a nonlinear equation, so linear techniques cannot be used to design a controller for it. The approach that many designers of controller rectifiers have taken is to use a technique called "feedback linearization" [13] [51] [66]. This technique is sometimes called "decoupling" in the literature. The basic idea of feedback linearization is to design a controller for the linear part of the system, and then add the nonlinear term(s) to the output of the controller to find the control signal [67, p. 656]. The linear part of (7.3), neglecting the last term, can be written in the Laplace domain as

$$v_q(s) = \frac{2}{3p\psi}(R\tau_e(s) + sL_s\tau_e(s)). \tag{7.4}$$

Equation (7.4) can then be rearranged into transfer function form as

$$\frac{\tau_e(s)}{v_q(s)} = \frac{3p\psi}{2L_s s + 2R}. \tag{7.5}$$

Then (7.5) can be used with conventional linear design techniques, such as root locus or Bode, to design a controller. Using the 10kW system as an example, (7.5) has an open loop pole at -65.8. The MATLAB Control Systems Toolbox SISO Design Tool was used to design a parallel proportional-integral (PI) controller for (7.5). A parallel PI controller has the transfer function

$$G(s) = \frac{K_P\left(1 + \frac{K_I}{K_P}\right)}{s}. \tag{7.6}$$

K_P and K_I were selected to be 7 and 10.5 respectively for the 10 kW system so that the resulting closed loop system poles are at -0.666 and -4.71*10^4. Because both poles are real and negative, the system will be stable and well-damped. The step response for the closed loop linear part of the 10kW system is shown in Figure 7.2.

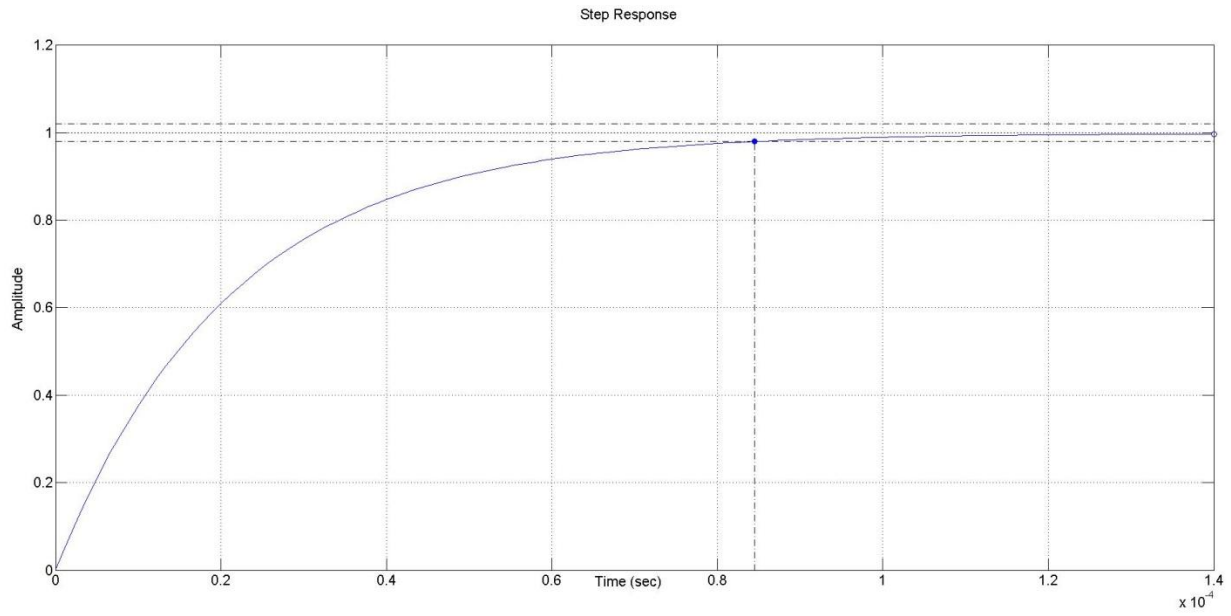

Figure 7.2 Torque Controller Step Response

Then the nonlinear part of (7.3), cross-coupling term 2 (CCT_2) can be added to the output of the PI;

$$CCT_2 \triangleq L_s(p\omega_r i_d) + p\omega_r \psi. \tag{7.7}$$

Thus, v_q is used to control generator torque, but what is v_d used for? Because torque is only dependent on i_q, i_d is left as a degree of freedom. One popular use for i_d in the literature is to simply make it 0 to minimize resistive losses in the machine [51] [68]. Other authors have used a slightly more sophisticated view of losses in the machine, taking more than just resistive losses into account, and thus used i_d to minimize losses [13]. A controller can be designed for i_d using feedback linearization to allow for these or virtually any other use for i_d. Considering only the linear parts of (5.41), repeated here:

$$v_d = Ri_d + L_s\left(\frac{di_d}{dt} - p\omega_r i_q\right), \tag{7.8}$$

the v_d-to-i_d transfer function can be found for the linear part of (7.8) as

$$\frac{i_d}{v_d} = \frac{1}{sL_s + R}. \tag{7.9}$$

The same design procedure as was used for the torque controller can be used here too, with

$$CCT_1 \triangleq -L_s\left(p\omega_r i_q\right). \tag{7.10}$$

The gains for the torque and i_d controllers for both the 10 kW and 5 MW systems are given in Table 5.

Table 5 Torque and i_d Controller Gains

Gain	10 kW	5 MW
K_p, torque control	7	0.01
K_I, torque control	10.5	20
K_p, i_d control	27	0.5
K_I, i_d control	1.2	0.12

Simulation results showing torque control for both systems can be found in Chapter 11.

7.2 Speed Control

As previously stated, the whole reason for controlling torque in a PMSG is so that the speed can then be controlled. Designing a speed controller is not quite as straightforward as designing a torque controller, however. Consider (5.4), repeated here:

$$\dot{\omega_r} = \frac{1}{J}(\tau_e - C_D\omega_r - \tau_{aero}). \tag{7.11}$$

It is not difficult to find a state space realization or a transfer function for (7.11) with ω_r as the output, but in both cases the input must be the difference between τ_e and τ_{aero}. While it is possible to affect τ_{aero} by changing the pitch angle of the blades or the yaw angle of the tower, those are not practical options for most turbines, especially small ones. Even with pitch and active yaw controls, estimating τ_{aero} would be very difficult as it may require taking quantities like blade torsion into account. Therefore, the "black art" of designing a linear controller using only τ_e was employed to realize speed control. The design was completed iteratively by starting the with PI's zero close to the jω axis, then progressively moving it left (more negative) in the complex plane until a satisfactory response was obtained. As a general rule, the more negative the real part of a PI zero, the faster the response. To further complicate matters, v_q (used to control τ_e) is limited by the DC link voltage. It is quite possible for the control system to reach that limit by trying to change the rotor speed too quickly. This is dealt with in two ways: first, the rate at which the controller is allowed to change the rotor speed setpoint is limited. This is quite practical in fact because the rotor generally does not need to change its speed very quickly. The

second is to employ anti-windup on the integral control. When the limit placed on the output of the integrator is reached, it saturates, the integrator is clamped at the saturation value. A PI with clamping is shown in block diagram form in Figure 7.3.

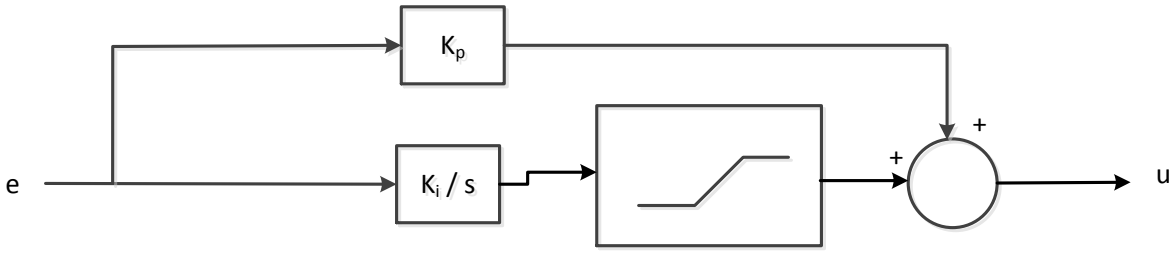

Figure 7.3 PI Controller with Anti-Windup

For the speed controller, e in Figure 7.3 is $\omega_r^* - \omega_r$ and u is τ_e^*. If the maximum rated generator torque is specified by the manufacturer, that should be the level at which the speed controller saturates. If that maximum rated torque is not known, it can be estimated based on the generator's maximum power and voltage ratings,

$$\hat{I} = \sqrt{\frac{2}{3}} \frac{S_{max}}{V_{LL,max}}. \tag{7.12}$$

Assuming $i_d = 0$, $i_q = \hat{I}$. Then (7.12) can be substituted into (5.43) to find an estimate for the machine's maximum torque,

$$\tau_{e,max} \cong \frac{3}{2} p\psi \sqrt{\frac{2}{3}} \frac{S_{max}}{V_{LL,max}}. \tag{7.13}$$

The controller parameters in were determined through the iterative process described above and presented in Table 6.

Table 6 Speed Controller Parameters

Parameter	10 kW Generator	5 MW Generator
K_P	900	$3*10^7$
K_I	12460	$1.5*10^7$
Saturation Level	-406 Nm	$-4.44*10^6$ Nm

Results showing the speed being arbitrarily controlled are presented in Chapter 11.

7.2.1 Blade Pitch Controller for 5 MW system

In order to prevent the turbine from failing mechanically, the amount of power captured at high wind speeds must be limited. Essentially this means that some mechanism must be used to reduce the amount of wind incident to the blades to prevent them from failing or the generator from overheating. The 10 kW system has passive yaw, called furl, to control its power capture at high wind speeds. This means that if the wind gets too high, the turbine will yaw out of the wind as discussed in Chapter 2. This sort of passive control is not practical in commercial-scale wind turbines like the 5 MW system. Large wind turbines generally have two mechanisms to limit the amount of power they capture: blade pitch control and active yaw. Blade pitch control consists of changing the angle of the blades so that they catch less wind at high wind speeds. This is sometimes called "feathering" the blades. The aerodynamics behind this process are outside the scope of this thesis, but they can be found in [10, pp. 83-138]. If the wind speed is so high that even pitching the blades isn't sufficient to reduce the load on them, then the turbine can be yawed out of the wind and have its blades locked by a mechanical brake.

A blade pitch controller has been designed by Jonkman et. al for the NREL 5 MW turbine, which was based heavily on work by Hansen et. al. [25] [69]. That controller has been tuned for the 5 MW system in this thesis and implemented. The controller is a PI-type with gain scheduling based on the blade pitch. The same gain schedule was used in the 5 MW system as was used by Jonkman et. al [25]. The controller gains for the 5 MW system in this thesis are K_p=-0.617484 and K_I=-1.32318. Simulation results showing the validity of the pitch controller are provided in Chapter 11.

Chapter 8 - Filter and Inverter Control Design

As mentioned in Chapter 6 it is most common for the DC link voltage to be controlled by the inverter, which is how the systems in this thesis operate. Therefore a control system must be designed in order to keep the DC link voltage somewhat steady at a level that is appropriate for controlling both the PMSG and the power injected into the grid. A filter must be used in order to reduce harmonic content in the inverter's output to acceptable levels and a transformer is needed to provide isolation between the inverter and the grid. A schematic for the inverter, filter, transformer, and grid is shown in Figure 8.1. The sensors needed for feedback signals are also shown.

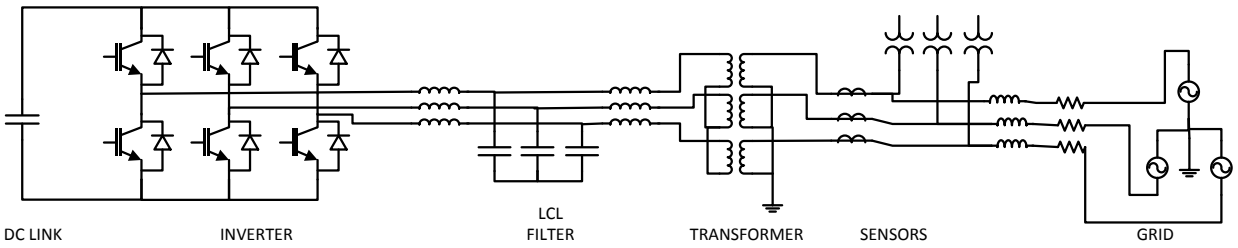

Figure 8.1 Inverter, Filter, Transformer, and Grid Schematic

The first subsection of this chapter will discuss the design of LCL filter, and the second subsection will explore the design of the phase-locked loop needed for the controller. Next, expressions for active and reactive power will be formulated in the synchronous reference frame. Finally, controller design for reactive power and DC link voltage will be presented.

8.1 LCL Filter Design and Transformer

As discussed in Chapter 6, it is necessary to use a filter in order to reduce the harmonics injected to the grid to acceptable levels. The simplest type of filter that can be used is a purely inductive one. However, it may take an unreasonably large inductor to provide enough filtering [70]. Therefore, many designers have chosen to use an LCL filter such as the one shown in Figure 8.1 instead [71] [72] [73] [74]. Lowpass LCL filters provide 60 dB/dec of attenuation, so they are more effective at filtering harmonics with smaller component values than lower-order filters.

They have an inherent weakness, though, around their resonant frequency. Consider Figure 8.2 where a single phase of the filter with a resistor in series with the capacitor is shown.

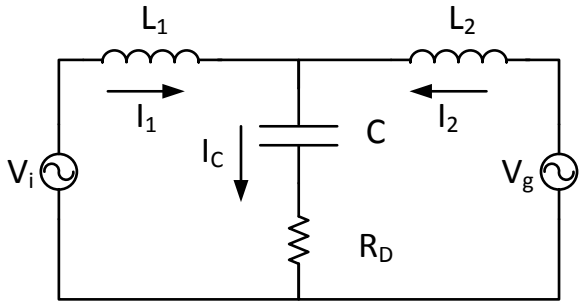

Figure 8.2 Single Phase of an LCL Filter with Passive Damping

Let three state variables be defined as:

$$\begin{aligned} x_1 &= I_1 \\ x_2 &= I_2 \\ x_3 &= q_c, \end{aligned} \tag{8.1}$$

where q_c is the capacitor's charge. And inputs:

$$\begin{aligned} u_1 &= V_i \\ u_2 &= V_g. \end{aligned} \tag{8.2}$$

Then, the following state space formulation can be found from two KVL equations for Figure 8.2:

$$\begin{bmatrix} \dot{x_1} \\ \dot{x_2} \\ \dot{x_3} \end{bmatrix} = \underbrace{\begin{bmatrix} -\frac{R_D}{L_1} & -\frac{R_D}{L_1} & \frac{-1}{CL_1} \\ -\frac{R_D}{L_2} & -\frac{R_D}{L_2} & -\frac{1}{CL_2} \\ 1 & 1 & 0 \end{bmatrix}}_{\text{(F)}} \begin{bmatrix} x_1 \\ x_2 \\ x_3 \end{bmatrix} + \underbrace{\begin{bmatrix} \frac{1}{L_1} & 0 \\ 0 & \frac{1}{L_2} \\ 0 & 0 \end{bmatrix}}_{\text{(G)}} \begin{bmatrix} u_1 \\ u_2 \end{bmatrix} \tag{8.3}$$

$$y = \underbrace{\begin{bmatrix} 1 & 0 & 0 \\ 0 & 1 & 0 \end{bmatrix}}_{\text{(H)}} \begin{bmatrix} x_1 \\ x_2 \\ x_3 \end{bmatrix}. \tag{8.4}$$

The transfer functions can then be found with the equation [67, p. 465]:

$$TF(s) = H[sI - F]^{-1}G. \tag{8.5}$$

Using (8.5) to find the transfer functions of (8.3) and (8.4) gives:

$$\frac{I_1(s)}{V_i(s)} = \frac{s^2 + \frac{sR_D}{L_2} + \frac{1}{L_2C}}{s^3L_1 + s^2\frac{R_D(L_1 + L_2)}{L_2} + s\frac{L_1 + L_2}{L_2C}} \tag{8.6}$$

and

$$\frac{I_2(s)}{V_i(s)} = \frac{-\left(\frac{sR_D}{L_2} + \frac{1}{L_2C}\right)}{s^3L_1 + s^2\frac{R_D(L_1 + L_2)}{L_2} + s\frac{L_1 + L_2}{L_2C}} \tag{8.7}$$

Equation (8.6) is called the "forward self-admittance", while (8.7) is known as the "forward transadmittance." The resistor in series with the capacitor in Figure 8.2 is a form of passive damping [75, p. 302] [76]. To illustrate the need for that resistor, consider what (8.6) becomes if $R_D = 0$,

$$\frac{I_1(s)}{V_i(s)} = \frac{s^2 + \frac{1}{L_2C}}{s^3L_1 + s\frac{L_1 + L_2}{L_2C}}. \tag{8.8}$$

As an example, let $L_1 = 10\ mH, L_2 = 2\ mH$, and $C = 10\ \mu F$. The resulting system has a pole at the origin and complex conjugate poles on the jω axis of the complex plane, so the system is oscillatory. The problem with this system is also clearly seen in the Bode plot in Figure 8.3.

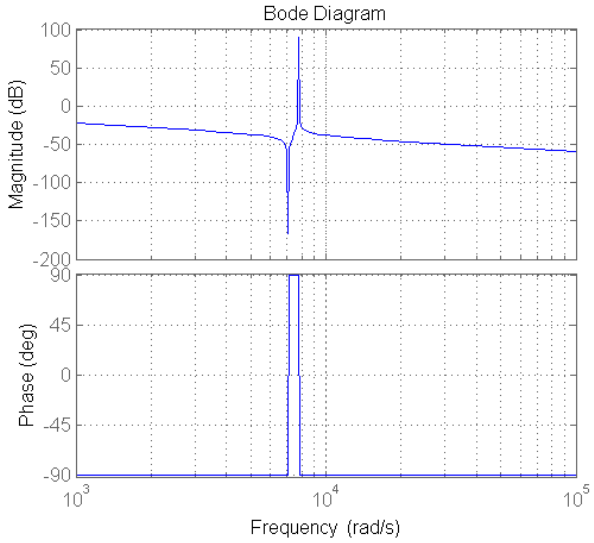

Figure 8.3 LCL Exemplar Bode Plot

Clearly there is a resonant peak around 7.5 kHz. The resonant frequency can be calculated from [70]:

$$\omega_{res} = \sqrt{\frac{L_1 + L_2}{L_1 L_2 C}}, \tag{8.9}$$

which works out to 7.746 kHz for the values above. This means that if there was a component of the inverter voltage at or near 7.746 kHz (which is likely), very high currents would flow through the filter, which is undesirable for obvious reasons. In contrast, Figure 8.4 shows the system's Bode plot if $R_D = 5\ \Omega$. The damped system has only a small "blip" around the resonant frequency. Including the damping resistor does increase the losses in the filter, which can be calculated by [75, p. 303]

$$P_{loss} = \frac{3}{R_D} \sum_h \left[v_c(h) - v_g(h) \right]^2, \tag{8.10}$$

where h is the harmonic number, v_c is the capacitor voltage, and v_g is the grid voltage. There are alternate methods to passive damping called "active damping" that use control techniques to reduce the resonant effect, but they were not considered for this thesis [75, pp. 304-306].

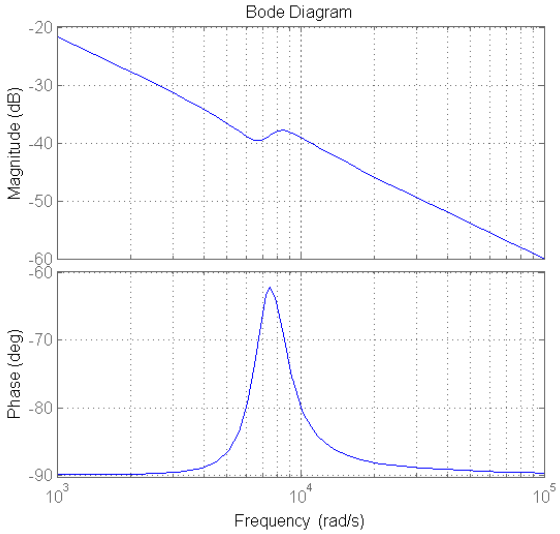

Figure 8.4 LCL with Passive Damping Exemplar Bode Plot

A procedure for designing LCL filters published by Lisesrre, Blaabjerg, and Hansen was used as a guide for the filters designed for this thesis [70]. The procedure is written in terms of base impedance and base capacitance, which are defined as [70]

$$Z_b = \frac{(V_g)^2}{P_n} \tag{8.11}$$

and

$$C_b = \frac{1}{\omega_n Z_b}, \tag{8.12}$$

where the subscript "n" denotes nominal quantities. There are four basic guidelines for the design of the filter [70]:

1. $C <$ 5% of C_b to limit the power factor decrease at rated power.
2. $L_1 + L_2 < 0.1$ p.u to limit AC voltage drop.
3. $10\omega_{line} < \omega_{res} < \frac{1}{2}\omega_s$, where ω_s is the inverter's switching frequency and ω_{line} the grid frequency (both in rad/s), to avoid resonance issues.
4. R_D must be chosen so as to avoid oscillation but not decrease efficiency too much.

For the 10 kW system:

$$Z_b = \frac{(208\ V)^2}{10\ kW} = 4.3264\ \Omega, \tag{8.13}$$

$$L_b = \frac{4.3264}{2\pi 60} = 11.476\ mH, \tag{8.14}$$

and

$$C_b = \frac{1}{2\pi 60 * 4.3264} = 613.115\ \mu F. \tag{8.15}$$

For the 5 MW system:

$$Z_b = \frac{(650)^2}{6\ MVA} = 0.704\ \Omega, \tag{8.16}$$

$$L_b = \frac{0.704}{2\pi 60} = 186.786\ \mu H, \tag{8.17}$$

and

$$C_b = \frac{1}{2\pi 60 * 3.2} = 828.932\ \mu F. \tag{8.18}$$

Satisfactory values for the 10 kW system filter were found using the guidelines above. Those values are given in Table 7. The resonant frequency was slightly higher than recommended (24943.9 rad/s vs. 21991.5 rad/s), but no resonance problems were seen in the results. Also, when the transformer was introduced to the system the filter values were not changed, making the per unit values of L_1 and L_2 large. However, no adverse effects were observed so the design is still valid.

Table 7 10 kW System LCL Filter Values

Parameter	10 kW
f_s	7 kHz
L_1	0.574 mH
L_2	0.574 mH
C	5.6 μF
R_D	5 Ω
ω_{res}	24943.9 rad/s

The Bode plot for the 10 kW system's filter is shown in Figure 8.5. The filter has poles at the origin and -8711 ± j23374, so it is stable.

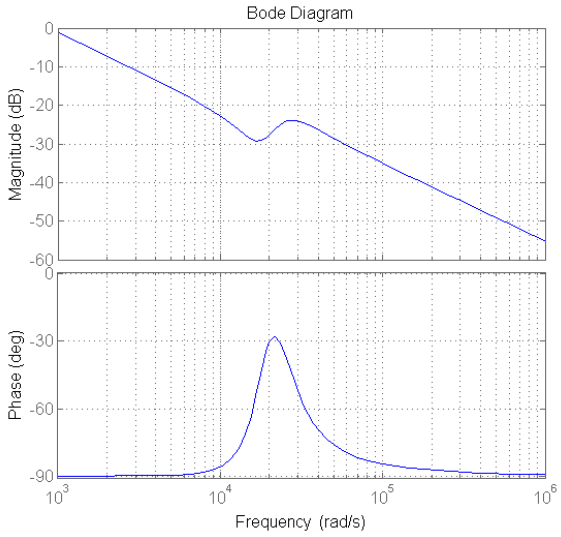

Figure 8.5 10 kW System Filter Bode Plot

The design of the filter for the 5 MW system was more complicated than that for the 10 kW system. It is common practice to use relatively low switching frequencies for utility-scale systems in order to minimize losses. The tradeoff, though, is that a larger filter is necessary in order to meet the requirements for harmonics given in IEEE 519-1992 [77]. Also, the losses from the damping resistor become more important at high power levels, so additional components are sometimes uses to mitigate them [76]. Figure 8.6 shows the LCL filter with an additional

inductor in parallel with R_D to minimize the losses from it at low frequencies. This is called "selective lowpass damping."

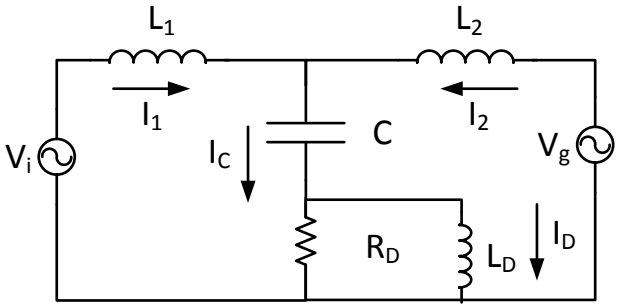

Figure 8.6 LCL Filter with Selective Lowpass Damping

In much the same way as above, a state space formulation for this filter can be found as

$$\begin{bmatrix} \dot{x_1} \\ \dot{x_2} \\ \dot{x_3} \\ \dot{x_4} \end{bmatrix} = \begin{bmatrix} -\frac{R_D}{L_1} & -\frac{R_D}{L1} & \frac{R_D}{L_1} & -\frac{1}{L_1 C} \\ -\frac{R_D}{L_2} & -\frac{R_D}{L_2} & \frac{R_D}{L_2} & -\frac{1}{L_2 C} \\ \frac{R_D}{L_D} & \frac{R_D}{L_D} & -\frac{R_D}{L_D} & 0 \\ 1 & 1 & 0 & 0 \end{bmatrix} \begin{bmatrix} x_1 \\ x_2 \\ x_3 \\ x_4 \end{bmatrix} + \begin{bmatrix} \frac{1}{L_1} & 0 \\ 0 & \frac{1}{L_2} \\ 0 & 0 \\ 0 & 0 \end{bmatrix} \begin{bmatrix} u_1 \\ u_2 \end{bmatrix} \tag{8.19}$$

$$y = \begin{bmatrix} 1 & 0 & 0 & 0 \\ 0 & 1 & 0 & 0 \end{bmatrix} \begin{bmatrix} x_1 \\ x_2 \\ x_3 \\ x_4 \end{bmatrix}, \tag{8.20}$$

where

$$\begin{aligned} I_1 &= x_1 \\ I_2 &= x_2 \\ I_D &= x_3 \\ q_c &= x_4, \end{aligned} \tag{8.21}$$

with the inputs still defined by (8.2). The forward self-admittance and forward transadmittance can be found in the same way as above. They are

$$\frac{I_1(s)}{V_i(s)} = \frac{s^3CL_2L_D + s^2R_D(L_2 + L_D) + sL_D + R_D}{s^4CL_1L_2L_D + s^3CR_D(L_1L_2 + L_1L_D + L_2L_D) + s^2L_D(L_1 + L_2) + sR_D(L_1 + L_2)} \quad (8.22)$$

and

$$\frac{I_2(s)}{V_1(s)} = \frac{-(s^2CL_DR_D + sL_D + R_D)}{s^4CL_1L_2L_D + s^3CR_D(L_1L_2 + L_1L_D + L_2L_D) + s^2L_D(L_1 + L_2) + sR_D(L_1 + L_2)}. \quad (8.23)$$

The four guidelines given above proved impossible to follow and still achieve sufficient harmonic attenuation for the 5 MW system. Therefore, an iterative process of varying the filter parameters and checking the performance via simulation was used, with (8.22) and (8.23) as guides. The final filter parameters are given in Table 8.

Table 8 5 MW LCL Filter Values

Parameter	**10 kW**
f_s	4 kHz
L_1	54.168 μH
L_2	54.168 μH
L_D	100 μH
C	2.6 mF
R_D	0.5 Ω

Though it is not shown this way in Figure 8.1, L_2 was considered to be the series inductance of the primary side of the transformer for each system. The transformer properties are given in Table 9.

Table 9 Transformer Properties

Property	10 kW System	5 MW System
V (primary)	90.13 V	650 V
V (secondary)	208 V	34.5 kV
Nominal power	20 kVA	6 MVA
Series resistance (primary)	0.0043264 Ω	211.25 μΩ
Series resistance (secondary)	$8.124*10^{-4}$ Ω	0.198375 Ω
Series inductance (primary)	0.574 mH	54.168 μH
Series inductance (secondary)	86.198 μH	526.21 μH
Magnetizing resistance	1086.6 Ω	99188 Ω
Magnetizing inductance	2.869 H	263.1 H

8.2 Phase-Locked Loop

As will be shown in the next sections, it is relatively easy to design controllers for a three-phase inverter in the synchronous (dq) reference frame. That is because all of the sinusoidal quantities become like DC values when the reference frame is rotating with the grid. As implied by Figure 8.1, all three line-to-neutral voltages and all three phase currents are measured in this system. Then, those quantities are referred to the synchronous reference frame (attached to the grid voltage) and used in controllers. In order to refer those variables to the synchronous reference frame, however, the grid angle must be known. The grid angle, ωt, becomes θ in (4.16), which is used to find the d- and q-axis values. It is the job of a phase-locked loop (PLL) to estimate the grid angle.

Interestingly, the dq transform is part of the process of grid angle estimation. The PLL used in this thesis is a modified version of the one contained in the "Discrete 3-phase PLL" Simulink block. The modified sub-blocks of that block are shown in Figure 8.7. Basically, the PLL in Figure 8.7 works by taking the dq transform of the three-phase voltage and adjusting θ until $v_q = 0$. At that point, the output of the PLL, ωt, will be synchronized with the zero crossings of phase A voltage. In other words, if one were to use (4.16) on the voltages, the result would be as if the voltages were defined as

$$\begin{bmatrix} v_a \\ v_b \\ v_c \end{bmatrix} \triangleq \hat{V} \begin{bmatrix} \sin(\omega t) \\ \sin\left(\omega t - \frac{2\pi}{3}\right) \\ \sin\left(\omega t + \frac{2\pi}{3}\right) \end{bmatrix} \tag{8.24}$$

from the perspective of the voltage measurements.

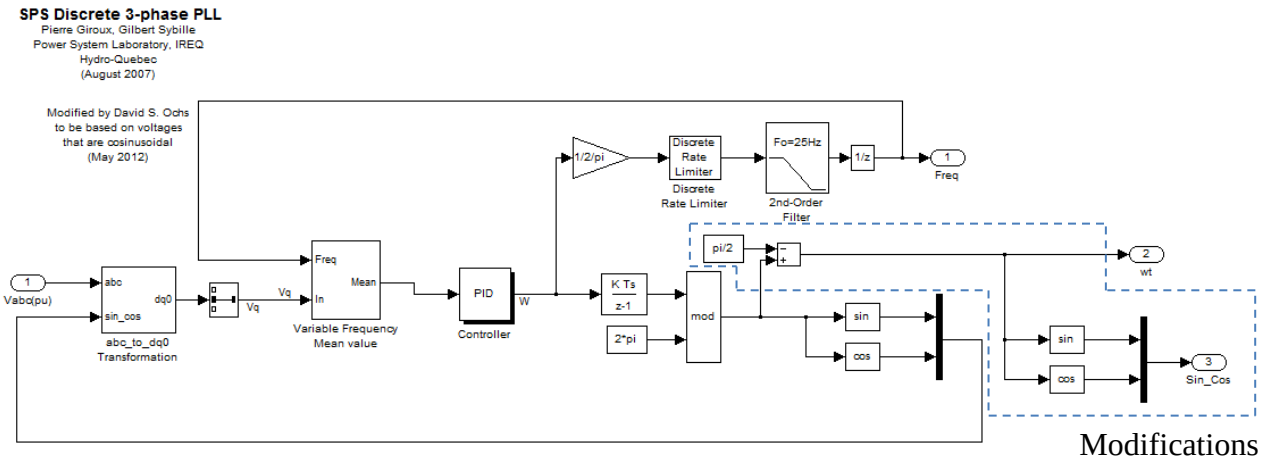

Modifications

Figure 8.7 Discrete PLL

For no other reasons but convenience and preference, this author defines the line-to-neutral voltage as

$$\begin{bmatrix} v_a \\ v_b \\ v_c \end{bmatrix} \triangleq \hat{V} \begin{bmatrix} \cos(\omega t) \\ \cos\left(\omega t - \frac{2\pi}{3}\right) \\ \cos\left(\omega t + \frac{2\pi}{3}\right) \end{bmatrix}. \tag{8.25}$$

This is why pi/2 has been subtracted from the original output in Figure 8.7. Doing so synchronizes ωt with the voltage peaks instead of the zero crossings, ensuring that the reference frame is oriented the proper way when (4.16) is used on the voltages. Sine and cosine of ωt are outputs of the PLL only because it reduces the number of blocks needed to implement (4.16). It should be noted that subtracting pi/2 from the output of the modulus block assumes that input voltages are purely sinusoidal. Because they are the grid voltages, this is generally a good assumption. This author has found that it is valid both in simulations and in lab tests [78].

8.3 Active and Reactive Power in the Synchronous Reference Frame

Consider the simplified model for the inverter and the grid in Figure 8.8, where the filter capacitor, the transformer, and the harmonic content of the inverter have been neglected.

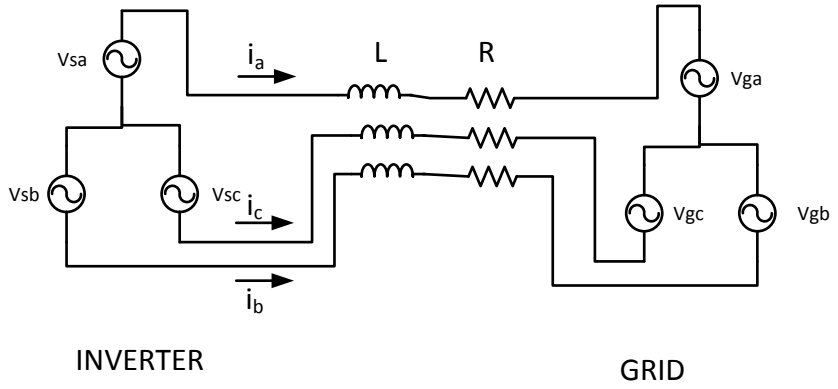

Figure 8.8 Simplified Inverter and Grid Circuit

Assuming that the circuit is balanced so no current flows through the neutral, a KVL equation can be written for each phase of the circuit,

$$\begin{bmatrix} v_{sa} \\ v_{sb} \\ v_{sc} \end{bmatrix} = \begin{bmatrix} R+L\rho & 0 & 0 \\ 0 & R+L\rho & 0 \\ 0 & 0 & R+L\rho \end{bmatrix} \begin{bmatrix} i_a \\ i_b \\ i_c \end{bmatrix} + \begin{bmatrix} v_{ga} \\ v_{gb} \\ v_{gc} \end{bmatrix}, \tag{8.26}$$

where ρ is the time derivative operator. Let the line-to-line voltages be defined as:

$$\begin{bmatrix} v_{ga} \\ v_{gb} \\ v_{gc} \end{bmatrix} \triangleq \hat{V} \begin{bmatrix} \cos(\omega t) \\ \cos\left(\omega t - \frac{2\pi}{3}\right) \\ \cos\left(\omega t + \frac{2\pi}{3}\right) \end{bmatrix}. \tag{8.27}$$

The combined Clark and Park Transform can be applied to (8.26) by multiplying every term by K from (4.16). Note that at this point, θ is arbitrary so this is a transformation to the arbitrary reference frame.

$$K\bar{v}_{iabc} = KRI\bar{\imath}_{abc} + KLpI\bar{\imath}_{abc} + K\bar{v}_{gabc} \tag{8.28}$$

where I is the identity matrix. Using the same reasoning as for (5.9), (8.28) may be rewritten as:

$$K\bar{v}_{iabc} = KRIK^{-1}\bar{\imath}_{dq} + KLpIK^{-1}\bar{\imath}_{dq} + K\bar{v}_{gabc}. \tag{8.29}$$

Because R is a scalar, $KRIK^{-1} = RI$. By the chain rule:

$$KLpIK^{-1}\bar{\imath}_{dq} = LK(pK^{-1})\bar{\imath}_{dq} + LKK^{-1}\left(p\bar{\imath}_{dq}\right), \tag{8.30}$$

where $KL = LK$ because L is a scalar. KpK^{-1} was found to be (5.14) for a PMSG. It can be easily adapted to this formulation by substituting ω, the grid angular frequency, for ω_e, the back-emf angular frequency of a PMSM:

$$pK^{-1} = \frac{dK^{-1}}{dt} = \begin{bmatrix} 0 & -\omega \\ \omega & 0 \end{bmatrix}. \tag{8.31}$$

Therefore, the KVL equations can be written in the synchronous reference frame as:

$$v_{sq} = Ri_q + \omega Li_d + L\dot{i_q} + v_{gq} \tag{8.32}$$

and

$$v_{sd} = Ri_d - \omega Li_q + L\dot{i_d} + v_{gd}. \tag{8.33}$$

Next, consider what v_{gq} and v_{qd} become when the combined Clark and Park Transform is applied to (8.27),

$$K\hat{V}\begin{bmatrix} \cos(\omega t) \\ \cos\left(\omega t - \frac{2\pi}{3}\right) \\ \cos\left(\omega t + \frac{2\pi}{3}\right) \end{bmatrix} = \begin{bmatrix} 0 \\ \hat{V} \end{bmatrix} = \begin{bmatrix} v_{gd} \\ v_{gq} \end{bmatrix}. \tag{8.34}$$

Similarly, if the line currents are defined as:

$$\begin{bmatrix} i_a \\ i_b \\ i_c \end{bmatrix} \triangleq \hat{I}\begin{bmatrix} \cos(\omega t + \gamma) \\ \cos\left(\omega t - \frac{2\pi}{3} + \gamma\right) \\ \cos\left(\omega t + \frac{2\pi}{3} + \gamma\right) \end{bmatrix}, \tag{8.35}$$

then

$$K\hat{I}\begin{bmatrix} \cos(\omega t + \gamma) \\ \cos\left(\omega t - \frac{2\pi}{3} + \gamma\right) \\ \cos\left(\omega t + \frac{2\pi}{3} + \gamma\right) \end{bmatrix} = \hat{I}\begin{bmatrix} -\sin(\gamma) \\ \cos(\gamma) \end{bmatrix} = \begin{bmatrix} i_d \\ i_q \end{bmatrix}. \tag{8.36}$$

The time domain expressions for 3-phase active and reactive power are [56, pp. 65-69]:

$$P = 3V_{LN}I\cos(\gamma) \tag{8.37}$$

and

$$Q = -3V_{LN}I\sin(\gamma), \tag{8.38}$$

where V_{LN} and I are rms values. Then, it can be shown from (8.34) and (8.36) that:

$$v_{gq}i_q = \hat{V}\hat{I}\cos(\gamma) \tag{8.39}$$

and

$$v_{gq}i_d = -\hat{V}\hat{I}\sin(\gamma). \tag{8.40}$$

By inspection (8.39) and (8.40) only differ from (8.37) and (8.38) by a scaling factor of 3/2. Therefore:

$$P = \frac{3}{2}v_{gq}i_q \tag{8.41}$$

and

$$Q = \frac{3}{2}v_{gq}i_d. \tag{8.42}$$

8.4 Reactive Power Control

Because v_q is set by the grid, as implied by (8.42), Q can be independently controlled by controlling i_d. This gives the inverter the ability to act as a STATCOM and support the grid voltage by sourcing or sinking VARs [14]. In a process very similar to that in Chapter 7, a feedback-linearized PI controller can be designed to control i_d. This practice is well-documented in the literature [13] [51] [71] [79]. Note: the references for this practice and for DC link voltage control may interchange the uses of i_d and i_q, because of differences in reference frame orientation. The linear part of (8.33), excluding v_{gq}, taken to the Laplace domain and rearranged into transfer function form is:

$$\frac{i_d}{v_{sd}} = \frac{1}{sL + R}. \tag{8.43}$$

The grid definitely has some inductance and resistance from the inverter's point of view, but it is very difficult to estimate what they may be. Therefore, the L and R used to design the controller are the total series inductance and series resistance of the filter and the primary of the transformer. The block diagram for reactive power controller is shown in Figure 8.9. Because of

the placement of the sensors, all of the voltage and current feedback signals must be referred to the primary (inverter-side) of the transformer before they can be used by the controllers.

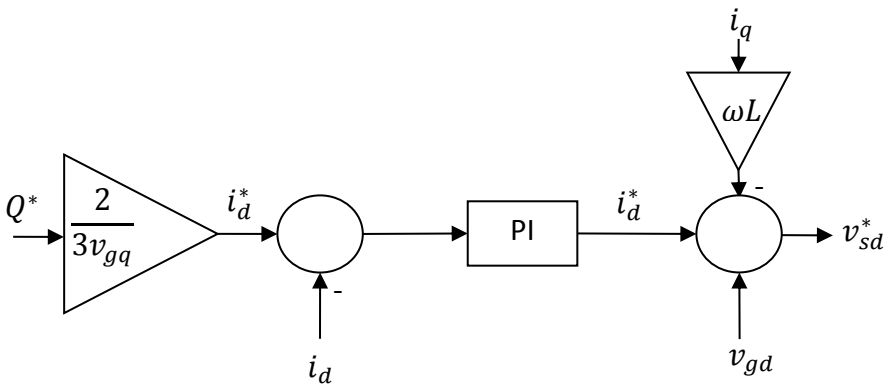

Figure 8.9 Reactive Power Controller Block Diagram

The PI gains can then be found in the same way as those in Section 7.1 and they are given in Table 10 for each system.

Table 10 Reactive Power Controller Gains

System	K_P	K_I
10 kW	0.24	0.85
5 MW	0.0106	0.148

8.5 DC Link Voltage Control

The previous section explained how i_d is used to control the reactive power output of the inverter. From examining (8.41) and (8.42), it seems logical that this section would be dedicated to how i_q is used to control the inverter's active power output. It is true, i_q is used to control P, but not directly. Instead, it is common practice to use i_q to regulate the DC link voltage [13] [51] [71] [75, pp. 221-226] [79]. Then, because of (8.41), the active power output of the inverter is also regulated. This is intuitive because if the DC link voltage stays constant, all of the energy output of the active rectifier must then be transferred to the inverter, less losses of course.

The V_{DC} controller is feedback-linearized and its block diagram is shown in Figure 8.10. Again, all voltage and current feedback signals must be referred to the primary of the transformer.

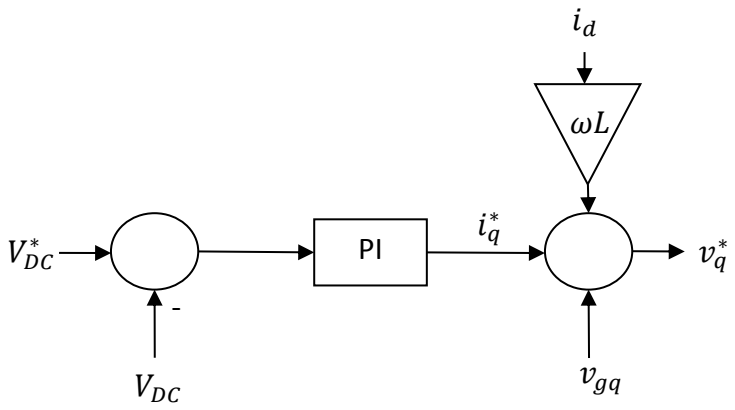

Figure 8.10 DC Link Voltage Controller Block Diagram

Unlike the reactive power controller, there is no easy way to find a linearized transfer function with which to find appropriate PI gains for this controller. Therefore, a technique developed by J.G. Ziegler and N.B. Nichols was used to find a good starting point for K_P and K_I [67, pp. 198-199]. To use the technique, the step response of the system must be known. The idea behind it is that many processes exhibit similar step responses. Ziegler and Nichols called this response a "process reaction curve" [67, pp. 198-199]. A general transfer function that exhibits such a curve is [67, p. 198]:

$$\frac{Y(s)}{U(s)} = \frac{Ae^{-st_d}}{\tau s + 1}. \tag{8.44}$$

The variables in (8.44) are defined in Figure 8.11, which shows an example of such curve.

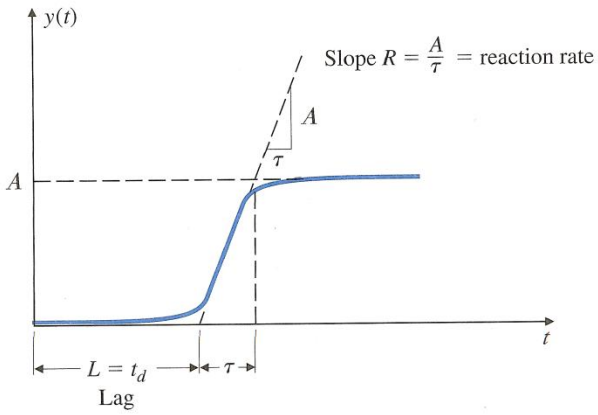

Figure 8.11 General Process Reaction Curve [67, p. 198]

The open-loop step response was found for the inverter and DC link for the 10 kW system with the turbine outputting 3 kW and the reactive power setpoint = 0. The response is shown in Figure 8.12. It is important to realize that the V_{DC} controller has what is called "reverse action" [80, p. 361]**.** A controller for a system with reverse action must have negative gains in order to function properly. To illustrate the reverse action of this system, consider an example: if the voltage is greater than the setpoint, i_q should increase in order to draw more current from the DC link capacitor, thereby lowering its voltage. The error, $V_{DC}^* - V_{DC}$, would be negative, so if the gains were positive, i_q would actually decrease, thereby making the error increase further. But if the gains were negative, i_q would increase, decreasing the size of the error. With that in mind, i_q^* (see Figure 8.10) was stepped from 4 to 3.8 at t=2.5 s to find the curve in Figure 8.12.

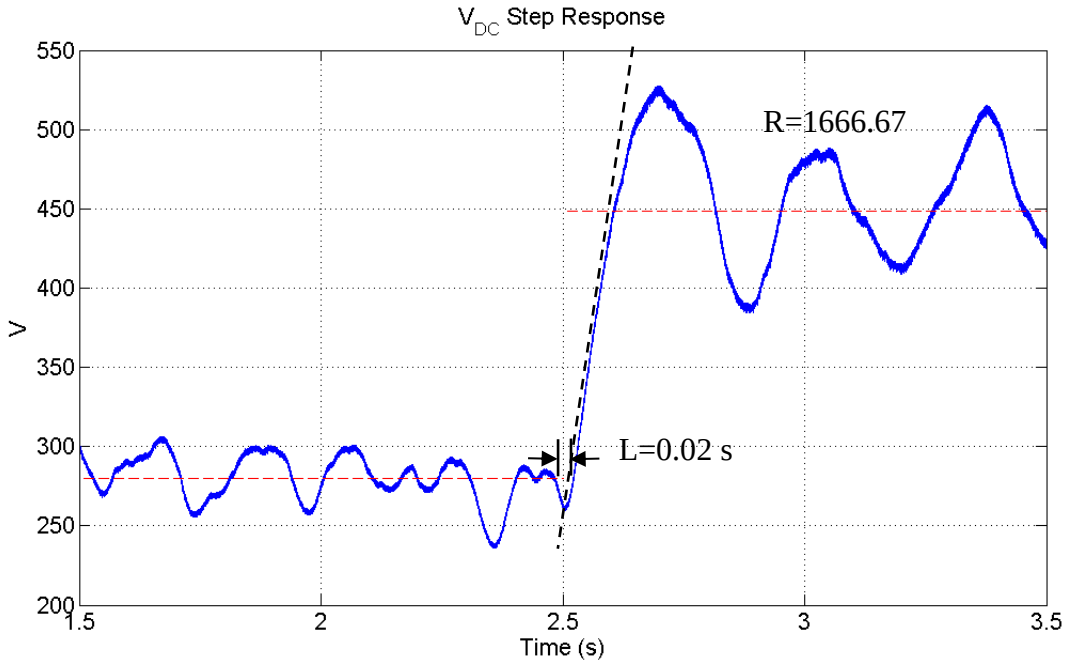

Figure 8.12 V_{DC} Closed-Loop Step Response – 10 kW System

Zeigler and Nichols provided guidelines from which to start the iterative tuning process based on a good tradeoff between fast response and good stability margins for the system given by (8.44) [67, p. 199]. For a PI controller, those guidelines are

$$K_p = \frac{-0.9}{RL} \tag{8.45}$$

and

$$K_I = \frac{0.3K_p}{L}. \tag{8.46}$$

Using (8.45) and (8.46), the initial gains for the 10 kW system were found to be $K_p = -0.027$ and $K_I = -0.405$. Next, iterative tuning was used to find gains that gave an acceptable response. Note: the 5 MW system did not exhibit a useable process reaction curve, so the DC link voltage controller was found iteratively. The final gains and system response characteristics are presented in Table 11.

Table 11 DC Link Voltage Controller Gains and Response Characteristics

System	K_P	K_I	K_D
10 kW	-0.56	-0.32	0
5 MW	-0.029	-0.06	-0.001

The final step response for the 10 kW system is shown in Figure 8.13.

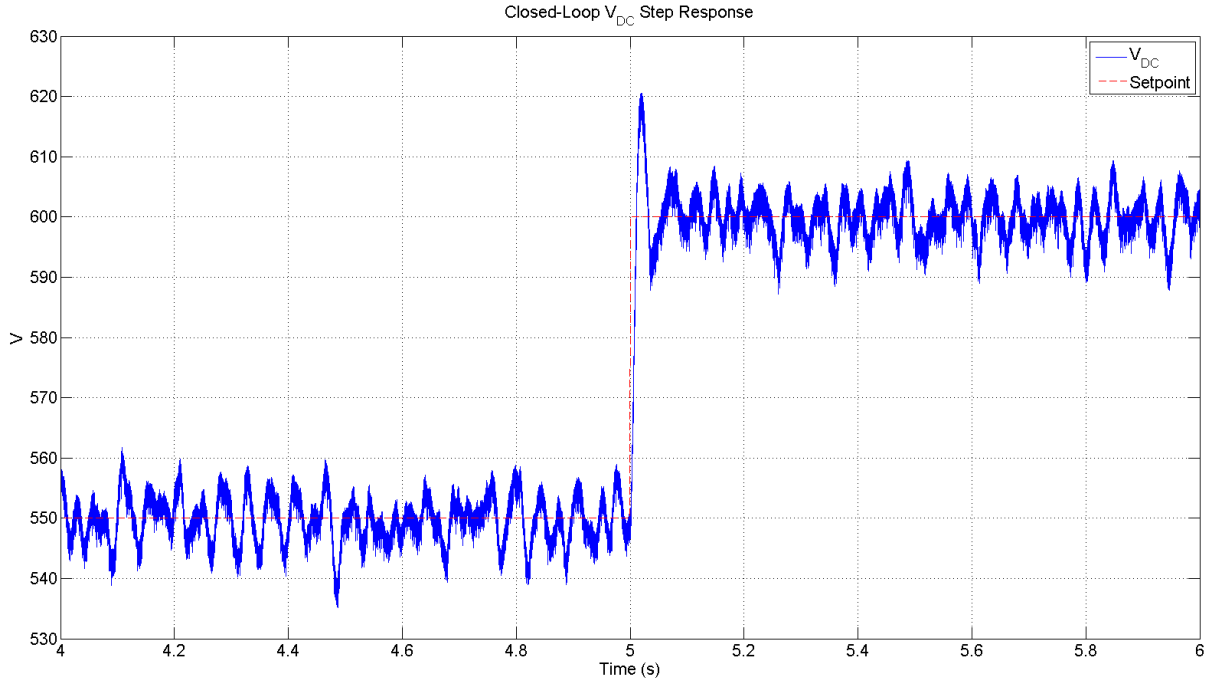

Figure 8.13 10 kW System Closed-Loop V_{DC} Step Response – Final Gains

Chapter 9 - System Overview

Each of the previous chapters has provided theory and background on a part of the wind turbines being modeled in this thesis. The purpose of this short chapter is to provide a high-level summary of the entire system and clarify how the different parts interact. Figure 9.1 shows the simulation process at the highest level possible.

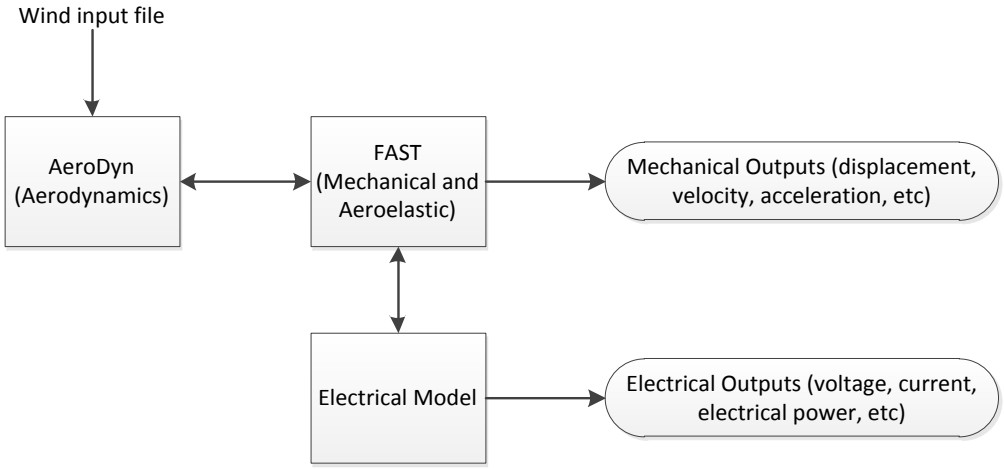

Figure 9.1 High-Level View of Simulations

As seen in Figure 9.1, AeroDyn handles the input to the system, which is a file containing information on the wind. During simulation, AeroDyn and FAST share information back and forth as part of the process of simulating the mechanical and aeroelastic parts of the wind turbine. Likewise, the electrical model and FAST share information during simulation. Simulation outputs come from two different places: FAST and the electrical model.

The electrical model used in this thesis is unique to FAST simulations. Figure 9.2 shows all of the electrical components being modeled. A control system for the active rectifier was designed so that the speed of the generator could be controlled. Control was performed in the reference frame attached to the PMSG's rotor. Referring all of the machine variables to such a reference frame turns sinusoidally-varying quantities, such as voltage and current, into DC quantities aligned with either the direct or quadrature axis. Likewise, a control system was designed to control the DC link voltage and the reactive power injected into the grid. This controller was also designed using direct and quadrature axis variables, but they are unrelated to those of the

generator controller. The d- and q-axis quantities for the grid-side controller stem from referring variables to the synchronous reference frame.

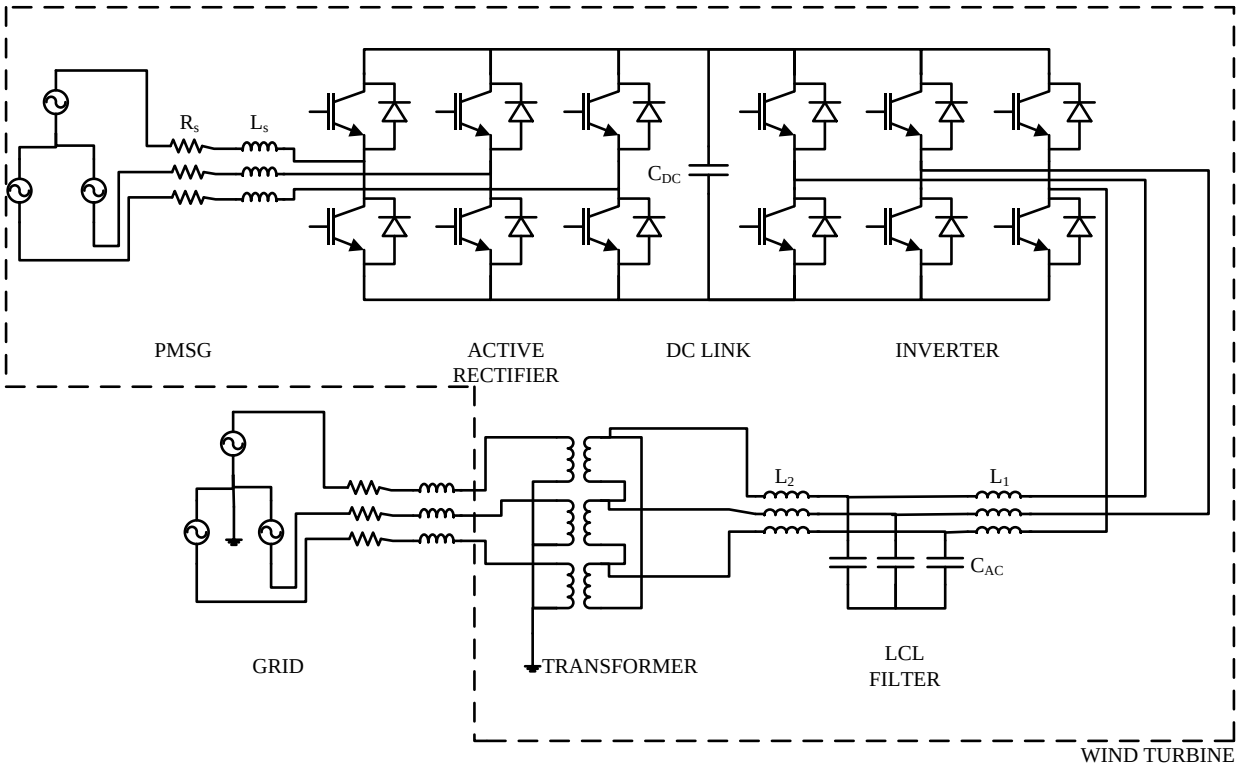

Figure 9.2 System Schematic

Important characteristics of the electrical model for each system are given in Table 12. Note that the conducting resistance of the IGBTs in the 5 MW model is significantly less than that of the 10 kW system. This was done to increase the efficiency of the 5 MW system to something reasonable (~85 %). It is probably impractical to use a 3-phase bridge inverter such as the one shown in Figure 9.2 for such a large wind turbine. Rather, a multilevel inverter that is inherently more efficient should be used. The same type of control used in this thesis could be used with a multilevel inverter, only with different implementation. Lowering the conducting resistance of the IGBTs is merely a way to observe efficiency that would be consistent with a system using a multilevel inverter.

Table 12 Electrical Model Parameters

Parameter	**10 kW System**	**5 MW System**
Nominal grid voltage	208 V	34.5 kV
Nominal grid frequency	60 Hz	60 Hz
Nominal PMSG voltage	260 V	690 V
C_{DC}	600 μF	2000 μF
IGBT forward voltage drop	2.0 V	2.0 V
Diode forward voltage drop	1.0 V	1.0 V
IGBT conducting resistance	55 mΩ	7 mΩ
IGBT fall time	70 ns	200 ns
Switching frequency	7 kHz	4 kHz
Transformer turns ratio	1:2.3077	1: 53.0769

The two main parts of the Simulink model, FAST and the electrical model, are shown in Figure 9.3. Figure 9.3 shows the 10kW system, but the differences between the two systems are mainly in values of gains and components, many of which are not shown in the figure. The complete Simulink model is given in Appendix B. Note: the Transfer Function blocks in Figure 9.3 as well as the figures in Appendix B (sometimes shown as 1/den(s)), are only present so that Simulink does not try to compute a value and use it in a controller at the same time step. For instance, V_{DC} is used to calculate m; without the transfer function block on the V_{DC} measurement, at every time step Simulink will try to calculate the new V_{DC} value, while trying to use that value to calculate m simultaneously, which is impossible. The transfer functions each have very fast poles, so they delay the measurements very slightly. The transfer functions are all

$$H(s) = \frac{1}{1x10^{-6}s + 1}. \tag{9.1}$$

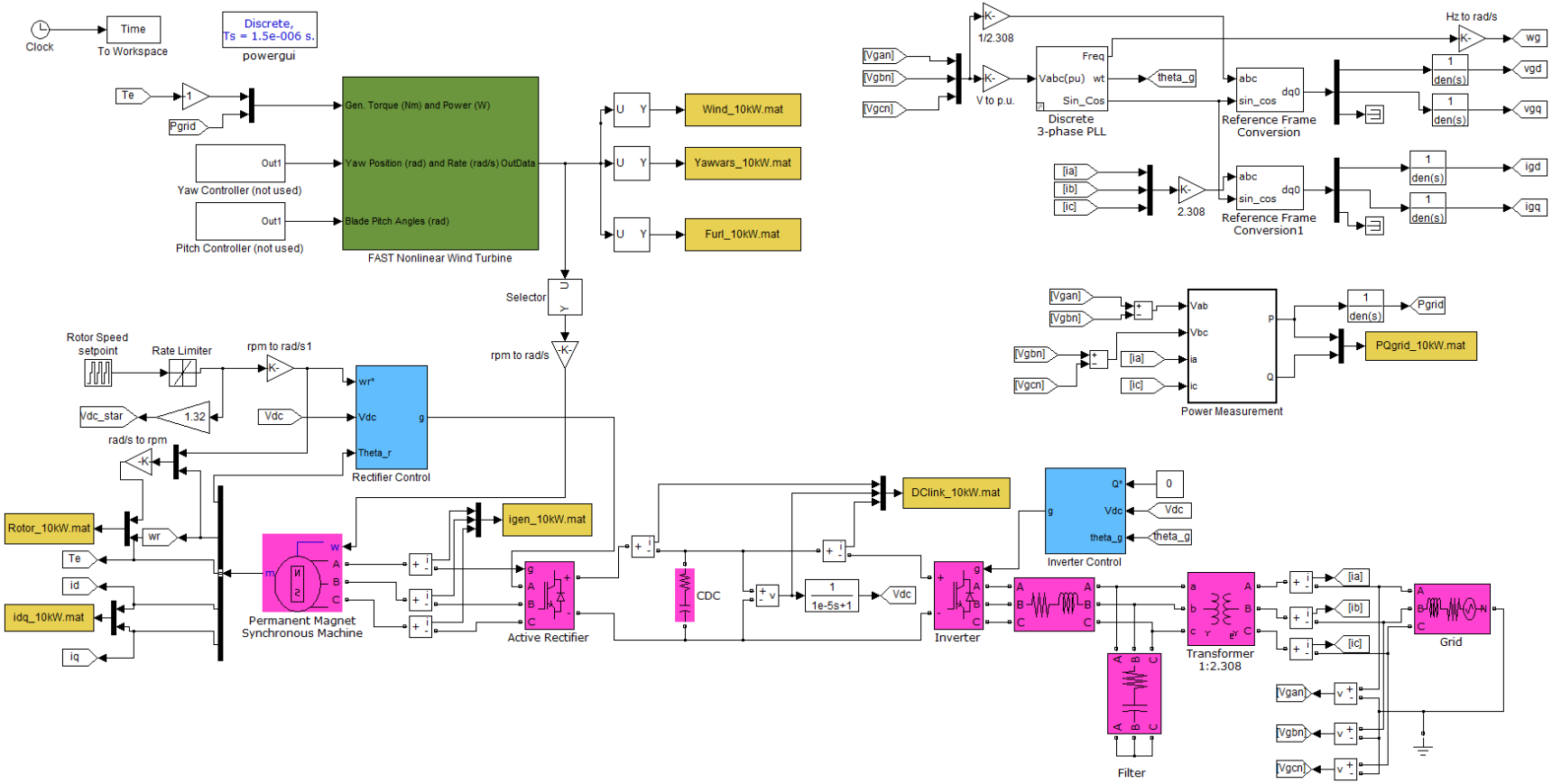

Figure 9.3 Simulink Electrical Model for 10 kW System

Chapter 10 - DC Link Magnitude Determination

The final section of Chapter 8 dealt with how the DC link voltage can be controlled by controlling the q-axis grid current. Very little is written in the published literature, though, on what magnitude the DC link voltage should be controlled to. It is often merely stated in the literature that keeping the DC link voltage constant ensures all the power passed through the rectifier is then injected to the grid [13]. This is true, but the magnitude of the DC link voltage affects other parts of the turbine as is made clear in Chapter 11.

First, it was shown in Chapter 6 that the modulation index is limited for linear modulation techniques by (6.16), which is repeated here:

$$0 \leq m \leq \frac{\sqrt{3}}{3}. \tag{10.1}$$

In order for a grid-tied inverter to work properly, it must be able to approximately match the grid voltage. With that in mind, the DC link voltage magnitude plays a role in the operating range of the inverter via (6.13), which is repeated here:

$$m = \frac{V}{V_{DC}}. \tag{10.2}$$

In order for the inverter to work properly, V in (10.2) must be:

$$V \cong \frac{\sqrt{2}V_{g,LL}}{\sqrt{3}}. \tag{10.3}$$

An alternate view is that (10.3) puts a lower bound on the DC link voltage:

$$V_{DC} \geq \frac{V_{g,LL}\sqrt{2/3}}{m}. \tag{10.4}$$

If m is equal to its upper bound, (10.4) becomes:

$$V_{DC} \geq \sqrt{2}V_{g,LL}. \tag{10.5}$$

Next, consider the rectifier side of the DC link, where (10.2) is also valid. This time, though, instead of V being the grid voltage, it is whatever the generator controllers make it. In that sense,

the rectifier works more like a true voltage-source converter than the inverter does. It can be shown with (10.2) and Figure 4.3 that:

$$V_{DC} = \frac{\sqrt{v_d^2 + v_q^2}}{m}. \tag{10.6}$$

Then (5.41) and (5.42), with the current derivative terms neglected and $i_d = 0$, can be substituted into (10.6) and simplified to:

$$V_{DC} = \frac{\sqrt{i_q^2(R^2 + p^2\omega_r^2 L_s^2) + i_q(2Rp\omega_r\psi) + (p\omega_r\psi)^2}}{m}. \tag{10.7}$$

Then (5.43) can be rearranged for i_q and substituted into (10.7), along with (10.1), to find the minimum DC link voltage needed to hold i_d to zero and achieve the necessary generator torque

$$V_{DC,min} = \sqrt{3\left(\frac{4\tau_e^2}{9p^2\psi^2}\left(R^2 + p^2\omega_r^2 {L_s}^2\right) + \frac{4\tau_e R\omega_r}{3} + (p\omega_r\psi)^2\right)}. \tag{10.8}$$

There are several good reasons to keep the DC link voltage as low as possible:

1. Minimize the rating, and therefore the cost, of the DC link capacitor(s).
2. Minimize the reverse blocking voltage of the IGBT/diode modules that make up the converters, prolonging their lives.

The third reason is a little less straightforward, so some explanation is in order. Consider Figure 10.1, which shows the equivalent circuit of the rectifier and the PMSG with the switch state equal to (1,0,0); the stator resistance and synchronous inductance are neglected because they are assumed to be small. This turns out to be a good assumption for the 10 kW system, but not so good for the 5 MW system. Therefore, the remainder of this discussion is restricted to the 10 kW system.

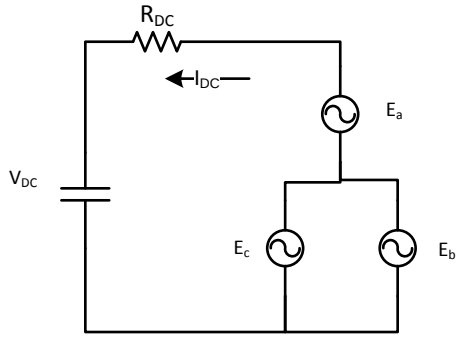

Figure 10.1 Rectifier and PMSG Equivalent Circuit in Switch State (1,0,0)

Figure 10.1 shows that in order for current to flow into, and not out of, the DC link capacitor,

$$V_{DC} < E_a - E_{b(c)}. \tag{10.9}$$

If current were to flow from the DC link into the PMSG, called "backfeeding," the generator currents would be unnecessarily distorted. As shown in Section 3.3.2 , it takes balanced, sinusoidal currents to have smooth torque in a PMSG. By extension, backfeeding the generator will make the torque less constant, which could conceivably lead to vibrations or other mechanical problems in the turbine.

Conceivably (10.8) could be used directly in a control system for choosing the magnitude setpoint of the DC link capacitor. However, any sudden changes in τ_e would then cause sudden changes in the voltage setpoint, possibly causing the system to go unstable. That situation is most likely to occur in gusty or turbulent wind. To avoid such problems, a linear relationship relating speed and $V_{DC,min}$ for the 10 kW system was found using (10.8) and torque and speed data from simulations,

$$V_{DC,min} \cong 1.32n \tag{10.10}$$

where n is the generator speed in rpm.

Care must be taken not to make the DC link voltage so low that the inverter cannot function properly, so the following rule can be used for choosing the DC link voltage setpoint:

if $V_{DC,min} \geq \sqrt{2}V_{g,LL}$

$$V_{DC}^* = V_{DC,min}$$

else

$$V_{DC}^* = \sqrt{2}V_{g,LL}.$$

This rule should make the advantage of a step-up transformer clear. Using one would increase the range over which $V_{DC,min}$ can be used by lowering the effective $V_{g,LL}$. A turns ratio of 1:2.3077 was used in the 10 kW system, which corresponds to the standard low voltage turns ratio of 208:480.

See the future work section of Chapter 12 for more on this subject.

Chapter 11 - Results

11.1 10 kW System

The simulation results for the 10 kW system are divided into two subsections: model verification and electromechanical interactions. All simulations were executed using a fixed-step solver with a 1.5 μs step size.

11.1.1 Model Validation

The 10 kW system was heavily based on the Bergey Excel 10 wind turbine. Though there are major differences in the two, especially the use of an active rectifier and 3-phase VSI in the model versus a passive rectifier and single-phase inverter in the real turbine, they should be fairly comparable. Before the two systems are directly compared, though, verification of the controllers presented in the previous chapters is presented.

Figure 11.1 shows the generator torque following a series of steps in the presence of very unsteady wind. The transient at the beginning of Figure 11.1 is merely due to the initialization of the model and is inconsequential. Note that because the torque is held steady, the generator speed varies with the wind speed.

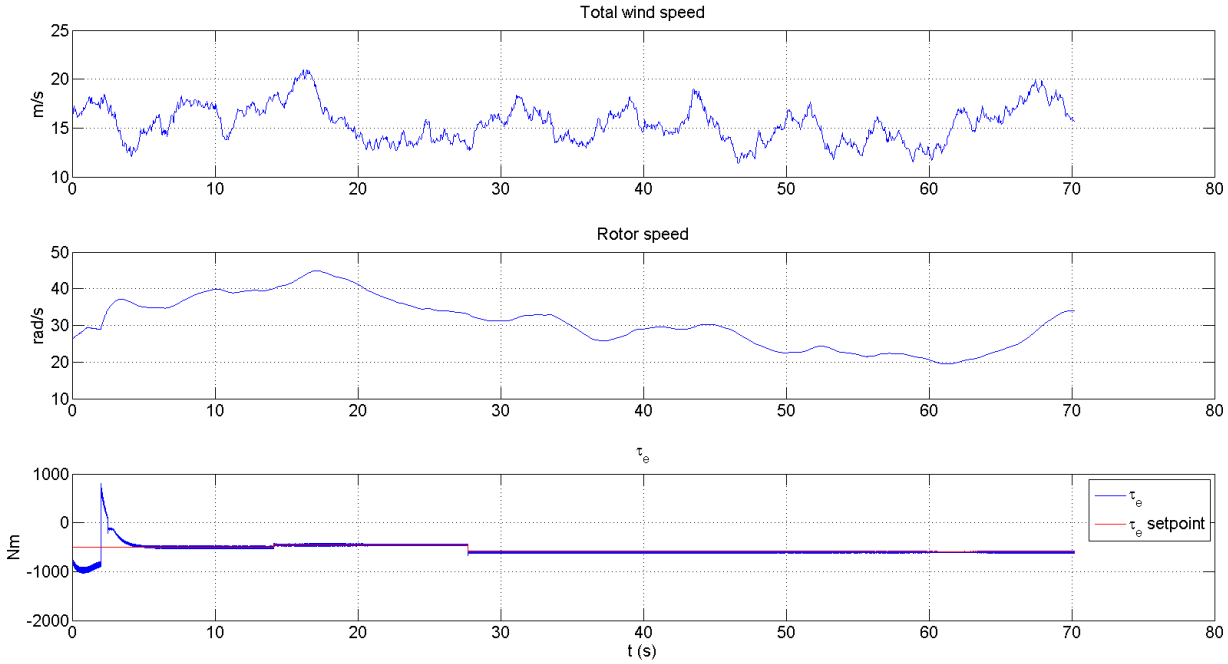

Figure 11.1 Torque Control

Figure 11.2 shows the generator speed following an arbitrary setpoint. Note that several times during the simulation the torque controller saturates at 0 or -400 N.m as it tries to make the speed follow the ramps in the setpoint.

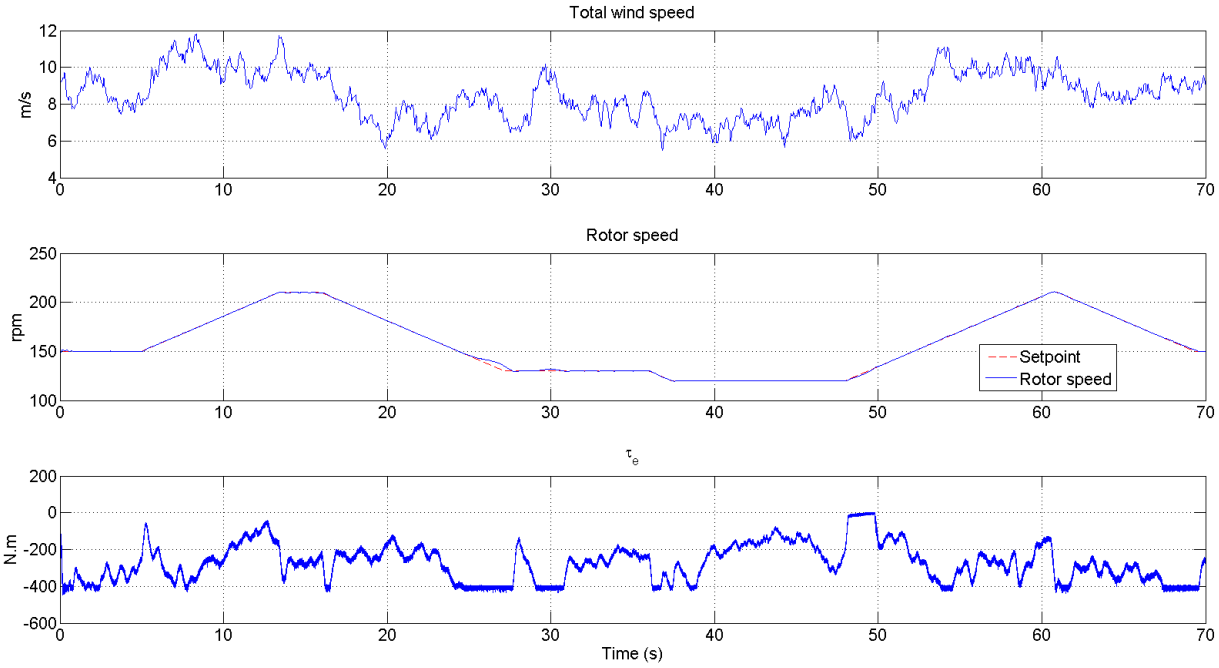

Figure 11.2 Speed Control

Figure 11.3 shows the d- and q-axis generator current control capabilities. As designed in Section 7.1, the q-axis current scales linearly with generator torque and the d-axis current is regulated to zero.

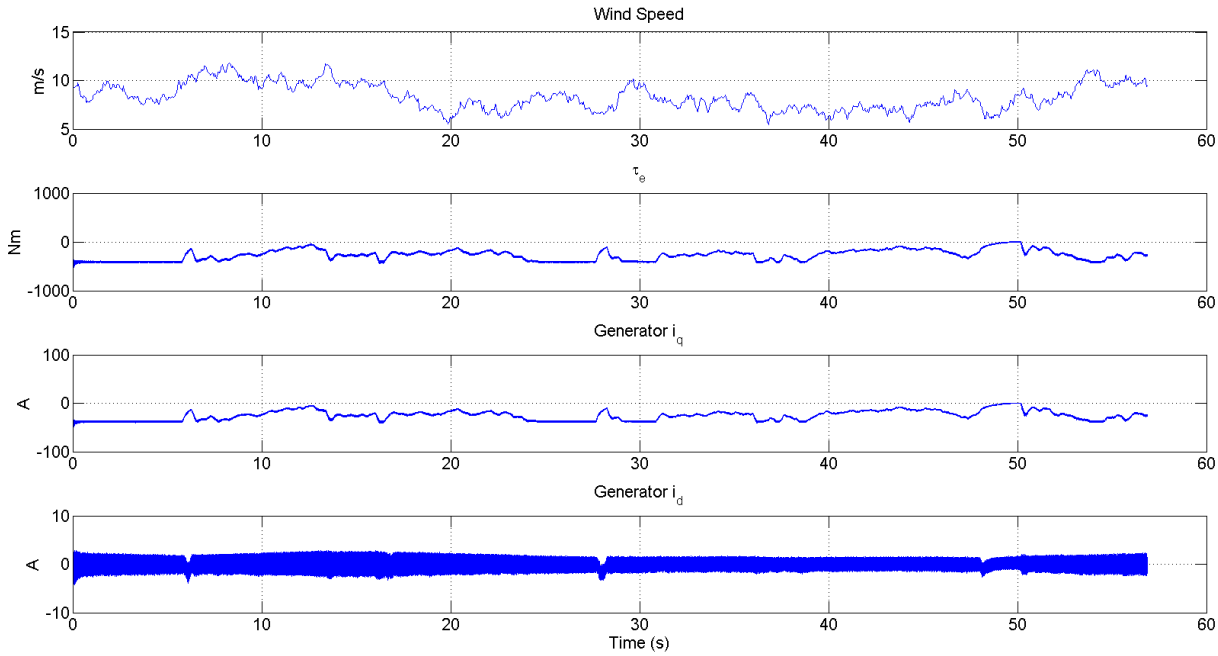

Figure 11.3 Generator i_{dq} Control

Figure 11.4 shows the reactive power injected to the grid being controlled arbitrarily between 0, +1000 VAR, -1000 VAR, and back to 0.

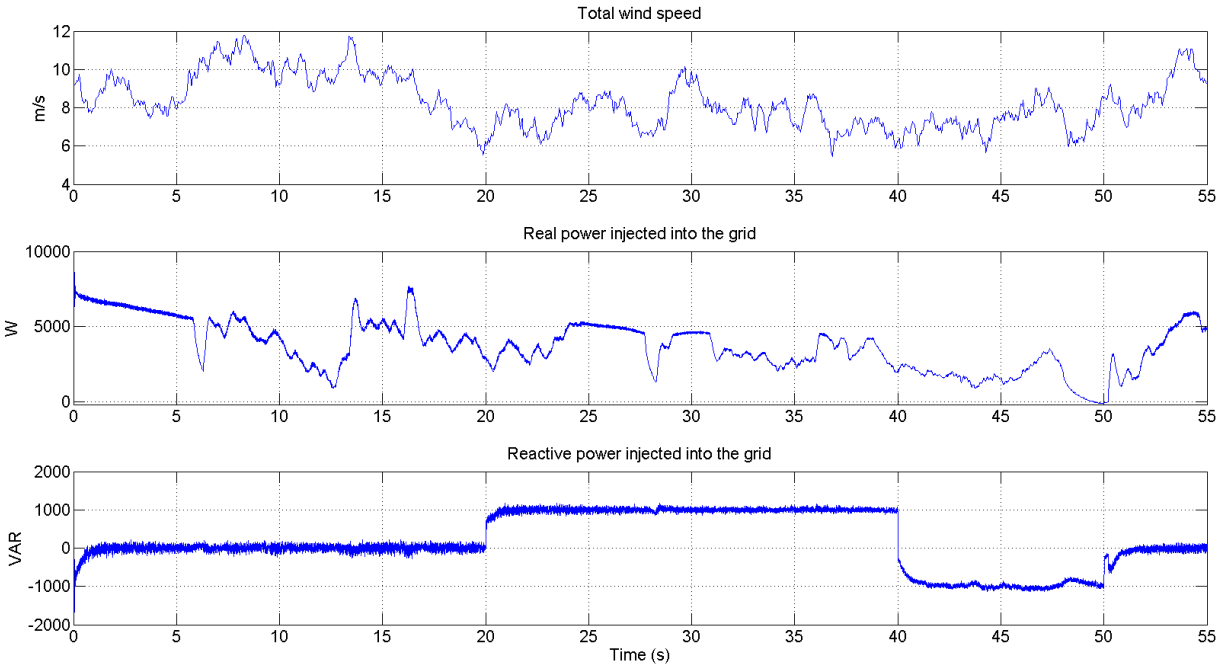

Figure 11.4 Reactive Power Control

Figure 11.5 shows the DC link voltage being controlled, using (10.10) to determine the setpoint. The controller performs reasonably well with only one minor problem around 50 s. The results from Figure 11.2 and Figure 11.5 are from the same simulation. Figure 11.2 shows that near 50 s the torque drops to essentially zero as the system tries to keep up with the speed setpoint. Because the torque goes to zero there is little or no power being passed to the DC link from the generator. In order to keep the DC link voltage equal to the setpoint, the controller drops the power output of the inverter to basically zero as well, except it actually dips barely negative for an instant. For that instant, a small amount of power flows into the DC link, where the voltage quickly increases because no power was flowing in from the generator side. Further results concerned with DC link magnitude are presented in the next subsection.

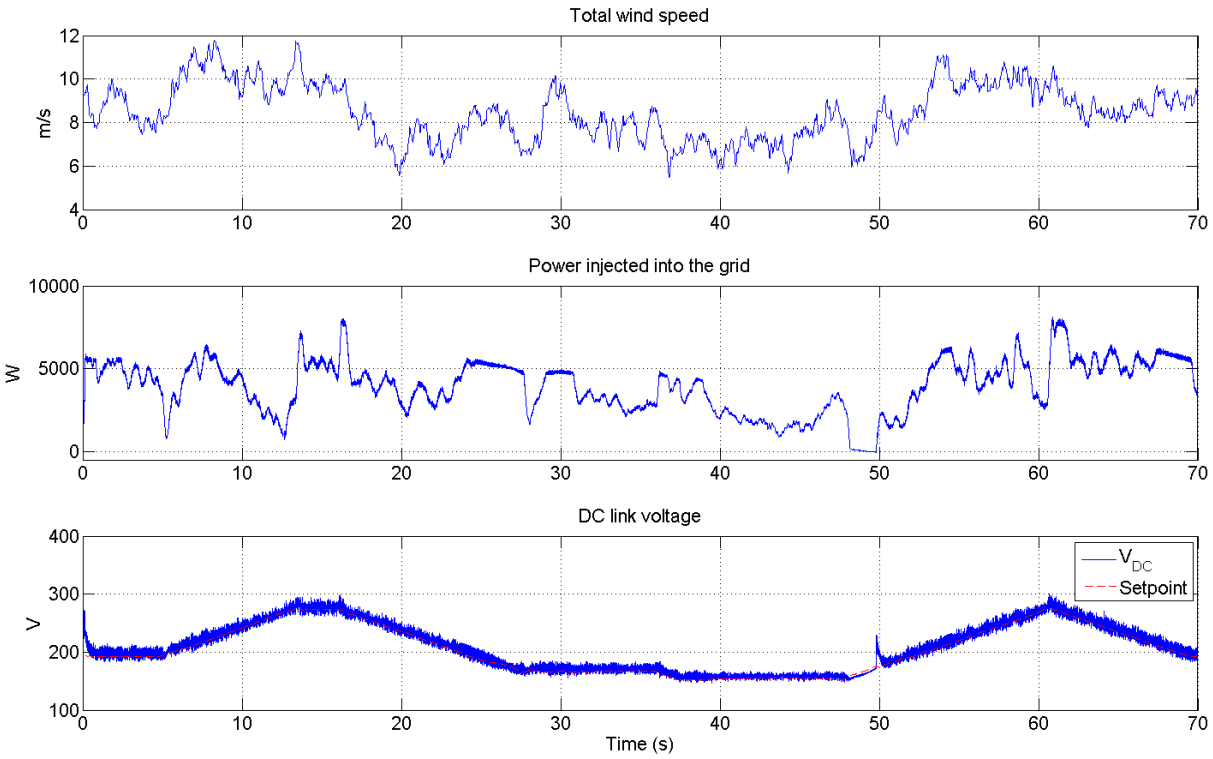

Figure 11.5 DC Link Voltage Control

Figure 11.6 shows a comparison between the power curve of the model in this thesis and that of the Bergey Excel 10. The Bergey's power curve was found through actual test data collected in 2011 [81]. The model's power curve was found by setting the wind to a constant value, and then stepping through successive speed setpoints until the maximum steady-state electrical power was found. This process is shown in Figure 11.7, which shows that the maximum power output at 7 m/s is 2633 W at 130 rpm. Clearly, the power curve from the model in this thesis is not perfect, but then no model is. This power output from the model is within the tolerance of the power curve all the way through 15 m/s, except for at 9 m/s, where it is barely outside of it. It is well documented that models based on the SWRT over-perform at high wind speeds because FAST does not model blade-tip torsion, which is significant at high wind speeds [22]. The model compensates for this in the range of 11-15 m/s due to increased i^2R losses that occur because of the lower primary voltage used.

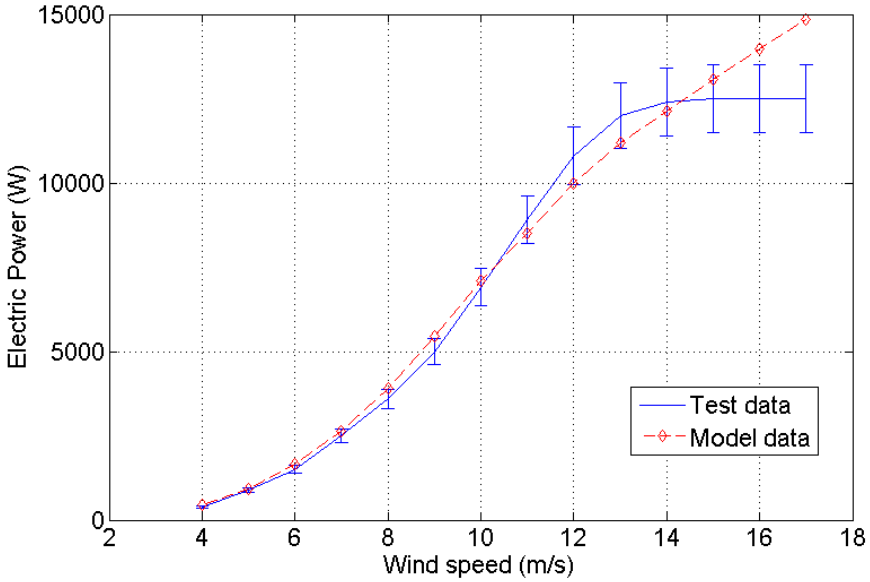

Figure 11.6 Power Curve Comparison

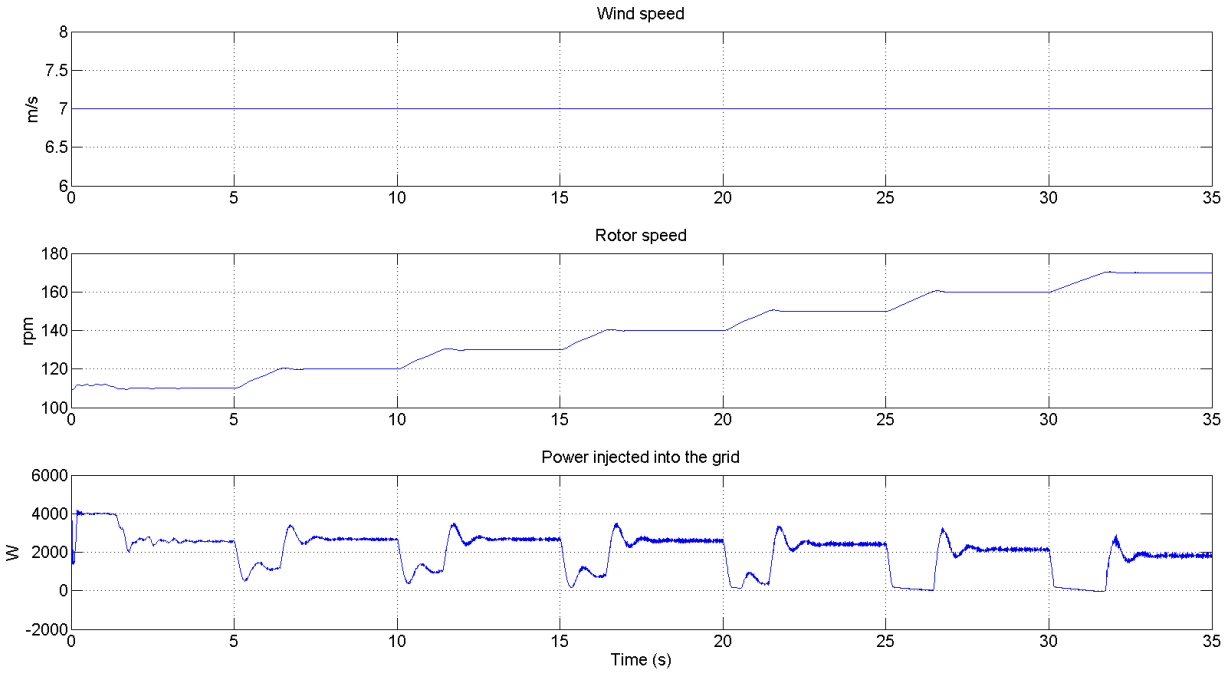

Figure 11.7 Finding a Power Curve Data Point for 7 m/s Wind

11.1.2 Electromechanical Interactions

The main contributions of this work are detailed electromechanical models and investigations in the effects of the DC link voltage, and the two overlap in this subsection. It was stated in Chapter

10 that making the DC link voltage too high could ultimately lead to increased vibrations in the turbine. A test was performed that made use of the detailed electromechanical model developed in this work to validate that claim.

The test was very simple: for the same wind speed, one simulation was run with the transformer's turns ratio = 1:1. Then, another simulation was run with the transformer's turns ratio = 1:2.3077, with the wind turbine on the low side. Figure 11.8 shows the wind speed for this test. Figure 11.9 (a) and (b) show the DC link voltage and the current into the DC link from the generator respectively for the 1:1 turns ratio case. Figure 11.9 (c) and (d) show the same for the 1:2.3077 turns ratio case. Figure 11.9 (b) shows that the current actually flows out of the DC link capacitor during the simulation (the generator is backfed). This is because the DC link voltage is greater than the line to line back-emf as discussed in Chapter 10. Figure 11.9 (d) shows that current never flows from the DC link to the generator when the larger turns ratio was used (except for during initialization, which is inconsequential). This is because $V_{g,LL}$ is lower in the larger turns ratio case, so $V_{DC,min}$ was attainable, whereas it was not in the 1:1 case.

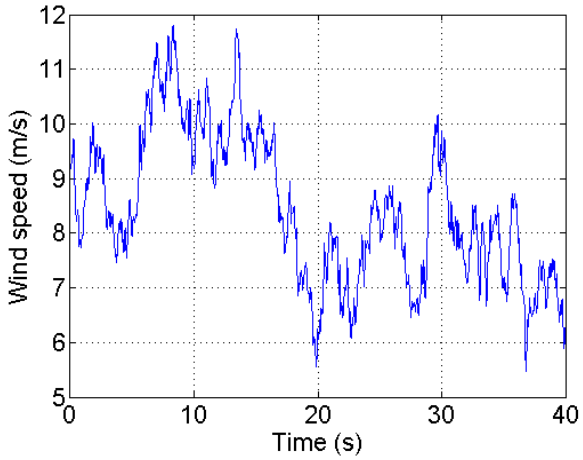

Figure 11.8 Wind speed input

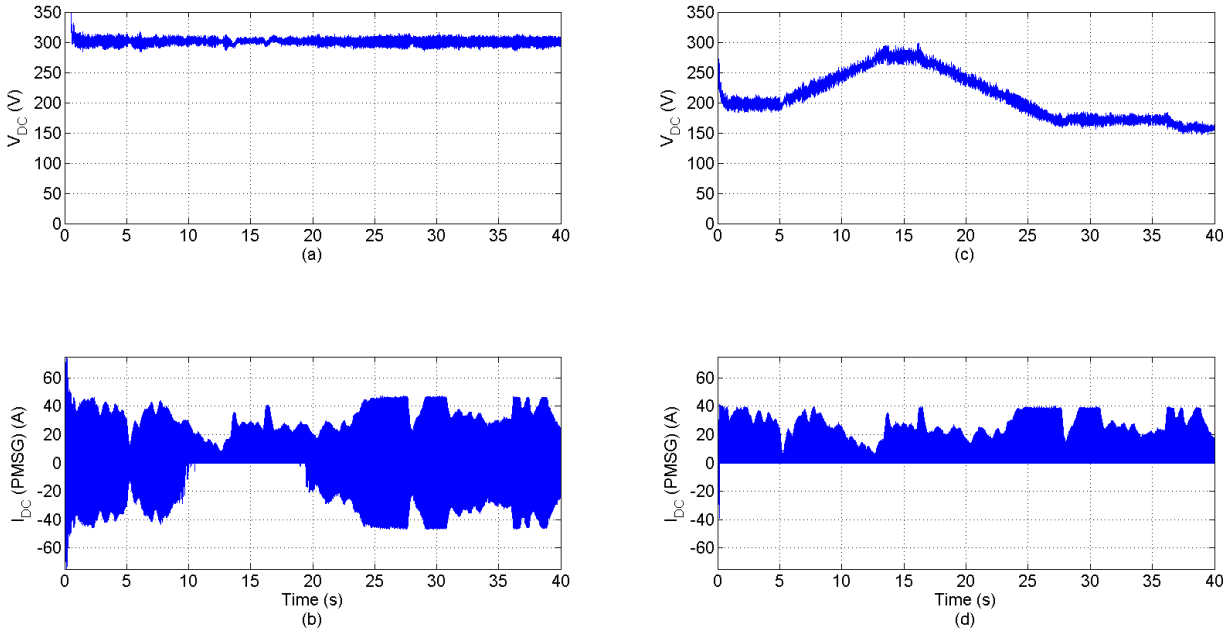

Figure 11.9 DC Link Voltage and Current Comparison

The consequences of backfeeding the generator are shown in the following figures. Figure 11.10 shows the difference in the generator phase currents for the two cases. Figure 11.10 shows that backfeeding the generator greatly distorts the phase currents. The THD of the currents in Figure 11.10 (a) is 6.79%, while the THD of the currents in (b) is 2.30%, a decrease of 66.1%. Figure 11.11 gives a comparison of the rotor speed and generator torque between the two cases. Section 3.3.2 showed that balanced, sinusoidal generator currents produce constant torque. With that in mind, one would predict that the currents in Figure 11.10 (a) would produce torque that is much less constant than that in (b). Figure 11.11 confirms that prediction. The worst-case high-frequency peak-to-peak torque ripple in Figure 11.11 (d) was 80.35% less than in (b).

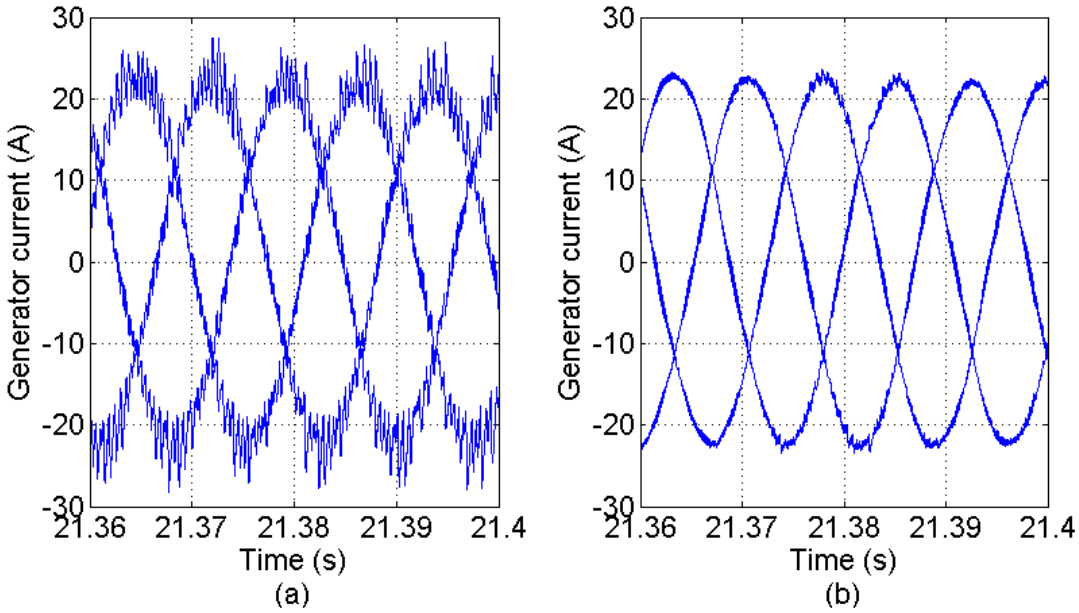

Figure 11.10 Generator Phase Current Comparison

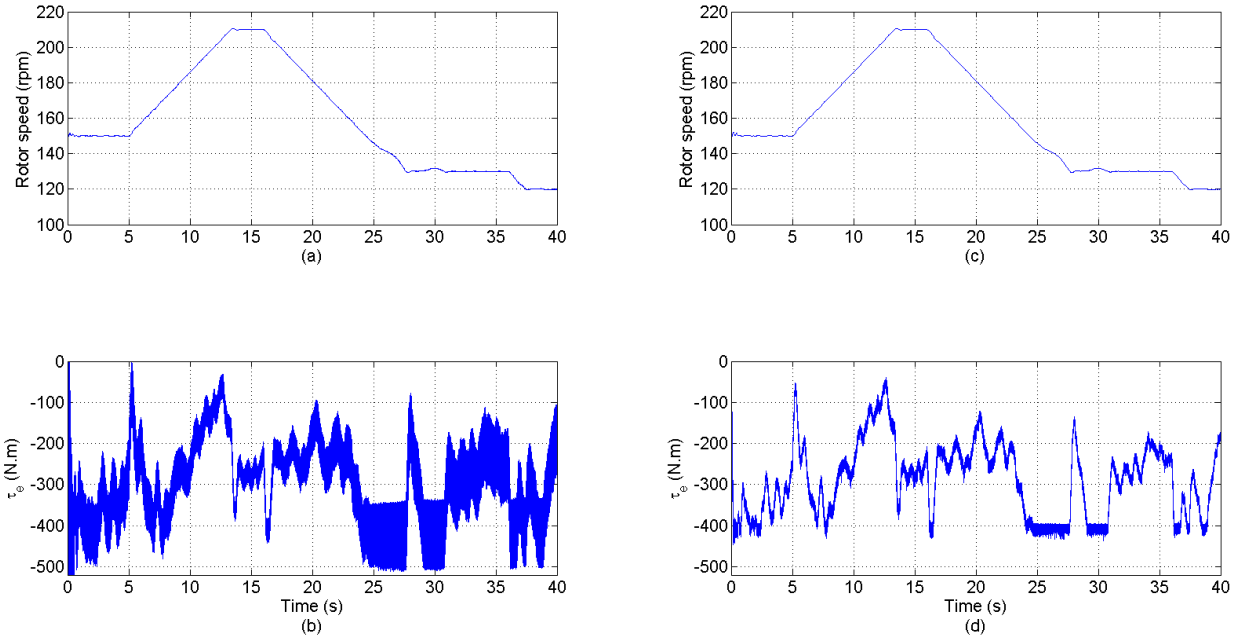

Figure 11.11 Rotor Speed and Generator Torque Comparison

Figure 11.12 shows one mechanical result of the decreased torque ripple in the 1:2.3077 case. It shows a comparison of the top-tower acceleration between the two cases. The high frequency

peak to peak top-tower acceleration was decreased by 91.3% in the 1:2.3077 case. Top-tower acceleration is a method of quantifying tower vibration [29]. Vibration can cause wear and tear on many components of the turbine, so any decrease in vibrations is a positive. The high frequency vibrations in Figure 11.12 are around 2 kHz, which is within the audible range. Therefore, using $V_{DC,min}$ would decrease audible noise for this turbine. Also, vibrations in the tower could potentially interfere with the operation of any ancillary equipment attached to it, such as anemometers or dataloggers.

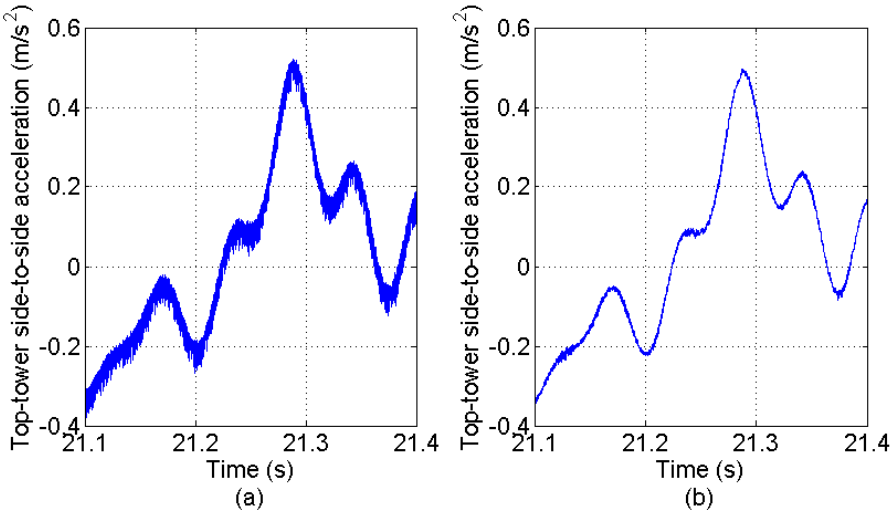

Figure 11.12 Top-Tower Acceleration Comparison

11.2 5 MW System

As with the previous section, results from the 5 MW system are divided into two subsections: model verification and electromechanical interactions. All simulations were executed using a fixed-step solver with a 2 μs step size.

11.2.1 Model Validation

Figure 11.13 shows the torque controller working in the presence of very unsteady wind. The generator torque is arbitrarily controlled to demonstrate the validity of the controller.

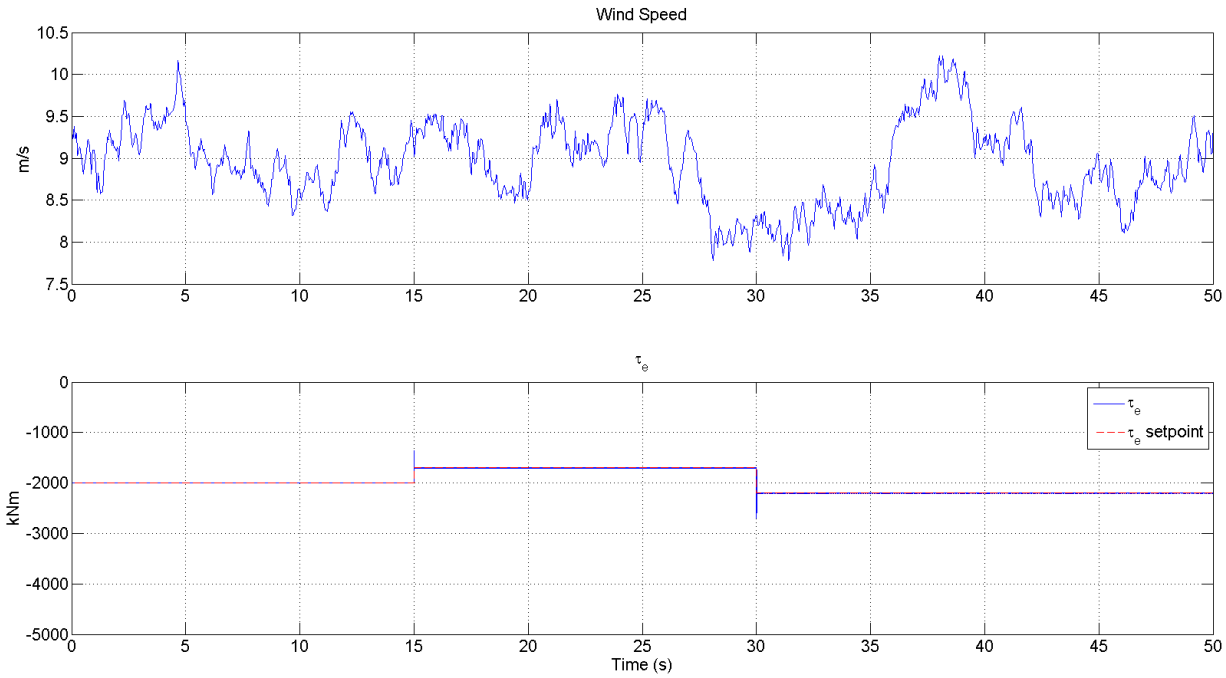

Figure 11.13 Torque Control

Figure 11.14 shows the generator speed controller working. The speed setpoint is arbitrarily controlled in the presence of very unsteady wind after 5 seconds of initialization.

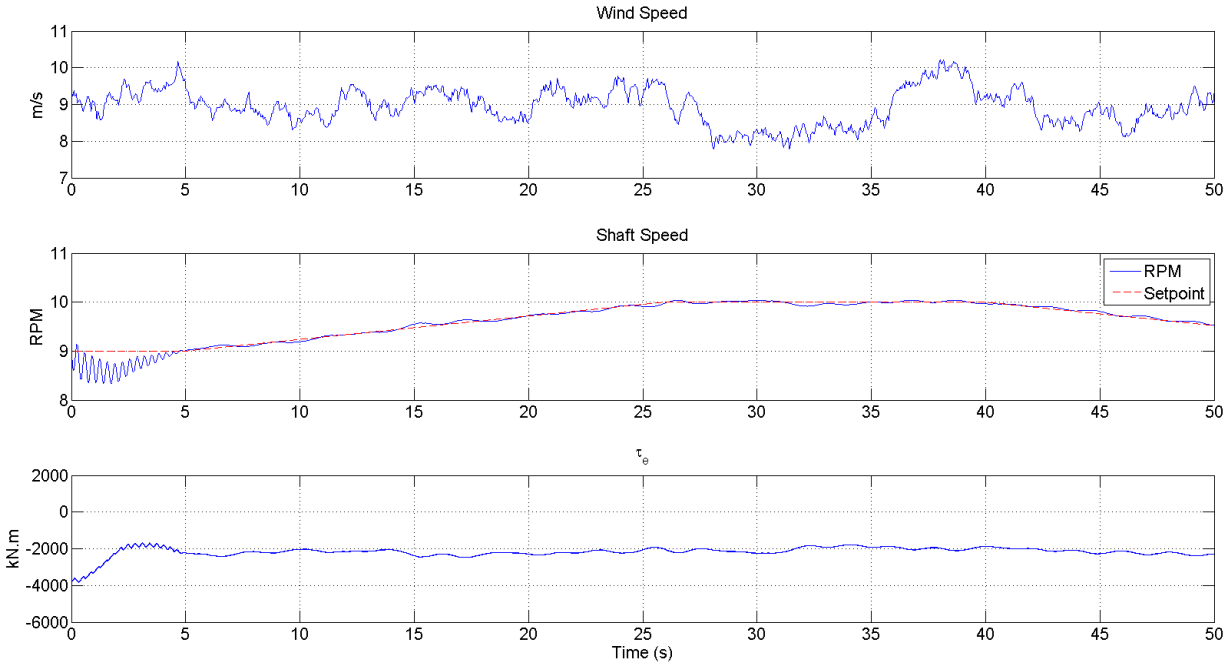

Figure 11.14 Rotor Speed Control

Figure 11.15 shows the functionality of the blade pitch controller, as it successfully controls the generator speed after τ_e has reached its maximum (-4.44 M.N.m).

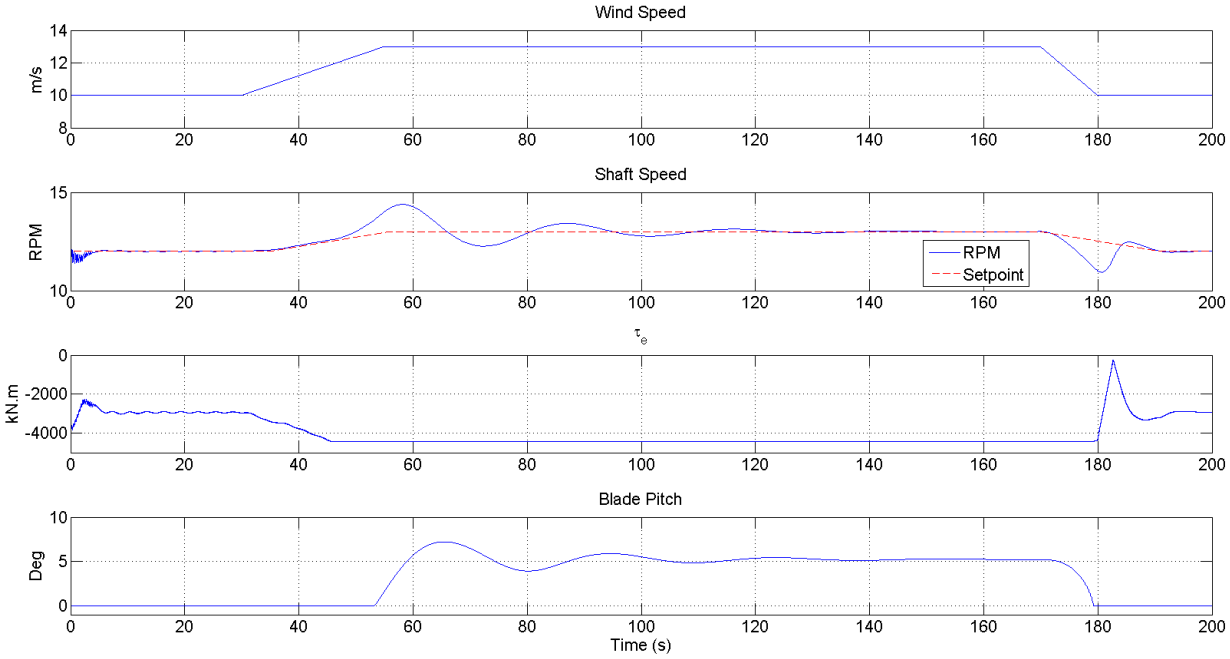

Figure 11.15 Rotor Speed Control in High Wind

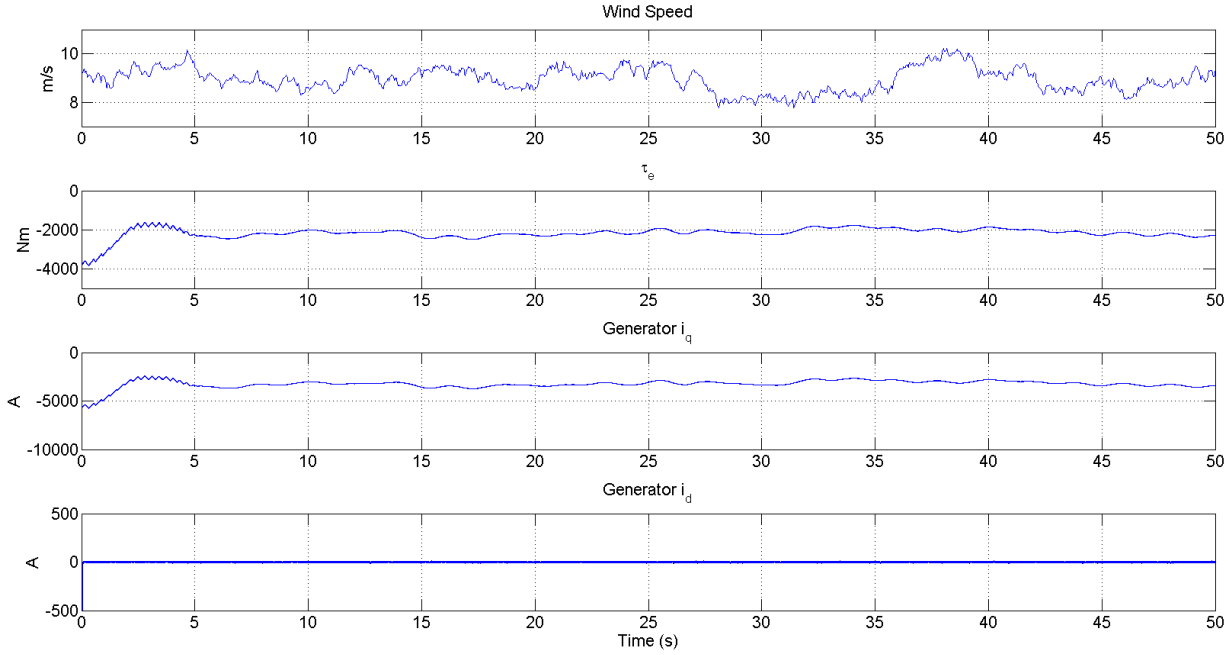

Figure 11.16 Generator i_{dq} Control

Figure 11.16 shows that the generator d- and q-axis currents behave as expected. Just as in Figure 11.3, the q-axis current follows the torque, and the d-axis current is zero.

Figure 11.17 shows the reactive power control capabilities of the 5 MW system. It shows the reactive power being set to +1 MVAR and -1 MVAR, which at 2 MW real power output is approximately pf=0.9 leading and lagging.

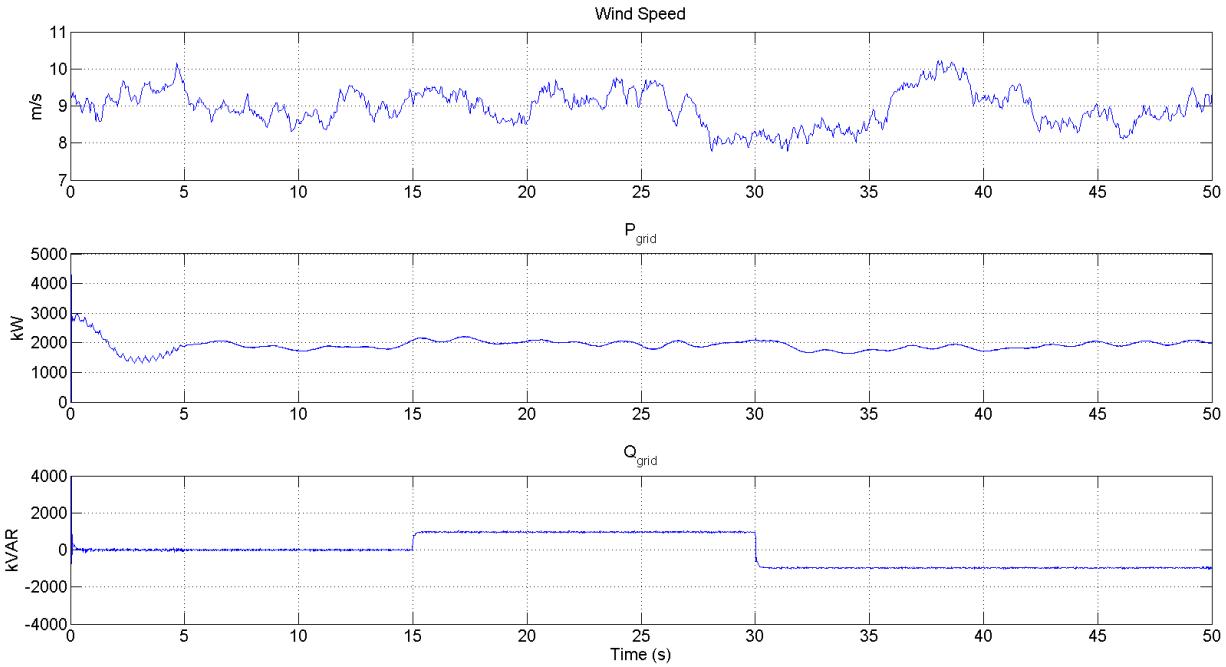

Figure 11.17 Reactive Power Control

Figure 11.18 shows the DC link voltage being arbitrarily controlled. The setpoint was initially 1500 V, and it underwent step changes to 1750 V and 1200 V at t=15 s and t=30 s respectively.

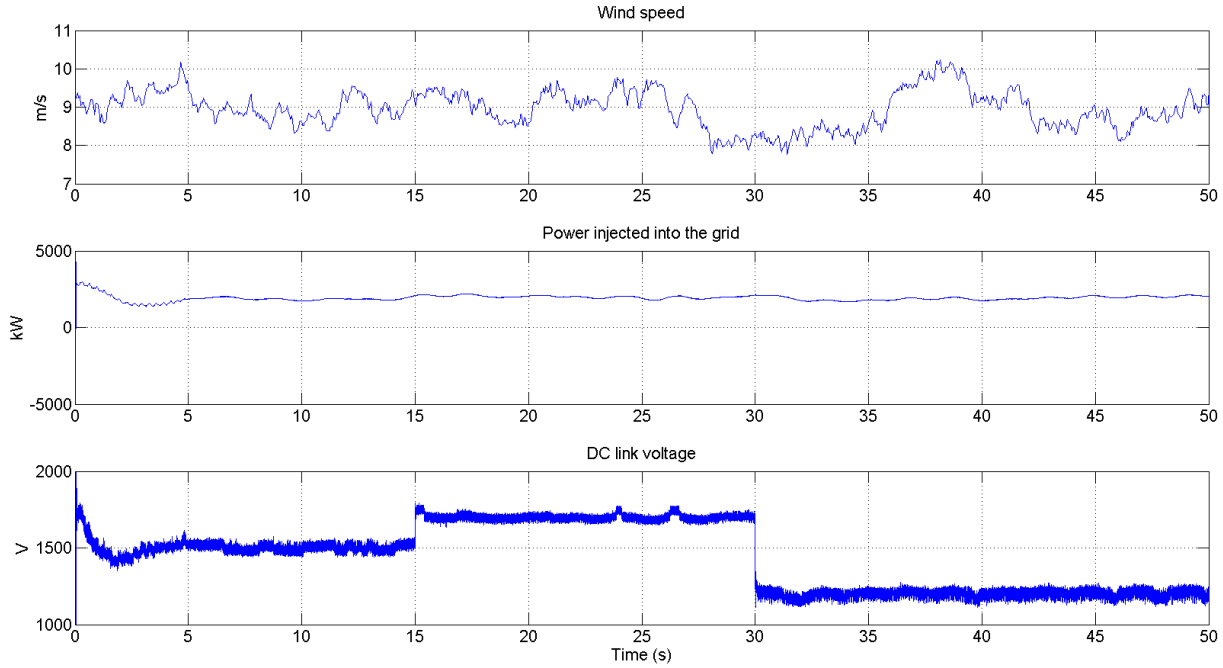

Figure 11.18 DC Link Voltage Control

Figure 11.19 shows the power curve obtained for the 5 MW model. The same process of applying steady wind to the turbine, changing the rotor speed, and observing the output power was used to find the curve. The curve follows a cubic trajectory with increasing wind speed, as predicted by (1.4), until its rated power is reached.

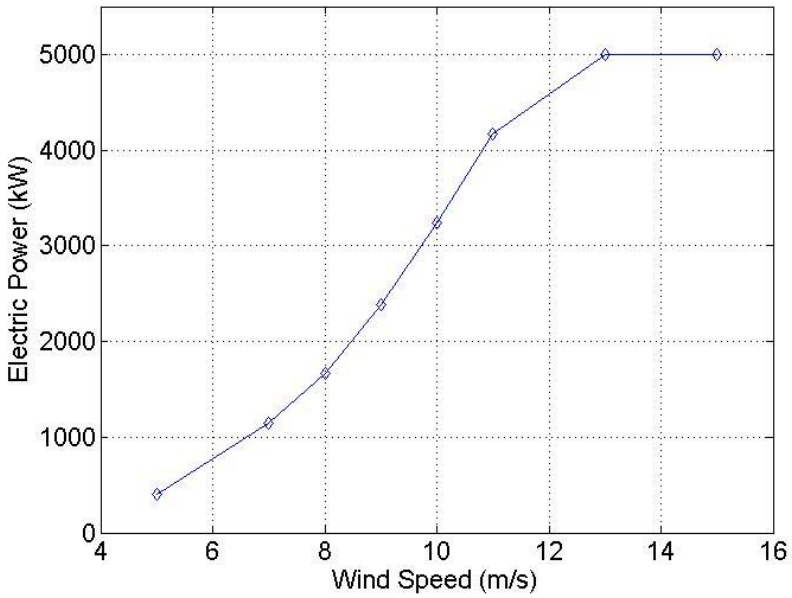

Figure 11.19 5 MW System Power Curve

Chapter 12 - Conclusions and Future Work

The preceding chapters have developed, in detail, the formulation of comprehensive models of PMDD wind turbines. The models include aerodynamic, mechanical, and electrical simulations through a combination of the FAST aeroelastic simulator and the SimPowerSystems toolbox for MATLAB/Simulink. The aeroelastic model includes realistic wind data incident to models for the blades, as well as mechanical models for many other parts of the turbine as was discussed in Chapter 2. The electrical model includes a PMSG, an active rectifier, a DC link capacitor, a 3-phase inverter, an LCL filter with passive damping, a transformer, and the grid. The generator model was developed in detail in Chapter 3. Chapter 4 introduced the concept of changing reference frames in order to turn sinusoidal quantities into constant ones for use in controller design. The generator model was completed in Chapter 5 with the use of reference frame conversions. One of the main features of a PMDD wind turbine is its back-to-back, or full, converter. This consists of a rectifier, a DC link, and an inverter. The same circuit topology, the 3-phase IGBT bridge, was used for both the rectifier and inverter for both systems. These circuits, as well as SVPWM, which was used to operate them, were developed in Chapter 6. Having implemented useful models for the turbine, generator, and power electronics, the first controller design was introduced in Chapter 7. In Chapter 7, feedback linearization in the dq frame attached to the generator's rotor was used to design controllers for generator torque, d-axis current, and generator speed. Also, a blade pitch controller for the 5 MW system was discussed in Chapter 7. That controller allows for speed control after the generator torque reaches its maximum value. These controllers and the active rectifier model are useful because they allow one to find the rotor speed at which maximum power capture occurs, or to design and test a maximum power capture scheme. They were used to find the power curves presented in Chapter 11. Chapter 8 dealt with the rest of the electrical model, including the filter, the transformer, and the inverter controllers. The inverter controllers consist of a DC link voltage controller that indirectly controls how much active power the inverter outputs, and a reactive power controller. These controllers were designed in the dq reference frame synchronous with the grid. Along with the inverter model, these controllers allow one to simulate interactions of the power system and the wind turbine, such as low voltage ride through or proper control of the DC link voltage. This capability was shown in the electromechanical interactions results presented in Chapter 11.

Chapter 10 discussed an idea for minimizing torque ripple in the 10 kW system through proper selection of the DC link voltage level. Simulations supporting this idea were presented in Chapter 11.

While the models presented in this thesis are very detailed and useful, they are by no means perfect. There are several aspects of the models that, if improved upon, would make them more realistic. The first is the inclusion of blade tip torsion in FAST. As was displayed in Chapter 11, the lack of blade tip torsion in FAST degraded the performance of the 10 kW model at high wind speeds.

The biggest problem with the electrical model is the presence of low-frequency content in the inverter output at low wind speeds. In many cases there was significant (1-2%) 2^{nd} and 4^{th} harmonic content at low wind speeds. Also at low wind speeds, significant fluctuations in the output current occurred, which can be seen as frequency components of the output current between 18 and 48 Hz. It's this author's belief that the problem is a combination of the DC link voltage and reactive power controllers, and the filter. A possible remedy may be some sort of gain scheduling that adjusts the controller gains depending on the output current level.

As was mentioned in Chapter 7, the use of a 3-phase IGBT bridge inverter for a 5 MW system is probably unrealistic. The inclusion of a multilevel inverter model in the 5 MW system would make it more accurately reflect reality.

Another area in which the 5MW system could be made more realistic is in its mechanical model. The NREL 5 MW model was originally designed for a DFIG. For this thesis, it was assumed that the mechanical properties of the turbine, such as its center of mass, generator inertia, generator mass, etc. were unchanged when the DFIG was removed and the PMSG was inserted. As one might guess from Figure 12.1, the mechanical properties of a DFIG turbine vs. a PMSG turbine would probably differ quite a bit. Figure 12.1 shows a rendering of a PMDD wind turbine next to a DFIG turbine. This is an extreme example of the difference in nacelle shape between PMSG and DFIG turbines, but the point is clear: the mechanical properties of the two systems are

different, and that difference must be accounted for in the 5 MW model if accurate electromechanical interaction results are to be obtained.

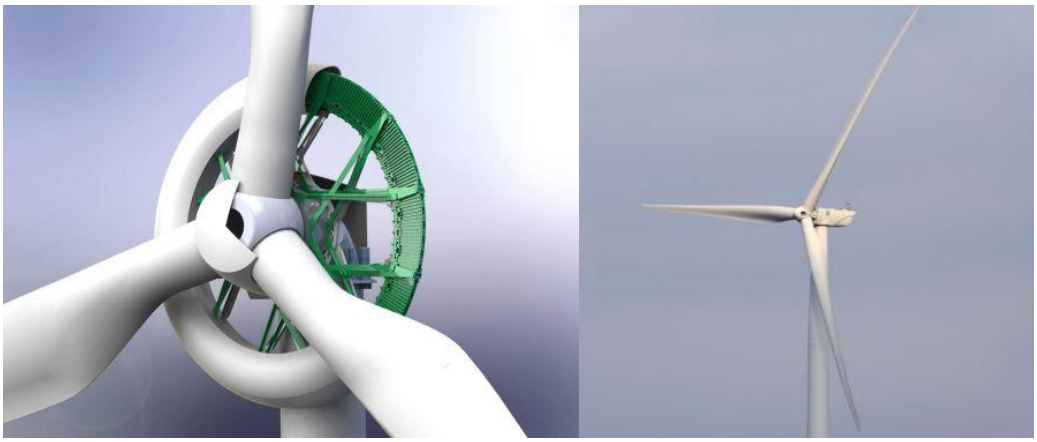

Figure 12.1 PMSG (left) and DFIG (right) Wind Turbine Comparison [82] [83]

An interesting use for the models developed in this thesis would be to complete the work started in Chapter 10. The issue of proper DC link voltage magnitude is one that this author has never seen addressed in the published literature on PMDD wind turbines. As was seen in Chapter 11, improper DC link voltage can lead to backfeeding, generator current distortion, and increased vibrations. Consider Figure 12.2, which is Figure 10.1 with the generator series resistance and inductance included.

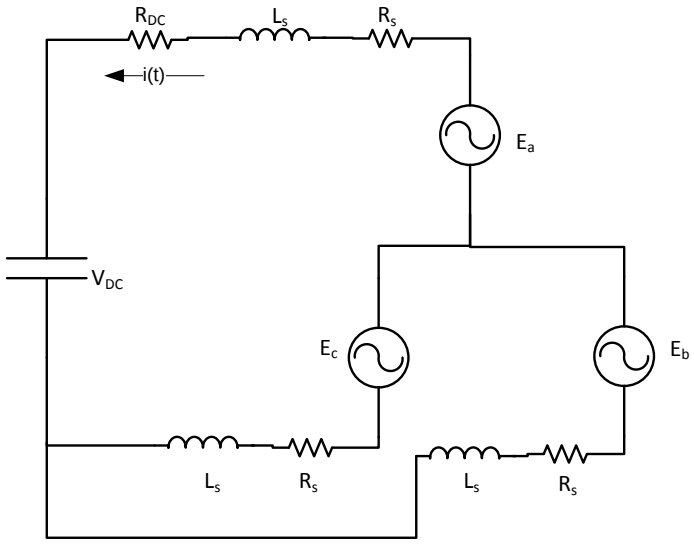

Figure 12.2 Generator and DC Link Circuit for Switch State (1,0,0)

KVL equations can be written for the circuit in Figure 12.2 as:

$$V_{DC} - E_{ab} = R(i_b - i_a) + \rho L(i_b - i_a), \tag{12.1}$$

$$V_{DC} - E_{ac} = R(i_c - i_a) + \rho L(i_c - i_a) \tag{12.2}$$

$$E_{bc} = R(i_c - i_b) + \rho L(i_c - i_b). \tag{12.3}$$

A KCL equation can also be written for Figure 12.2:

$$i_a + i_b + i_c = 0. \tag{12.4}$$

The sign of $i(t)$ depends on the DC link voltage, the line-to-line back-emf, the generator inductance and resistance, and the time spent in each switch state. To further complicate matters, the time spent in each switch state is not constant throughout a cycle. Also, the i^2R losses in the inverter, filter, and transformer depend on the DC link voltage. Assuming that the generator resistance and inductance cannot be changed, there is an optimization problem to be solved between the DC link voltage and the switching frequency to prevent backfeeding (if possible) and minimize losses.

Despite the shortcoming of the models presented in this thesis, they are still among the most detailed models for PMDD wind turbines available to date. It is this author's hope that they are used to design better wind turbines and controllers in the future.

References

[1] G. Klempner and I. Kerszenbaum, Operation and Maintenance of Large Scale Turbo Generators, John Wiley & Sons, 2004.

[2] F. T. Ulaby, Electromagnetics for Engineers, Upper Saddle River: Pearson Prentice Hall, 2005.

[3] M. Brian, April 2000. [Online]. Available: http://science.howstuffworks.com/environmental/energy/power.htm.

[4] 2012. [Online]. Available: http://www.ucsusa.org/clean_energy/coalvswind/c01.html.

[5] American Wind Energy Association, January 2012. [Online]. Available: http://www.awea.org/learnabout/publications/reports/upload/4Q-2011-AWEA-Public-Market-Report_1-31.pdf.

[6] DOE, NREL, AWEA, B&V et al., "20% wind energy by 2030," Golden, CO, 2008.

[7] Renewable Energy World, January 2011. [Online]. Available: http://www.renewableenergyworld.com/rea/news/article/2011/01/obama-calls-for-80-clean-energy-by-2035.

[8] J. Ribrant and L. Bertling, "Survey of failures in wind power plant systems focus on Swedish wind power plants during 1997 - 2005," in *IEEE Power Engineering Society General Meeting*, Tampa, 2007.

[9] W. Wu, V. Ramsden, T. Crawford and G. Hill, "A low speed, high torque, direct drive permanent magnet generator for wind turbines," in *Conf. Rec. IEEE Industry Applications Conference*, Rome, 2000.

[10] J. Manwell, J. McGowan and A. Rogers, Wind Energy Explained, 2nd ed., Chichester: John Wiley & Sons Ltd., 2002.

[11] T. Hawkins, W. White, G. Hu and F. D. Sahneh, "Region II wind power capture maximization using robust control and estimation with alternating gradient search," in *American Control Conference (ACC)*, San Francisco, 2011.

[12] D. Vilathgaumwa, S. Jayasinghe and U. Madawala, "Space vector modulated cascade multi-level inverter for PMSG wind generation systems," in *35th Annual Conference of IEEE Industrial Electronics*, Porto, Portugal, 2009.

[13] M. Chinchilla, S. Arnaltes and J. Burgos, "Control of permanent-magnet generators applied to variable-speed wind-energy systems connected to the grid," *IEEE Transactions on Energy Conversion*, vol. 21, no. 1, pp. 130-135, March 2006.

[14] C. Tareila, *"A single-phase D-STATCOM inverter for distributed energy sources"*, 2011.

[15] J. M. Jonkman and M. L. B. Jr., FAST user's guide, NREL/EL-500-29798, Golden, CO: National Renewable Energy Laboratory, 2005.

[16] M. Buhl, April 2001. [Online]. Available: http://wind.nrel.gov/designcodes/preprocessors/modes/.

[17] B. J. Jonkman, "TurbSim User's Guide: Version 1.50," National Renewable Energy Laboratory, Golden, Co, 2009.

[18] P. Moriarty and A. C. Hansen, "AeroDyn Theory Manual. NREL/EL-500-36881," National Renewable Energy Laboratory, Golden, Co, 2005.

[19] D. J. Laino and A. C. Hansen, "User's Guide to the Wind Turbine Aerodynamics Computer Software AeroDyn," Windward Engineering, Salt Lake City, UT, 2002.

[20] A. Manjock, "Evaluation Report: Design Codes FAST and ADAMS for Load Calculations of Onshore Wind Turbines. Report No. 72042," Germanischer Lloyd WindEnergie GmbH, Humburg Germany, 2006.

[21] J. Jonkman, *Overview of the FAST Servo-Elastic Module (Powerpoint),* Golden, CO: National Renewable Energy Laboratory, 2012.

[22] D. Corbus and M. Meadors, "Small Wind Research Turbine Final Report," National Renewable Energy Laboratory, Golden, CO, 2005.

[23] J. Jonkman, "Modeling of the UAE Wind Turbine for the Refinement of FAST_AD," National Renewable Energy Laboratory, Golden, CO, 2003.

[24] T. Hanley, *Personal Communication*, 2012.

[25] J. Jonkman, S. Butterfield, W. Musial and G. Scott, "Definition of a 5-MW Reference Wind Turbine for Offshore System Development, NREL/TP-500-38060," National Renewable Energy Laboratory, Golden, CO, 2009.

[26] R. Fadaeinedjad, G. Moschopoulos and M. Moallern, "The Impact of Tower Shadow, Yaw Error, and Wind Shears on Power Quality in a Wind-Diesel System," *IEEE Transactions on Energy Conversion*, vol. 24, no. 1, pp. 102-111, 2009.

[27] R. Fadaeinedjad, G. Moschopoloulos and M. Moallem, "A New Wind Power Plant Simulation Method to Study Power Quality," in *Canadian Conference on Electrical and Computer Engineering*, London, ON, 2007.

[28] R. Fadaeinedjad, G. Moschopoulos and M. Mohammadian, "The impact of mechanical dynamics of wind turbines on the flicker level in a wind diesel system," in *24th Canadian Conference on Electrical and Computer Engineering*, 2011.

[29] R. Fadaeinedjad, G. Moschopoulos and M. Moallern, "Voltage Sag Impact on Wind Turbine Tower Vibration," in *IEEE Power Engineering Society General Meeting*, London, ON, 2007.

[30] R. Fadaeinedjad, M. Moallern and G. Moschopoulos, "Simulation of a Wind Turbine With Doubly Fed Induction Generator by FAST and Simulink," *IEEE Transactions on Energy Conversion*, vol. 23, no. 2, pp. 690-700, 2008.

[31] B. Boukhezzar and H. Siguerdidjane, "Nonlinear control with wind estimation of DFIG variable speed turbine for power capture optimization," *Elsevier Energy Conversion and Management*, vol. 50, no. 4, pp. 885-892, 2009.

[32] B. Boukhezzar and H. Siquerdidjane, "Nonlinear Control of a Variable-Speed Wind Turbine Using a Two-Mass Model," *IEEE Transactions on Energy Conversion*, vol. 26, no. 1, pp. 149-162, 2011.

[33] B. Beltran, T. Ahmed-Ali and M. E. H. Benbouzid, "Sliding Mode Power Control of Variable-Speed Wind Energy Conversion Systems," *IEEE Transactions on Energy Conversion*, vol. 23, no. 2, pp. 551-558, 2008.

[34] B. Beltran, T. Ahmed-Ali and M. Benbouzid, "High-Order Sliding Mode Control of Variable-Speed Wind Turbines," *IEEE Transactions on Industrial Electronics*, vol. 56, no. 9, pp. 3314-3321, 2009.

[35] B. Beltran, M. Benbouzid and T. Ahmed-Ali, "High-order sliding mode control of a DFIG-based Wind Turbine for power maximization and grid fault tolerance," in *IEEE International Electric Machines and Drives Conference*, 2009.

[36] Y. Xing-Jia, L. Shu, J. Hong-Liang and G. Chang-chun, "Control strategy for variable speed wind turbine," in *IEEE 6th International Power Electronics and Motion Control Conference*, Shenyang, China, 2009.

[37] S. Frost, M. Balas and A. Wright, "Direct adaptive control of a utility-scale wind turbine for speed regulation," *International Journal of Robust and Nonlinear Control*, vol. 19, no. 1, pp. 59-71, 2009.

[38] X. Gong and W. Qiao, "Imbalance Fault Detection of Direct-Drive Wind Turbines Using Generator Current Signals," *IEEE Transactions on Energy Conversion*, vol. 27, no. 2, pp. 468-476, 2012.

[39] G. Bywaters, V. John, J. Lynch, P. Mattila, G. Norton, J. Stowell, M. Salata, O. Labath, A. Chertok and D. Hablanian, "Northern Power Systems WindPACT Drive Train Alternative Design Study Report," National Renewable Energy Laboratory, Golden, CO, 2005.

[40] J. Zhang, M. Cheng and Z. Chen, "Design of wind turbine controller by using wind turbine codes," in *International Conference on Electrical Machines and Systems*, 2008.

[41] J. Mevey, *Sensorless field oriented control of brushless permanent magnet synchronous motors,* 2009.

[42] P. Krause, O. Wasynczuk and S. Sudhoff, Analysis of Electric Machinery and Drive Systems, 2nd ed., Piscataway, NJ: IEEE Press, 2002.

[43] M. El-Hawary, Principles of Electric Machines with Power Electronics Applications, 2nd ed., Piscataway, NJ: IEEE Press, 2002.

[44] T. Gonen, Electrical Machines, Carmichael, CA: Power International Press, 1998.

[45] W. C. Duesdterhoeft, M. W. Schulz and E. Clarke, "Determination of Instantaneous Currents and Voltages by Means of Alpha, Beta, and Zero Components," *Transactions of the American Institute of Electrical Engineers*, vol. 70, no. 2, pp. 1248-1255, 1951.

[46] G. R. Slemon, Electric Machines and Drives, Reading, MA: Addison-Wesley, 1992.

[47] B. Lathi, Signal Processing & Linear Systems, New York, NY: Oxford University Press, 1998.

[48] R. Park, "Two-Reaction Theory of Synchronous Machines - Generalized Method of Analysis, Part I," *AIEE Transactions,* vol. 48, pp. 716-727, July 1929.

[49] D. Ohm, ""Dynamic model of PM synchronous motors"," Drivetech Inc., 2000. [Online]. Available: http://www.drivetechinc.com/articles/IM97PM_Rev1forPDF.pdf.

[50] P. Krause and C. Thomas, "Simulation of Symmetrical Induction Machinery," *IEEE Transactions on Power Apparatus and Systems,* vol. 84, no. 11, pp. 1038-1053, 1965.

[51] I. Schiemenz and M. Stiebler, "Control of a permanent magnet synchronous generator used in a variable speed wind energy system," in *IEEE International Electric Machines and Drives Conference*, Cambridge, MA, 2001.

[52] A. Cimpoeru, *Encoderless vector control of PMSG for wind turbine applications,* Masters

thesis, Aalborg University, 2010.

[53] A. Hansen and G. Michalke, "Modelling and control of variable-speed multi-pole permanent magnet synchronous generator wind turbine," *Wind Energy,* vol. 11, no. 5, pp. 537-554, September/October 2008.

[54] K. Tan and S. Islam, "Optimum control strategies in energy conversion of PMSG wind turbine system without mechanical sensors," *IEEE Transactions on Energy Conversion,* vol. 19, no. 2, pp. 392-399, June 2004.

[55] K. E. Johnson, L. Pao, M. Balas and L. Fingersh, "Control of Variable-Speed Wind Turbines," *IEEE Control Systems Magazine,* pp. 70-81, June 2006.

[56] J. Glover, M. Sarma and T. Overbye, Power System Analysis and Design, 4th ed., 2007.

[57] M. H. Rashid, Power Electronics Circuits, Devices, and Applications, 2nd ed., Englewood Cliffs, NJ: Prentice-Hall, 1993.

[58] N. Mohan, T. Undeland and W. Robbins, Power Electronics - Converters, Applications, and Design, 3rd ed., John Wiley & Sons, 2003.

[59] M. Malinowski, *Sensorless Control Strategies for Three-Phase PWM Rectifiers,* 2001.

[60] J. Kassakian, M. Schlecht and G. Verhese, Principles of Power Electronics, Reading, MA: Addison-Wesley, 1991.

[61] A. Lidozzi, L. Solero, F. Crescibini and A. D. Napoli, "SVM PMSM Drive with Low Resolution Hall-Effect Sensors," *IEEE Transactions on Power Electronics,* vol. 22, no. 1, pp. 282-290, January 2007.

[62] H. v. d. Broeck, "Analysis and realization of a pulsewidth modulator based on voltage space vectors," *IEEE Transactions on Industry Applications,* vol. 24, no. 1, pp. 142-150, Jan/Feb. 1988.

[63] V. Prasad, *Analysis and comparison of space vector modulation schemes for three-leg and four-leg voltage source inverters,* 1998.

[64] R. Valentine, Ed., Motor Control Electronics Handbook, New York: McGraw-Hill, 1998.

[65] B. Hariram and N. Marimuth, "Space vector switching patterns for different applications - a comparative analysis," in *IEEE International Conference on Industrial Technology*, Hong Kong, 2005.

[66] S. Zhang and e. al, "Design of a Robust Grid Interface System for PMSG-Based Wind Turbine Generators," *IEEE Transactions on Industrial Electronics,* vol. 58, no. 1,

pp. 316 - 328, Jan. 2011.

[67] G. Franklin, J. Powell and A. Emami-Naeini, Feedback Control of Dynamic Systems, Upper Saddle River, NJ: Pearson Prentice Hall, 2006.

[68] M. S. I. Schiemenz, "Control of a permanent magnet synchronous generator used in a variable speed wind energy system," in *IEEE International Electric Machines and Drives Conference*, Cambridge, MA, 2001.

[69] M. Hansen, A. Hansen, T. Larsen, S. Oye, Sorensen and P. Fuglsang, "Control Design for a Pitch-Regulated, Variable-Speed Wind Turbine," Riso National Laboratory, Roskilde, Denmark, 2005.

[70] M. Liserre, S. F. Blaabjerg and Hanson, "Design and Control of an LCL-Filter-Based Three-Phase Active Rectifier," *IEEE Transactions on Industy Applications*, vol. 41, no. 5, pp. 1281-1291, 2005.

[71] R. Teodorescu and F. Blaabjerg, "Flexible control of small wind turbines with grid failure detection operating in stand-alone and grid-connected modes," *IEEE Transactions on Power Electronics*, vol. 19, no. 5, pp. 1323-1332, 2004.

[72] S. Jung, Y. Bae, S. Choi and H. Kim, "A Low Cost Utility Interactive Inverter for Residential Fuel Cell Generation," *IEEE Transactions on Power Electronics*, vol. 22, no. 6, pp. 2293-2298, 2007.

[73] M. Liserre, F. Blaabjerg and A. Dell'Aquila, "Step-by-step design procedure for a grid-connected three-phase PWM Voltage Source Converter," *Int. J. Electron*, vol. 91, no. 8, pp. 445-460, 2004.

[74] M. Lindgren and J. Svensson, "Control of a voltage-source converter connected to the grid through an LCL-filter-application to active filtering," in *Proc. IEEE PESC '98*, 1998.

[75] R. Teodorescu, M. Liserre and P. Rodriguez, Grid Converters for Photovoltaic and Wind Power Systems, Chichester: John Wiley & Sons, 2011.

[76] A. Rockhill, M. Liserre, R. Teodorescu and P. Rodriguez, "Grid-Filter Design for a Multimegawatt Medium-Voltage Voltage-Source Inverter," *IEEE Transactions on Industrial Electronics*, vol. 58, no. 4, pp. 1205-1217, 2011.

[77] I. S. 519-1992, "IEEE Recommended Practices and Requirements for Harmonic Control in Electrical Power Systems," IEEE, 1993.

[78] D. Ochs, P. Sotoodeh and B. Mirafzal, "A technique for voltage source inverter seamless transitions between grid-connected and standalone modes," in *2013 IEEE Applied*

Power Electronics Conference, Long Beach, CA (To be published March 2013).

[79] S. Dehghan, M. Mohamadian and A. Varjani, "A New Variable-Speed Wind Energy Conversion System Using Permanent-Magnet Synchronous Generator and Z-Source Inverter," *IEEE Transactions on Energy Conversion*, vol. 24, no. 3, pp. 714-724, 2009.

[80] C. D. Johnson, Process Control Instrumentation Technology, Englewood Cliffs, NJ: Prentice Hall, 1993.

[81] SWCC, 2011. [Online]. Available: http://www.smallwindcertification.org/wp-content/new-uploads/2011/11/Summary-Report-10-12.pdf.

[82] "Boulder Wind Power," 2012. [Online]. Available: http://www.boulderwindpower.com/. [Accessed 3 October 2012].

[83] "GE Energy 2.75-103 Wind Turbine," 2012. [Online]. Available: http://www.ge-energy.com/products_and_services/products/wind_turbines/ge_2.75_103_wind_turbine.jsp. [Accessed 3 October 2012].

[84] "GE Energy 4.1-113 Wind Turbine," 2012. [Online]. Available: http://www.ge-energy.com/products_and_services/products/wind_turbines/fourone_113.jsp. [Accessed 3 October 2012].

Appendix A - The Forward and Inverse Clarke Transforms

First, the forward Clarke Transform is derived using trigonometric relationships.

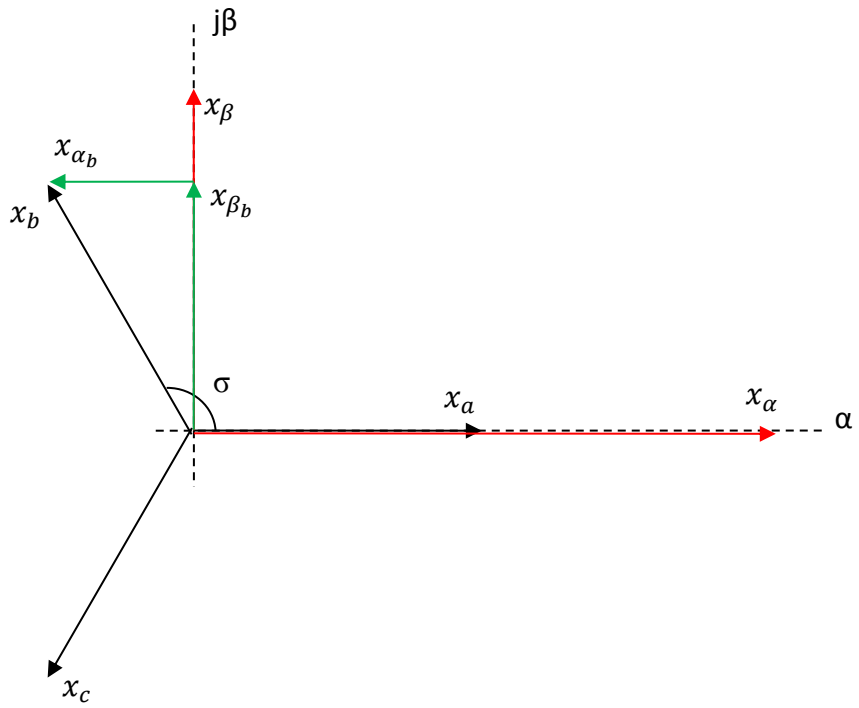

Figure A.1 Graphical Clarke Transform

Figure A.1 shows how trigonometry may be used to break each abc component into its αβ ones. The red vectors are the final results of breaking the abc vectors into their αβ components with a magnitude invariant Clarke Transform. That is, $|x_{abc}| = |x_{\alpha\beta}|$. The green vectors shown how the b vector may be formed by α and β components. Trigonometry may be used to find those components. When the αβ components are found for each abc vector, their sums give x_α and x_β. Using Figure A.1 as a guide, with σ=120^o, it is easily shown that

$$\begin{aligned} x_{\alpha_a} &= x_a, \\ x_{\beta_a} &= 0, \end{aligned} \tag{A.1}$$

$$\begin{aligned} x_{\beta_b} &= |x_b|\cos(30°) = \frac{\sqrt{3}}{2}x_b, \\ x_{\alpha_b} &= -|x_b|\sin(30°) = -\frac{1}{2}x_b, \end{aligned} \tag{A.2}$$

$$x_{\beta_c} = -|x_c|\cos(30°) = -\frac{\sqrt{3}}{2}x_c,$$
$$x_{\alpha_c} = -|x_c|\sin(30°) = -\frac{1}{2}x_c, \tag{A.3}$$

$$\begin{bmatrix} x_\alpha \\ x_\beta \end{bmatrix} = \begin{bmatrix} x_{\alpha_a} + x_{\alpha_b} + x_{\alpha_c} \\ x_{\beta_a} + x_{\beta_b} + x_{\beta_c} \end{bmatrix} = \begin{bmatrix} 1 & -\frac{1}{2} & -\frac{1}{2} \\ 0 & \frac{\sqrt{3}}{2} & -\frac{\sqrt{3}}{2} \end{bmatrix} \begin{bmatrix} x_a \\ x_b \\ x_c \end{bmatrix}. \tag{A.4}$$

Obviously, if the magnitudes of all the abc components were equal, the αβ components would both be zero. However, for a positive sequence, 3-phase system, the magnitudes of all three phase (or line) quantities are never all zero simultaneously. Also, the scaling factor that Section 4.1 made clear the necessity for is missing from (A.4). When the scaling factor is included, (A.4) becomes

$$\begin{bmatrix} x_\alpha \\ x_\beta \end{bmatrix} = \frac{2}{3}\begin{bmatrix} 1 & -\frac{1}{2} & -\frac{1}{2} \\ 0 & \frac{\sqrt{3}}{2} & -\frac{\sqrt{3}}{2} \end{bmatrix} \begin{bmatrix} x_a \\ x_b \\ x_c \end{bmatrix} = \frac{2}{3} C \boldsymbol{x_{abc}}. \tag{A.5}$$

Next, trigonometry is used to derive the inverse Clark Transform.

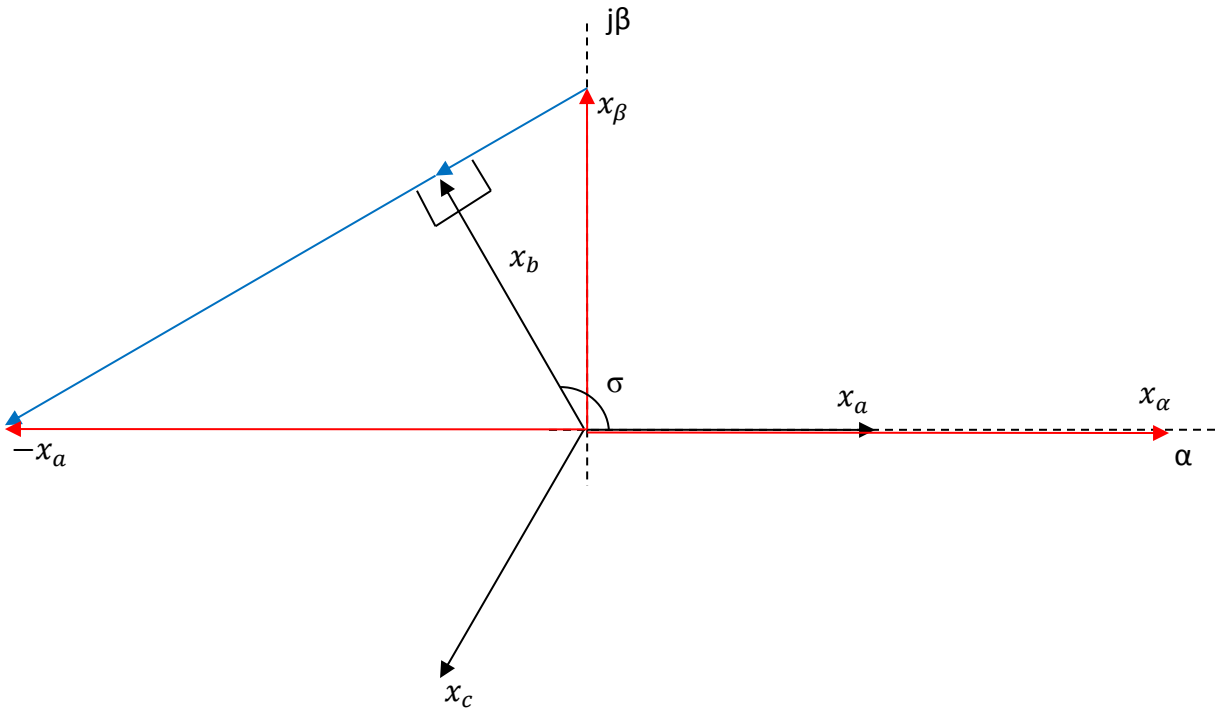

Figure A.2 Graphical Inverse Clarke Transform

Figure A.2 may be used to find the trigonometric relationships needed to find x_b from x_α and x_β. Similar vectors may be drawn for x_a and x_c, assuming σ=120°,

$$\begin{aligned} x_{a_\beta} &= 0, \\ x_{a_\alpha} &= x_\alpha, \end{aligned} \tag{A.6}$$

$$\begin{aligned} x_{b_\beta} &= x_\beta \cos(30°) = \frac{\sqrt{3}}{2} x_\beta, \\ x_{b_\alpha} &= -x_\alpha \cos(60°) = -\frac{1}{2} x_\alpha, \end{aligned} \tag{A.7}$$

$$\begin{aligned} x_{c_\beta} &= -x_\beta \cos(30°) = -\frac{\sqrt{3}}{2} x_\beta, \\ x_{c_\alpha} &= -x_\alpha \cos(60°) = -\frac{1}{2} x_\beta, \end{aligned} \tag{A.8}$$

$$\begin{bmatrix} x_a \\ x_b \\ x_c \end{bmatrix} = \begin{bmatrix} 1 & 0 \\ -\frac{1}{2} & \frac{\sqrt{3}}{2} \\ -\frac{1}{2} & -\frac{\sqrt{3}}{2} \end{bmatrix} \begin{bmatrix} x_\alpha \\ x_\beta \end{bmatrix}. \tag{A.9}$$

In order that the x_α and x_β vectors in Figure A.2 have the same magnitude as their abc counterparts, the same scaling factor must be employed [41]

$$\begin{bmatrix} x_a \\ x_b \\ x_c \end{bmatrix} = \frac{2}{3} \begin{bmatrix} 1 & 0 \\ -\frac{1}{2} & \frac{\sqrt{3}}{2} \\ -\frac{1}{2} & -\frac{\sqrt{3}}{2} \end{bmatrix} \begin{bmatrix} x_\alpha \\ x_\beta \end{bmatrix} = \frac{2}{3} C^{-1} \boldsymbol{x_{\alpha\beta}}. \tag{A.10}$$

Finally, the Clarke Transform using two line-to-line voltages is derived. From (4.10),

$$\begin{bmatrix} v_\alpha \\ v_\beta \end{bmatrix} = \frac{2}{3} \begin{bmatrix} 1 & -\frac{1}{2} & -\frac{1}{2} \\ 0 & \frac{\sqrt{3}}{2} & -\frac{\sqrt{3}}{2} \end{bmatrix} \begin{bmatrix} v_{an} \\ v_{bn} \\ v_{cn} \end{bmatrix} = \begin{bmatrix} \frac{2}{3} v_{an} - \frac{1}{3} v_{bn} - \frac{1}{3} v_{cn} \\ \frac{\sqrt{3}}{3} v_{bn} - \frac{\sqrt{3}}{3} v_{cn} \end{bmatrix} \tag{A.11}$$

and

$$\begin{aligned} v_{ab} &= v_{an} - v_{bn} \rightarrow v_{an} = v_{ab} + v_{bn} \\ v_{bc} &= v_{bn} - v_{cn}. \end{aligned} \tag{A.12}$$

Making use of (A.12), (A.11) can be rewritten as

$$\begin{aligned} \begin{bmatrix} v_\alpha \\ v_\beta \end{bmatrix} &= \begin{bmatrix} \frac{2}{3} v_{ab} + \frac{2}{3} v_{bn} - \frac{1}{3} v_{bn} - \frac{1}{3} v_{cn} \\ \frac{\sqrt{3}}{3} v_{bc} \end{bmatrix} = \begin{bmatrix} \frac{2}{3} v_{ab} + \frac{1}{3} v_{bn} - \frac{1}{3} v_{cn} \\ \frac{\sqrt{3}}{3} v_{bc} \end{bmatrix} \\ &= \begin{bmatrix} \frac{2}{3} v_{ab} + \frac{1}{3} v_{bc} \\ \frac{\sqrt{3}}{3} v_{bc} \end{bmatrix}. \end{aligned} \tag{A.13}$$

Then

$$\begin{bmatrix} v_\alpha \\ v_\beta \end{bmatrix} = \frac{1}{3} \begin{bmatrix} 2 & 1 \\ 0 & \sqrt{3} \end{bmatrix} \begin{bmatrix} v_{ab} \\ v_{bc} \end{bmatrix}. \tag{A.14}$$

Appendix B - Simulink Model

The top level of the Simulink model for the 10 kW system was given in Figure 9.3. The models used for simulating each system are almost identical. Screenshots of each part of the 10 kW model not shown in Figure 9.3 are given below. The parts of the models that are identical between the two systems are denoted “Identical” in the caption. The model hierarchy is included in each screenshot to help clarify where each part fits into the whole.

10 kW System and Identical Parts

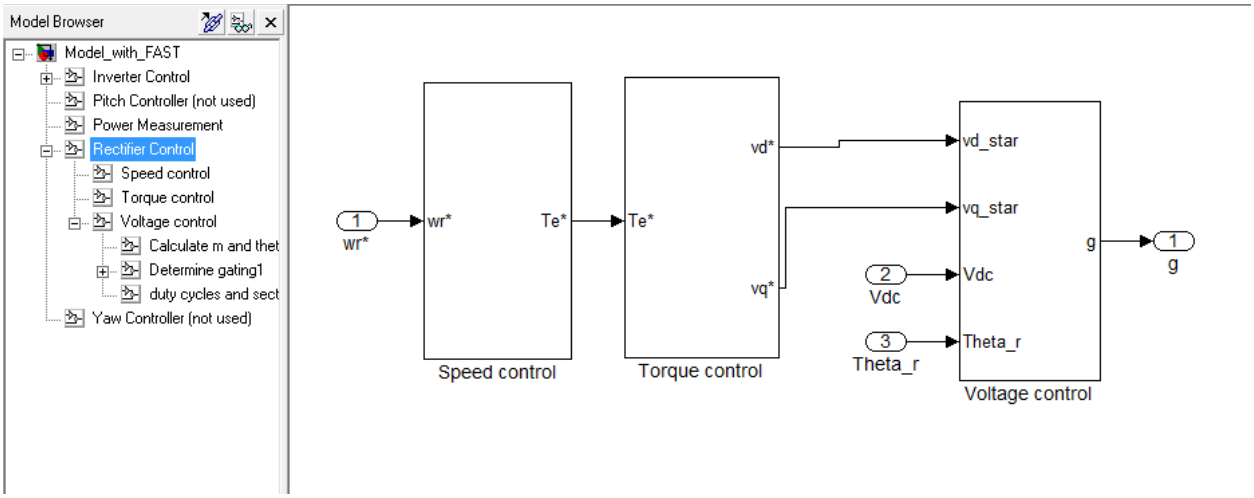

Figure B.1 Rectifier Control Simulink Model (Identical)

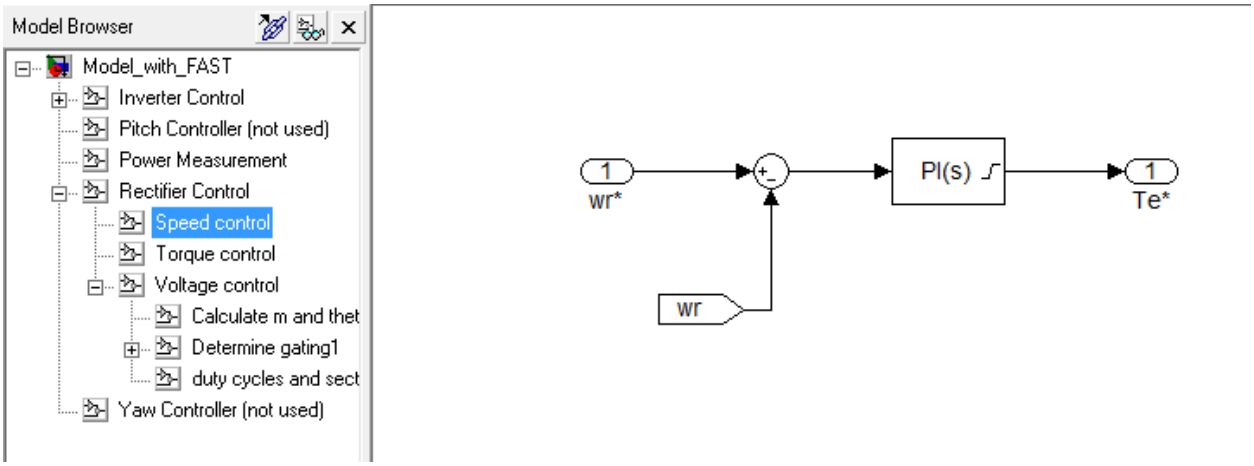

Figure B.2 Speed Control Simulink Model

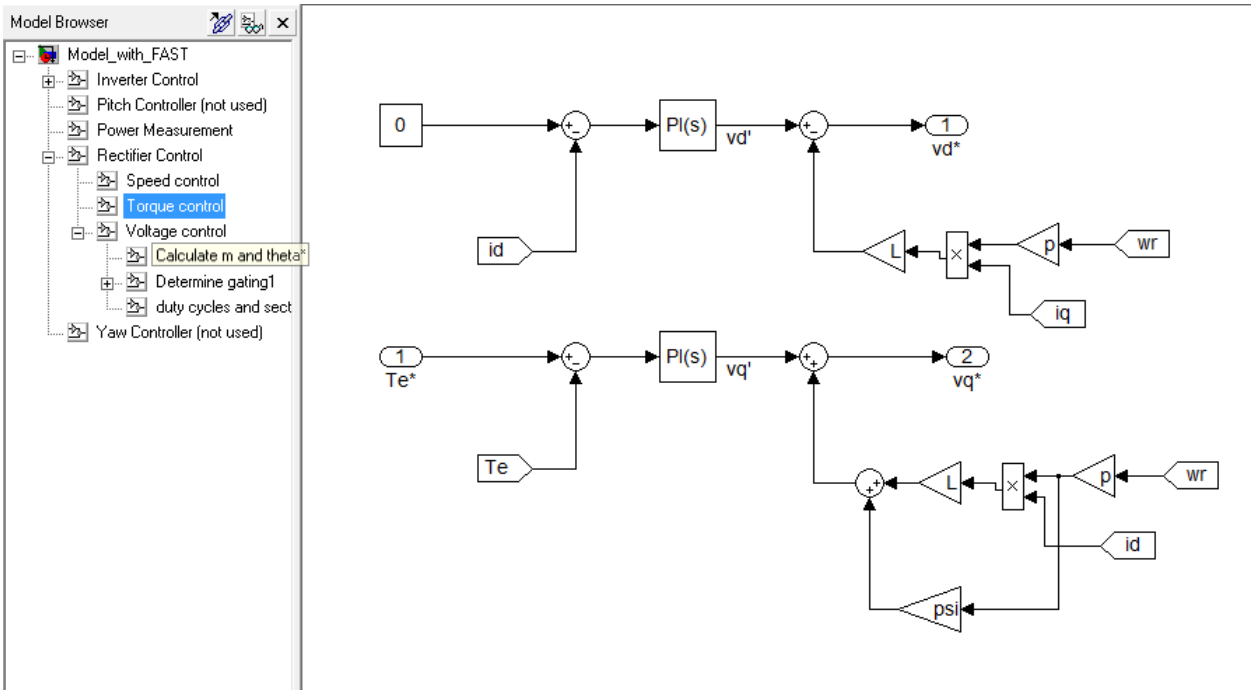

Figure B.3 Torque Control Simulink Model (Identical)

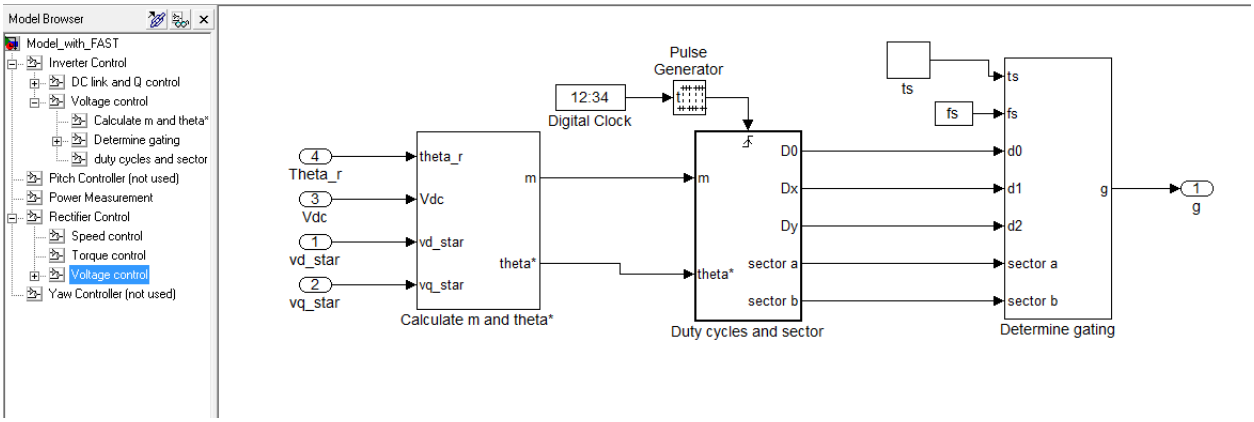

Figure B.4 Rectifier Voltage Control Simulink Model (Identical)

The "ts" block in Figure B.4 is a repeating sequence block with time and output values both [0 1/fs]. The Pulse Generator block has amplitude = 1, period = floor(DT/fs) samples, pulse width = 2 samples, phase delay=0.

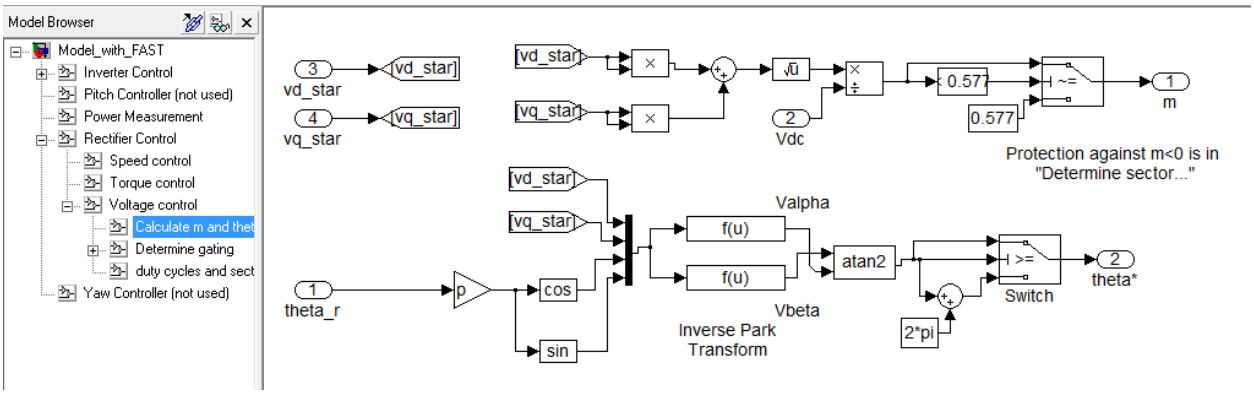

Figure B.5 m and θ^* Calculation Simulink Model (Rectifier, Identical)

Figure B.6 - Figure B.8 show blocks that are used in both the rectifier and inverter controllers, i.e. identical sets of blocks are used in each.

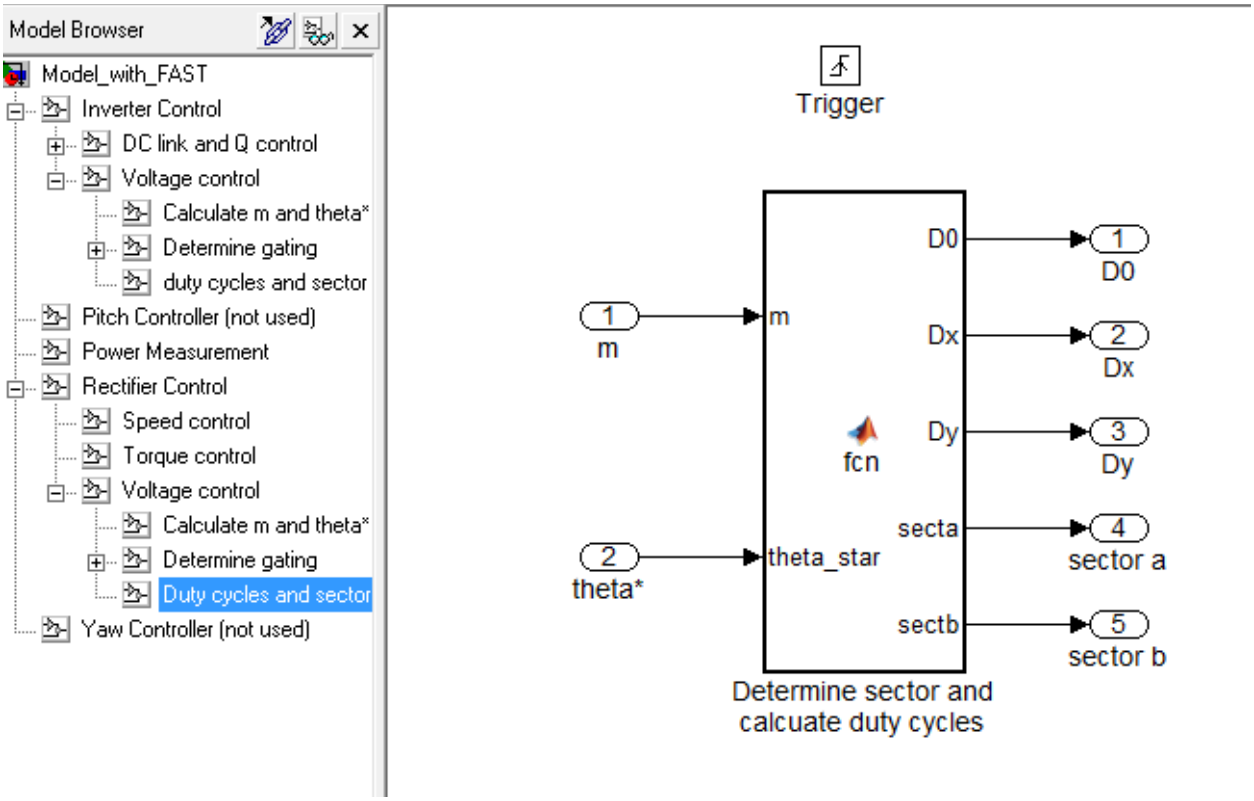

Figure B.6 Sector Determination and Duty Cycle Calculation Simulink Model (Rectifier and Inverter, Identical)

The MATLAB code used in the "Determine…" block in Figure B.6 is given below.

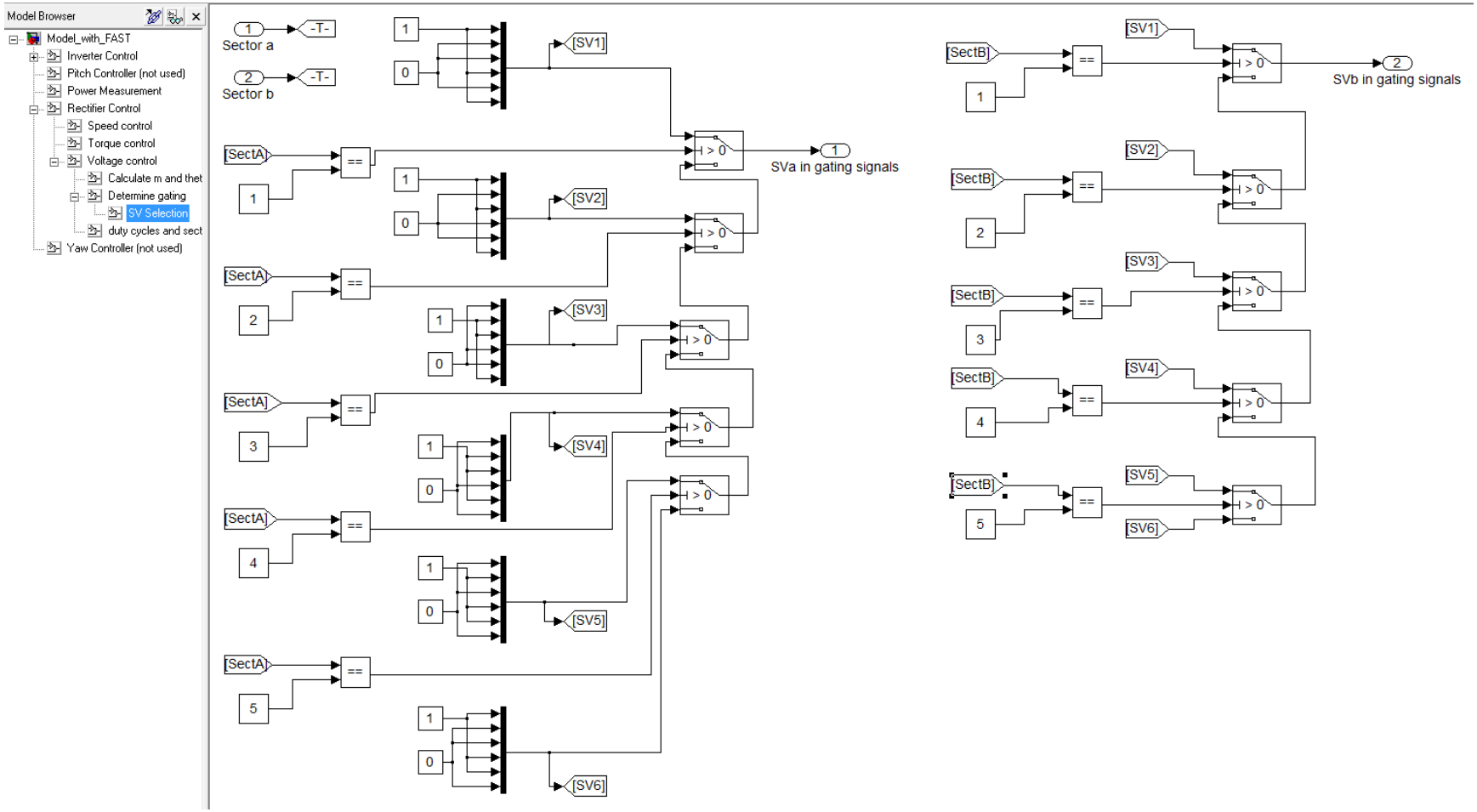

Figure B.7 Space-vector Selection Simulink Model (Rectifier and Inverter, Identical)

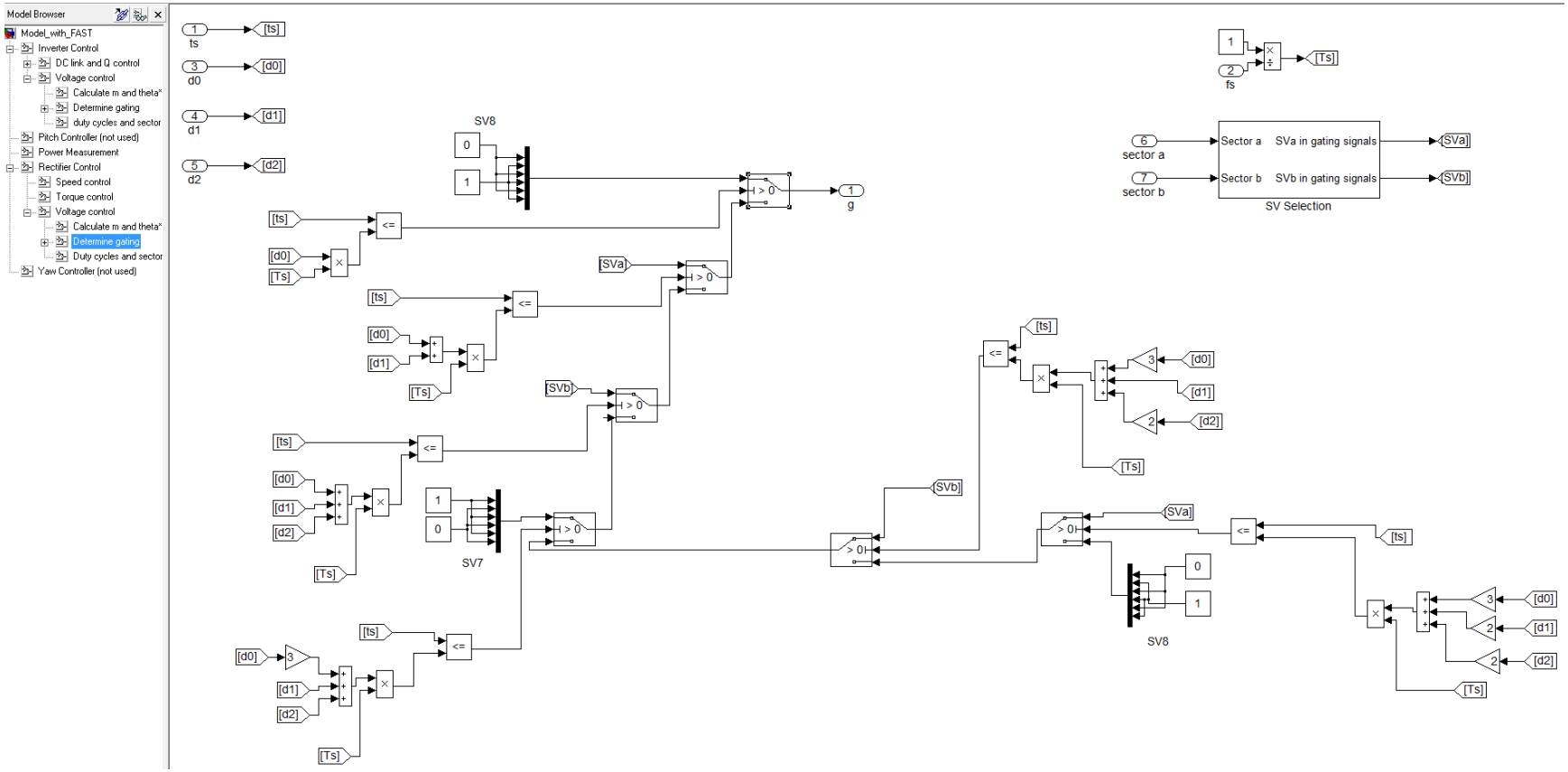

Figure B.8 Gating Signal Determination Simulink Model (Rectifier and Inverter, Identical)

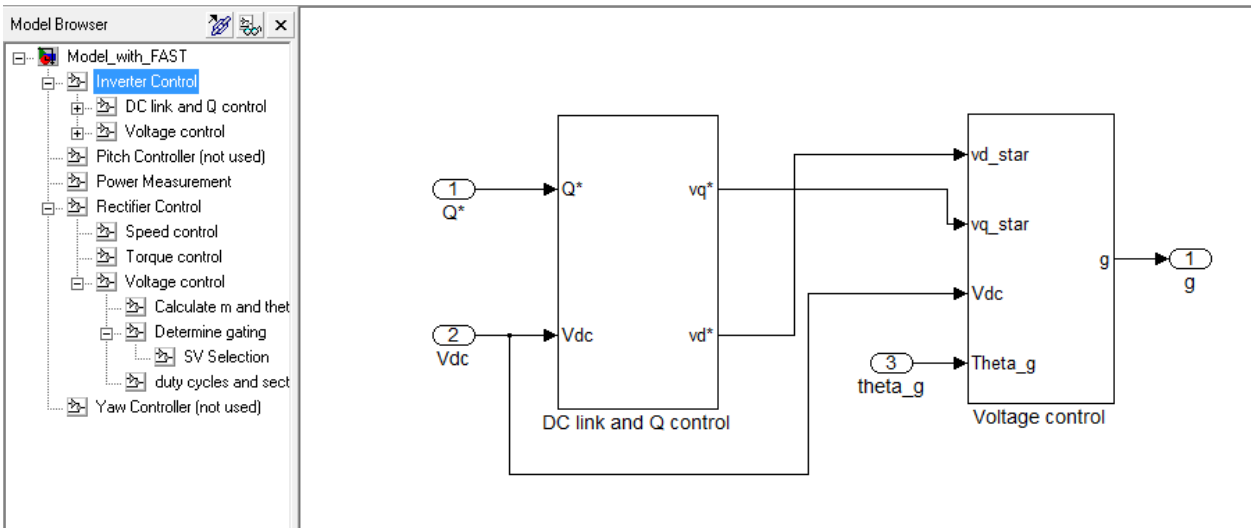

Figure B.9 Inverter Control Simulink Model (Identical)

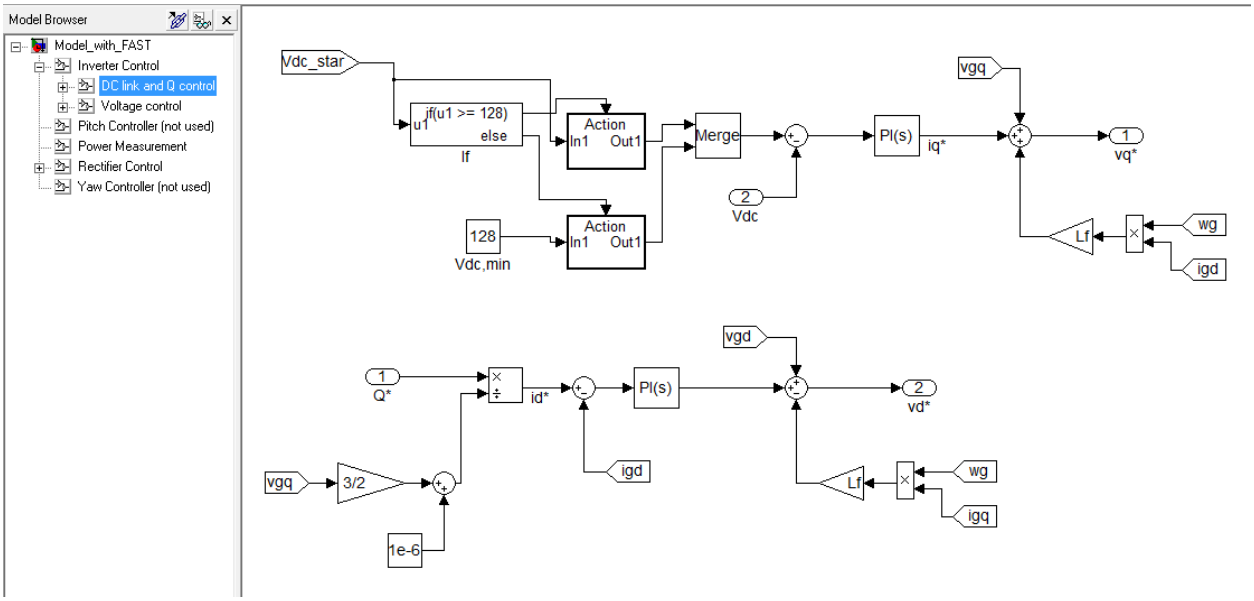

Figure B.10 DC Link Voltage and Reactive Power Control Simulink Model

Vdc,min in Figure B.10 is 128 V for the 10kW system only. For the 5 MW system, it is 920 V. The Action subsystems in Figure B.10 simply pass their input directly to their output.

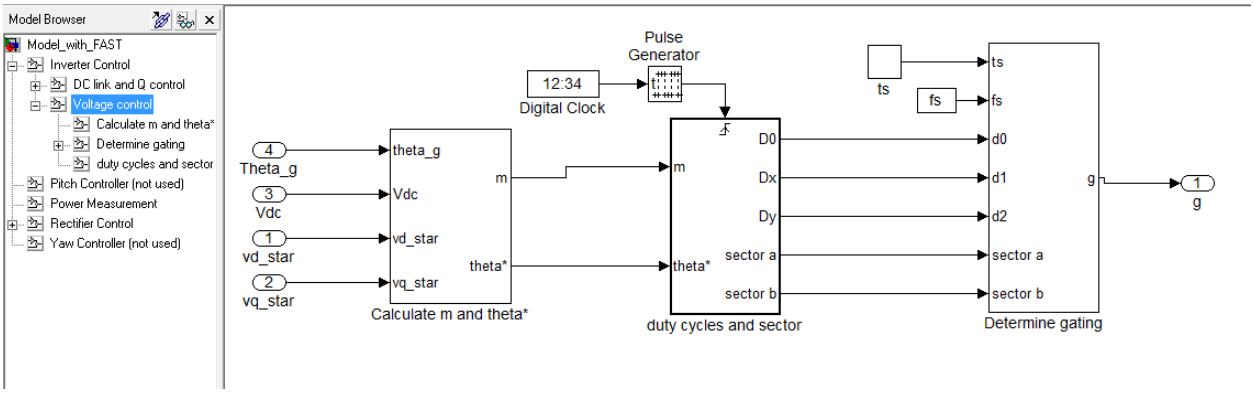

Figure B.11 Inverter Voltage Control Simulink Model (Identical)

The Pulse Generator and ts blocks in Figure B.11 are the same as those in Figure B.4.

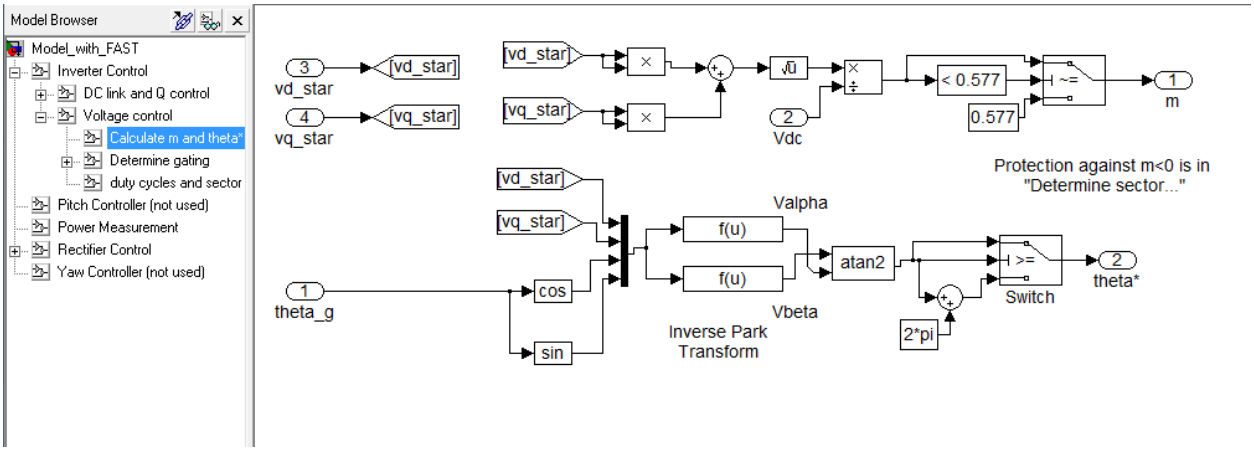

Figure B.12 m and θ^* Calculation Simulink Model (Inverter, Identical)

The rest of the inverter control blocks are the same as those in Figure B.6 - Figure B.8.

Figure B.13 shows the blocks used to implement the two wattmeter method, which was used to measure the real and reactive power outputs of the inverter [44, pp. 34-38].

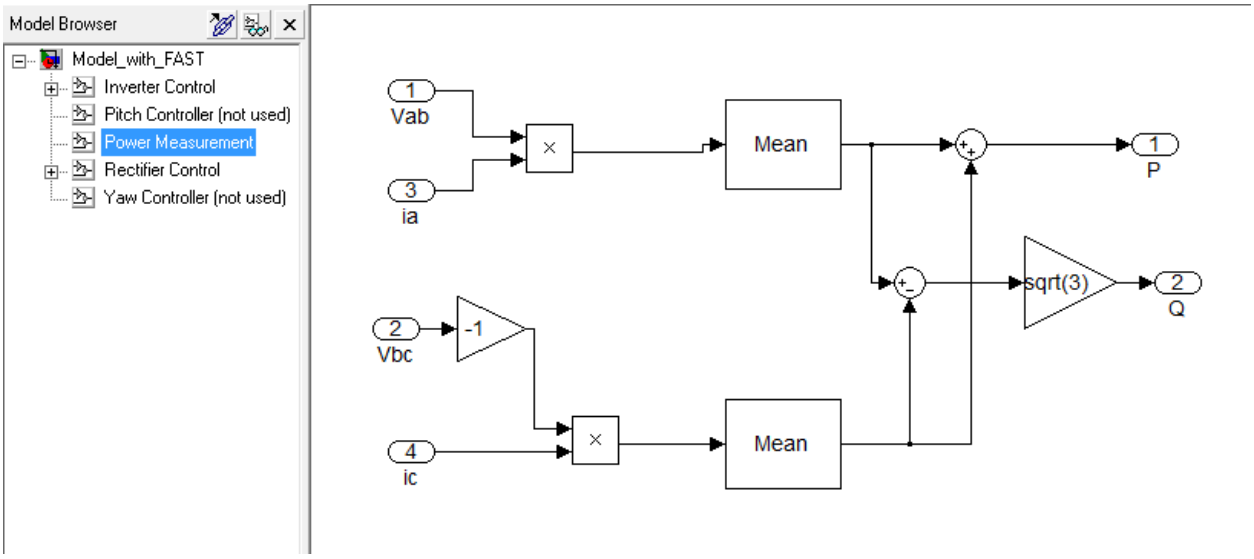

Figure B.13 Power Measurement Simulink Model

The MATLAB code used in the "determine sector…" block in Figure B.6 is:

```
function [D0,Dx,Dy,secta,sectb]  = fcn(m,theta_star)

SV_angle=[0 pi/3 2*pi/3 pi 4*pi/3 5*pi/3];  %ANGLES OF BASE SPACE-VECTORS
reverse=0;
sect=[0 0];
theta_rel=0;    %RELATIVE ANGLE B/W THE IDEAL SV LOCATION AND THE MORE CCW
BASE SPACE-VECTOR FOR A SECTOR

theta_set=theta_star;     %ANGLE OF THE SV THE CONTROLLER'S TRYING TO
SYNTHESIZE

while theta_set>2*pi
    theta_set=theta_set-2*pi;
end
if theta_set<SV_angle(2) && theta_set>=SV_angle(1)
    sect=[1 2];
    theta_rel=theta_set-SV_angle(1);
    reverse=0;
elseif theta_set<SV_angle(3) && theta_set>=SV_angle(2)
    sect=[2 3];
    theta_rel=theta_set-SV_angle(2);
    reverse=1;
elseif theta_set<SV_angle(4) && theta_set>=SV_angle(3)
    sect=[3 4];
    theta_rel=theta_set-SV_angle(3);
    reverse=0;
elseif theta_set<SV_angle(5) && theta_set>=SV_angle(4)
    sect=[4 5];
    theta_rel=theta_set-SV_angle(4);
    reverse=1;
```

```
elseif theta_set<SV_angle(6) && theta_set>=SV_angle(5)
    sect=[5 6];
    theta_rel=theta_set-SV_angle(5);
    reverse=0;
elseif theta_set<2*pi || theta_set>=SV_angle(6)
    sect=[6 1];
    theta_rel=theta_set-SV_angle(6);
    reverse=1;
end

if m<0
    M=0.01;
else
    M=m;
end

dy=sqrt(3)*M*sin(theta_rel);
dx=sqrt(3)*M*cos(theta_rel+pi/6);
d0=1-dx-dy;

if reverse==1;
    d_one=dx;
    d_two=dy;
    dx=d_two;
    dy=d_one;
    sect=[sect(2) sect(1)];
end

% THE OUTPUTS TO THE GATING FUNCTION ARE DIVIDED BY 2 (d1 AND d2) OR 4 (d0)
% TO ACCOUNT FOR SYMMETRICAL SEQUENCING.
D0=d0/4;         %SPLIT THE 0 VECTOR INTO FOUR SECTIONS
Dx=dx/2;         %SPLIT INTO TWO SECTIONS
Dy=dy/2;         %SPLIT INTO TWO SECTIONS
secta=sect(1);
sectb=sect(2);
```

5 MW System Unique Parts

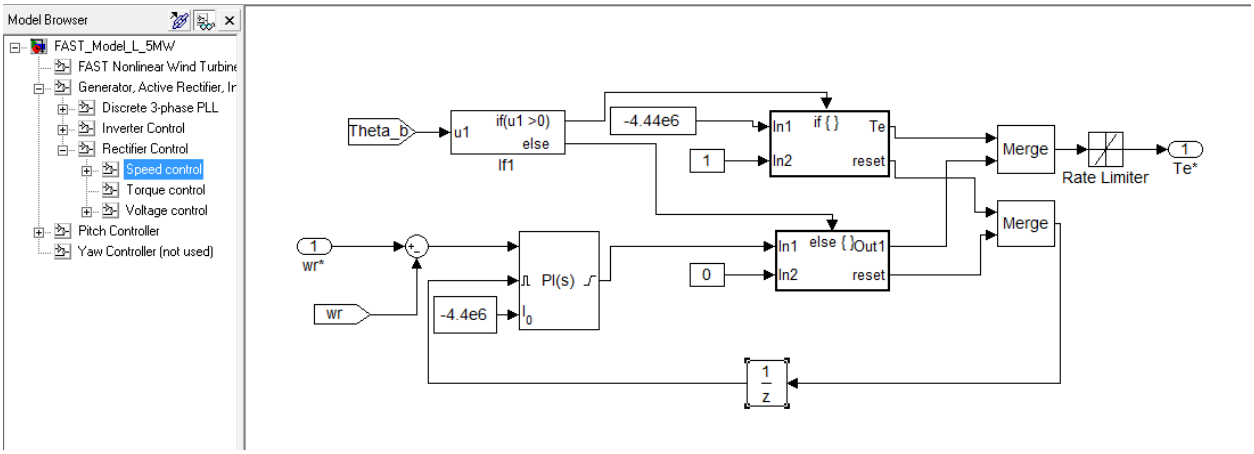

Figure B.14 Speed Control Simulink Model

Figure B.14 shows the Simulink blocks used to implement speed control in the 5 MW system. They are different from those in the 10 kW system to account for the blade pitch speed control (see below). To ensure maximum power capture, and to prevent the pitch and torque controllers from working at the same time, the "if" block in Figure B.14 sets the generator torque to its maximum value if the blade pitch is nonzero. Also, if the blade pitch is nonzero, the PI controller is reset and its new initial value is set to the maximum generator torque. This ensures that the torque controller is ready to take over speed control when the blade pitch goes to zero.

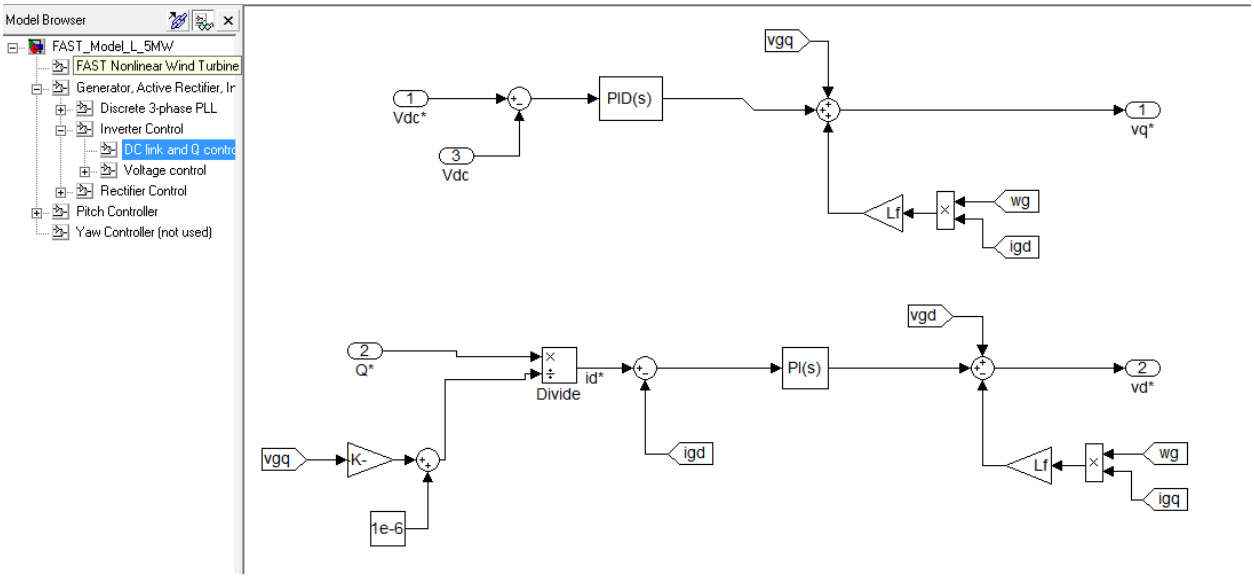

Figure B.15 DC Link and Reactive Power Controllers

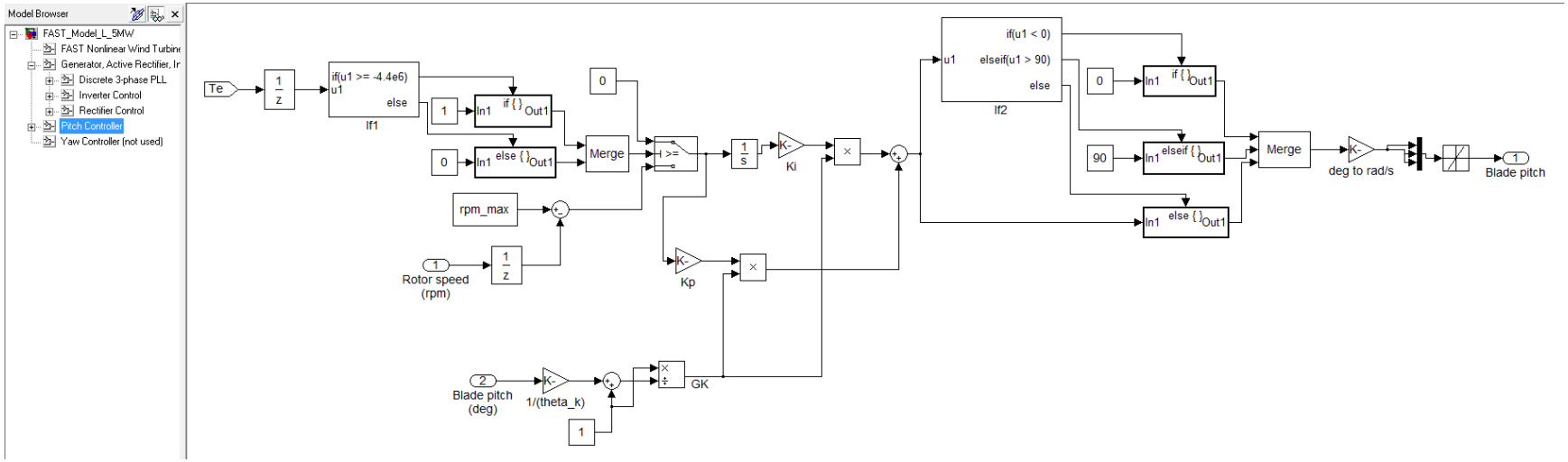

Figure B.16 Blade Pitch Controller Model

Appendix C - NREL CAE Tools Input Files

10 kW System

The following NREL CAE tools were used as part of, or in the development of, the 10 kW system model:

1. Modes
2. TurbSim
3. AeroDyn
4. FAST

Following are the input files used for each of the tools.

Modes

UAE_Tower_SWRT.inp:

```
False     Blade Switch:  True = Blade, False = Tower
   0.0    Steady state angular velocity of rotor (rpm)  [Ignored for towers]
   0.0    Pitch angle for blades (degrees)  [Ignored for towers]
  11.5    Total beam length (m)
   0.0    Rigid beam length (m)
301.252  End mass (kg)
   5      Number of modes shapes or coefficients
   2      Order of first coefficient
   6      Number of input stations for distributed parameters
   1.0    Factor to adjust mass
   1.0    Factor to adjust tower stiffness
   1.0    Factor to adjust in-plane stiffness  [Ignored for towers]
0.00000  260.467  235869817.7
0.29565  260.467  235869817.7
0.29574  260.467  235869817.7
0.33904  207.107  79470442.3
0.33913  207.107  79470442.3
1.00000  207.107  79470442.3

For the lines of distributed parameters, the first column is the fractional
distance along the flexible portion of the tower.  It must go from 0 to 1.
The second column is the mass/length in kg/m, and the third column is the
stiffness in N m^2.
```

TurbSim

TurbSim_7.inp:

```
TurbSim Input File. Valid for TurbSim v1.50, 25-Sep-2009
```

```
---------Runtime Options-----------------------------------
2318573             RandSeed1       - First random seed  (-2147483648 to
2147483647)
RANLUX              RandSeed2       - Second random seed (-2147483648 to
2147483647) for intrinsic pRNG, or an alternative pRNG: "RanLux" or "RNSNLW"
False               WrBHHTP         - Output hub-height turbulence parameters
in binary form?  (Generates RootName.bin)
False               WrFHHTP         - Output hub-height turbulence parameters
in formatted form?  (Generates RootName.dat)
False               WrADHH          - Output hub-height time-series data in
AeroDyn form?  (Generates RootName.hh)
True                WrADFF          - Output full-field time-series data in
TurbSim/AeroDyn form? (Generates Rootname.bts)
False               WrBLFF          - Output full-field time-series data in
BLADED/AeroDyn form?  (Generates RootName.wnd)
True                WrADTWR         - Output tower time-series data?
(Generates RootName.twr)
False               WrFMTFF         - Output full-field time-series data in
formatted (readable) form?  (Generates RootName.u, RootName.v, RootName.w)
False               WrACT           - Output coherent turbulence time steps
in AeroDyn form? (Generates RootName.cts)
True                Clockwise       - Clockwise rotation looking downwind?
(used only for full-field binary files - not necessary for AeroDyn)
 0                  ScaleIEC        - Scale IEC turbulence models to exact
target standard deviation? [0=no additional scaling; 1=use hub scale
uniformly; 2=use individual scales]

--------Turbine/Model Specifications-----------------------
6                  NumGrid_Z       - Vertical grid-point matrix dimension
6                  NumGrid_Y       - Horizontal grid-point matrix dimension
0.05                TimeStep        - Time step [seconds]
600                 AnalysisTime    - Length of analysis time series
[seconds] (program will add time if necessary: AnalysisTime =
MAX(AnalysisTime, UsableTime+GridWidth/MeanHHWS) )
70                  UsableTime      - Usable length of output time series
[seconds] (program will add GridWidth/MeanHHWS seconds)
11.5             HubHt           - Hub height [m] (should be >
0.5*GridHeight)
8.0               GridHeight      - Grid height [m]
8.0               GridWidth       - Grid width [m] (should be >=
2*(RotorRadius+ShaftLength))
0                   VFlowAng        - Vertical mean flow (uptilt) angle
[degrees]
0                   HFlowAng        - Horizontal mean flow (skew) angle
[degrees]

--------Meteorological Boundary Conditions-------------------
"IECKAI"            TurbModel       - Turbulence model ("IECKAI"=Kaimal,
"IECVKM"=von Karman, "GP_LLJ", "NWTCUP", "SMOOTH", "WF_UPW", "WF_07D",
"WF_14D", or "NONE")
"1-ED3"             IECstandard     - Number of IEC 61400-x standard (x=1,2,
or 3 with optional 61400-1 edition number (i.e. "1-Ed2") )
"A"                 IECturbc        - IEC turbulence characteristic ("A",
"B", "C" or the turbulence intensity in percent) ("KHTEST" option with NWTCUP
model, not used for other models)
```

```
"NTM"               IEC_WindType    - IEC turbulence type ("NTM"=normal,
"xETM"=extreme turbulence, "xEWM1"=extreme 1-year wind, "xEWM50"=extreme 50-
year wind, where x=wind turbine class 1, 2, or 3)
default             ETMc            - IEC Extreme Turbulence Model "c"
parameter [m/s]
default             WindProfileType - Wind profile type
("JET","LOG"=logarithmic,"PL"=power law,"IEC"=PL on rotor disk,LOG elsewhere,
or "default")
11.5                RefHt           - Height of the reference wind speed [m]
7.0                URef            - Mean (total) wind speed at the reference
height [m/s] (or "default" for JET wind profile)
default             ZJetMax         - Jet height [m] (used only for JET wind
profile, valid 70-490 m)
default             PLExp           - Power law exponent [-] (or "default")
default             Z0              - Surface roughness length [m] (or
"default")

--------Non-IEC Meteorological Boundary Conditions------------
default             Latitude        - Site latitude [degrees] (or "default")
0.05                RICH_NO         - Gradient Richardson number
default             UStar           - Friction or shear velocity [m/s] (or
"default")
default             ZI              - Mixing layer depth [m] (or "default")
default             PC_UW           - Hub mean u'w' Reynolds stress (or
"default")
default             PC_UV           - Hub mean u'v' Reynolds stress (or
"default")
default             PC_VW           - Hub mean v'w' Reynolds stress (or
"default")
default             IncDec1         - u-component coherence parameters (e.g.
"10.0  0.3e-3" in quotes) (or "default")
default             IncDec2         - v-component coherence parameters (e.g.
"10.0  0.3e-3" in quotes) (or "default")
default             IncDec3         - w-component coherence parameters (e.g.
"10.0  0.3e-3" in quotes) (or "default")
default             CohExp          - Coherence exponent (or "default")

--------Coherent Turbulence Scaling Parameters-------------------
"E:\Program Files\TurbSim\Test\EventData"  CTEventPath     - Name of the path
where event data files are located
"Random"            CTEventFile     - Type of event files ("LES", "DNS", or
"RANDOM")
true                Randomize       - Randomize the disturbance scale and
locations? (true/false)
 1.0                DistScl         - Disturbance scale (ratio of wave height
to rotor disk). (Ignored when Randomize = true.)
 0.5                CTLy            - Fractional location of tower centerline
from right (looking downwind) to left side of the dataset. (Ignored when
Randomize = true.)
 0.5                CTLz            - Fractional location of hub height from
the bottom of the dataset. (Ignored when Randomize = true.)
30.0                CTStartTime     - Minimum start time for coherent
structures in RootName.cts [seconds]

================================================
```

NOTE: Do not add or remove any lines in this file!

Test17_AD_FMN.ipt:

```
SWRT rotor aerodynamic parameters for FAST certification test #17 (modified).
SI                                  SysUnits - System of units for used
for input and output [must be SI for FAST] (unquoted string)
BEDDOES                             StallMod - Dynamic stall included
[BEDDOES or STEADY] (unquoted string)
NO_CM                               UseCm    - Use aerodynamic pitching
moment model? [USE_CM or NO_CM] (unquoted string)
DYNIN                               InfModel - Inflow model [DYNIN or
EQUIL] (unquoted string)
SWIRL                               IndModel - Induction-factor model
[NONE or WAKE or SWIRL] (unquoted string)
   0.005                            AToler   - Induction-factor tolerance
(convergence criteria) (-)
PRANDtl                             TLModel  - Tip-loss model (EQUIL only)
[PRANDtl, GTECH, or NONE] (unquoted string)
NONE                                HLModel  - Hub-loss model (EQUIL only)
[PRANdtl or NONE] (unquoted string)
"Wind\SWRT\NoShr.wnd"               WindFile - Name of file containing
wind data (quoted string)
  12.119                           HH       - Wind reference (hub) height
[TowerHt+Twr2Shft+OverHang*SIN(ShftTilt)] (m)
   0.0                              TwrShad  - Tower-shadow velocity
deficit (-)
9999.9                              ShadHWid - Tower-shadow half width (m)
9999.9                              T_Shad_Refpt - Tower-shadow reference
point (m)
   1.225                              AirDens  - Air density (kg/m^3)
   1.5100E-05                       KinVisc  - Kinematic air viscosity
(m^2/sec)
   1.0000E-03                       DTAero   - Time interval for
aerodynamic calculations (sec)
   4                                NumFoil  - Number of airfoil files (-)
"AeroData\SWRT\TailPlate.dat"       FoilNm   - Names of the airfoil files
[NumFoil lines] (quoted strings)
"AeroData\SWRT\SH3052Mod_AllRe_Hanley.dat"
"AeroData\SWRT\SH3052Mod_AllRe_Elem14_Hanley.dat"
"AeroData\SWRT\SH3052Mod_AllRe_Elem15_Hanley.dat"
  15                                BldNodes - Number of blade nodes used
for analysis (-)
RNodes    AeroTwst  DRNodes  Chord  NFoil  PrnElm
0.4667    0.00      0.2092   0.213  2      NOPRINT
0.6759    0.00      0.2092   0.213  2      NOPRINT
0.8851    0.00      0.2092   0.213  2      NOPRINT
1.0943    0.00      0.2092   0.213  2      NOPRINT
1.3035    0.00      0.2092   0.213  2      NOPRINT
1.5127    0.00      0.2092   0.213  2      NOPRINT
1.7219    0.00      0.2092   0.213  2      NOPRINT
1.9311    0.00      0.2092   0.213  2      NOPRINT
2.1403    0.00      0.2092   0.213  2      NOPRINT
2.3495    0.00      0.2092   0.213  2      NOPRINT
2.5587    0.00      0.2092   0.213  2      NOPRINT
```

```
2.7679    0.00      0.2092   0.213  2      NOPRINT
2.9770    0.00      0.2092   0.213  2      NOPRINT
3.18643    1.60      0.2092   0.201  3      NOPRINT
3.3955    3.20      0.2092   0.181  4      NOPRINT
ReNum
```

TailPlate.dat:

```
TailPlate.dat. Lift and drag on delta wing. See Hoerner Lift page 18-5,
Figure 7
Oct. 14, 2003, Foilchecked by Windward Engineering.
   1  Number of airfoil tables in this file
     0.00   Table ID parameter
     0.00   No longer used, enter zero
     0.00   No longer used, enter zero
     0.00   No longer used, enter zero
     0.00   No longer used, enter zero
    -4.23   Zero lift angle of attack (deg)
    2.71555 Cn slope for zero lift (dimensionless)
     1.8588 Cn at stall value for positive angle of attack
    -0.8000 Cn at stall value for negative angle of attack
     0.0000 Angle of attack for minimum CD (deg)
     0.0100 Minimum CD value
  -180.00     0.000      0.1820
  -170.00     0.144      0.2155
  -160.00     0.287      0.3114
  -150.00     0.431      0.4576
  -140.00     0.524      0.6353
  -130.00     0.479      0.8212
  -120.00     0.398      0.9910
  -110.00     0.285      1.1219
  -100.00     0.147      1.1954
   -90.00     0.000      1.2000
   -80.00    -0.147      1.1954
   -70.00    -0.285      1.1219
   -60.00    -0.398      0.9910
   -50.00    -0.479      0.8212
   -40.00    -0.524      0.6353
   -30.00    -0.404      0.4722
   -20.00    -0.223      0.3181
   -10.00    -0.041      0.1641
     0.00     0.200      0.0100
     4.00     0.390      0.0230
     8.00     0.576      0.0630
    12.00     0.758      0.1280
    16.00     0.861      0.2190
    20.00     0.963      0.3340
    24.00     1.041      0.4730
    35.00     1.106      0.7830
    37.00     0.759      0.5800
    40.00     0.748      0.6353
    50.00     0.684      0.8212
    60.00     0.569      0.9910
    70.00     0.407      1.1219
```

```
    80.00     0.210      1.1954
    90.00     0.000      1.2000
   100.00    -0.147      1.1954
   110.00    -0.285      1.1219
   120.00    -0.398      0.9910
   130.00    -0.479      0.8212
   140.00    -0.524      0.6353
   150.00    -0.431      0.4577
   160.00    -0.287      0.3114
   170.00    -0.144      0.2155
   180.00     0.000      0.1820
```

SH3052Mod_AllRe_Elem15_Hanley.dat:

```
SH3052 data from T Hanley XFOIL predictions
Reinterpolated and foilchecked by CH Feb04
3     Number of airfoil tables in this file
0.3   0.5   1.2   Table ID parameter, typically Re in millions
11.0  10.0  9.0   Stall angle (deg)
0     0     0     No longer used, enter zero
0     0     0     No longer used, enter zero
0     0     0     No longer used, enter zero
-10.152     -10.285     -10.251     Zero Cn angle of attack (deg)
6.249 6.261 6.372 Cn slope for zero lift (dimensionless)
2.307 2.217 2.141 Cn extrapolated to value at positive stall angle of attack
-0.8  -0.8  -0.8  Cn at stall value for negative angle of attack
-3.0  -3.0  -3.0  Angle of attack for minimum CD (deg)
0.0171      0.01335     0.01155     Minimum CD value
-180  0     0.04485     0     0.02745     0     0.054
-170  0.41544     0.1026      0.42561     0.0855      0.42471     0.1116
-160  0.83097     0.2685      0.85122     0.25215     0.84942     0.2772
-150  0.91332     0.5226      0.93285     0.5076      0.93105     0.53055
-140  0.74187     0.83385     0.75375     0.8205      0.75267     0.8409
-130  0.60201     1.16445     0.60903     1.1532      0.6084      1.1703
-120  0.45999     1.47375     0.46368     1.46505     0.46341     1.47825
-110  0.3078      1.72395     0.30942     1.7181      0.30924     1.7271
-100  0.15048     1.88445     0.15084     1.88145     0.15084     1.8861
-90   0     1.935 0     1.935 0     1.935
-80   -0.15048    1.88445     -0.15084    1.88145     -0.15084    1.8861
-70   -0.3078     1.72395     -0.30942    1.7181      -0.30924    1.7271
-60   -0.45999    1.47375     -0.46368    1.46505     -0.46341    1.47825
-50   -0.60201    1.16445     -0.60903    1.1532      -0.6084     1.1703
-40   -0.74187    0.83385     -0.75375    0.8205      -0.75267    0.8409
-30   -1.0148     0.3484      -1.0365     0.3384      -1.0345     0.3537
-20   -0.7899     0.1969      -0.7974     0.1880      -0.7912     0.1996
-10   -0.0575     0.1260      -0.0260     0.1165      -0.0133     0.1212
-5    0.3891      0.0298      0.4589      0.0218      0.4812      0.0184
-4    0.5716      0.0232      0.5877      0.0196      0.5967      0.0174
-3    0.6950      0.0228      0.7100      0.0178      0.7187      0.0154
-2    0.7940      0.0246      0.8094      0.0188      0.8212      0.0158
-1    0.8946      0.0254      0.9087      0.0198      0.9219      0.0166
0     0.9932      0.0262      1.0072      0.0206      1.0216      0.0172
1     1.0899      0.0270      1.1038      0.0214      1.1195      0.0182
2     1.1838      0.0282      1.1981      0.0226      1.2155      0.0192
3     1.2741      0.0296      1.2896      0.0238      1.3091      0.0204
```

```
4     1.3608      0.0314      1.3780      0.0254      1.4001      0.0218
5     1.4429      0.0334      1.4621      0.0272      1.4875      0.0234
6     1.5190      0.0358      1.5411      0.0294      1.5691      0.0254
7     1.5857      0.0386      1.6109      0.0322      1.6397      0.0288
8     1.6325      0.0424      1.6631      0.0360      1.6947      0.0332
9     1.6392      0.0463      1.6697      0.0407      1.6715      0.0407
10    1.6247      0.0517      1.6497      0.0485      1.6126      0.0535
11    1.5964      0.0617      1.5840      0.0639      1.5701      0.0660
12    1.5398      0.0778      1.4960      0.0867      1.5398      0.0782
13    1.4550      0.1037      1.4337      0.1094      1.4956      0.0952
14    1.3557      0.1382      1.3788      0.1328      1.4424      0.1157
15    1.2786      0.1707      1.3242      0.1579      1.3777      0.1419
16    1.2196      0.1991      1.2683      0.1841      1.3114      0.1705
17    1.1720      0.2242      1.2147      0.2105      1.2577      0.1958
18    1.1271      0.2479      1.1626      0.2368      1.2062      0.2207
19    1.0907      0.2654      1.1153      0.2609      1.1591      0.2436
20    1.1479      0.2723      1.1557      0.2777      1.1974      0.2640
21    1.2120      0.2734      1.2098      0.2872      1.2362      0.2832
22    1.2787      0.2720      1.2672      0.2943      1.2813      0.2981
23    1.3408      0.2735      1.3271      0.2978      1.3310      0.3092
24    1.3958      0.2794      1.3866      0.3005      1.3846      0.3173
25    1.4089      0.3160      1.4432      0.3031      1.4402      0.3229
30    1.4497      0.3484      1.4807      0.3384      1.4779      0.3537
40    1.05975     0.83385     1.07676     0.8205      1.07523     0.8409
50    0.86004     1.16445     0.87012     1.1532      0.86922     1.1703
60    0.65709     1.47375     0.6624      1.46505     0.66195     1.47825
70    0.43965     1.72395     0.44199     1.7181      0.44181     1.7271
80    0.21492     1.88445     0.21546     1.88145     0.21546     1.8861
90    0     1.935 0     1.935 0     1.935
100   -0.15048    1.88445     -0.15084    1.88145     -0.15084    1.8861
110   -0.3078     1.72395     -0.30942    1.7181      -0.30924    1.7271
120   -0.45999    1.47375     -0.46368    1.46505     -0.46341    1.47825
130   -0.60201    1.16445     -0.60903    1.1532      -0.6084     1.1703
140   -0.74187    0.83385     -0.75375    0.8205      -0.75267    0.8409
150   -0.91332    0.5226      -0.93285    0.5076      -0.93105    0.53055
160   -0.83097    0.2685      -0.85122    0.25215     -0.84942    0.2772
170   -0.41544    0.1026      -0.42561    0.0855      -0.42471    0.1116
180   0     0.04485     0     0.02745     0     0.054
```

SH3052Mod_AllRe_Elem14_Hanley.dat:

```
SH3052 _6te (14th element) data from T Hanley XFOIL predictions
Reinterpolated and foilchecked by CH Feb04
3     Number of airfoil tables in this file
0.3   0.6   1.2   Table ID parameter, Re in millions
12.0  11.0  10.0  Stall angle (deg)
0     0     0     No longer used, enter zero
0     0     0     No longer used, enter zero
0     0     0     No longer used, enter zero
-7.300      -7.265      -7.214      Zero Cn angle of attack (deg)
6.075 6.127 6.228 Cn slope for zero lift (dimensionless)
2.046 1.953 1.871 Cn extrapolated to value at positive stall angle of attack
-0.8  -0.8  -0.8  Cn at stall value for negative angle of attack
-3.0  -2.0  -2.0  Angle of attack for minimum CD (deg)
0.01058     0.00829     0.00678     Minimum CD value
```

-180.0 0.0000 -0.0261 0.0000 -0.0203 0.0000 -
0.0015
-170.0 0.3963 0.0132 0.3975 0.0189 0.3919
0.0375
-160.0 0.7926 0.1263 0.7950 0.1319 0.7837
0.1495
-150.0 0.9401 0.2999 0.9427 0.3049 0.9307
0.3212
-140.0 0.7788 0.5130 0.7804 0.5175 0.7731
0.5319
-130.0 0.6421 0.7402 0.6430 0.7440 0.6387
0.7561
-120.0 0.4967 0.9544 0.4972 0.9574 0.4949
0.9668
-110.0 0.3358 1.1302 0.3360 1.1322 0.3350
1.1386
-100.0 0.1656 1.2466 0.1657 1.2476 0.1654
1.2508
-90.0 0.0000 1.2900 0.0000 1.2900 0.0000 1.2900
-80.0 -0.1656 1.2466 -0.1657 1.2476 -0.1654 1.2508
-70.0 -0.3358 1.1302 -0.3360 1.1322 -0.3350 1.1386
-60.0 -0.4967 0.9544 -0.4972 0.9574 -0.4949 0.9668
-50.0 -0.6421 0.7402 -0.6430 0.7440 -0.6387 0.7561
-40.0 -0.7788 0.5130 -0.7804 0.5175 -0.7731 0.5319
-30 -0.9401 0.2999 -0.9427 0.3049 -0.9307 0.3212
-20 -0.7243 0.1732 -0.7175 0.1642 -0.7070 0.1671
-10 -0.1999 0.1465 -0.1780 0.0918 -0.1747 0.0575
-9 -0.2293 0.1375 -0.1938 0.0766 -0.1900 0.0369
-8 -0.1327 0.0972 -0.0817 0.0646 -0.0862 0.0299
-7 -0.0123 0.0584 0.0146 0.0319 0.0202 0.0269
-6 0.1063 0.0365 0.1203 0.0265 0.1226 0.0213
-5 0.2000 0.0300 0.2085 0.0232 0.2109 0.0188
-4 0.3032 0.0256 0.3079 0.0200 0.3101 0.0172
-3 0.4048 0.0212 0.4060 0.0172 0.4090 0.0160
-2 0.5033 0.0224 0.5031 0.0166 0.5064 0.0136
-1 0.5988 0.0232 0.6003 0.0172 0.6049 0.0138
0 0.6939 0.0234 0.6966 0.0176 0.7021 0.0144
1 0.7879 0.0238 0.7912 0.0182 0.7982 0.0150
2 0.8801 0.0244 0.8839 0.0190 0.8934 0.0156
3 0.9701 0.0254 0.9749 0.0198 0.9867 0.0164
4 1.0573 0.0266 1.0640 0.0208 1.0776 0.0174
5 1.1409 0.0280 1.1499 0.0222 1.1657 0.0186
6 1.2204 0.0296 1.2319 0.0236 1.2508 0.0200
7 1.2972 0.0316 1.3081 0.0254 1.3299 0.0218
8 1.3710 0.0336 1.3714 0.0278 1.3977 0.0242
9 1.3932 0.0362 1.4126 0.0299 1.4213 0.0274
10 1.4025 0.0399 1.4239 0.0342 1.4192 0.0332
11 1.3968 0.0457 1.4113 0.0412 1.3882 0.0429
12 1.3739 0.0544 1.3633 0.0538 1.3289 0.0576
13 1.3241 0.0691 1.2939 0.0729 1.3035 0.0695
14 1.2568 0.0905 1.2235 0.0967 1.2649 0.0857
15 1.1758 0.1191 1.1763 0.1179 1.2265 0.1034
16 1.0962 0.1512 1.1287 0.1407 1.1810 0.1242
17 1.0393 0.1785 1.0739 0.1669 1.1300 0.1476
18 0.9932 0.2028 1.0200 0.1932 1.0787 0.1717
19 0.9485 0.2264 0.9772 0.2159 1.0291 0.1955
20 0.9872 0.2406 1.0074 0.2358 1.0529 0.2180

```
21    1.0355      0.2491      1.0434      0.2514      1.0784      0.2390
22    1.0912      0.2521      1.0868      0.2625      1.1057      0.2580
23    1.1578      0.2468      1.1366      0.2693      1.1402      0.2717
24    1.2232      0.2421      1.1902      0.2729      1.1874      0.2794
25    1.2729      0.2469      1.2468      0.2736      1.2368      0.2860
26    1.3006      0.2652      1.3047      0.2715      1.2861      0.2914
30    1.3430      0.2999      1.3467      0.3049      1.3296      0.3212
40.0  1.1126      0.5130      1.1149      0.5175      1.1045      0.5319
50.0  0.9172      0.7402      0.9186      0.7440      0.9124      0.7561
60.0  0.7095      0.9544      0.7103      0.9574      0.7070      0.9668
70.0  0.4797      1.1302      0.4800      1.1322      0.4786      1.1386
80.0  0.2366      1.2466      0.2367      1.2476      0.2363      1.2508
90.0  0.0000      1.2900      0.0000      1.2900      0.0000      1.2900
100.0 -0.1656     1.2466      -0.1657     1.2476      -0.1654     1.2508
110.0 -0.3358     1.1302      -0.3360     1.1322      -0.3350     1.1386
120.0 -0.4967     0.9544      -0.4972     0.9574      -0.4949     0.9668
130.0 -0.6421     0.7402      -0.6430     0.7440      -0.6387     0.7561
140.0 -0.7788     0.5130      -0.7804     0.5175      -0.7731     0.5319
150.0 -0.9401     0.2999      -0.9427     0.3049      -0.9307     0.3212
160.0 -0.7926     0.1263      -0.7950     0.1319      -0.7837     0.1495
170.0 -0.3963     0.0132      -0.3975     0.0189      -0.3919     0.0375
180.0 0.0000      -0.0261     0.0000      -0.0203     0.0000      -0.0015
```

SH3052Mod_AllRe_Elem15_Hanley.dat:

```
SH3052 _15te (15th element) data from T Hanley XFOIL predictions
Reinterpolated and foilchecked by CH Feb04
3     Number of airfoil tables in this file
0.3   0.6   1.2   Table ID parameter, Re in millions
12.0  12.0  11.0  Stall angle (deg)
0     0     0     No longer used, enter zero
0     0     0     No longer used, enter zero
0     0     0     No longer used, enter zero
-6.093      -6.076      -6.032      Zero Cn angle of attack (deg)
5.977 6.002 6.108 Cn slope for zero lift (dimensionless)
1.887 1.894 1.816 Cn extrapolated to value at positive stall angle of attack
-0.8  -0.8  -0.8  Cn at stall value for negative angle of attack
-3.0  -2.0  -2.0  Angle of attack for minimum CD (deg)
0.01075     0.00822     0.00673     Minimum CD value
-180.0      0.0000      -0.0432     0.0000      -0.0476     0.0000      -
0.0224
-170.0      0.3508      -0.0036     0.3571      -0.0080     0.3510
      0.0168
-160.0      0.7015      0.1103      0.7142      0.1061      0.7019
      0.1298
-150.0      0.8900      0.2851      0.9047      0.2812      0.8905
      0.3031
-140.0      0.7484      0.4999      0.7573      0.4965      0.7486
      0.5158
-130.0      0.6241      0.7293      0.6294      0.7264      0.6242
      0.7426
-120.0      0.4870      0.9459      0.4899      0.9437      0.4871
      0.9563
-110.0      0.3316      1.1243      0.3329      1.1228      0.3317
      1.1314
```

-100.0	0.1646	1.2436	0.1649	1.2428	0.1646	1.2472
-90.0	0.0000	1.2900	0.0000	1.2900	0.0000	1.2900
-80.0	-0.1646	1.2436	-0.1649	1.2428	-0.1646	1.2472
-70.0	-0.3316	1.1243	-0.3329	1.1228	-0.3317	1.1314
-60.0	-0.4870	0.9459	-0.4899	0.9437	-0.4871	0.9563
-50.0	-0.6241	0.7293	-0.6294	0.7264	-0.6242	0.7426
-40.0	-0.7484	0.4999	-0.7573	0.4965	-0.7486	0.5158
-30	-0.8900	0.2851	-0.9047	0.2812	-0.8905	0.3031
-20	-0.6574	0.1601	-0.6568	0.1484	-0.6464	0.1609
-10	-0.2275	0.1065	-0.2033	0.0687	-0.2018	0.0657
-8	-0.2222	0.0803	-0.1795	0.0356	-0.1798	0.0274
-7	-0.1122	0.0437	-0.0827	0.0295	-0.0861	0.0246
-6	0.0080	0.0344	0.0139	0.0257	0.0061	0.0205
-5	0.1004	0.0296	0.1031	0.0232	0.0991	0.0188
-4	0.1933	0.0258	0.1954	0.0204	0.1941	0.0174
-3	0.2844	0.0216	0.2853	0.0166	0.2901	0.0160
-2	0.3822	0.0224	0.3813	0.0164	0.3824	0.0134
-1	0.4762	0.0226	0.4770	0.0168	0.4793	0.0136
0	0.5709	0.0228	0.5716	0.0172	0.5754	0.0140
1	0.6641	0.0230	0.6642	0.0176	0.6710	0.0144
2	0.7556	0.0236	0.7555	0.0182	0.7647	0.0150
3	0.8425	0.0242	0.8446	0.0190	0.8561	0.0158
4	0.9266	0.0250	0.9308	0.0198	0.9447	0.0168
5	1.0058	0.0256	1.0127	0.0208	1.0315	0.0176
6	1.0857	0.0274	1.0850	0.0218	1.1113	0.0188
7	1.1651	0.0292	1.1474	0.0246	1.1860	0.0202
8	1.2249	0.0316	1.2096	0.0276	1.2494	0.0228
9	1.2528	0.0340	1.2474	0.0297	1.2876	0.0248
10	1.2658	0.0372	1.2826	0.0317	1.3031	0.0286
11	1.2653	0.0421	1.2854	0.0371	1.2815	0.0365
12	1.2518	0.0495	1.2609	0.0462	1.2358	0.0485
13	1.2221	0.0601	1.2111	0.0606	1.1852	0.0640
14	1.1718	0.0765	1.1438	0.0814	1.1618	0.0769
15	1.1099	0.0984	1.0840	0.1043	1.1275	0.0933
16	1.0329	0.1273	1.0433	0.1245	1.0930	0.1109
17	0.9670	0.1558	0.9999	0.1464	1.0522	0.1311
18	0.9182	0.1804	0.9509	0.1708	1.0073	0.1527
19	0.8786	0.2021	0.9035	0.1949	0.9621	0.1749
20	0.9022	0.2217	0.9296	0.2147	0.9830	0.1967
21	0.9442	0.2318	0.9602	0.2314	1.0025	0.2183
22	0.9952	0.2365	0.9975	0.2440	1.0216	0.2386
23	1.0526	0.2370	1.0424	0.2520	1.0527	0.2530
24	1.1203	0.2309	1.0920	0.2570	1.0944	0.2631
25	1.1776	0.2301	1.1498	0.2555	1.1398	0.2704
26	1.2083	0.2431	1.2127	0.2487	1.1873	0.2755
27	1.2348	0.2584	1.2572	0.2539	1.2356	0.2794
30	1.2715	0.2851	1.2925	0.2812	1.2722	0.3031
40.0	1.0691	0.4999	1.0819	0.4965	1.0695	0.5158
50.0	0.8915	0.7293	0.8991	0.7264	0.8918	0.7426
60.0	0.6958	0.9459	0.6998	0.9437	0.6959	0.9563
70.0	0.4738	1.1243	0.4755	1.1228	0.4738	1.1314
80.0	0.2352	1.2436	0.2356	1.2428	0.2352	1.2472
90.0	0.0000	1.2900	0.0000	1.2900	0.0000	1.2900
100.0	-0.1646	1.2436	-0.1649	1.2428	-0.1646	1.2472
110.0	-0.3316	1.1243	-0.3329	1.1228	-0.3317	1.1314
120.0	-0.4870	0.9459	-0.4899	0.9437	-0.4871	0.9563

```
130.0 -0.6241     0.7293      -0.6294     0.7264      -0.6242     0.7426
140.0 -0.7484     0.4999      -0.7573     0.4965      -0.7486     0.5158
150.0 -0.8900     0.2851      -0.9047     0.2812      -0.8905     0.3031
160.0 -0.7015     0.1103      -0.7142     0.1061      -0.7019     0.1298
170.0 -0.3508     -0.0036     -0.3571     -0.0080     -0.3510     0.0168
180.0 0.0000      -0.0432     0.0000      -0.0476     0.0000      -0.0224
```

NoShr.wnd:

```
! Wind file for Trivial turbine.
! Time      Wind  Wind  Vert. Horiz.      Vert. LinV  Gust
!                 Speed Dir   Speed Shear       Shear Shear Speed
  0.0       5.0   0.0   0.0   0.0         0.0   0.0   0.0
  0.1       5.0   0.0   0.0   0.0         0.0   0.0   0.0
999.9       5.0   0.0   0.0   0.0         0.0   0.0   0.0
```

TurbSim_7.bts: Unreadable in text form.

FAST

T17_FMP_10kW.fst:

```
------------------------------------------------------------------------
---
------- FAST INPUT FILE -------------------------------------------------
---
FAST certification Test #17 (modified): FAST model of a SWRT 3-bladed upwind
turbine.  Note- SWRT rotates in CCW direction- some inputs will be mirror
image of the actual turbine.
Model properties from "SWRTv1p2.adm" and SWRT "AdamsWT_MakeBladeDat_v12.xls".
JEM Jan., 2004.  Updated by J. Jonkman, NREL, Feb, 2004.  Compatible with
FAST v7.00.00.
---------------------- SIMULATION CONTROL ----------------------------------
---
False       Echo        - Echo input data to "echo.out" (flag)
   1        ADAMSPrep   - ADAMS preprocessor mode {1: Run FAST, 2: use FAST
as a preprocessor to create an ADAMS model, 3: do both} (switch)
   1        AnalMode    - Analysis mode {1: Run a time-marching simulation,
2: create a periodic linearized model} (switch)
   3        NumBl       - Number of blades (-)
  14      TMax        - Total run time (s)
   1.5E-6    DT          - Integration time step (s)
---------------------- TURBINE CONTROL -------------------------------------
---
   0        YCMode      - Yaw control mode {0: none, 1: user-defined from
routine UserYawCont, 2: user-defined from Simulink} (switch)
9999.9      TYCOn       - Time to enable active yaw control (s) [unused when
YCMode=0]
   0        PCMode      - Pitch control mode {0: none, 1: user-defined from
routine PitchCntrl, 2: user-defined from Simulink} (switch)
9999.9      TPCOn       - Time to enable active pitch control (s) [unused
when PCMode=0]
```

```
   3        VSContrl    - Variable-speed control mode {0: none, 1: simple VS,
2: user-defined from routine UserVSCont, 3: user-defined from Simulink}
(switch)
9999.9      VS_RtGnSp   - Rated generator speed for simple variable-speed
generator control (HSS side) (rpm) [used only when VSContrl=1]
9999.9      VS_RtTq     - Rated generator torque/constant generator torque in
Region 3 for simple variable-speed generator control (HSS side) (N-m) [used
only when VSContrl=1]
9999.9      VS_Rgn2K    - Generator torque constant in Region 2 for simple
variable-speed generator control (HSS side) (N-m/rpm^2) [used only when
VSContrl=1]
9999.9      VS_SlPc     - Rated generator slip percentage in Region 2 1/2 for
simple variable-speed generator control (%) [used only when VSContrl=1]
   1        GenModel    - Generator model {1: simple, 2: Thevenin, 3: user-
defined from routine UserGen} (switch) [used only when VSContrl=0]
True        GenTiStr    - Method to start the generator {T: timed using
TimGenOn, F: generator speed using SpdGenOn} (flag)
True        GenTiStp    - Method to stop the generator {T: timed using
TimGenOf, F: when generator power = 0} (flag)
9999.9      SpdGenOn    - Generator speed to turn on the generator for a
startup (HSS speed) (rpm) [used only when GenTiStr=False]
   0.0      TimGenOn    - Time to turn on the generator for a startup (s)
[used only when GenTiStr=True]
9999.9      TimGenOf    - Time to turn off the generator (s) [used only when
GenTiStp=True]
   1        HSSBrMode   - HSS brake model {1: simple, 2: user-defined from
routine UserHSSBr} (switch)
9999.9      THSSBrDp    - Time to initiate deployment of the HSS brake (s)
9999.9      TiDynBrk    - Time to initiate deployment of the dynamic
generator brake [CURRENTLY IGNORED] (s)
9999.9      TTpBrDp(1)  - Time to initiate deployment of tip brake 1 (s)
9999.9      TTpBrDp(2)  - Time to initiate deployment of tip brake 2 (s)
9999.9      TTpBrDp(3)  - Time to initiate deployment of tip brake 3 (s)
[unused for 2 blades]
9999.9      TBDepISp(1) - Deployment-initiation speed for the tip brake on
blade 1 (rpm)
9999.9      TBDepISp(2) - Deployment-initiation speed for the tip brake on
blade 2 (rpm)
9999.9      TBDepISp(3) - Deployment-initiation speed for the tip brake on
blade 3 (rpm) [unused for 2 blades]
9999.9      TYawManS    - Time to start override yaw maneuver and end
standard yaw control (s)
9999.9      TYawManE    - Time at which override yaw maneuver reaches final
yaw angle (s)
   0.0      NacYawF     - Final yaw angle for yaw maneuvers (degrees)
9999.9      TPitManS(1) - Time to start override pitch maneuver for blade 1
and end standard pitch control (s)
9999.9      TPitManS(2) - Time to start override pitch maneuver for blade 2
and end standard pitch control (s)
9999.9      TPitManS(3) - Time to start override pitch maneuver for blade 3
and end standard pitch control (s) [unused for 2 blades]
9999.9      TPitManE(1) - Time at which override pitch maneuver for blade 1
reaches final pitch (s)
9999.9      TPitManE(2) - Time at which override pitch maneuver for blade 2
reaches final pitch (s)
9999.9      TPitManE(3) - Time at which override pitch maneuver for blade 3
reaches final pitch (s) [unused for 2 blades]
```

```
  9.75     BlPitch(1)  - Blade 1 initial pitch (degrees)
  9.75     BlPitch(2)  - Blade 2 initial pitch (degrees)
  9.75     BlPitch(3)  - Blade 3 initial pitch (degrees) [unused for 2
blades]
  9.75     BlPitchF(1) - Blade 1 final pitch for pitch maneuvers (degrees)
  9.75     BlPitchF(2) - Blade 2 final pitch for pitch maneuvers (degrees)
  9.75     BlPitchF(3) - Blade 3 final pitch for pitch maneuvers (degrees)
[unused for 2 blades]
---------------------- ENVIRONMENTAL CONDITIONS ----------------------------
---
   9.81     Gravity     - Gravitational acceleration (m/s^2)
---------------------- FEATURE FLAGS ---------------------------------------
---
True        FlapDOF1    - First flapwise blade mode DOF (flag)
True        FlapDOF2    - Second flapwise blade mode DOF (flag)
True        EdgeDOF     - First edgewise blade mode DOF (flag)
False       TeetDOF     - Rotor-teeter DOF (flag) [unused for 3 blades]
False       DrTrDOF     - Drivetrain rotational-flexibility DOF (flag)
True        GenDOF      - Generator DOF (flag)
True        YawDOF      - Yaw DOF (flag)
True       TwFADOF1    - First fore-aft tower bending-mode DOF (flag)
True       TwFADOF2    - Second fore-aft tower bending-mode DOF (flag)
True       TwSSDOF1    - First side-to-side tower bending-mode DOF (flag)
True       TwSSDOF2    - Second side-to-side tower bending-mode DOF (flag)
True        CompAero    - Compute aerodynamic forces (flag)
False       CompNoise   - Compute aerodynamic noise (flag)
---------------------- INITIAL CONDITIONS ----------------------------------
---
   0.0      OoPDefl     - Initial out-of-plane blade-tip displacement
(meters)
   0.0      IPDefl      - Initial in-plane blade-tip deflection (meters)
   0.0      TeetDefl    - Initial or fixed teeter angle (degrees) [unused for
3 blades]
   0.0      Azimuth     - Initial azimuth angle for blade 1 (degrees)
   60      RotSpeed    - Initial or fixed rotor speed (rpm)
   -10.0      NacYaw      - Initial or fixed nacelle-yaw angle (degrees)
   0.0      TTDspFA     - Initial fore-aft tower-top displacement (meters)
   0.0      TTDspSS     - Initial side-to-side tower-top displacement
(meters)
---------------------- TURBINE CONFIGURATION -------------------------------
---
   3.5      TipRad      - The distance from the rotor apex to the blade tip
(meters)
   0.362    HubRad      - The distance from the rotor apex to the blade root
(meters)
   1        PSpnElN     - Number of the innermost blade element which is
still part of the pitchable portion of the blade for partial-span pitch
control [1 to BldNodes] [CURRENTLY IGNORED] (-)
   0.0      UndSling    - Undersling length [distance from teeter pin to the
rotor apex] (meters) [unused for 3 blades]
   0.1536   HubCM       - Distance from rotor apex to hub mass [positive
downwind] (meters)
  -0.7456   OverHang    - Distance from yaw axis to rotor apex [3 blades] or
teeter pin [2 blades] (meters)
  -0.2307   NacCMxn     - Downwind distance from the tower-top to the nacelle
CM (meters)
```

```
   0.0910   NacCMyn     - Lateral  distance from the tower-top to the nacelle
CM (meters)
   0.5475   NacCMzn     - Vertical distance from the tower-top to the nacelle
CM (meters)
  11.5      TowerHt     - Height of tower above ground level [onshore] or MSL
[offshore] (meters)
   0.515112 Twr2Shft    - Vertical distance from the tower-top to the rotor
shaft (meters)
   0.0      TwrRBHt     - Tower rigid base height (meters)
  -8.0      ShftTilt    - Rotor shaft tilt angle (degrees).  Negative for an
upwind rotor.
   0.0      Delta3      - Delta-3 angle for teetering rotors (degrees)
[unused for 3 blades]
   0.0      PreCone(1)  - Blade 1 cone angle (degrees)
   0.0      PreCone(2)  - Blade 2 cone angle (degrees)
   0.0      PreCone(3)  - Blade 3 cone angle (degrees) [unused for 2 blades]
   0.0      AzimB1Up    - Azimuth value to use for I/O when blade 1 points up
(degrees)
---------------------- MASS AND INERTIA ----------------------------------
---
   0.0      YawBrMass   - Yaw bearing mass (kg)
 260.5      NacMass     - Nacelle mass (kg)
 113.0      HubMass     - Hub mass (kg)
   0.0      TipMass(1)  - Tip-brake mass, blade 1 (kg)
   0.0      TipMass(2)  - Tip-brake mass, blade 2 (kg)
   0.0      TipMass(3)  - Tip-brake mass, blade 3 (kg) [unused for 2 blades]
  39.81     NacYIner    - Nacelle inertia about yaw axis (kg m^2)
   0.5      GenIner     - Generator inertia about HSS (kg m^2)
   7.71     HubIner     - Hub inertia about rotor axis [3 blades] or teeter
axis [2 blades] (kg m^2)
---------------------- DRIVETRAIN ----------------------------------------
---
 100.0      GBoxEff     - Gearbox efficiency (%)
  83.0      GenEff      - Generator efficiency [ignored by the Thevenin and
user-defined generator models] (%)
   1.0      GBRatio     - Gearbox ratio (-)
False       GBRevers    - Gearbox reversal {T: if rotor and generator rotate
in opposite directions} (flag)
9999.9      HSSBrTqF    - Fully deployed HSS-brake torque (N-m)
9999.9      HSSBrDT     - Time for HSS-brake to reach full deployment once
initiated (sec) [used only when HSSBrMode=1]
""          DynBrkFi    - File containing a mech-gen-torque vs HSS-speed
curve for a dynamic brake [CURRENTLY IGNORED] (quoted string)
9999.9      DTTorSpr    - Drivetrain torsional spring (N-m/rad)
9999.9      DTTorDmp    - Drivetrain torsional damper (N-m/(rad/s))
---------------------- SIMPLE INDUCTION GENERATOR ------------------------
---
9999.9      SIG_SlPc    - Rated generator slip percentage (%) [used only when
VSContrl=0 and GenModel=1]
9999.9      SIG_SySp    - Synchronous (zero-torque) generator speed (rpm)
[used only when VSContrl=0 and GenModel=1]
9999.9      SIG_RtTq    - Rated torque (N-m) [used only when VSContrl=0 and
GenModel=1]
9999.9      SIG_PORt    - Pull-out ratio (Tpullout/Trated) (-) [used only
when VSContrl=0 and GenModel=1]
---------------------- THEVENIN-EQUIVALENT INDUCTION GENERATOR -----------
---
```

```
9999.9      TEC_Freq    - Line frequency [50 or 60] (Hz) [used only when
VSContrl=0 and GenModel=2]
9998        TEC_NPol    - Number of poles [even integer > 0] (-) [used only
when VSContrl=0 and GenModel=2]
9999.9      TEC_SRes    - Stator resistance (ohms) [used only when VSContrl=0
and GenModel=2]
9999.9      TEC_RRes    - Rotor resistance (ohms) [used only when VSContrl=0
and GenModel=2]
9999.9      TEC_VLL     - Line-to-line RMS voltage (volts) [used only when
VSContrl=0 and GenModel=2]
9999.9      TEC_SLR     - Stator leakage reactance (ohms) [used only when
VSContrl=0 and GenModel=2]
9999.9      TEC_RLR     - Rotor leakage reactance (ohms) [used only when
VSContrl=0 and GenModel=2]
9999.9      TEC_MR      - Magnetizing reactance (ohms) [used only when
VSContrl=0 and GenModel=2]
---------------------- PLATFORM ----------------------------------------
---
   0        PtfmModel   - Platform model {0: none, 1: onshore, 2: fixed
bottom offshore, 3: floating offshore} (switch)
""          PtfmFile    - Name of file containing platform properties (quoted
string) [unused when PtfmModel=0]
---------------------- TOWER -------------------------------------------
---
  10        TwrNodes    - Number of tower nodes used for analysis (-)
"UAE_Ames_Tower_SWRT.dat"        TwrFile - Name of file containing tower
properties (quoted string)
---------------------- NACELLE-YAW -------------------------------------
---
   0.0      YawSpr      - Nacelle-yaw spring constant (N-m/rad)
   0.0      YawDamp     - Nacelle-yaw damping constant (N-m/(rad/s))
   0.0      YawNeut     - Neutral yaw position--yaw spring force is zero at
this yaw (degrees)
---------------------- FURLING -----------------------------------------
---
True        Furling     - Read in additional model properties for furling
turbine (flag)
"SWRT_Furl.dat"         FurlFile    - Name of file containing furling
properties (quoted string) [unused when Furling=False]
---------------------- ROTOR-TEETER ------------------------------------
---
   0        TeetMod     - Rotor-teeter spring/damper model {0: none, 1:
standard, 2: user-defined from routine UserTeet} (switch) [unused for 3
blades]
   0.0      TeetDmpP    - Rotor-teeter damper position (degrees) [used only
for 2 blades and when TeetMod=1]
   0.0      TeetDmp     - Rotor-teeter damping constant (N-m/(rad/s)) [used
only for 2 blades and when TeetMod=1]
   0.0      TeetCDmp    - Rotor-teeter rate-independent Coulomb-damping
moment (N-m) [used only for 2 blades and when TeetMod=1]
   0.0      TeetSStP    - Rotor-teeter soft-stop position (degrees) [used
only for 2 blades and when TeetMod=1]
   0.0      TeetHStP    - Rotor-teeter hard-stop position (degrees) [used
only for 2 blades and when TeetMod=1]
   0.0      TeetSSSp    - Rotor-teeter soft-stop linear-spring constant (N-
m/rad) [used only for 2 blades and when TeetMod=1]
```

```
   0.0      TeetHSSp    - Rotor-teeter hard-stop linear-spring constant (N-
m/rad) [used only for 2 blades and when TeetMod=1]
---------------------- TIP-BRAKE ----------------------------------------
---
   0.0      TBDrConN    - Tip-brake drag constant during normal operation,
Cd*Area (m^2)
   0.0      TBDrConD    - Tip-brake drag constant during fully-deployed
operation, Cd*Area (m^2)
   0.0      TpBrDT      - Time for tip-brake to reach full deployment once
released (sec)
---------------------- BLADE --------------------------------------------
---
"SWRT_Blade.dat"        BldFile(1)  - Name of file containing properties for
blade 1 (quoted string)
"SWRT_Blade.dat"        BldFile(2)  - Name of file containing properties for
blade 2 (quoted string)
"SWRT_Blade.dat"        BldFile(3)  - Name of file containing properties for
blade 3 (quoted string) [unused for 2 blades]
---------------------- AERODYN ------------------------------------------
---
"Test17_AD_FMN.ipt"         ADFile      - Name of file containing AeroDyn
input parameters (quoted string)
---------------------- NOISE --------------------------------------------
---
""          NoiseFile   - Name of file containing aerodynamic noise input
parameters (quoted string) [used only when CompNoise=True]
---------------------- ADAMS --------------------------------------------
---
"SWRT_ADAMS.dat"        ADAMSFile   - Name of file containing ADAMS-specific
input parameters (quoted string) [unused when ADAMSPrep=1]
---------------------- LINEARIZATION CONTROL ----------------------------
---
"SWRT_Linear.dat"       LinFile     - Name of file containing FAST
linearization parameters (quoted string) [unused when AnalMode=1]
---------------------- OUTPUT -------------------------------------------
---
True        SumPrint    - Print summary data to "<RootName>.fsm" (flag)
True        TabDelim    - Generate a tab-delimited tabular output file.
(flag)
"ES10.3E2"  OutFmt      - Format used for tabular output except time.
Resulting field should be 10 characters. (quoted string)  [not checked for
validity!]
  0.0      TStart      - Time to begin tabular output (s)
   7        DecFact     - Decimation factor for tabular output {1: output
every time step} (-)
   1.0      SttsTime    - Amount of time between screen status messages (sec)
   0.0      NcIMUxn     - Downwind distance from the tower-top to the nacelle
IMU (meters)
   0.0      NcIMUyn     - Lateral  distance from the tower-top to the nacelle
IMU (meters)
   0.0      NcIMUzn     - Vertical distance from the tower-top to the nacelle
IMU (meters)
   0.1      ShftGagL    - Distance from rotor apex [3 blades] or teeter pin
[2 blades] to shaft strain gages [positive for upwind rotors] (meters)
   0        NTwGages    - Number of tower nodes that have strain gages for
output [0 to 9] (-)
```

```
   0        TwrGagNd    - List of tower nodes that have strain gages [1 to
TwrNodes] (-) [unused if NTwGages=0]
   0        NBlGages    - Number of blade nodes that have strain gages for
output [0 to 9] (-)
   0        BldGagNd    - List of blade nodes that have strain gages [1 to
BldNodes] (-) [unused if NBlGages=0]
            OutList     - The next line(s) contains a list of output
parameters.  See OutList.txt for a listing of available output channels, (-)
"RotSpeed"                          - Rotor speed
"TotWindV"
"YawPos"
"YawAzn"
"YawBrTAxp"
"YawBrTAyp"
"YawBrTAzp"
"TailFurlP"
"TailFurlV"
"TailFurlA"
"TipDyb1"
"TipDyb2"
"TipDyb3"
"TipALyb1"
"TipALyb2"
"TipALyb3"
"Spn4ALyb1"
"Spn4ALyb2"
"Spn4ALyb3"
"Spn8ALyb1"
"Spn8ALyb2"
"Spn8ALyb3"
END of FAST input file (the word "END" must appear in the first 3 columns of
this last line).
---------------------------------------------------------------------------
---
```

UAE_Ames_Tower_SWRT.dat:

```
---------------------------------------------------------------------------
---
---------------------- FAST TOWER FILE ------------------------------------
---
 UAE Phase VI (Ames) tower data, adjusted for use with the SWRT.
---------------------- TOWER PARAMETERS -----------------------------------
---
   6        NTwInpSt    - Number of input stations to specify tower geometry
False       CalcTMode   - Calculate tower mode shapes internally {T: ignore
mode shapes from below, F: use mode shapes from below} [CURRENTLY IGNORED]
(flag)
   0.55     TwrFADmp(1) - Tower 1st fore-aft mode structural damping ratio
(%)
   0.80     TwrFADmp(2) - Tower 2nd fore-aft mode structural damping ratio
(%)
   0.55     TwrSSDmp(1) - Tower 1st side-to-side mode structural damping
ratio (%)
```

```
   0.80     TwrSSDmp(2) - Tower 2nd side-to-side mode structural damping
ratio (%)
---------------------- TOWER ADJUSTMUNT FACTORS ----------------------------
---
   1.0      FAStTunr(1) - Tower fore-aft modal stiffness tuner, 1st mode (-)
   1.0      FAStTunr(2) - Tower fore-aft modal stiffness tuner, 2nd mode (-)
   1.0      SSStTunr(1) - Tower side-to-side stiffness tuner, 1st mode (-)
   1.0      SSStTunr(2) - Tower side-to-side stiffness tuner, 2nd mode (-)
   1.0      AdjTwMa     - Factor to adjust tower mass density (-)
   1.0      AdjFASt     - Factor to adjust tower fore-aft stiffness (-)
   1.0      AdjSSSt     - Factor to adjust tower side-to-side stiffness (-)
---------------------- DISTRIBUTED TOWER PROPERTIES ------------------------
---
HtFract    TMassDen     TwFAStif     TwSSStif     TwGJStif     TwEAStif
TwFAIner     TwSSIner    TwFAcgOf     TwSScgOf
    (-)      (kg/m)       (Nm^2)       (Nm^2)       (Nm^2)          (N)
(kg m)       (kg m)         (m)          (m)
0.00000     260.467  235869817.7  235869817.7       1.0E12       1.0E12
0.0          0.0         0.0          0.0
0.29565     260.467  235869817.7  235869817.7       1.0E12       1.0E12
0.0          0.0         0.0          0.0
0.29574     260.467  235869817.7  235869817.7       1.0E12       1.0E12
0.0          0.0         0.0          0.0
0.33904     207.107   79470442.3   79470442.3       1.0E12       1.0E12
0.0          0.0         0.0          0.0
0.33913     207.107   79470442.3   79470442.3       1.0E12       1.0E12
0.0          0.0         0.0          0.0
1.00000     207.107   79470442.3   79470442.3       1.0E12       1.0E12
0.0          0.0         0.0          0.0
---------------------- TOWER FORE-AFT MODE SHAPES --------------------------
---
   1.2789   TwFAM1Sh(2) - Mode 1, coefficient of x^2 term
  -2.5586   TwFAM1Sh(3) -       , coefficient of x^3 term
   6.8578   TwFAM1Sh(4) -       , coefficient of x^4 term
  -6.8267   TwFAM1Sh(5) -       , coefficient of x^5 term
   2.2486   TwFAM1Sh(6) -       , coefficient of x^6 term
 -9.4878    TwFAM2Sh(2) - Mode 2, coefficient of x^2 term
  -4.2045   TwFAM2Sh(3) -       , coefficient of x^3 term
  43.4360   TwFAM2Sh(4) -       , coefficient of x^4 term
 -38.1498   TwFAM2Sh(5) -       , coefficient of x^5 term
   9.4062   TwFAM2Sh(6) -       , coefficient of x^6 term
---------------------- TOWER SIDE-TO-SIDE MODE SHAPES ----------------------
---
   1.2789   TwSSM1Sh(2) - Mode 1, coefficient of x^2 term
  -2.5586   TwSSM1Sh(3) -       , coefficient of x^3 term
   6.8578   TwSSM1Sh(4) -       , coefficient of x^4 term
  -6.8267   TwSSM1Sh(5) -       , coefficient of x^5 term
   2.2486   TwSSM1Sh(6) -       , coefficient of x^6 term
 -9.4878   TwSSM2Sh(2) - Mode 2, coefficient of x^2 term
  -4.2045   TwSSM2Sh(3) -       , coefficient of x^3 term
  43.4360   TwSSM2Sh(4) -       , coefficient of x^4 term
 -38.1498   TwSSM2Sh(5) -       , coefficient of x^5 term
   9.4062   TwSSM2Sh(6) -       , coefficient of x^6 term
```

SWRT_Furl.dat:

```
------------------------------------------------------------------------
---
---------------------- FAST FURLING FILE -------------------------------
---
SWRT input properties. Windward Engineering.  January, 2004.  Updated by J.
Jonkman, NREL, Feb, 2004.
---------------------- FEATURE FLAGS (CONT) ----------------------------
---
False       RFrlDOF     - Rotor-furl DOF (flag)
True        TFrlDOF     - Tail-furl DOF (flag)
---------------------- INITIAL CONDITIONS (CONT) -----------------------
---
   0.0      RotFurl     - Initial or fixed rotor-furl angle (degrees)
   0.0      TailFurl    - Initial or fixed tail-furl angle (degrees)
---------------------- TURBINE CONFIGURATION (CONT) --------------------
---
   0.106    Yaw2Shft    - Lateral distance from the yaw axis to the rotor
shaft (meters)
   0.0      ShftSkew    - Rotor shaft skew angle (degrees)
   0.0      RFrlCMxn    - Downwind distance from the tower-top to the CM of
the structure that furls with the rotor [not including rotor] (meters)
   0.0      RFrlCMyn    - Lateral  distance from the tower-top to the CM of
the structure that furls with the rotor [not including rotor] (meters)
   0.0      RFrlCMzn    - Vertical distance from the tower-top to the CM of
the structure that furls with the rotor [not including rotor] (meters)
   1.7667   BoomCMxn    - Downwind distance from the tower-top to the tail
boom CM (meters)
   0.106    BoomCMyn    - Lateral  distance from the tower-top to the tail
boom CM (meters)
   0.2668   BoomCMzn    - Vertical distance from the tower-top to the tail
boom CM (meters)
   0.0      TFinCMxn    - Downwind distance from the tower-top to the tail
fin CM (meters)
   0.0      TFinCMyn    - Lateral  distance from the tower-top to the tail
fin CM (meters)
   0.0      TFinCMzn    - Vertical distance from the tower-top to the tail
fin CM (meters)
   2.7674   TFinCPxn    - Downwind distance from the tower-top to the tail
fin center-of-pressure (m)
   0.106    TFinCPyn    - Lateral  distance from the tower-top to the tail
fin center-of-pressure (m)
   0.1262   TFinCPzn    - Vertical distance from the tower-top to the tail
fin center-of-pressure (m)
   0.0      TFinSkew    - Tail fin chordline skew angle (degrees)
  -8.0      TFinTilt    - Tail fin chordline tilt angle (degrees)
   8.0      TFinBank    - Tail fin planform  bank angle (degrees)
   0.0      RFrlPntxn   - Downwind distance from the tower-top to an
arbitrary point on the rotor-furl axis (meters)
   0.0      RFrlPntyn   - Lateral  distance from the tower-top to an
arbitrary point on the rotor-furl axis (meters)
   0.0      RFrlPntzn   - Vertical distance from the tower-top to an
arbitrary point on the rotor-furl axis (meters)
   0.0      RFrlSkew    - Rotor-furl axis skew angle (degrees)
   0.0      RFrlTilt    - Rotor-furl axis tilt angle (degrees)
   0.318    TFrlPntxn   - Downwind distance from the tower-top to an
arbitrary point on the tail-furl axis (meters)
```

```
   0.106    TFrlPntyn   - Lateral  distance from the tower-top to an
arbitrary point on the tail-furl axis (meters)
   0.470    TFrlPntzn   - Vertical distance from the tower-top to an
arbitrary point on the tail-furl axis (meters)
 -45.2802   TFrlSkew    - Tail-furl axis skew angle (degrees)
  78.7047   TFrlTilt    - Tail-furl axis tilt angle (degrees)
---------------------- MASS AND INERTIA (CONT) -----------------------------
---
   0.0      RFrlMass    - Mass of structure that furls with the rotor [not
including rotor] (kg)
  86.8      BoomMass    - Tail boom mass (kg)
   0.0      TFinMass    - Tail fin mass (kg)
   0.0      RFrlIner    - Inertia of the structure that furls with the rotor
about the rotor-furl axis (kg m^2) [not including rotor]
 264.7      TFrlIner    - Tail boom inertia about tail-furl axis (kg m^2)
---------------------- ROTOR-FURL ------------------------------------------
---
   0        RFrlMod     - Rotor-furl spring/damper model {0: none, 1:
standard, 2: user-defined from routine UserRFrl} (switch)
   0.0      RFrlSpr     - Rotor-furl spring constant (N-m/rad) [used only
when RFrlMod=1]
   0.0      RFrlDmp     - Rotor-furl damping constant (N-m/(rad/s)) [used
only when RFrlMod=1]
   0.0      RFrlCDmp    - Rotor-furl rate-independent Coulomb-damping moment
(N-m) [used only when RFrlMod=1]
   0.0      RFrlUSSP    - Rotor-furl up-stop spring position (degrees) [used
only when RFrlMod=1]
   0.0      RFrlDSSP    - Rotor-furl down-stop spring position (degrees)
[used only when RFrlMod=1]
   0.0      RFrlUSSpr   - Rotor-furl up-stop spring constant (N-m/rad) [used
only when RFrlMod=1]
   0.0      RFrlDSSpr   - Rotor-furl down-stop spring constant (N-m/rad)
[used only when RFrlMod=1]
   0.0      RFrlUSDP    - Rotor-furl up-stop damper position (degrees) [used
only when RFrlMod=1]
   0.0      RFrlDSDP    - Rotor-furl down-stop damper position (degrees)
[used only when RFrlMod=1]
   0.0      RFrlUSDmp   - Rotor-furl up-stop damping constant (N-m/(rad/s))
[used only when RFrlMod=1]
   0.0      RFrlDSDmp   - Rotor-furl down-stop damping constant (N-m/(rad/s))
[used only when RFrlMod=1]
---------------------- TAIL-FURL -------------------------------------------
---
   1        TFrlMod     - Tail-furl spring/damper model {0: none, 1:
standard, 2: user-defined from routine UserTFrl} (switch)
   0.0      TFrlSpr     - Tail-furl spring constant (N-m/rad) [used only when
TFrlMod=1]
  10.0      TFrlDmp     - Tail-furl damping constant (N-m/(rad/s)) [used only
when TFrlMod=1]
   0.0      TFrlCDmp    - Tail-furl rate-independent Coulomb-damping moment
(N-m) [used only when TFrlMod=1]
  85.0      TFrlUSSP    - Tail-furl up-stop spring position (degrees) [used
only when TFrlMod=1]
   3.0      TFrlDSSP    - Tail-furl down-stop spring position (degrees) [used
only when TFrlMod=1]
   1.0E3    TFrlUSSpr   - Tail-furl up-stop spring constant (N-m/rad) [used
only when TFrlMod=1]
```

```
   1.7E4    TFrlDSSpr   - Tail-furl down-stop spring constant (N-m/rad) [used
only when TFrlMod=1]
  85.0      TFrlUSDP    - Tail-furl up-stop damper position (degrees) [used
only when TFrlMod=1]
   0.0      TFrlDSDP    - Tail-furl down-stop damper position (degrees) [used
only when TFrlMod=1]
   1.0E3    TFrlUSDmp   - Tail-furl up-stop damping constant (N-m/(rad/s))
[used only when TFrlMod=1]
 137.0      TFrlDSDmp   - Tail-furl down-stop damping constant (N-m/(rad/s))
[used only when TFrlMod=1]
---------------------- TAIL FIN AERODYNAMICS --------------------------------
---
   1        TFinMod     - Tail fin aerodynamics model (0: none, 1: standard,
2: user-defined from routine UserTFin) (switch)
   1        TFinNFoil   - Tail fin airfoil number [1 to NumFoil] [used only
when TFinMod=1]
   1.017    TFinArea    - Tail fin planform area (m^2) [used only when
TFinMod=1]
True        SubAxInd    - Subtract average rotor axial induction when
computing relative wind-inflow at tail fin? (flag) [used only when TFinMod=1]
```

SWRT_blade.dat:

```
---------------------------------------------------------------------------
---
---------------------- FAST INDIVIDUAL BLADE FILE ---------------------------
---
SWRT blade.  Windward Engineering. January, 2004.  Updated by J. Jonkman,
NREL, Feb, 2004.
---------------------- BLADE PARAMETERS -------------------------------------
---
   4        NBlInpSt    - Number of blade input stations (-)
False       CalcBMode   - Calculate blade mode shapes internally {T: ignore
mode shapes from below, F: use mode shapes from below} [CURRENTLY IGNORED]
(flag)
   3.0      BldFlDmp(1) - Blade flap mode #1 structural damping in percent of
critical (%)
   3.0      BldFlDmp(2) - Blade flap mode #2 structural damping in percent of
critical (%)
   5.0      BldEdDmp(1) - Blade edge mode #1 structural damping in percent of
critical (%)
---------------------- BLADE ADJUSTMENT FACTORS -----------------------------
---
   1.0      FlStTunr(1) - Blade flapwise modal stiffness tuner, 1st mode (-)
   1.0      FlStTunr(2) - Blade flapwise modal stiffness tuner, 2nd mode (-)
   1.0      AdjBlMs     - Factor to adjust blade mass density (-)
   1.0      AdjFlSt     - Factor to adjust blade flap stiffness (-)
   1.0      AdjEdSt     - Factor to adjust blade edge stiffness (-)
---------------------- DISTRIBUTED BLADE PROPERTIES -------------------------
---
BlFract  AeroCent  StrcTwst  BMassDen    FlpStff    EdgStff    GJStff
EAStff   Alpha   FlpIner   EdgIner   PrecrvRef   PreswpRef   FlpcgOf
EdgcgOf   FlpEAOf   EdgEAOf
```

```
    (-)        (-)      (deg)     (kg/m)      (Nm^2)      (Nm^2)     (Nm^2)
(N)      (-)     (kg m)     (kg m)          (m)          (m)        (m)        (m)
(m)        (m)
   0.00       0.25       0.0     4.192   4.53E+03   1.99E+05  4.48E+03
2.04E+06     0.0 0.005890117 0.021739021     0.0         0.0        0.0
0.0       0.0       0.0
   0.90       0.25       0.0     4.192   4.53E+03   1.99E+05  4.48E+03
2.04E+06     0.0 0.005890117 0.021739021     0.0         0.0        0.0
0.0       0.0       0.0
   0.95       0.25       0.0     4.020   4.53E+03   1.99E+05  4.48E+03
2.04E+06     0.0 0.005648443 0.020847058     0.0         0.0        0.0
0.0       0.0       0.0
   1.00       0.25       0.0     3.848   4.53E+03   1.99E+05  4.48E+03
2.04E+06     0.0 0.005406768 0.019955094     0.0         0.0        0.0
0.0       0.0       0.0
---------------------- BLADE MODE SHAPES-------------------------------------
---
   2.572    BldFl1Sh(2) - Flap , coeff of x^2
  -2.772    BldFl1Sh(3) -      , coeff of x^3
   1.551    BldFl1Sh(4) -      , coeff of x^4
  -0.330    BldFl1Sh(5) -      , coeff of x^5
  -0.021    BldFl1Sh(6) -      , coeff of x^6
  -9.847    BldFl2Sh(2) - Flap , coeff of x^2
  13.882    BldFl2Sh(3) -      , coeff of x^3
   9.529    BldFl2Sh(4) -      , coeff of x^4
 -19.873    BldFl2Sh(5) -      , coeff of x^5
   7.309    BldFl2Sh(6) -      , coeff of x^6
   1.617    BldEdgSh(2) - Edge , coeff of x^2
  -0.065    BldEdgSh(3) -      , coeff of x^3
  -1.424    BldEdgSh(4) -      , coeff of x^4
   1.201    BldEdgSh(5) -      , coeff of x^5
  -0.329    BldEdgSh(6) -      , coeff of x^6
```

5 MW System

The NREL CAE tools AeroDyn and FAST were used in simulations of the 5 MW system. The input files used are given below.

AeroDyn

NRELOffshrBsline5MW_AeroDyn.ipt:

```
NREL 5.0 MW offshore baseline aerodynamic input properties; Compatible with
AeroDyn v13.00.
SI           SysUnits    - System of units for used for input and output [must
be SI for FAST] (unquoted string)
STEADY       StallMod    - Dynamic stall included [BEDDOES or STEADY]
(unquoted string)
USE_CM       UseCm       - Use aerodynamic pitching moment model? [USE_CM or
NO_CM] (unquoted string)
EQUIL        InfModel    - Inflow model [DYNIN or EQUIL] (unquoted string)
SWIRL        IndModel    - Induction-factor model [NONE or WAKE or SWIRL]
(unquoted string)
```

```
   0.005    AToler      - Induction-factor tolerance (convergence criteria)
(-)
PRANDtl     TLModel     - Tip-loss model (EQUIL only) [PRANDtl, GTECH, or
NONE] (unquoted string)
PRANDtl     HLModel     - Hub-loss model (EQUIL only) [PRANdtl or NONE]
(unquoted string)
"Wind\NREL5MW\NoShr_gust.wnd"                    WindFile    - Name of file
containing wind data (quoted string)
  90.0      HH          - Wind reference (hub) height
[TowerHt+Twr2Shft+OverHang*SIN(ShftTilt)] (m)
   0.0      TwrShad     - Tower-shadow velocity deficit (-)
9999.9      ShadHWid    - Tower-shadow half width (m)
9999.9      T_Shad_Refpt- Tower-shadow reference point (m)
   1.225    AirDens     - Air density (kg/m^3)
   1.464E-5 KinVisc     - Kinematic air viscosity [CURRENTLY IGNORED]
(m^2/sec)
   0.02479  DTAero      - Time interval for aerodynamic calculations (sec)
   8        NumFoil     - Number of airfoil files (-)
"AeroData\NREL 5MW\Cylinder1.dat"                  FoilNm      - Names of
the airfoil files [NumFoil lines] (quoted strings)
"AeroData\NREL 5MW\Cylinder2.dat"
"AeroData\NREL 5MW\DU40_A17.dat"
"AeroData\NREL 5MW\DU35_A17.dat"
"AeroData\NREL 5MW\DU30_A17.dat"
"AeroData\NREL 5MW\DU25_A17.dat"
"AeroData\NREL 5MW\DU21_A17.dat"
"AeroData\NREL 5MW\NACA64_A17.dat"
  17        BldNodes    - Number of blade nodes used for analysis (-)
RNodes   AeroTwst  DRNodes  Chord  NFoil  PrnElm
 2.8667  13.308    2.7333   3.542  1      NOPRINT
 5.6000  13.308    2.7333   3.854  1      NOPRINT
 8.3333  13.308    2.7333   4.167  2      NOPRINT
11.7500  13.308    4.1000   4.557  3      NOPRINT
15.8500  11.480    4.1000   4.652  4      NOPRINT
19.9500  10.162    4.1000   4.458  4      NOPRINT
24.0500   9.011    4.1000   4.249  5      NOPRINT
28.1500   7.795    4.1000   4.007  6      NOPRINT
32.2500   6.544    4.1000   3.748  6      NOPRINT
36.3500   5.361    4.1000   3.502  7      NOPRINT
40.4500   4.188    4.1000   3.256  7      NOPRINT
44.5500   3.125    4.1000   3.010  8      NOPRINT
48.6500   2.319    4.1000   2.764  8      NOPRINT
52.7500   1.526    4.1000   2.518  8      NOPRINT
56.1667   0.863    2.7333   2.313  8      NOPRINT
58.9000   0.370    2.7333   2.086  8      NOPRINT
61.6333   0.106    2.7333   1.419  8      NOPRINT
```

NoShr_gust.wnd:

```
! Wind file for Trivial turbine.
! Time  Wind    Wind    Vert.   Horiz.  Vert.   LinV    Gust
!           Speed   Dir Speed   Shear       Shear   Shear   Speed
  0.0       10.0    0.0 0.0 0.0     0.0 0.0 0.0
  0.1       10.0    0.0 0.0 0.0     0.0 0.0 0.0
 30.0       10.0    0.0 0.0 0.0     0.0 0.0 0.0
```

```
55.0        13.0    0.0 0.0 0.0     0.0 0.0 0.0
110.0        13.0    0.0 0.0 0.0     0.0 0.0 0.0
130.0        10.0    0.0 0.0 0.0     0.0 0.0 0.0
999.9       10.0    0.0 0.0 0.0     0.0 0.0 0.0
```

Cylinder1.dat:

```
Round root section with a Cd of 0.50
Made by Jason Jonkman
   1        Number of airfoil tables in this file
   0.0      Table ID parameter
   0.0      Stall angle (deg)
   0.0      No longer used, enter zero
   0.0      No longer used, enter zero
   0.0      No longer used, enter zero
   0.0      Zero Cn angle of attack (deg)
   0.0      Cn slope for zero lift (dimensionless)
   0.0      Cn extrapolated to value at positive stall angle of attack
   0.0      Cn at stall value for negative angle of attack
   0.0      Angle of attack for minimum CD (deg)
   0.50     Minimum CD value
-180.00    0.000   0.5000   0.000
   0.00    0.000   0.5000   0.000
 180.00    0.000   0.5000   0.000
```

Cylinder2.dat:

```
Round root section with a Cd of 0.35
Made by Jason Jonkman
   1        Number of airfoil tables in this file
   0.0      Table ID parameter
   0.0      Stall angle (deg)
   0.0      No longer used, enter zero
   0.0      No longer used, enter zero
   0.0      No longer used, enter zero
   0.0      Zero Cn angle of attack (deg)
   0.0      Cn slope for zero lift (dimensionless)
   0.0      Cn extrapolated to value at positive stall angle of attack
   0.0      Cn at stall value for negative angle of attack
   0.0      Angle of attack for minimum CD (deg)
   0.35     Minimum CD value
-180.00    0.000   0.3500   0.000
   0.00    0.000   0.3500   0.000
 180.00    0.000   0.3500   0.000
```

DU40_A17.dat:

```
DU40 airfoil with an aspect ratio of 17.  Original -180 to 180deg Cl, Cd, and
Cm versus AOA data taken from Appendix A of DOWEC document 10046_009.pdf
(numerical values obtained from Koert Lindenburg of ECN).
Cl and Cd values corrected for rotational stall delay and Cd values corrected
using the Viterna method for 0 to 90deg AOA by Jason Jonkman using
AirfoilPrep_v2p0.xls.
   1        Number of airfoil tables in this file
```

```
   0.0      Table ID parameter
   9.00     Stall angle (deg)
   0.0      No longer used, enter zero
   0.0      No longer used, enter zero
   0.0      No longer used, enter zero
  -1.3430   Zero Cn angle of attack (deg)
   7.4888   Cn slope for zero lift (dimensionless)
   1.3519   Cn extrapolated to value at positive stall angle of attack
  -0.3226   Cn at stall value for negative angle of attack
   0.00     Angle of attack for minimum CD (deg)
   0.0113   Minimum CD value
-180.00    0.000   0.0602   0.0000
-175.00    0.218   0.0699   0.0934
-170.00    0.397   0.1107   0.1697
-160.00    0.642   0.3045   0.2813
-155.00    0.715   0.4179   0.3208
-150.00    0.757   0.5355   0.3516
-145.00    0.772   0.6535   0.3752
-140.00    0.762   0.7685   0.3926
-135.00    0.731   0.8777   0.4048
-130.00    0.680   0.9788   0.4126
-125.00    0.613   1.0700   0.4166
-120.00    0.532   1.1499   0.4176
-115.00    0.439   1.2174   0.4158
-110.00    0.337   1.2716   0.4117
-105.00    0.228   1.3118   0.4057
-100.00    0.114   1.3378   0.3979
 -95.00   -0.002   1.3492   0.3887
 -90.00   -0.120   1.3460   0.3781
 -85.00   -0.236   1.3283   0.3663
 -80.00   -0.349   1.2964   0.3534
 -75.00   -0.456   1.2507   0.3394
 -70.00   -0.557   1.1918   0.3244
 -65.00   -0.647   1.1204   0.3084
 -60.00   -0.727   1.0376   0.2914
 -55.00   -0.792   0.9446   0.2733
 -50.00   -0.842   0.8429   0.2543
 -45.00   -0.874   0.7345   0.2342
 -40.00   -0.886   0.6215   0.2129
 -35.00   -0.875   0.5067   0.1906
 -30.00   -0.839   0.3932   0.1670
 -25.00   -0.777   0.2849   0.1422
 -24.00   -0.761   0.2642   0.1371
 -23.00   -0.744   0.2440   0.1320
 -22.00   -0.725   0.2242   0.1268
 -21.00   -0.706   0.2049   0.1215
 -20.00   -0.685   0.1861   0.1162
 -19.00   -0.662   0.1687   0.1097
 -18.00   -0.635   0.1533   0.1012
 -17.00   -0.605   0.1398   0.0907
 -16.00   -0.571   0.1281   0.0784
 -15.00   -0.534   0.1183   0.0646
 -14.00   -0.494   0.1101   0.0494
 -13.00   -0.452   0.1036   0.0330
 -12.00   -0.407   0.0986   0.0156
 -11.00   -0.360   0.0951  -0.0026
 -10.00   -0.311   0.0931  -0.0213
```

-8.00	-0.208	0.0930	-0.0600
-6.00	-0.111	0.0689	-0.0500
-5.50	-0.090	0.0614	-0.0516
-5.00	-0.072	0.0547	-0.0532
-4.50	-0.065	0.0480	-0.0538
-4.00	-0.054	0.0411	-0.0544
-3.50	-0.017	0.0349	-0.0554
-3.00	0.003	0.0299	-0.0558
-2.50	0.014	0.0255	-0.0555
-2.00	0.009	0.0198	-0.0534
-1.50	0.004	0.0164	-0.0442
-1.00	0.036	0.0147	-0.0469
-0.50	0.073	0.0137	-0.0522
0.00	0.137	0.0113	-0.0573
0.50	0.213	0.0114	-0.0644
1.00	0.292	0.0118	-0.0718
1.50	0.369	0.0122	-0.0783
2.00	0.444	0.0124	-0.0835
2.50	0.514	0.0124	-0.0866
3.00	0.580	0.0123	-0.0887
3.50	0.645	0.0120	-0.0900
4.00	0.710	0.0119	-0.0914
4.50	0.776	0.0122	-0.0933
5.00	0.841	0.0125	-0.0947
5.50	0.904	0.0129	-0.0957
6.00	0.967	0.0135	-0.0967
6.50	1.027	0.0144	-0.0973
7.00	1.084	0.0158	-0.0972
7.50	1.140	0.0174	-0.0972
8.00	1.193	0.0198	-0.0968
8.50	1.242	0.0231	-0.0958
9.00	1.287	0.0275	-0.0948
9.50	1.333	0.0323	-0.0942
10.00	1.368	0.0393	-0.0926
10.50	1.400	0.0475	-0.0908
11.00	1.425	0.0580	-0.0890
11.50	1.449	0.0691	-0.0877
12.00	1.473	0.0816	-0.0870
12.50	1.494	0.0973	-0.0870
13.00	1.513	0.1129	-0.0876
13.50	1.538	0.1288	-0.0886
14.50	1.587	0.1650	-0.0917
15.00	1.614	0.1845	-0.0939
15.50	1.631	0.2052	-0.0966
16.00	1.649	0.2250	-0.0996
16.50	1.666	0.2467	-0.1031
17.00	1.681	0.2684	-0.1069
17.50	1.699	0.2900	-0.1110
18.00	1.719	0.3121	-0.1157
19.00	1.751	0.3554	-0.1242
19.50	1.767	0.3783	-0.1291
20.50	1.798	0.4212	-0.1384
21.00	1.810	0.4415	-0.1416
22.00	1.830	0.4830	-0.1479
23.00	1.847	0.5257	-0.1542
24.00	1.861	0.5694	-0.1603
25.00	1.872	0.6141	-0.1664

```
 26.00    1.881   0.6593  -0.1724
 28.00    1.894   0.7513  -0.1841
 30.00    1.904   0.8441  -0.1954
 32.00    1.915   0.9364  -0.2063
 35.00    1.929   1.0722  -0.2220
 40.00    1.903   1.2873  -0.2468
 45.00    1.820   1.4796  -0.2701
 50.00    1.690   1.6401  -0.2921
 55.00    1.522   1.7609  -0.3127
 60.00    1.323   1.8360  -0.3321
 65.00    1.106   1.8614  -0.3502
 70.00    0.880   1.8347  -0.3672
 75.00    0.658   1.7567  -0.3830
 80.00    0.449   1.6334  -0.3977
 85.00    0.267   1.4847  -0.4112
 90.00    0.124   1.3879  -0.4234
 95.00    0.002   1.3912  -0.4343
100.00   -0.118   1.3795  -0.4437
105.00   -0.235   1.3528  -0.4514
110.00   -0.348   1.3114  -0.4573
115.00   -0.453   1.2557  -0.4610
120.00   -0.549   1.1864  -0.4623
125.00   -0.633   1.1041  -0.4606
130.00   -0.702   1.0102  -0.4554
135.00   -0.754   0.9060  -0.4462
140.00   -0.787   0.7935  -0.4323
145.00   -0.797   0.6750  -0.4127
150.00   -0.782   0.5532  -0.3863
155.00   -0.739   0.4318  -0.3521
160.00   -0.664   0.3147  -0.3085
170.00   -0.410   0.1144  -0.1858
175.00   -0.226   0.0702  -0.1022
180.00    0.000   0.0602   0.0000
```

DU35_A17.dat:

```
DU35 airfoil with an aspect ratio of 17.  Original -180 to 180deg Cl, Cd, and
Cm versus AOA data taken from Appendix A of DOWEC document 10046_009.pdf
(numerical values obtained from Koert Lindenburg of ECN).
Cl and Cd values corrected for rotational stall delay and Cd values corrected
using the Viterna method for 0 to 90deg AOA by Jason Jonkman using
AirfoilPrep_v2p0.xls.
   1        Number of airfoil tables in this file
   0.0      Table ID parameter
  11.50     Stall angle (deg)
   0.0      No longer used, enter zero
   0.0      No longer used, enter zero
   0.0      No longer used, enter zero
  -1.8330   Zero Cn angle of attack (deg)
   7.1838   Cn slope for zero lift (dimensionless)
   1.6717   Cn extrapolated to value at positive stall angle of attack
  -0.3075   Cn at stall value for negative angle of attack
   0.00     Angle of attack for minimum CD (deg)
   0.0094   Minimum CD value
```

-180.00	0.000	0.0407	0.0000
-175.00	0.223	0.0507	0.0937
-170.00	0.405	0.1055	0.1702
-160.00	0.658	0.2982	0.2819
-155.00	0.733	0.4121	0.3213
-150.00	0.778	0.5308	0.3520
-145.00	0.795	0.6503	0.3754
-140.00	0.787	0.7672	0.3926
-135.00	0.757	0.8785	0.4046
-130.00	0.708	0.9819	0.4121
-125.00	0.641	1.0756	0.4160
-120.00	0.560	1.1580	0.4167
-115.00	0.467	1.2280	0.4146
-110.00	0.365	1.2847	0.4104
-105.00	0.255	1.3274	0.4041
-100.00	0.139	1.3557	0.3961
-95.00	0.021	1.3692	0.3867
-90.00	-0.098	1.3680	0.3759
-85.00	-0.216	1.3521	0.3639
-80.00	-0.331	1.3218	0.3508
-75.00	-0.441	1.2773	0.3367
-70.00	-0.544	1.2193	0.3216
-65.00	-0.638	1.1486	0.3054
-60.00	-0.720	1.0660	0.2884
-55.00	-0.788	0.9728	0.2703
-50.00	-0.840	0.8705	0.2512
-45.00	-0.875	0.7611	0.2311
-40.00	-0.889	0.6466	0.2099
-35.00	-0.880	0.5299	0.1876
-30.00	-0.846	0.4141	0.1641
-25.00	-0.784	0.3030	0.1396
-24.00	-0.768	0.2817	0.1345
-23.00	-0.751	0.2608	0.1294
-22.00	-0.733	0.2404	0.1243
-21.00	-0.714	0.2205	0.1191
-20.00	-0.693	0.2011	0.1139
-19.00	-0.671	0.1822	0.1086
-18.00	-0.648	0.1640	0.1032
-17.00	-0.624	0.1465	0.0975
-16.00	-0.601	0.1300	0.0898
-15.00	-0.579	0.1145	0.0799
-14.00	-0.559	0.1000	0.0682
-13.00	-0.539	0.0867	0.0547
-12.00	-0.519	0.0744	0.0397
-11.00	-0.499	0.0633	0.0234
-10.00	-0.480	0.0534	0.0060
-5.54	-0.385	0.0245	-0.0800
-5.04	-0.359	0.0225	-0.0800
-4.54	-0.360	0.0196	-0.0800
-4.04	-0.355	0.0174	-0.0800
-3.54	-0.307	0.0162	-0.0800
-3.04	-0.246	0.0144	-0.0800
-3.00	-0.240	0.0240	-0.0623
-2.50	-0.163	0.0188	-0.0674
-2.00	-0.091	0.0160	-0.0712
-1.50	-0.019	0.0137	-0.0746
-1.00	0.052	0.0118	-0.0778

-0.50	0.121	0.0104	-0.0806
0.00	0.196	0.0094	-0.0831
0.50	0.265	0.0096	-0.0863
1.00	0.335	0.0098	-0.0895
1.50	0.404	0.0099	-0.0924
2.00	0.472	0.0100	-0.0949
2.50	0.540	0.0102	-0.0973
3.00	0.608	0.0103	-0.0996
3.50	0.674	0.0104	-0.1016
4.00	0.742	0.0105	-0.1037
4.50	0.809	0.0107	-0.1057
5.00	0.875	0.0108	-0.1076
5.50	0.941	0.0109	-0.1094
6.00	1.007	0.0110	-0.1109
6.50	1.071	0.0113	-0.1118
7.00	1.134	0.0115	-0.1127
7.50	1.198	0.0117	-0.1138
8.00	1.260	0.0120	-0.1144
8.50	1.318	0.0126	-0.1137
9.00	1.368	0.0133	-0.1112
9.50	1.422	0.0143	-0.1100
10.00	1.475	0.0156	-0.1086
10.50	1.523	0.0174	-0.1064
11.00	1.570	0.0194	-0.1044
11.50	1.609	0.0227	-0.1013
12.00	1.642	0.0269	-0.0980
12.50	1.675	0.0319	-0.0953
13.00	1.700	0.0398	-0.0925
13.50	1.717	0.0488	-0.0896
14.00	1.712	0.0614	-0.0864
14.50	1.703	0.0786	-0.0840
15.50	1.671	0.1173	-0.0830
16.00	1.649	0.1377	-0.0848
16.50	1.621	0.1600	-0.0880
17.00	1.598	0.1814	-0.0926
17.50	1.571	0.2042	-0.0984
18.00	1.549	0.2316	-0.1052
19.00	1.544	0.2719	-0.1158
19.50	1.549	0.2906	-0.1213
20.00	1.565	0.3085	-0.1248
21.00	1.565	0.3447	-0.1317
22.00	1.563	0.3820	-0.1385
23.00	1.558	0.4203	-0.1452
24.00	1.552	0.4593	-0.1518
25.00	1.546	0.4988	-0.1583
26.00	1.539	0.5387	-0.1647
28.00	1.527	0.6187	-0.1770
30.00	1.522	0.6978	-0.1886
32.00	1.529	0.7747	-0.1994
35.00	1.544	0.8869	-0.2148
40.00	1.529	1.0671	-0.2392
45.00	1.471	1.2319	-0.2622
50.00	1.376	1.3747	-0.2839
55.00	1.249	1.4899	-0.3043
60.00	1.097	1.5728	-0.3236
65.00	0.928	1.6202	-0.3417
70.00	0.750	1.6302	-0.3586

```
  75.00    0.570   1.6031  -0.3745
  80.00    0.396   1.5423  -0.3892
  85.00    0.237   1.4598  -0.4028
  90.00    0.101   1.4041  -0.4151
  95.00   -0.022   1.4053  -0.4261
 100.00   -0.143   1.3914  -0.4357
 105.00   -0.261   1.3625  -0.4437
 110.00   -0.374   1.3188  -0.4498
 115.00   -0.480   1.2608  -0.4538
 120.00   -0.575   1.1891  -0.4553
 125.00   -0.659   1.1046  -0.4540
 130.00   -0.727   1.0086  -0.4492
 135.00   -0.778   0.9025  -0.4405
 140.00   -0.809   0.7883  -0.4270
 145.00   -0.818   0.6684  -0.4078
 150.00   -0.800   0.5457  -0.3821
 155.00   -0.754   0.4236  -0.3484
 160.00   -0.677   0.3066  -0.3054
 170.00   -0.417   0.1085  -0.1842
 175.00   -0.229   0.0510  -0.1013
 180.00    0.000   0.0407   0.0000
```

DU30_A17.dat:

```
DU30 airfoil with an aspect ratio of 17.  Original -180 to 180deg Cl, Cd, and
Cm versus AOA data taken from Appendix A of DOWEC document 10046_009.pdf
(numerical values obtained from Koert Lindenburg of ECN).
Cl and Cd values corrected for rotational stall delay and Cd values corrected
using the Viterna method for 0 to 90deg AOA by Jason Jonkman using
AirfoilPrep_v2p0.xls.
   1        Number of airfoil tables in this file
   0.0      Table ID parameter
   9.00     Stall angle (deg)
   0.0      No longer used, enter zero
   0.0      No longer used, enter zero
   0.0      No longer used, enter zero
  -2.3220   Zero Cn angle of attack (deg)
   7.3326   Cn slope for zero lift (dimensionless)
   1.4490   Cn extrapolated to value at positive stall angle of attack
  -0.6138   Cn at stall value for negative angle of attack
   0.00     Angle of attack for minimum CD (deg)
   0.0087   Minimum CD value
-180.00    0.000   0.0267   0.0000
-175.00    0.274   0.0370   0.1379
-170.00    0.547   0.0968   0.2778
-160.00    0.685   0.2876   0.2740
-155.00    0.766   0.4025   0.3118
-150.00    0.816   0.5232   0.3411
-145.00    0.836   0.6454   0.3631
-140.00    0.832   0.7656   0.3791
-135.00    0.804   0.8807   0.3899
-130.00    0.756   0.9882   0.3965
-125.00    0.690   1.0861   0.3994
-120.00    0.609   1.1730   0.3992
-115.00    0.515   1.2474   0.3964
```

-110.00	0.411	1.3084	0.3915
-105.00	0.300	1.3552	0.3846
-100.00	0.182	1.3875	0.3761
-95.00	0.061	1.4048	0.3663
-90.00	-0.061	1.4070	0.3551
-85.00	-0.183	1.3941	0.3428
-80.00	-0.302	1.3664	0.3295
-75.00	-0.416	1.3240	0.3153
-70.00	-0.523	1.2676	0.3001
-65.00	-0.622	1.1978	0.2841
-60.00	-0.708	1.1156	0.2672
-55.00	-0.781	1.0220	0.2494
-50.00	-0.838	0.9187	0.2308
-45.00	-0.877	0.8074	0.2113
-40.00	-0.895	0.6904	0.1909
-35.00	-0.889	0.5703	0.1696
-30.00	-0.858	0.4503	0.1475
-25.00	-0.832	0.3357	0.1224
-24.00	-0.852	0.3147	0.1156
-23.00	-0.882	0.2946	0.1081
-22.00	-0.919	0.2752	0.1000
-21.00	-0.963	0.2566	0.0914
-20.00	-1.013	0.2388	0.0823
-19.00	-1.067	0.2218	0.0728
-18.00	-1.125	0.2056	0.0631
-17.00	-1.185	0.1901	0.0531
-16.00	-1.245	0.1754	0.0430
-15.25	-1.290	0.1649	0.0353
-14.24	-1.229	0.1461	0.0240
-13.24	-1.148	0.1263	0.0100
-12.22	-1.052	0.1051	-0.0090
-11.22	-0.965	0.0886	-0.0230
-10.19	-0.867	0.0740	-0.0336
-9.70	-0.822	0.0684	-0.0375
-9.18	-0.769	0.0605	-0.0440
-8.18	-0.756	0.0270	-0.0578
-7.19	-0.690	0.0180	-0.0590
-6.65	-0.616	0.0166	-0.0633
-6.13	-0.542	0.0152	-0.0674
-6.00	-0.525	0.0117	-0.0732
-5.50	-0.451	0.0105	-0.0766
-5.00	-0.382	0.0097	-0.0797
-4.50	-0.314	0.0092	-0.0825
-4.00	-0.251	0.0091	-0.0853
-3.50	-0.189	0.0089	-0.0884
-3.00	-0.120	0.0089	-0.0914
-2.50	-0.051	0.0088	-0.0942
-2.00	0.017	0.0088	-0.0969
-1.50	0.085	0.0088	-0.0994
-1.00	0.152	0.0088	-0.1018
-0.50	0.219	0.0088	-0.1041
0.00	0.288	0.0087	-0.1062
0.50	0.354	0.0087	-0.1086
1.00	0.421	0.0088	-0.1107
1.50	0.487	0.0089	-0.1129
2.00	0.554	0.0090	-0.1149
2.50	0.619	0.0091	-0.1168

3.00	0.685	0.0092	-0.1185
3.50	0.749	0.0093	-0.1201
4.00	0.815	0.0095	-0.1218
4.50	0.879	0.0096	-0.1233
5.00	0.944	0.0097	-0.1248
5.50	1.008	0.0099	-0.1260
6.00	1.072	0.0101	-0.1270
6.50	1.135	0.0103	-0.1280
7.00	1.197	0.0107	-0.1287
7.50	1.256	0.0112	-0.1289
8.00	1.305	0.0125	-0.1270
9.00	1.390	0.0155	-0.1207
9.50	1.424	0.0171	-0.1158
10.00	1.458	0.0192	-0.1116
10.50	1.488	0.0219	-0.1073
11.00	1.512	0.0255	-0.1029
11.50	1.533	0.0307	-0.0983
12.00	1.549	0.0370	-0.0949
12.50	1.558	0.0452	-0.0921
13.00	1.470	0.0630	-0.0899
13.50	1.398	0.0784	-0.0885
14.00	1.354	0.0931	-0.0885
14.50	1.336	0.1081	-0.0902
15.00	1.333	0.1239	-0.0928
15.50	1.326	0.1415	-0.0963
16.00	1.329	0.1592	-0.1006
16.50	1.326	0.1743	-0.1042
17.00	1.321	0.1903	-0.1084
17.50	1.331	0.2044	-0.1125
18.00	1.333	0.2186	-0.1169
18.50	1.340	0.2324	-0.1215
19.00	1.362	0.2455	-0.1263
19.50	1.382	0.2584	-0.1313
20.00	1.398	0.2689	-0.1352
20.50	1.426	0.2814	-0.1406
21.00	1.437	0.2943	-0.1462
22.00	1.418	0.3246	-0.1516
23.00	1.397	0.3557	-0.1570
24.00	1.376	0.3875	-0.1623
25.00	1.354	0.4198	-0.1676
26.00	1.332	0.4524	-0.1728
28.00	1.293	0.5183	-0.1832
30.00	1.265	0.5843	-0.1935
32.00	1.253	0.6492	-0.2039
35.00	1.264	0.7438	-0.2193
40.00	1.258	0.8970	-0.2440
45.00	1.217	1.0402	-0.2672
50.00	1.146	1.1686	-0.2891
55.00	1.049	1.2779	-0.3097
60.00	0.932	1.3647	-0.3290
65.00	0.799	1.4267	-0.3471
70.00	0.657	1.4621	-0.3641
75.00	0.509	1.4708	-0.3799
80.00	0.362	1.4544	-0.3946
85.00	0.221	1.4196	-0.4081
90.00	0.092	1.3938	-0.4204
95.00	-0.030	1.3943	-0.4313

```
 100.00   -0.150   1.3798  -0.4408
 105.00   -0.267   1.3504  -0.4486
 110.00   -0.379   1.3063  -0.4546
 115.00   -0.483   1.2481  -0.4584
 120.00   -0.578   1.1763  -0.4597
 125.00   -0.660   1.0919  -0.4582
 130.00   -0.727   0.9962  -0.4532
 135.00   -0.777   0.8906  -0.4441
 140.00   -0.807   0.7771  -0.4303
 145.00   -0.815   0.6581  -0.4109
 150.00   -0.797   0.5364  -0.3848
 155.00   -0.750   0.4157  -0.3508
 160.00   -0.673   0.3000  -0.3074
 170.00   -0.547   0.1051  -0.2786
 175.00   -0.274   0.0388  -0.1380
 180.00    0.000   0.0267   0.0000
```

DU25_A17.dat:

```
DU25 airfoil with an aspect ratio of 17.  Original -180 to 180deg Cl, Cd, and
Cm versus AOA data taken from Appendix A of DOWEC document 10046_009.pdf
(numerical values obtained from Koert Lindenburg of ECN).
Cl and Cd values corrected for rotational stall delay and Cd values corrected
using the Viterna method for 0 to 90deg AOA by Jason Jonkman using
AirfoilPrep_v2p0.xls.
   1        Number of airfoil tables in this file
   0.0      Table ID parameter
   8.50     Stall angle (deg)
   0.0      No longer used, enter zero
   0.0      No longer used, enter zero
   0.0      No longer used, enter zero
  -4.2422   Zero Cn angle of attack (deg)
   6.4462   Cn slope for zero lift (dimensionless)
   1.4336   Cn extrapolated to value at positive stall angle of attack
  -0.6873   Cn at stall value for negative angle of attack
   0.00     Angle of attack for minimum CD (deg)
   0.0065   Minimum CD value
-180.00    0.000   0.0202   0.0000
-175.00    0.368   0.0324   0.1845
-170.00    0.735   0.0943   0.3701
-160.00    0.695   0.2848   0.2679
-155.00    0.777   0.4001   0.3046
-150.00    0.828   0.5215   0.3329
-145.00    0.850   0.6447   0.3540
-140.00    0.846   0.7660   0.3693
-135.00    0.818   0.8823   0.3794
-130.00    0.771   0.9911   0.3854
-125.00    0.705   1.0905   0.3878
-120.00    0.624   1.1787   0.3872
-115.00    0.530   1.2545   0.3841
-110.00    0.426   1.3168   0.3788
-105.00    0.314   1.3650   0.3716
-100.00    0.195   1.3984   0.3629
 -95.00    0.073   1.4169   0.3529
 -90.00   -0.050   1.4201   0.3416
```

-85.00	-0.173	1.4081	0.3292
-80.00	-0.294	1.3811	0.3159
-75.00	-0.409	1.3394	0.3017
-70.00	-0.518	1.2833	0.2866
-65.00	-0.617	1.2138	0.2707
-60.00	-0.706	1.1315	0.2539
-55.00	-0.780	1.0378	0.2364
-50.00	-0.839	0.9341	0.2181
-45.00	-0.879	0.8221	0.1991
-40.00	-0.898	0.7042	0.1792
-35.00	-0.893	0.5829	0.1587
-30.00	-0.862	0.4616	0.1374
-25.00	-0.803	0.3441	0.1154
-24.00	-0.792	0.3209	0.1101
-23.00	-0.789	0.2972	0.1031
-22.00	-0.792	0.2730	0.0947
-21.00	-0.801	0.2485	0.0849
-20.00	-0.815	0.2237	0.0739
-19.00	-0.833	0.1990	0.0618
-18.00	-0.854	0.1743	0.0488
-17.00	-0.879	0.1498	0.0351
-16.00	-0.905	0.1256	0.0208
-15.00	-0.932	0.1020	0.0060
-14.00	-0.959	0.0789	-0.0091
-13.00	-0.985	0.0567	-0.0243
-13.00	-0.985	0.0567	-0.0243
-12.01	-0.953	0.0271	-0.0349
-11.00	-0.900	0.0303	-0.0361
-9.98	-0.827	0.0287	-0.0464
-8.98	-0.753	0.0271	-0.0534
-8.47	-0.691	0.0264	-0.0650
-7.45	-0.555	0.0114	-0.0782
-6.42	-0.413	0.0094	-0.0904
-5.40	-0.271	0.0086	-0.1006
-5.00	-0.220	0.0073	-0.1107
-4.50	-0.152	0.0071	-0.1135
-4.00	-0.084	0.0070	-0.1162
-3.50	-0.018	0.0069	-0.1186
-3.00	0.049	0.0068	-0.1209
-2.50	0.115	0.0068	-0.1231
-2.00	0.181	0.0068	-0.1252
-1.50	0.247	0.0067	-0.1272
-1.00	0.312	0.0067	-0.1293
-0.50	0.377	0.0067	-0.1311
0.00	0.444	0.0065	-0.1330
0.50	0.508	0.0065	-0.1347
1.00	0.573	0.0066	-0.1364
1.50	0.636	0.0067	-0.1380
2.00	0.701	0.0068	-0.1396
2.50	0.765	0.0069	-0.1411
3.00	0.827	0.0070	-0.1424
3.50	0.890	0.0071	-0.1437
4.00	0.952	0.0073	-0.1448
4.50	1.013	0.0076	-0.1456
5.00	1.062	0.0079	-0.1445
6.00	1.161	0.0099	-0.1419
6.50	1.208	0.0117	-0.1403

7.00	1.254	0.0132	-0.1382
7.50	1.301	0.0143	-0.1362
8.00	1.336	0.0153	-0.1320
8.50	1.369	0.0165	-0.1276
9.00	1.400	0.0181	-0.1234
9.50	1.428	0.0211	-0.1193
10.00	1.442	0.0262	-0.1152
10.50	1.427	0.0336	-0.1115
11.00	1.374	0.0420	-0.1081
11.50	1.316	0.0515	-0.1052
12.00	1.277	0.0601	-0.1026
12.50	1.250	0.0693	-0.1000
13.00	1.246	0.0785	-0.0980
13.50	1.247	0.0888	-0.0969
14.00	1.256	0.1000	-0.0968
14.50	1.260	0.1108	-0.0973
15.00	1.271	0.1219	-0.0981
15.50	1.281	0.1325	-0.0992
16.00	1.289	0.1433	-0.1006
16.50	1.294	0.1541	-0.1023
17.00	1.304	0.1649	-0.1042
17.50	1.309	0.1754	-0.1064
18.00	1.315	0.1845	-0.1082
18.50	1.320	0.1953	-0.1110
19.00	1.330	0.2061	-0.1143
19.50	1.343	0.2170	-0.1179
20.00	1.354	0.2280	-0.1219
20.50	1.359	0.2390	-0.1261
21.00	1.360	0.2536	-0.1303
22.00	1.325	0.2814	-0.1375
23.00	1.288	0.3098	-0.1446
24.00	1.251	0.3386	-0.1515
25.00	1.215	0.3678	-0.1584
26.00	1.181	0.3972	-0.1651
28.00	1.120	0.4563	-0.1781
30.00	1.076	0.5149	-0.1904
32.00	1.056	0.5720	-0.2017
35.00	1.066	0.6548	-0.2173
40.00	1.064	0.7901	-0.2418
45.00	1.035	0.9190	-0.2650
50.00	0.980	1.0378	-0.2867
55.00	0.904	1.1434	-0.3072
60.00	0.810	1.2333	-0.3265
65.00	0.702	1.3055	-0.3446
70.00	0.582	1.3587	-0.3616
75.00	0.456	1.3922	-0.3775
80.00	0.326	1.4063	-0.3921
85.00	0.197	1.4042	-0.4057
90.00	0.072	1.3985	-0.4180
95.00	-0.050	1.3973	-0.4289
100.00	-0.170	1.3810	-0.4385
105.00	-0.287	1.3498	-0.4464
110.00	-0.399	1.3041	-0.4524
115.00	-0.502	1.2442	-0.4563
120.00	-0.596	1.1709	-0.4577
125.00	-0.677	1.0852	-0.4563
130.00	-0.743	0.9883	-0.4514

```
 135.00   -0.792   0.8818  -0.4425
 140.00   -0.821   0.7676  -0.4288
 145.00   -0.826   0.6481  -0.4095
 150.00   -0.806   0.5264  -0.3836
 155.00   -0.758   0.4060  -0.3497
 160.00   -0.679   0.2912  -0.3065
 170.00   -0.735   0.0995  -0.3706
 175.00   -0.368   0.0356  -0.1846
 180.00    0.000   0.0202   0.0000
```

DU21_A17.dat:

```
DU21 airfoil with an aspect ratio of 17.  Original -180 to 180deg Cl, Cd, and
Cm versus AOA data taken from Appendix A of DOWEC document 10046_009.pdf
(numerical values obtained from Koert Lindenburg of ECN).
Cl and Cd values corrected for rotational stall delay and Cd values corrected
using the Viterna method for 0 to 90deg AOA by Jason Jonkman using
AirfoilPrep_v2p0.xls.
   1        Number of airfoil tables in this file
   0.0      Table ID parameter
   8.00     Stall angle (deg)
   0.0      No longer used, enter zero
   0.0      No longer used, enter zero
   0.0      No longer used, enter zero
  -5.0609   Zero Cn angle of attack (deg)
   6.2047   Cn slope for zero lift (dimensionless)
   1.4144   Cn extrapolated to value at positive stall angle of attack
  -0.5324   Cn at stall value for negative angle of attack
  -1.50     Angle of attack for minimum CD (deg)
   0.0057   Minimum CD value
-180.00    0.000   0.0185   0.0000
-175.00    0.394   0.0332   0.1978
-170.00    0.788   0.0945   0.3963
-160.00    0.670   0.2809   0.2738
-155.00    0.749   0.3932   0.3118
-150.00    0.797   0.5112   0.3413
-145.00    0.818   0.6309   0.3636
-140.00    0.813   0.7485   0.3799
-135.00    0.786   0.8612   0.3911
-130.00    0.739   0.9665   0.3980
-125.00    0.675   1.0625   0.4012
-120.00    0.596   1.1476   0.4014
-115.00    0.505   1.2206   0.3990
-110.00    0.403   1.2805   0.3943
-105.00    0.294   1.3265   0.3878
-100.00    0.179   1.3582   0.3796
 -95.00    0.060   1.3752   0.3700
 -90.00   -0.060   1.3774   0.3591
 -85.00   -0.179   1.3648   0.3471
 -80.00   -0.295   1.3376   0.3340
 -75.00   -0.407   1.2962   0.3199
 -70.00   -0.512   1.2409   0.3049
 -65.00   -0.608   1.1725   0.2890
 -60.00   -0.693   1.0919   0.2722
 -55.00   -0.764   1.0002   0.2545
```

-50.00	-0.820	0.8990	0.2359
-45.00	-0.857	0.7900	0.2163
-40.00	-0.875	0.6754	0.1958
-35.00	-0.869	0.5579	0.1744
-30.00	-0.838	0.4405	0.1520
-25.00	-0.791	0.3256	0.1262
-24.00	-0.794	0.3013	0.1170
-23.00	-0.805	0.2762	0.1059
-22.00	-0.821	0.2506	0.0931
-21.00	-0.843	0.2246	0.0788
-20.00	-0.869	0.1983	0.0631
-19.00	-0.899	0.1720	0.0464
-18.00	-0.931	0.1457	0.0286
-17.00	-0.964	0.1197	0.0102
-16.00	-0.999	0.0940	-0.0088
-15.00	-1.033	0.0689	-0.0281
-14.50	-1.050	0.0567	-0.0378
-12.01	-0.953	0.0271	-0.0349
-11.00	-0.900	0.0303	-0.0361
-9.98	-0.827	0.0287	-0.0464
-8.12	-0.536	0.0124	-0.0821
-7.62	-0.467	0.0109	-0.0924
-7.11	-0.393	0.0092	-0.1015
-6.60	-0.323	0.0083	-0.1073
-6.50	-0.311	0.0089	-0.1083
-6.00	-0.245	0.0082	-0.1112
-5.50	-0.178	0.0074	-0.1146
-5.00	-0.113	0.0069	-0.1172
-4.50	-0.048	0.0065	-0.1194
-4.00	0.016	0.0063	-0.1213
-3.50	0.080	0.0061	-0.1232
-3.00	0.145	0.0058	-0.1252
-2.50	0.208	0.0057	-0.1268
-2.00	0.270	0.0057	-0.1282
-1.50	0.333	0.0057	-0.1297
-1.00	0.396	0.0057	-0.1310
-0.50	0.458	0.0057	-0.1324
0.00	0.521	0.0057	-0.1337
0.50	0.583	0.0057	-0.1350
1.00	0.645	0.0058	-0.1363
1.50	0.706	0.0058	-0.1374
2.00	0.768	0.0059	-0.1385
2.50	0.828	0.0061	-0.1395
3.00	0.888	0.0063	-0.1403
3.50	0.948	0.0066	-0.1406
4.00	0.996	0.0071	-0.1398
4.50	1.046	0.0079	-0.1390
5.00	1.095	0.0090	-0.1378
5.50	1.145	0.0103	-0.1369
6.00	1.192	0.0113	-0.1353
6.50	1.239	0.0122	-0.1338
7.00	1.283	0.0131	-0.1317
7.50	1.324	0.0139	-0.1291
8.00	1.358	0.0147	-0.1249
8.50	1.385	0.0158	-0.1213
9.00	1.403	0.0181	-0.1177
9.50	1.401	0.0211	-0.1142

10.00	1.358	0.0255	-0.1103
10.50	1.313	0.0301	-0.1066
11.00	1.287	0.0347	-0.1032
11.50	1.274	0.0401	-0.1002
12.00	1.272	0.0468	-0.0971
12.50	1.273	0.0545	-0.0940
13.00	1.273	0.0633	-0.0909
13.50	1.273	0.0722	-0.0883
14.00	1.272	0.0806	-0.0865
14.50	1.273	0.0900	-0.0854
15.00	1.275	0.0987	-0.0849
15.50	1.281	0.1075	-0.0847
16.00	1.284	0.1170	-0.0850
16.50	1.296	0.1270	-0.0858
17.00	1.306	0.1368	-0.0869
17.50	1.308	0.1464	-0.0883
18.00	1.308	0.1562	-0.0901
18.50	1.308	0.1664	-0.0922
19.00	1.308	0.1770	-0.0949
19.50	1.307	0.1878	-0.0980
20.00	1.311	0.1987	-0.1017
20.50	1.325	0.2100	-0.1059
21.00	1.324	0.2214	-0.1105
22.00	1.277	0.2499	-0.1172
23.00	1.229	0.2786	-0.1239
24.00	1.182	0.3077	-0.1305
25.00	1.136	0.3371	-0.1370
26.00	1.093	0.3664	-0.1433
28.00	1.017	0.4246	-0.1556
30.00	0.962	0.4813	-0.1671
32.00	0.937	0.5356	-0.1778
35.00	0.947	0.6127	-0.1923
40.00	0.950	0.7396	-0.2154
45.00	0.928	0.8623	-0.2374
50.00	0.884	0.9781	-0.2583
55.00	0.821	1.0846	-0.2782
60.00	0.740	1.1796	-0.2971
65.00	0.646	1.2617	-0.3149
70.00	0.540	1.3297	-0.3318
75.00	0.425	1.3827	-0.3476
80.00	0.304	1.4202	-0.3625
85.00	0.179	1.4423	-0.3763
90.00	0.053	1.4512	-0.3890
95.00	-0.073	1.4480	-0.4004
100.00	-0.198	1.4294	-0.4105
105.00	-0.319	1.3954	-0.4191
110.00	-0.434	1.3464	-0.4260
115.00	-0.541	1.2829	-0.4308
120.00	-0.637	1.2057	-0.4333
125.00	-0.720	1.1157	-0.4330
130.00	-0.787	1.0144	-0.4294
135.00	-0.836	0.9033	-0.4219
140.00	-0.864	0.7845	-0.4098
145.00	-0.869	0.6605	-0.3922
150.00	-0.847	0.5346	-0.3682
155.00	-0.795	0.4103	-0.3364
160.00	-0.711	0.2922	-0.2954

```
 170.00   -0.788   0.0969  -0.3966
 175.00   -0.394   0.0334  -0.1978
 180.00    0.000   0.0185   0.0000
```

NACA64_A17.dat:

```
NACA64 airfoil with an aspect ratio of 17.  Original -180 to 180deg Cl, Cd,
and Cm versus AOA data taken from Appendix A of DOWEC document 10046_009.pdf
(numerical values obtained from Koert Lindenburg of ECN).
Cl and Cd values corrected for rotational stall delay and Cd values corrected
using the Viterna method for 0 to 90deg AOA by Jason Jonkman using
AirfoilPrep_v2p0.xls.
   1        Number of airfoil tables in this file
   0.0      Table ID parameter
   9.00     Stall angle (deg)
   0.0      No longer used, enter zero
   0.0      No longer used, enter zero
   0.0      No longer used, enter zero
  -4.4320   Zero Cn angle of attack (deg)
   6.0031   Cn slope for zero lift (dimensionless)
   1.4073   Cn extrapolated to value at positive stall angle of attack
  -0.7945   Cn at stall value for negative angle of attack
  -1.00     Angle of attack for minimum CD (deg)
   0.0052   Minimum CD value
-180.00    0.000   0.0198   0.0000
-175.00    0.374   0.0341   0.1880
-170.00    0.749   0.0955   0.3770
-160.00    0.659   0.2807   0.2747
-155.00    0.736   0.3919   0.3130
-150.00    0.783   0.5086   0.3428
-145.00    0.803   0.6267   0.3654
-140.00    0.798   0.7427   0.3820
-135.00    0.771   0.8537   0.3935
-130.00    0.724   0.9574   0.4007
-125.00    0.660   1.0519   0.4042
-120.00    0.581   1.1355   0.4047
-115.00    0.491   1.2070   0.4025
-110.00    0.390   1.2656   0.3981
-105.00    0.282   1.3104   0.3918
-100.00    0.169   1.3410   0.3838
 -95.00    0.052   1.3572   0.3743
 -90.00   -0.067   1.3587   0.3636
 -85.00   -0.184   1.3456   0.3517
 -80.00   -0.299   1.3181   0.3388
 -75.00   -0.409   1.2765   0.3248
 -70.00   -0.512   1.2212   0.3099
 -65.00   -0.606   1.1532   0.2940
 -60.00   -0.689   1.0731   0.2772
 -55.00   -0.759   0.9822   0.2595
 -50.00   -0.814   0.8820   0.2409
 -45.00   -0.850   0.7742   0.2212
 -40.00   -0.866   0.6610   0.2006
 -35.00   -0.860   0.5451   0.1789
 -30.00   -0.829   0.4295   0.1563
 -25.00   -0.853   0.3071   0.1156
```

-24.00	-0.870	0.2814	0.1040
-23.00	-0.890	0.2556	0.0916
-22.00	-0.911	0.2297	0.0785
-21.00	-0.934	0.2040	0.0649
-20.00	-0.958	0.1785	0.0508
-19.00	-0.982	0.1534	0.0364
-18.00	-1.005	0.1288	0.0218
-17.00	-1.082	0.1037	0.0129
-16.00	-1.113	0.0786	-0.0028
-15.00	-1.105	0.0535	-0.0251
-14.00	-1.078	0.0283	-0.0419
-13.50	-1.053	0.0158	-0.0521
-13.00	-1.015	0.0151	-0.0610
-12.00	-0.904	0.0134	-0.0707
-11.00	-0.807	0.0121	-0.0722
-10.00	-0.711	0.0111	-0.0734
-9.00	-0.595	0.0099	-0.0772
-8.00	-0.478	0.0091	-0.0807
-7.00	-0.375	0.0086	-0.0825
-6.00	-0.264	0.0082	-0.0832
-5.00	-0.151	0.0079	-0.0841
-4.00	-0.017	0.0072	-0.0869
-3.00	0.088	0.0064	-0.0912
-2.00	0.213	0.0054	-0.0946
-1.00	0.328	0.0052	-0.0971
0.00	0.442	0.0052	-0.1014
1.00	0.556	0.0052	-0.1076
2.00	0.670	0.0053	-0.1126
3.00	0.784	0.0053	-0.1157
4.00	0.898	0.0054	-0.1199
5.00	1.011	0.0058	-0.1240
6.00	1.103	0.0091	-0.1234
7.00	1.181	0.0113	-0.1184
8.00	1.257	0.0124	-0.1163
8.50	1.293	0.0130	-0.1163
9.00	1.326	0.0136	-0.1160
9.50	1.356	0.0143	-0.1154
10.00	1.382	0.0150	-0.1149
10.50	1.400	0.0267	-0.1145
11.00	1.415	0.0383	-0.1143
11.50	1.425	0.0498	-0.1147
12.00	1.434	0.0613	-0.1158
12.50	1.443	0.0727	-0.1165
13.00	1.451	0.0841	-0.1153
13.50	1.453	0.0954	-0.1131
14.00	1.448	0.1065	-0.1112
14.50	1.444	0.1176	-0.1101
15.00	1.445	0.1287	-0.1103
15.50	1.447	0.1398	-0.1109
16.00	1.448	0.1509	-0.1114
16.50	1.444	0.1619	-0.1111
17.00	1.438	0.1728	-0.1097
17.50	1.439	0.1837	-0.1079
18.00	1.448	0.1947	-0.1080
18.50	1.452	0.2057	-0.1090
19.00	1.448	0.2165	-0.1086
19.50	1.438	0.2272	-0.1077

```
  20.00    1.428   0.2379  -0.1099
  21.00    1.401   0.2590  -0.1169
  22.00    1.359   0.2799  -0.1190
  23.00    1.300   0.3004  -0.1235
  24.00    1.220   0.3204  -0.1393
  25.00    1.168   0.3377  -0.1440
  26.00    1.116   0.3554  -0.1486
  28.00    1.015   0.3916  -0.1577
  30.00    0.926   0.4294  -0.1668
  32.00    0.855   0.4690  -0.1759
  35.00    0.800   0.5324  -0.1897
  40.00    0.804   0.6452  -0.2126
  45.00    0.793   0.7573  -0.2344
  50.00    0.763   0.8664  -0.2553
  55.00    0.717   0.9708  -0.2751
  60.00    0.656   1.0693  -0.2939
  65.00    0.582   1.1606  -0.3117
  70.00    0.495   1.2438  -0.3285
  75.00    0.398   1.3178  -0.3444
  80.00    0.291   1.3809  -0.3593
  85.00    0.176   1.4304  -0.3731
  90.00    0.053   1.4565  -0.3858
  95.00   -0.074   1.4533  -0.3973
 100.00   -0.199   1.4345  -0.4075
 105.00   -0.321   1.4004  -0.4162
 110.00   -0.436   1.3512  -0.4231
 115.00   -0.543   1.2874  -0.4280
 120.00   -0.640   1.2099  -0.4306
 125.00   -0.723   1.1196  -0.4304
 130.00   -0.790   1.0179  -0.4270
 135.00   -0.840   0.9064  -0.4196
 140.00   -0.868   0.7871  -0.4077
 145.00   -0.872   0.6627  -0.3903
 150.00   -0.850   0.5363  -0.3665
 155.00   -0.798   0.4116  -0.3349
 160.00   -0.714   0.2931  -0.2942
 170.00   -0.749   0.0971  -0.3771
 175.00   -0.374   0.0334  -0.1879
 180.00    0.000   0.0198   0.0000
```

FAST

NREL_5MW_5MWFMA.fst:

```
------------------------------------------------------------------------
---
------- FAST INPUT FILE -------------------------------------------------
---
NREL 5.0 MW Baseline Wind Turbine for Use in Offshore Analysis.
Properties from Dutch Offshore Wind Energy Converter (DOWEC) 6MW Pre-Design
(10046_009.pdf) and REpower 5M 5MW (5m_uk.pdf); Compatible with FAST v7.01.
This file is a modified version of "NRELOffshrBsline5MW_Onshore.fst" DSO 6-
29-12
---------------------- SIMULATION CONTROL ----------------------------------
---
False       Echo        - Echo input data to "echo.out" (flag)
```

```
   1        ADAMSPrep   - ADAMS preprocessor mode {1: Run FAST, 2: use FAST
as a preprocessor to create an ADAMS model, 3: do both} (switch)
   1        AnalMode    - Analysis mode {1: Run a time-marching simulation,
2: create a periodic linearized model} (switch)
   3        NumBl       - Number of blades (-)
 250      TMax        - Total run time (s)
  2E-6   DT          - Integration time step (s)
---------------------- TURBINE CONTROL ------------------------------------
---
   0        YCMode      - Yaw control mode {0: none, 1: user-defined from
routine UserYawCont, 2: user-defined from Simulink} (switch)
9999.9      TYCOn       - Time to enable active yaw control (s) [unused when
YCMode=0]
   2        PCMode      - Pitch control mode {0: none, 1: user-defined from
routine PitchCntrl, 2: user-defined from Simulink} (switch)
   0.0      TPCOn       - Time to enable active pitch control (s) [unused
when PCMode=0]
   3        VSContrl    - Variable-speed control mode {0: none, 1: simple VS,
2: user-defined from routine UserVSCont, 3: user-defined from Simulink}
(switch)
9999.9      VS_RtGnSp   - Rated generator speed for simple variable-speed
generator control (HSS side) (rpm) [used only when VSContrl=1]
9999.9      VS_RtTq     - Rated generator torque/constant generator torque in
Region 3 for simple variable-speed generator control (HSS side) (N-m) [used
only when VSContrl=1]
9999.9      VS_Rgn2K    - Generator torque constant in Region 2 for simple
variable-speed generator control (HSS side) (N-m/rpm^2) [used only when
VSContrl=1]
9999.9      VS_SlPc     - Rated generator slip percentage in Region 2 1/2 for
simple variable-speed generator control (%) [used only when VSContrl=1]
   2        GenModel    - Generator model {1: simple, 2: Thevenin, 3: user-
defined from routine UserGen} (switch) [used only when VSContrl=0]
True        GenTiStr    - Method to start the generator {T: timed using
TimGenOn, F: generator speed using SpdGenOn} (flag)
True        GenTiStp    - Method to stop the generator {T: timed using
TimGenOf, F: when generator power = 0} (flag)
9999.9      SpdGenOn    - Generator speed to turn on the generator for a
startup (HSS speed) (rpm) [used only when GenTiStr=False]
   0.0      TimGenOn    - Time to turn on the generator for a startup (s)
[used only when GenTiStr=True]
9999.9      TimGenOf    - Time to turn off the generator (s) [used only when
GenTiStp=True]
   1        HSSBrMode   - HSS brake model {1: simple, 2: user-defined from
routine UserHSSBr} (switch)
9999.9      THSSBrDp    - Time to initiate deployment of the HSS brake (s)
9999.9      TiDynBrk    - Time to initiate deployment of the dynamic
generator brake [CURRENTLY IGNORED] (s)
9999.9      TTpBrDp(1)  - Time to initiate deployment of tip brake 1 (s)
9999.9      TTpBrDp(2)  - Time to initiate deployment of tip brake 2 (s)
9999.9      TTpBrDp(3)  - Time to initiate deployment of tip brake 3 (s)
[unused for 2 blades]
9999.9      TBDepISp(1) - Deployment-initiation speed for the tip brake on
blade 1 (rpm)
9999.9      TBDepISp(2) - Deployment-initiation speed for the tip brake on
blade 2 (rpm)
9999.9      TBDepISp(3) - Deployment-initiation speed for the tip brake on
blade 3 (rpm) [unused for 2 blades]
```

```
9999.9      TYawManS    - Time to start override yaw maneuver and end
standard yaw control (s)
9999.9      TYawManE    - Time at which override yaw maneuver reaches final
yaw angle (s)
   0.0      NacYawF     - Final yaw angle for yaw maneuvers (degrees)
9999.9      TPitManS(1) - Time to start override pitch maneuver for blade 1
and end standard pitch control (s)
9999.9      TPitManS(2) - Time to start override pitch maneuver for blade 2
and end standard pitch control (s)
9999.9      TPitManS(3) - Time to start override pitch maneuver for blade 3
and end standard pitch control (s) [unused for 2 blades]
9999.9      TPitManE(1) - Time at which override pitch maneuver for blade 1
reaches final pitch (s)
9999.9      TPitManE(2) - Time at which override pitch maneuver for blade 2
reaches final pitch (s)
9999.9      TPitManE(3) - Time at which override pitch maneuver for blade 3
reaches final pitch (s) [unused for 2 blades]
   0.0      BlPitch(1)  - Blade 1 initial pitch (degrees)
   0.0      BlPitch(2)  - Blade 2 initial pitch (degrees)
   0.0      BlPitch(3)  - Blade 3 initial pitch (degrees) [unused for 2
blades]
   0.0      B1PitchF(1) - Blade 1 final pitch for pitch maneuvers (degrees)
   0.0      B1PitchF(2) - Blade 2 final pitch for pitch maneuvers (degrees)
   0.0      B1PitchF(3) - Blade 3 final pitch for pitch maneuvers (degrees)
[unused for 2 blades]
---------------------- ENVIRONMENTAL CONDITIONS -----------------------------
---
   9.80665  Gravity     - Gravitational acceleration (m/s^2)
---------------------- FEATURE FLAGS ----------------------------------------
---
True        FlapDOF1    - First flapwise blade mode DOF (flag)
True        FlapDOF2    - Second flapwise blade mode DOF (flag)
True        EdgeDOF     - First edgewise blade mode DOF (flag)
False       TeetDOF     - Rotor-teeter DOF (flag) [unused for 3 blades]
True        DrTrDOF     - Drivetrain rotational-flexibility DOF (flag)
True       GenDOF      - Generator DOF (flag)
True        YawDOF      - Yaw DOF (flag)
True        TwFADOF1    - First fore-aft tower bending-mode DOF (flag)
True        TwFADOF2    - Second fore-aft tower bending-mode DOF (flag)
True        TwSSDOF1    - First side-to-side tower bending-mode DOF (flag)
True        TwSSDOF2    - Second side-to-side tower bending-mode DOF (flag)
True        CompAero    - Compute aerodynamic forces (flag)
False       CompNoise   - Compute aerodynamic noise (flag)
---------------------- INITIAL CONDITIONS -----------------------------------
---
   0.0      OoPDefl     - Initial out-of-plane blade-tip displacement
(meters)
   0.0      IPDefl      - Initial in-plane blade-tip deflection (meters)
   0.0      TeetDefl    - Initial or fixed teeter angle (degrees) [unused for
3 blades]
   0.0      Azimuth     - Initial azimuth angle for blade 1 (degrees)
   12      RotSpeed    - Initial or fixed rotor speed (rpm)
   0.0      NacYaw      - Initial or fixed nacelle-yaw angle (degrees)
   0.0      TTDspFA     - Initial fore-aft tower-top displacement (meters)
   0.0      TTDspSS     - Initial side-to-side tower-top displacement
(meters)
```

```
---------------------- TURBINE CONFIGURATION -------------------------------
---
  63.0      TipRad      - The distance from the rotor apex to the blade tip
(meters)
   1.5      HubRad      - The distance from the rotor apex to the blade root
(meters)
   1        PSpnElN     - Number of the innermost blade element which is
still part of the pitchable portion of the blade for partial-span pitch
control [1 to BldNodes] [CURRENTLY IGNORED] (-)
   0.0      UndSling    - Undersling length [distance from teeter pin to the
rotor apex] (meters) [unused for 3 blades]
   0.0      HubCM       - Distance from rotor apex to hub mass [positive
downwind] (meters)
  -5.01910  OverHang    - Distance from yaw axis to rotor apex [3 blades] or
teeter pin [2 blades] (meters)
   1.9      NacCMxn     - Downwind distance from the tower-top to the nacelle
CM (meters)
   0.0      NacCMyn     - Lateral  distance from the tower-top to the nacelle
CM (meters)
   1.75     NacCMzn     - Vertical distance from the tower-top to the nacelle
CM (meters)
  87.6      TowerHt     - Height of tower above ground level [onshore] or MSL
[offshore] (meters)
   1.96256  Twr2Shft    - Vertical distance from the tower-top to the rotor
shaft (meters)
   0.0      TwrRBHt     - Tower rigid base height (meters)
  -5.0      ShftTilt    - Rotor shaft tilt angle (degrees)
   0.0      Delta3      - Delta-3 angle for teetering rotors (degrees)
[unused for 3 blades]
  -2.5      PreCone(1)  - Blade 1 cone angle (degrees)
  -2.5      PreCone(2)  - Blade 2 cone angle (degrees)
  -2.5      PreCone(3)  - Blade 3 cone angle (degrees) [unused for 2 blades]
   0.0      AzimB1Up    - Azimuth value to use for I/O when blade 1 points up
(degrees)
---------------------- MASS AND INERTIA ------------------------------------
---
   0.0      YawBrMass   - Yaw bearing mass (kg)
 240.00E3   NacMass     - Nacelle mass (kg)
  56.78E3   HubMass     - Hub mass (kg)
   0.0      TipMass(1)  - Tip-brake mass, blade 1 (kg)
   0.0      TipMass(2)  - Tip-brake mass, blade 2 (kg)
   0.0      TipMass(3)  - Tip-brake mass, blade 3 (kg) [unused for 2 blades]
2607.89E3   NacYIner    - Nacelle inertia about yaw axis (kg m^2)
 534.116    GenIner     - Generator inertia about HSS (kg m^2)
 115.926E3  HubIner     - Hub inertia about rotor axis [3 blades] or teeter
axis [2 blades] (kg m^2)
---------------------- DRIVETRAIN ------------------------------------------
---
 100.0      GBoxEff     - Gearbox efficiency (%)
  94.4      GenEff      - Generator efficiency [ignored by the Thevenin and
user-defined generator models] (%)
  1.0      GBRatio     - Gearbox ratio (-)
False       GBRevers    - Gearbox reversal {T: if rotor and generator rotate
in opposite directions} (flag)
  28.1162E3 HSSBrTqF    - Fully deployed HSS-brake torque (N-m)
   0.6      HSSBrDT     - Time for HSS-brake to reach full deployment once
initiated (sec) [used only when HSSBrMode=1]
```

```
            DynBrkFi    - File containing a mech-gen-torque vs HSS-speed
curve for a dynamic brake [CURRENTLY IGNORED] (quoted string)
 867.637E6  DTTorSpr    - Drivetrain torsional spring (N-m/rad)
   6.215E6  DTTorDmp    - Drivetrain torsional damper (N-m/(rad/s))
---------------------- SIMPLE INDUCTION GENERATOR --------------------------
---
9999.9      SIG_SlPc    - Rated generator slip percentage (%) [used only when
VSContrl=0 and GenModel=1]
9999.9      SIG_SySp    - Synchronous (zero-torque) generator speed (rpm)
[used only when VSContrl=0 and GenModel=1]
9999.9      SIG_RtTq    - Rated torque (N-m) [used only when VSContrl=0 and
GenModel=1]
9999.9      SIG_PORt    - Pull-out ratio (Tpullout/Trated) (-) [used only
when VSContrl=0 and GenModel=1]
---------------------- THEVENIN-EQUIVALENT INDUCTION GENERATOR -------------
---
9999.9      TEC_Freq    - Line frequency [50 or 60] (Hz) [used only when
VSContrl=0 and GenModel=2]
9998        TEC_NPol    - Number of poles [even integer > 0] (-) [used only
when VSContrl=0 and GenModel=2]
9999.9      TEC_SRes    - Stator resistance (ohms) [used only when VSContrl=0
and GenModel=2]
9999.9      TEC_RRes    - Rotor resistance (ohms) [used only when VSContrl=0
and GenModel=2]
9999.9      TEC_VLL     - Line-to-line RMS voltage (volts) [used only when
VSContrl=0 and GenModel=2]
9999.9      TEC_SLR     - Stator leakage reactance (ohms) [used only when
VSContrl=0 and GenModel=2]
9999.9      TEC_RLR     - Rotor leakage reactance (ohms) [used only when
VSContrl=0 and GenModel=2]
9999.9      TEC_MR      - Magnetizing reactance (ohms) [used only when
VSContrl=0 and GenModel=2]
---------------------- PLATFORM --------------------------------------------
---
 0.0        PtfmModel   - Platform model {0: none, 1: onshore, 2: fixed
bottom offshore, 3: floating offshore} (switch)
            PtfmFile    - Name of file containing platform properties (quoted
string) [unused when PtfmModel=0]
---------------------- TOWER -----------------------------------------------
---
  20        TwrNodes    - Number of tower nodes used for analysis (-)
"NRELOffshrBsline5MW_Tower_Onshore.dat"          TwrFile     - Name of file
containing tower properties (quoted string)
---------------------- NACELLE-YAW -----------------------------------------
---
9028.32E6   YawSpr      - Nacelle-yaw spring constant (N-m/rad)
  19.16E6   YawDamp     - Nacelle-yaw damping constant (N-m/(rad/s))
   0.0      YawNeut     - Neutral yaw position--yaw spring force is zero at
this yaw (degrees)
---------------------- FURLING ---------------------------------------------
---
False       Furling     - Read in additional model properties for furling
turbine (flag)
            FurlFile    - Name of file containing furling properties (quoted
string) [unused when Furling=False]
---------------------- ROTOR-TEETER ----------------------------------------
---
```

```
   0        TeetMod     - Rotor-teeter spring/damper model {0: none, 1:
standard, 2: user-defined from routine UserTeet} (switch) [unused for 3
blades]
   0.0      TeetDmpP    - Rotor-teeter damper position (degrees) [used only
for 2 blades and when TeetMod=1]
   0.0      TeetDmp     - Rotor-teeter damping constant (N-m/(rad/s)) [used
only for 2 blades and when TeetMod=1]
   0.0      TeetCDmp    - Rotor-teeter rate-independent Coulomb-damping
moment (N-m) [used only for 2 blades and when TeetMod=1]
   0.0      TeetSStP    - Rotor-teeter soft-stop position (degrees) [used
only for 2 blades and when TeetMod=1]
   0.0      TeetHStP    - Rotor-teeter hard-stop position (degrees) [used
only for 2 blades and when TeetMod=1]
   0.0      TeetSSSp    - Rotor-teeter soft-stop linear-spring constant (N-
m/rad) [used only for 2 blades and when TeetMod=1]
   0.0      TeetHSSp    - Rotor-teeter hard-stop linear-spring constant (N-
m/rad) [used only for 2 blades and when TeetMod=1]
---------------------- TIP-BRAKE ---------------------------------------------
---
   0.0      TBDrConN    - Tip-brake drag constant during normal operation,
Cd*Area (m^2)
   0.0      TBDrConD    - Tip-brake drag constant during fully-deployed
operation, Cd*Area (m^2)
   0.0      TpBrDT      - Time for tip-brake to reach full deployment once
released (sec)
---------------------- BLADE -------------------------------------------------
---
"NRELOffshrBsline5MW_Blade.dat"                  BldFile(1)  - Name of file
containing properties for blade 1 (quoted string)
"NRELOffshrBsline5MW_Blade.dat"                  BldFile(2)  - Name of file
containing properties for blade 2 (quoted string)
"NRELOffshrBsline5MW_Blade.dat"                  BldFile(3)  - Name of file
containing properties for blade 3 (quoted string) [unused for 2 blades]
---------------------- AERODYN -----------------------------------------------
---
"NRELOffshrBsline5MW_AeroDyn.ipt"                ADFile      - Name of file
containing AeroDyn input parameters (quoted string)
---------------------- NOISE -------------------------------------------------
---
            NoiseFile   - Name of file containing aerodynamic noise input
parameters (quoted string) [used only when CompNoise=True]
---------------------- ADAMS -------------------------------------------------
---
            ADAMSFile   - Name of file containing ADAMS-specific input
parameters (quoted string) [unused when ADAMSPrep=1]
---------------------- LINEARIZATION CONTROL ---------------------------------
---
            LinFile     - Name of file containing FAST linearization
parameters (quoted string) [unused when AnalMode=1]
---------------------- OUTPUT ------------------------------------------------
---
True        SumPrint    - Print summary data to "<RootName>.fsm" (flag)
True        TabDelim    - Generate a tab-delimited tabular output file.
(flag)
"ES10.3E2"  OutFmt      - Format used for tabular output except time.
Resulting field should be 10 characters. (quoted string)  [not checked for
validity!]
```

```
   0.0      TStart      - Time to begin tabular output (s)
   1        DecFact     - Decimation factor for tabular output {1: output
every time step} (-)
   1.0      SttsTime    - Amount of time between screen status messages (sec)
  -3.09528  NcIMUxn     - Downwind distance from the tower-top to the nacelle
IMU (meters)
   0.0      NcIMUyn     - Lateral  distance from the tower-top to the nacelle
IMU (meters)
   2.23336  NcIMUzn     - Vertical distance from the tower-top to the nacelle
IMU (meters)
   1.912    ShftGagL    - Distance from rotor apex [3 blades] or teeter pin
[2 blades] to shaft strain gages [positive for upwind rotors] (meters)
   0        NTwGages    - Number of tower nodes that have strain gages for
output [0 to 9] (-)
            TwrGagNd    - List of tower nodes that have strain gages [1 to
TwrNodes] (-) [unused if NTwGages=0]
   3        NBlGages    - Number of blade nodes that have strain gages for
output [0 to 9] (-)
 5,9,13     BldGagNd    - List of blade nodes that have strain gages [1 to
BldNodes] (-) [unused if NBlGages=0]
            OutList     - The next line(s) contains a list of output
parameters.  See OutList.txt for a listing of available output channels, (-)
"RotSpeed"                          - Rotor speed
"HSShftTq"
"RotAccel"
"TotWindV"
"BlPitch1"
END of FAST input file (the word "END" must appear in the first 3 columns of
this last line).
--------------------------------------------------------------------------
---
```

NRELOffshrBsline5MW_Tower_Onshore.dat:

```
--------------------------------------------------------------------------
---
---------------------- FAST TOWER FILE -----------------------------------
---
NREL 5.0 MW offshore baseline tower input properties.
---------------------- TOWER PARAMETERS ----------------------------------
---
  11        NTwInpSt    - Number of input stations to specify tower geometry
False       CalcTMode   - Calculate tower mode shapes internally {T: ignore
mode shapes from below, F: use mode shapes from below} [CURRENTLY IGNORED]
(flag)
   1.0      TwrFADmp(1) - Tower 1st fore-aft mode structural damping ratio
(%)
   1.0      TwrFADmp(2) - Tower 2nd fore-aft mode structural damping ratio
(%)
   1.0      TwrSSDmp(1) - Tower 1st side-to-side mode structural damping
ratio (%)
   1.0      TwrSSDmp(2) - Tower 2nd side-to-side mode structural damping
ratio (%)
---------------------- TOWER ADJUSTMUNT FACTORS --------------------------
---
   1.0      FAStTunr(1) - Tower fore-aft modal stiffness tuner, 1st mode (-)
```

```
   1.0      FAStTunr(2) - Tower fore-aft modal stiffness tuner, 2nd mode (-)
   1.0      SSStTunr(1) - Tower side-to-side stiffness tuner, 1st mode (-)
   1.0      SSStTunr(2) - Tower side-to-side stiffness tuner, 2nd mode (-)
   1.0      AdjTwMa     - Factor to adjust tower mass density (-)
   1.0      AdjFASt     - Factor to adjust tower fore-aft stiffness (-)
   1.0      AdjSSSt     - Factor to adjust tower side-to-side stiffness (-)
---------------------- DISTRIBUTED TOWER PROPERTIES -------------------------
---
HtFract  TMassDen  TwFAStif   TwSSStif   TwGJStif   TwEAStif   TwFAIner
TwSSIner  TwFAcgOf  TwSScgOf
(-)      (kg/m)    (Nm^2)     (Nm^2)     (Nm^2)     (N)        (kg m)    (kg
m)    (m)       (m)
0.0      5590.87   614.343E9  614.343E9  472.751E9  138.127E9  24866.3
24866.3   0.0       0.0
0.1      5232.43   534.821E9  534.821E9  411.558E9  129.272E9  21647.5
21647.5   0.0       0.0
0.2      4885.76   463.267E9  463.267E9  356.495E9  120.707E9  18751.3
18751.3   0.0       0.0
0.3      4550.87   399.131E9  399.131E9  307.141E9  112.433E9  16155.3
16155.3   0.0       0.0
0.4      4227.75   341.883E9  341.883E9  263.087E9  104.450E9  13838.1
13838.1   0.0       0.0
0.5      3916.41   291.011E9  291.011E9  223.940E9   96.758E9  11779.0
11779.0   0.0       0.0
0.6      3616.83   246.027E9  246.027E9  189.323E9   89.357E9   9958.2
9958.2   0.0       0.0
0.7      3329.03   206.457E9  206.457E9  158.874E9   82.247E9   8356.6
8356.6   0.0       0.0
0.8      3053.01   171.851E9  171.851E9  132.244E9   75.427E9   6955.9
6955.9   0.0       0.0
0.9      2788.75   141.776E9  141.776E9  109.100E9   68.899E9   5738.6
5738.6   0.0       0.0
1.0      2536.27   115.820E9  115.820E9   89.126E9   62.661E9   4688.0
4688.0   0.0       0.0
---------------------- TOWER FORE-AFT MODE SHAPES ---------------------------
---
   0.7004   TwFAM1Sh(2) - Mode 1, coefficient of x^2 term   !JASON:THESE
COEFFICIENTS UPDATED ON 8/22/2007 - THE MODE SHAPES CHANGED ONLY A SMALL
AMOUNT - I CORRECTED MODE USING THE EIGENANALYSIS DATA BY USING A LINEAR
COMBINATION WITH THE SECOND MODE COEFFICIENTS
   2.1963   TwFAM1Sh(3) -       , coefficient of x^3 term   !JASON:THESE
COEFFICIENTS UPDATED ON 8/22/2007 - THE MODE SHAPES CHANGED ONLY A SMALL
AMOUNT - I CORRECTED MODE USING THE EIGENANALYSIS DATA BY USING A LINEAR
COMBINATION WITH THE SECOND MODE COEFFICIENTS
  -5.6202   TwFAM1Sh(4) -       , coefficient of x^4 term   !JASON:THESE
COEFFICIENTS UPDATED ON 8/22/2007 - THE MODE SHAPES CHANGED ONLY A SMALL
AMOUNT - I CORRECTED MODE USING THE EIGENANALYSIS DATA BY USING A LINEAR
COMBINATION WITH THE SECOND MODE COEFFICIENTS
   6.2275   TwFAM1Sh(5) -       , coefficient of x^5 term   !JASON:THESE
COEFFICIENTS UPDATED ON 8/22/2007 - THE MODE SHAPES CHANGED ONLY A SMALL
AMOUNT - I CORRECTED MODE USING THE EIGENANALYSIS DATA BY USING A LINEAR
COMBINATION WITH THE SECOND MODE COEFFICIENTS
  -2.5040   TwFAM1Sh(6) -       , coefficient of x^6 term   !JASON:THESE
COEFFICIENTS UPDATED ON 8/22/2007 - THE MODE SHAPES CHANGED ONLY A SMALL
AMOUNT - I CORRECTED MODE USING THE EIGENANALYSIS DATA BY USING A LINEAR
COMBINATION WITH THE SECOND MODE COEFFICIENTS
```

```
 -70.5319   TwFAM2Sh(2) - Mode 2, coefficient of x^2 term   !JASON:THESE
COEFFICIENTS UPDATED ON 8/22/2007 - THE MODE SHAPES CHANGED ONLY A SMALL
AMOUNT - I CORRECTED MODE USING THE EIGENANALYSIS DATA BY USING A LINEAR
COMBINATION WITH THE FIRST MODE COEFFICIENTS
 -63.7623   TwFAM2Sh(3) -       , coefficient of x^3 term   !JASON:THESE
COEFFICIENTS UPDATED ON 8/22/2007 - THE MODE SHAPES CHANGED ONLY A SMALL
AMOUNT - I CORRECTED MODE USING THE EIGENANALYSIS DATA BY USING A LINEAR
COMBINATION WITH THE FIRST MODE COEFFICIENTS
 289.7369   TwFAM2Sh(4) -       , coefficient of x^4 term   !JASON:THESE
COEFFICIENTS UPDATED ON 8/22/2007 - THE MODE SHAPES CHANGED ONLY A SMALL
AMOUNT - I CORRECTED MODE USING THE EIGENANALYSIS DATA BY USING A LINEAR
COMBINATION WITH THE FIRST MODE COEFFICIENTS
-176.5134   TwFAM2Sh(5) -       , coefficient of x^5 term   !JASON:THESE
COEFFICIENTS UPDATED ON 8/22/2007 - THE MODE SHAPES CHANGED ONLY A SMALL
AMOUNT - I CORRECTED MODE USING THE EIGENANALYSIS DATA BY USING A LINEAR
COMBINATION WITH THE FIRST MODE COEFFICIENTS
  22.0706   TwFAM2Sh(6) -       , coefficient of x^6 term   !JASON:THESE
COEFFICIENTS UPDATED ON 8/22/2007 - THE MODE SHAPES CHANGED ONLY A SMALL
AMOUNT - I CORRECTED MODE USING THE EIGENANALYSIS DATA BY USING A LINEAR
COMBINATION WITH THE FIRST MODE COEFFICIENTS
---------------------- TOWER SIDE-TO-SIDE MODE SHAPES -----------------------
---
   1.3850   TwSSM1Sh(2) - Mode 1, coefficient of x^2 term   !JASON:THESE
COEFFICIENTS UPDATED ON 8/22/2007 - THE MODE SHAPES CHANGED ONLY A SMALL
AMOUNT - I CORRECTED MODE USING THE EIGENANALYSIS DATA BY USING A LINEAR
COMBINATION WITH THE SECOND MODE COEFFICIENTS
  -1.7684   TwSSM1Sh(3) -       , coefficient of x^3 term   !JASON:THESE
COEFFICIENTS UPDATED ON 8/22/2007 - THE MODE SHAPES CHANGED ONLY A SMALL
AMOUNT - I CORRECTED MODE USING THE EIGENANALYSIS DATA BY USING A LINEAR
COMBINATION WITH THE SECOND MODE COEFFICIENTS
   3.0871   TwSSM1Sh(4) -       , coefficient of x^4 term   !JASON:THESE
COEFFICIENTS UPDATED ON 8/22/2007 - THE MODE SHAPES CHANGED ONLY A SMALL
AMOUNT - I CORRECTED MODE USING THE EIGENANALYSIS DATA BY USING A LINEAR
COMBINATION WITH THE SECOND MODE COEFFICIENTS
  -2.2395   TwSSM1Sh(5) -       , coefficient of x^5 term   !JASON:THESE
COEFFICIENTS UPDATED ON 8/22/2007 - THE MODE SHAPES CHANGED ONLY A SMALL
AMOUNT - I CORRECTED MODE USING THE EIGENANALYSIS DATA BY USING A LINEAR
COMBINATION WITH THE SECOND MODE COEFFICIENTS
   0.5357   TwSSM1Sh(6) -       , coefficient of x^6 term   !JASON:THESE
COEFFICIENTS UPDATED ON 8/22/2007 - THE MODE SHAPES CHANGED ONLY A SMALL
AMOUNT - I CORRECTED MODE USING THE EIGENANALYSIS DATA BY USING A LINEAR
COMBINATION WITH THE SECOND MODE COEFFICIENTS
-121.2097   TwSSM2Sh(2) - Mode 2, coefficient of x^2 term   !JASON:THESE
COEFFICIENTS UPDATED ON 8/22/2007 - THE MODE SHAPES CHANGED ONLY A SMALL
AMOUNT - I CORRECTED MODE USING THE EIGENANALYSIS DATA BY USING A LINEAR
COMBINATION WITH THE FIRST MODE COEFFICIENTS
 184.4151   TwSSM2Sh(3) -       , coefficient of x^3 term   !JASON:THESE
COEFFICIENTS UPDATED ON 8/22/2007 - THE MODE SHAPES CHANGED ONLY A SMALL
AMOUNT - I CORRECTED MODE USING THE EIGENANALYSIS DATA BY USING A LINEAR
COMBINATION WITH THE FIRST MODE COEFFICIENTS
-224.9037   TwSSM2Sh(4) -       , coefficient of x^4 term   !JASON:THESE
COEFFICIENTS UPDATED ON 8/22/2007 - THE MODE SHAPES CHANGED ONLY A SMALL
AMOUNT - I CORRECTED MODE USING THE EIGENANALYSIS DATA BY USING A LINEAR
COMBINATION WITH THE FIRST MODE COEFFICIENTS
 298.5360   TwSSM2Sh(5) -       , coefficient of x^5 term   !JASON:THESE
COEFFICIENTS UPDATED ON 8/22/2007 - THE MODE SHAPES CHANGED ONLY A SMALL
```

```
AMOUNT - I CORRECTED MODE USING THE EIGENANALYSIS DATA BY USING A LINEAR
COMBINATION WITH THE FIRST MODE COEFFICIENTS
-135.8377   TwSSM2Sh(6) -       , coefficient of x^6 term   !JASON:THESE
COEFFICIENTS UPDATED ON 8/22/2007 - THE MODE SHAPES CHANGED ONLY A SMALL
AMOUNT - I CORRECTED MODE USING THE EIGENANALYSIS DATA BY USING A LINEAR
COMBINATION WITH THE FIRST MODE COEFFICIENTS
```

NRELOffshrBsline5MW_Blade.dat:

```
------------------------------------------------------------------------
---
---------------------- FAST INDIVIDUAL BLADE FILE --------------------------
---
NREL 5.0 MW offshore baseline blade input properties.
---------------------- BLADE PARAMETERS ----------------------------------
---
  49        NBlInpSt    - Number of blade input stations (-)
False       CalcBMode   - Calculate blade mode shapes internally {T: ignore
mode shapes from below, F: use mode shapes from below} [CURRENTLY IGNORED]
(flag)
   0.477465 BldFlDmp(1) - Blade flap mode #1 structural damping in percent of
critical (%)
   0.477465 BldFlDmp(2) - Blade flap mode #2 structural damping in percent of
critical (%)
   0.477465 BldEdDmp(1) - Blade edge mode #1 structural damping in percent of
critical (%)
---------------------- BLADE ADJUSTMENT FACTORS ---------------------------
---
   1.0      FlStTunr(1) - Blade flapwise modal stiffness tuner, 1st mode (-)
   1.0      FlStTunr(2) - Blade flapwise modal stiffness tuner, 2nd mode (-)
   1.04536  AdjBlMs     - Factor to adjust blade mass density (-)
   1.0      AdjFlSt     - Factor to adjust blade flap stiffness (-)
   1.0      AdjEdSt     - Factor to adjust blade edge stiffness (-)
---------------------- DISTRIBUTED BLADE PROPERTIES ------------------------
---
BlFract  AeroCent  StrcTwst  BMassDen  FlpStff     EdgStff     GJStff
EAStff      Alpha  FlpIner  EdgIner  PrecrvRef  PreswpRef  FlpcgOf  EdgcgOf
FlpEAOf  EdgEAOf
(-)      (-)       (deg)     (kg/m)    (Nm^2)      (Nm^2)      (Nm^2)     (N)
(-)    (kg m)    (kg m)    (m)         (m)         (m)       (m)        (m)
(m)
0.00000  0.25000   13.308    678.935   18110.00E6  18113.60E6  5564.40E6
9729.48E6  0.0     972.86   973.04  0.0         0.0         0.0        0.00017
0.0      0.0
0.00325  0.25000   13.308    678.935   18110.00E6  18113.60E6  5564.40E6
9729.48E6  0.0     972.86   973.04  0.0         0.0         0.0        0.00017
0.0      0.0
0.01951  0.24951   13.308    773.363   19424.90E6  19558.60E6  5431.59E6
10789.50E6  0.0    1091.52  1066.38  0.0         0.0         0.0       -0.02309
0.0      0.0
0.03577  0.24510   13.308    740.550   17455.90E6  19497.80E6  4993.98E6
10067.23E6  0.0     966.09  1047.36  0.0         0.0         0.0        0.00344
0.0      0.0
```

```
0.05203  0.23284   13.308    740.042   15287.40E6  19788.80E6  4666.59E6
9867.78E6  0.0     873.81  1099.75  0.0        0.0         0.0       0.04345
0.0      0.0
0.06829  0.22059   13.308    592.496   10782.40E6  14858.50E6  3474.71E6
7607.86E6  0.0     648.55   873.02  0.0        0.0         0.0       0.05893
0.0      0.0
0.08455  0.20833   13.308    450.275    7229.72E6  10220.60E6  2323.54E6
5491.26E6  0.0     456.76   641.49  0.0        0.0         0.0       0.06494
0.0      0.0
0.10081  0.19608   13.308    424.054    6309.54E6   9144.70E6  1907.87E6
4971.30E6  0.0     400.53   593.73  0.0        0.0         0.0       0.07718
0.0      0.0
0.11707  0.18382   13.308    400.638    5528.36E6   8063.16E6  1570.36E6
4493.95E6  0.0     351.61   547.18  0.0        0.0         0.0       0.08394
0.0      0.0
0.13335  0.17156   13.308    382.062    4980.06E6   6884.44E6  1158.26E6
4034.80E6  0.0     316.12   490.84  0.0        0.0         0.0       0.10174
0.0      0.0
0.14959  0.15931   13.308    399.655    4936.84E6   7009.18E6  1002.12E6
4037.29E6  0.0     303.60   503.86  0.0        0.0         0.0       0.10758
0.0      0.0
0.16585  0.14706   13.308    426.321    4691.66E6   7167.68E6   855.90E6
4169.72E6  0.0     289.24   544.70  0.0        0.0         0.0       0.15829
0.0      0.0
0.18211  0.13481   13.181    416.820    3949.46E6   7271.66E6   672.27E6
4082.35E6  0.0     246.57   569.90  0.0        0.0         0.0       0.22235
0.0      0.0
0.19837  0.12500   12.848    406.186    3386.52E6   7081.70E6   547.49E6
4085.97E6  0.0     215.91   601.28  0.0        0.0         0.0       0.30756
0.0      0.0
0.21465  0.12500   12.192    381.420    2933.74E6   6244.53E6   448.84E6
3668.34E6  0.0     187.11   546.56  0.0        0.0         0.0       0.30386
0.0      0.0
0.23089  0.12500   11.561    352.822    2568.96E6   5048.96E6   335.92E6
3147.76E6  0.0     160.84   468.71  0.0        0.0         0.0       0.26519
0.0      0.0
0.24715  0.12500   11.072    349.477    2388.65E6   4948.49E6   311.35E6
3011.58E6  0.0     148.56   453.76  0.0        0.0         0.0       0.25941
0.0      0.0
0.26341  0.12500   10.792    346.538    2271.99E6   4808.02E6   291.94E6
2882.62E6  0.0     140.30   436.22  0.0        0.0         0.0       0.25007
0.0      0.0
0.29595  0.12500   10.232    339.333    2050.05E6   4501.40E6   261.00E6
2613.97E6  0.0     124.61   398.18  0.0        0.0         0.0       0.23155
0.0      0.0
0.32846  0.12500    9.672    330.004    1828.25E6   4244.07E6   228.82E6
2357.48E6  0.0     109.42   362.08  0.0        0.0         0.0       0.20382
0.0      0.0
0.36098  0.12500    9.110    321.990    1588.71E6   3995.28E6   200.75E6
2146.86E6  0.0      94.36   335.01  0.0        0.0         0.0       0.19934
0.0      0.0
0.39350  0.12500    8.534    313.820    1361.93E6   3750.76E6   174.38E6
1944.09E6  0.0      80.24   308.57  0.0        0.0         0.0       0.19323
0.0      0.0
0.42602  0.12500    7.932    294.734    1102.38E6   3447.14E6   144.47E6
1632.70E6  0.0      62.67   263.87  0.0        0.0         0.0       0.14994
0.0      0.0
```

```
0.45855  0.12500    7.321    287.120     875.80E6   3139.07E6   119.98E6
1432.40E6  0.0      49.42   237.06  0.0        0.0         0.0       0.15421
0.0      0.0
0.49106  0.12500    6.711    263.343     681.30E6   2734.24E6    81.19E6
1168.76E6  0.0      37.34   196.41  0.0        0.0         0.0       0.13252
0.0      0.0
0.52358  0.12500    6.122    253.207     534.72E6   2554.87E6    69.09E6
1047.43E6  0.0      29.14   180.34  0.0        0.0         0.0       0.13313
0.0      0.0
0.55610  0.12500    5.546    241.666     408.90E6   2334.03E6    57.45E6
922.95E6  0.0      22.16   162.43  0.0         0.0         0.0       0.14035
0.0      0.0
0.58862  0.12500    4.971    220.638     314.54E6   1828.73E6    45.92E6
760.82E6  0.0      17.33   134.83  0.0         0.0         0.0       0.13950
0.0      0.0
0.62115  0.12500    4.401    200.293     238.63E6   1584.10E6    35.98E6
648.03E6  0.0      13.30   116.30  0.0         0.0         0.0       0.15134
0.0      0.0
0.65366  0.12500    3.834    179.404     175.88E6   1323.36E6    27.44E6
539.70E6  0.0       9.96    97.98  0.0         0.0         0.0       0.17418
0.0      0.0
0.68618  0.12500    3.332    165.094     126.01E6   1183.68E6    20.90E6
531.15E6  0.0       7.30    98.93  0.0         0.0         0.0       0.24922
0.0      0.0
0.71870  0.12500    2.890    154.411     107.26E6   1020.16E6    18.54E6
460.01E6  0.0       6.22    85.78  0.0         0.0         0.0       0.26022
0.0      0.0
0.75122  0.12500    2.503    138.935      90.88E6    797.81E6    16.28E6
375.75E6  0.0       5.19    69.96  0.0         0.0         0.0       0.22554
0.0      0.0
0.78376  0.12500    2.116    129.555      76.31E6    709.61E6    14.53E6
328.89E6  0.0       4.36    61.41  0.0         0.0         0.0       0.22795
0.0      0.0
0.81626  0.12500    1.730    107.264      61.05E6    518.19E6     9.07E6
244.04E6  0.0       3.36    45.44  0.0         0.0         0.0       0.20600
0.0      0.0
0.84878  0.12500    1.342     98.776      49.48E6    454.87E6     8.06E6
211.60E6  0.0       2.75    39.57  0.0         0.0         0.0       0.21662
0.0      0.0
0.88130  0.12500    0.954     90.248      39.36E6    395.12E6     7.08E6
181.52E6  0.0       2.21    34.09  0.0         0.0         0.0       0.22784
0.0      0.0
0.89756  0.12500    0.760     83.001      34.67E6    353.72E6     6.09E6
160.25E6  0.0       1.93    30.12  0.0         0.0         0.0       0.23124
0.0      0.0
0.91382  0.12500    0.574     72.906      30.41E6    304.73E6     5.75E6
109.23E6  0.0       1.69    20.15  0.0         0.0         0.0       0.14826
0.0      0.0
0.93008  0.12500    0.404     68.772      26.52E6    281.42E6     5.33E6
100.08E6  0.0       1.49    18.53  0.0         0.0         0.0       0.15346
0.0      0.0
0.93821  0.12500    0.319     66.264      23.84E6    261.71E6     4.94E6
92.24E6  0.0       1.34    17.11  0.0         0.0         0.0       0.15382
0.0      0.0
0.94636  0.12500    0.253     59.340      19.63E6    158.81E6     4.24E6
63.23E6  0.0       1.10    11.55  0.0         0.0         0.0       0.09470
0.0      0.0
```

```
0.95447  0.12500    0.216     55.914      16.00E6    137.88E6     3.66E6
53.32E6  0.0       0.89     9.77  0.0        0.0        0.0       0.09018
0.0      0.0
0.96260  0.12500    0.178     52.484      12.83E6    118.79E6     3.13E6
44.53E6  0.0       0.71     8.19  0.0        0.0        0.0       0.08561
0.0      0.0
0.97073  0.12500    0.140     49.114      10.08E6    101.63E6     2.64E6
36.90E6  0.0       0.56     6.82  0.0        0.0        0.0       0.08035
0.0      0.0
0.97886  0.12500    0.101     45.818       7.55E6     85.07E6     2.17E6
29.92E6  0.0       0.42     5.57  0.0        0.0        0.0       0.07096
0.0      0.0
0.98699  0.12500    0.062     41.669       4.60E6     64.26E6     1.58E6
21.31E6  0.0       0.25     4.01  0.0        0.0        0.0       0.05424
0.0      0.0
0.99512  0.12500    0.023     11.453       0.25E6      6.61E6     0.25E6
4.85E6  0.0       0.04     0.94  0.0         0.0        0.0       0.05387  0.0
0.0
1.00000  0.12500    0.000     10.319       0.17E6      5.01E6     0.19E6
3.53E6  0.0       0.02     0.68  0.0         0.0        0.0       0.05181  0.0
0.0
---------------------- BLADE MODE SHAPES -------------------------------------
---
   0.0622   BldFl1Sh(2) - Flap mode 1, coeff of x^2
   1.7254   BldFl1Sh(3) -            , coeff of x^3
  -3.2452   BldFl1Sh(4) -            , coeff of x^4
   4.7131   BldFl1Sh(5) -            , coeff of x^5
  -2.2555   BldFl1Sh(6) -            , coeff of x^6
  -0.5809   BldFl2Sh(2) - Flap mode 2, coeff of x^2
   1.2067   BldFl2Sh(3) -            , coeff of x^3
 -15.5349   BldFl2Sh(4) -            , coeff of x^4
  29.7347   BldFl2Sh(5) -            , coeff of x^5
 -13.8255   BldFl2Sh(6) -            , coeff of x^6
   0.3627   BldEdgSh(2) - Edge mode 1, coeff of x^2
   2.5337   BldEdgSh(3) -            , coeff of x^3
  -3.5772   BldEdgSh(4) -            , coeff of x^4
   2.3760   BldEdgSh(5) -            , coeff of x^5
  -0.6952   BldEdgSh(6) -            , coeff of x^6
```